



UiT The Arctic University of Norway

Faculty of Science and Technology
Department of Technology and Safety

Hydrological Modelling and Climate Change Impact Assessment on Future Floods in the Norwegian Arctic Catchments

Minh Tuan Bui

A dissertation for the degree of Philosophiae Doctor

May 2022



Hydrological Modelling and Climate Change Impact Assessment on Future Floods in the Norwegian Arctic Catchments

By
Minh Tuan Bui

Thesis submitted in fulfilment of the requirements for the
degree of Philosophiae Doctor (PhD)



UiT The Arctic University of Norway

Faculty of Science and Technology
Department of Technology and Safety

May 2022

Abstract

Climate change is expected to alter the hydrological cycle in the Arctic, which would result in the increase in intensity and frequency of hydrological extreme events such as flooding. Noticeably, the changes in flooding due to climate change would severely affect human life, infrastructures, the environment, ecosystem, and socio-economic development in the impacted areas. Hydrological models are state-of-the-art tools for assessing the impact of climate change on hydrological processes. However, performing hydrological simulation/projection in the Arctic is challenging because of the complex hydrological processes and data-sparse features in the region. In consideration of those issues, this PhD research aims: (1) to assess the performances of hydrological models in the Arctic, (2) to investigate the alternative weather inputs for running the hydrological models in the Arctic region with scattered monitoring data, (3) to evaluate the effects of the models' structure and parameterization and the spatial resolution of weather inputs on the results of hydrological simulations, and (4) to project future hydrological events under climate change impacts using the current hydrological model, and analyse the reliability/uncertainty of the projection. To fulfil the research's objectives, several methodologies were applied. Firstly, a comprehensive review was conducted to address the current capacities and challenges of twelve well-known hydrological models, including surface hydrological models and subsurface hydrological models/groundwater models/cryo-hydrogeological models. These models have previously been applied or have the potential for application in the Arctic. Next, the physically based, semi-distributed model, SWAT (soil and water assessment tool), was selected as a suitable model, among other potential models, to assess its performance for hydrological simulations and to verify the potential application of reanalysis weather data. Moreover, the SWAT model was coupled with multiple ensemble global and regional climate models' (GCM_RCM) simulations to project the future hydrological impacts under climate change (in 2041-2070). The study areas were mainly focused in the Norwegian Arctic catchments.

This study found that both surface hydrological models and subsurface hydrological models/groundwater models/cryo-hydrogeological models have their capacities and limitations regarding dealing with complex hydrological processes in the Arctic. Besides, the selection of suitable models also depends on the targets and current conditions (e.g., available inputs, timing, funding, etc.) of each study. The SWAT model demonstrated considerable capacity for surface hydrological simulation under different temporal resolutions (e.g., monthly and daily simulation) in Norwegian Arctic catchments with variations in geographical distributions, latitudes, catchment's scales, and dominant hydrological regimes. However, the SWAT's performance varied among catchments as well as among sub-catchments within a large catchment. This explained the heterogeneous effects of catchments' characteristics, variation in local climate condition and dominant hydrological regimes in the Arctic environment. This study also found that the Climate Forecast System Reanalysis (CFSR) data had great capacity to drive the SWAT for hydrological simulations in the Norwegian Arctic catchments. Thus, the reanalysis products, like the CFSR, could be an alternative weather input to run the hydrological model in case of the existing monitoring networks being scattered. By altering model structures (e.g., number and size of sub-catchments, land use compositions and catchment characteristics, through the catchment delineation process), model parameters (through the calibration process), and quality of weather input (e.g., spatial resolution) for the SWAT, this would somewhat affect the results of hydrological simulations (e.g., annual mean values and spatial variation of snowmelt runoff, water balance components and streamflow (including peak flow)).

Under climate conditions in the near future period (2041-2070), the key projections for the Norwegian Arctic would be: (1) flood magnitudes would increase in the snowmelt-dominated catchments and decrease in the rainfall-dominated catchments, while the catchment with a mixed rainfall/snowmelt regime would experience both increase and decrease (only small flood) patterns; (2) extreme flood events would occur more frequently in the northern and southern catchments, while such behaviours would be the opposite in the inland catchments (with dominant snowmelt) in the centre of the Norwegian Arctic; (3) the changes in future extreme flood events would be more complicated in the rainfall-dominated catchment and near the coast due to high variation of future rainfall in this area; (4) small flood events would experience the opposite behaviours compared to the extreme floods. Finally, in the climate-hydrology modelling chain for flood projections, uncertainties from the ensemble climate models' simulations were found to be larger than those from the hydrological SWAT model. In addition, levels of uncertainties were varied greatly regarding catchments' scales and the dominant flood regimes.

Keyword: climate change, Norwegian Arctic catchments, global and regional climate models, hydrological SWAT model, reanalysis weather data, future floods, reliability and uncertainty.

Acknowledgments

This PhD thesis is an ending of my four-year journey (2018-2022) for doing a PhD research at Department of Technology and Safety (ITS), Faculty of Science and Technology, UiT The Arctic University of Norway. Doing a PhD is really an important milestone in my career as well as a great and unforgettable experience in my life. To be able to reach the final step of this challenged journey, I would like to express my sincere and deep gratitude to many people who helped and supported me.

First of all, I would like to give a special gratefulness to my main supervisor, Professor Jinmei Lu, who offered me a great chance to conduct a PhD research at ITS, UiT and provided me valuable advices, experiences and recommendations during my PhD period. I gained lots of great experiences in writing scientific papers, skills for teaching/supervising, and many other things from Jinmei. Besides, I would like to thank to my co-supervisor, Dr. Limei Nie, Director at Centre for Sustainable Development and Innovation of Water Technology-CSDI, Oslo, Norway, for all of her kindness, great helps and supports, especially her experiences in doing research, writing scientific papers, and many others.

Next, I would thank to all Team members in VanProd and Min-North projects which I had chances to involve during my PhD period. I gained great experience to work and go fieldtrip inside and outside Norway with those Teams. Especially, I had great time with the Team of VanProd project such as Dr. Tiina Leiviskä, project manager, at University of Oulu, Finland, Professor Mark Dopson at Linnæus University, Sweden, Dr. Ingar Walder at Kjeoy Research & Education Center, Norway, and PhD fellows, i.e., Ruichi Zhang and Rodrigo Embile. Being a member of this Team, I gained myself valuable knowledge and skills for international team work, public presentation, field works under cold climate conditions as well as doing experiments in the lab.

Moreover, my big thanks are also given to Associate Professor Bjørn-Morten Batalden (Head of Department, ITS), Gunn-Helene Turi (Head of Administration, ITS), Associate Professor Yngve Birkelund (former Head of Department, ITS) who supported and offered good conditions for me to conduct my PhD research. Also, I would like to thank to my colleagues at ITS for there sharing with me many interesting and funny things during tea/coffee breaks, trips or social gathering together during my PhD period. Especially, many thanks are given to Ronald Jann Hardersen and Svein Storbakk (University Lecturer) who were in the same office with me at the beginning of my work at ITS. Ronald and Svein shared with me lots of interesting knowledge about culture and society of Norway as well as many other things.

Thanks to all Vietnamese colleagues/friends at UiT and in Tromsø for their sharing and organizing indoor/outdoor activities during my time in Tromsø.

Especially, this PhD is a big gift that I would like to present to my parents who gave me a chance to appear in this earth and have supported me unconditionally. This present is also for all my siblings, and all my lovely nieces, nephews who are always proud of me and encourage me in every step of my life. They are always excited to well come me back home or pick up me at the airport. My family is a great spiritual support and motivation for me to complete my PhD. Many thanks are also for all my relatives and friends who are around me, and play an important part of my life.

Tromsø, Norway

May, 2022

Minh Tuan Bui

Table of Contents

1	Introduction	1
1.1	Background of the study	1
1.1.1	Climate change in the Arctic	1
1.1.2	Climate change impacts on Arctic's hydrological processes and the associated extreme events	1
1.1.3	The need for a modelling tool	4
1.2	Statement of the problems	4
1.2.1	Challenges for hydrological modelling in the Arctic environment	5
1.2.2	Uncertainties in the climate-hydrology modelling chain	5
1.3	Motivation	6
1.4	Research questions	6
1.5	Objectives of the study	7
1.6	Scope of the study.....	7
1.7	Thesis roadmap.....	8
2	Literature review on hydrological modelling	9
2.1	Deterministic models	10
2.1.1	Deterministic lumped model	10
2.1.2	Deterministic semi-distributed model	10
2.1.3	Deterministic distributed model	11
2.2	Stochastic models	11
2.3	Hydrological process description models.....	12
2.3.1	Empirical model (black-box model).....	12
2.3.2	Conceptual model (grey-box model).....	13
2.3.3	Physically based model (white-box model).....	14
3	Study areas, materials and methods	17
3.1	Study areas.....	17
3.1.1	Lakselva catchment	18
3.1.2	Strandvassbotn catchment	18
3.1.3	Marsvikelva catchment.....	18
3.1.4	Målselv catchment.....	19
3.1.5	Altavassdraget catchment.....	19
3.1.6	Halselva catchment.....	19

3.1.7	Karpelva catchment.....	19
3.1.8	Definition of study areas for each scientific paper.....	20
3.2	Data acquisition.....	22
3.2.1	Data acquisition – Paper I.....	22
3.2.2	Data acquisition – Papers II & III.....	22
3.2.3	Data acquisition – Paper IV.....	23
3.3	Methods.....	24
3.3.1	Comprehensive review.....	25
3.3.2	The selected model candidate SWAT.....	25
3.3.3	Modelling chain for climate change impact assessment.....	31
3.3.4	Evaluation of climate change impacts on future floods.....	33
4	Results.....	37
4.1	RQ1 – The current capacities and challenges for hydrological modelling in the Arctic environment.....	37
4.1.1	Models’ capacities.....	37
4.1.2	Models’ challenges.....	37
4.2	RQ2 – Suitable hydrological models and verification of their performance for hydrological simulation/projection in the Arctic catchments.....	38
4.2.1	Verification of the model candidate’s performances.....	39
4.2.2	Uncertainties of the modelling results.....	41
4.3	RQ3 – Potential for using reanalysis climate products to run the hydrological models in the data-sparse Arctic region.....	43
4.3.1	The simulated water balance components.....	43
4.3.2	The simulated streamflow.....	45
4.3.3	Uncertainties of the modelling results.....	47
4.4	RQ4 – The effect of hydrological models (e.g., structures and parameterizations) and quality of weather inputs (e.g., spatial resolution) on the simulation results.....	48
4.4.1	The changes in the simulation results of water balance components.....	49
4.4.2	The changes in the simulation results of snowmelt runoff volume.....	50
4.4.3	The changes in the simulation results of streamflow.....	51
4.5	RQ5 – The impacts of climate change on future flood.....	53
4.5.1	Projected changes in future climate.....	53
4.5.2	Projected changes in flood magnitudes.....	55
4.5.3	Projected changes in likelihood exceedance.....	56
4.5.4	Uncertainties analysis in the projection of future floods.....	58

5	Discussion	61
5.1	Connection between the papers	61
5.2	Strengths of the work.....	61
5.3	Limitations of the work	61
6	Concluding remarks.....	63
6.1	Conclusion	63
6.2	Research contributions	66
6.3	Suggestions for future works.....	66
	References.....	67
	Appended Papers	75
	Paper I.....	77
	Paper II	105
	Paper III.....	141
	Paper IV	175

List of Tables

Table 1 - Summary of research questions and objectives.	7
Table 2 - General characteristics of the studied Norwegian Arctic catchments.....	21
Table 3 - Summary of the selected model types used in the review in Paper I.	22
Table 4 - Data collection for the SWAT models applied in Papers II & III.....	23
Table 5 - Data collection for the SWAT models applied in Paper IV.....	23
Table 6 - Summary of GIS-coupled SWAT interfaces.	28
Table 7 - Thresholds of R^2 , NSE and RSR for evaluation of hydrological model's performance (daily simulation).....	29
Table 8 - Thresholds of R^2 , NSE and RSR for evaluation of hydrological model's performance (monthly simulation).....	30
Table 9 - Summary of all formulas used for flood frequency analysis.	35
Table 10 - Capacities of each modelling tool to simulate the important processes in permafrost environments (results from Paper I).....	37
Table 11 - Recommended model candidates for use in the Arctic region (results from Paper I).....	38
Table 12 - Performances of the SWAT for hydrological simulation in the small-scale Norwegian Arctic catchments (results from Paper IV).....	39
Table 13 - Performances of the SWAT for hydrological simulation in the large-scale, snowmelt-dominated Norwegian Arctic catchment Målselv (results from Papers II to IV).....	40
Table 14 - Transferability of the calibrated model parameters (validation for the period of 2008-2012) in the Norwegian Arctic catchments (results from Paper IV).	41
Table 15 - Uncertainties analysis of SWAT modelling in the large-scale, snowmelt-dominated Norwegian Arctic catchment Målselv (results from Papers II to IV).....	41
Table 16 - Uncertainties analysis of SWAT modelling in the small-scale Norwegian Arctic catchments (results from Paper IV).....	42
Table 17 - Comparison of the simulated water balance components.	43
Table 18 - Median changes in future magnitudes of small and extreme floods (results from Paper IV).	56
Table 19 - Quantification of uncertainties from the hydrological SWAT model (results from Paper IV).	58

List of Figures

Figure 1 - The impacts and responses of permafrost thaw on water fluxes and distribution (Walvoord & Kurylyk 2016; Bui et al. 2020).....	3
Figure 2 - Thesis roadmap.....	8
Figure 3 - Classification of hydrological models (Chow et al. 1988; Dwarakish & Ganasri 2015; Gupta et al. 2015).....	9
Figure 4 - Classification of deterministic models and use of them to predict discharge (Q) and soil moisture (θ): (a)-(c) lumped model; (d)-(f) semi-distributed model; (g)-(i) fully-distributed model (Koch 2016).....	10
Figure 5 - Example of soil moisture content (z) simulated by stochastic hydrological model: (a) deterministic model outputs (\hat{z}); (b) probability distribution of the modelling errors (e); (c) probability distribution of modelling outputs and the best estimation (\hat{z}) (Bierkens & Geer 2012).....	11
Figure 6 - Application of empirical curve number method to estimate runoff from rainfall (Sitterson et al. 2017).....	13
Figure 7 - Application of machine learning technique for runoff modelling (Mohammadi 2021).	13
Figure 8 - Conceptual structure of the HBV model (Killingtveit & Sælthun 1995; Bruland & Killingtveit 2002).....	14
Figure 9 - Overview of the hydrological processes described in the SWAT model (Neitsch et al. 2011; Zhang et al. 2016).....	15
Figure 10 - Map of Arctic region (top right, source: https://www.nasa.gov/topics/earth/features/earth20130610.html) and the studied Norwegian Arctic catchments.	17
Figure 11 - Number of recent publications related to hydrological models and cryo-hydrogeological models, found via https://www.scopus.com/ , supporting the review in Paper I.	22
Figure 12 - Spatial resolution of weather inputs (CFSR and RCMs) and hydro-gauging stations in seven Norwegian Arctic catchments.	23
Figure 13 - Summary of all the main methods applied in four scientific papers to solve the five research questions (RQ) of the thesis.	24
Figure 14 - Description of hydrological simulation in two different phases of the SWAT model (source: http://www.brc.tamus.edu/swat/).	26
Figure 15 - The algorithm for HRU definition in the SWAT (Her et al. 2015).	27
Figure 16 - The SUFI-2 algorithm in SWAT_CUP (Abbaspour 2015).	30
Figure 17 - Modelling chain for flood projections under global CC in the Norwegian Arctic catchments.	33
Figure 18 - Deviation between rainfall sources from CFSR and ground-based data for running hydrological model in the Norwegian Arctic catchment Målselv (results from Paper II).	44
Figure 19 - Monthly streamflow simulation with CFSR data after calibration (1998-2007): (a) at Lundberg; (b) at Lille Rostavatn; (c) at Høgskarhus; (d) at Skogly; and (e) at Målselvfossen hydro-gauging station of Målselv catchment (results from Paper II).	45
Figure 20 - Long-term average monthly streamflow (in m^3/s) during 1998-2007, generated from observed data and simulation with ground-based weather data and CFSR weather data (results from Paper II).....	46
Figure 21 - Uncertainty analysis for monthly streamflow simulation: (a) p-factors for calibration period; (b) r-factors for calibration period; (c) p-factors for validation period; and (d) r-factors for validation period (results from Paper II).	47

Figure 22 - The changes in number of sub-basins and integrated weather grids by changes in TDA schemes (results from Paper III).	48
Figure 23 - The changes in annual mean values of some water balance components in Målselv catchment by changes in TDA schemes (results from Paper III).	49
Figure 24 - The changes in spatial variation of annual mean values of some water balance components across the Målselv catchment by changes in TDA schemes: precipitation-PRECIP (a-d); actual evapotranspiration-ET (e-h); surface runoff-SURQ (i-l); and water yield-WYLD (m-p) (results from Paper III).	50
Figure 25 - The changes in spatial variation of simulated annual mean snowmelt runoff volume (1998-2007) across the Målselv catchment by changes in TDA schemes (results from Paper III).	51
Figure 26 - The changes in monthly mean streamflow (1998-2007) at five hydro-gauging stations within the Målselv catchment by changes in TDA schemes (results from Paper III).	52
Figure 27 - The changes in stream order levels and spatial variation of annual mean streamflow (1998-2007) in the Målselv catchment by changes in TDA schemes. Q1-Q5 denote streamflows in stream order levels from 1 to 5, respectively (results from Paper III).....	52
Figure 28 - Deviations in the near future (2041-2070) of annual precipitation-pcp (in %) and annual average air temperature-tmp (in °C) from the reference period (1976-2005), projected from five ensemble GCM_RCMs (results from Paper IV).	54
Figure 29 - The average (avg) changes in nine flood quantiles from the historical (1976-2005) to the future (2041-2070) in six Norwegian Arctic catchments under high scenario (RCP8.5) of CC (results from Paper IV). Q_U95PPU, Q_M95PPU, and Q_L95PPU denote the upper limited (at 97.5%), median and lower limited (at 2.5%) curves of the estimated discharges.	55
Figure 30 - Projected changes in likelihood exceedance of small and extreme floods, averaged from five ensemble GCM_RCMs inputs.....	57
Figure 31 - Uncertainties in the estimation of the probable peak discharges in the reference period (1971-2005) and the future period (2041-2070), in the small-scale Norwegian Arctic catchments (results from Paper IV).	59
Figure 32 - Uncertainties in the estimation of the probable peak discharges in the reference period (1971-2005) and the future period (2041-2070), in the large-scale Norwegian Arctic catchment Målselv (results from Paper IV).	60

Abbreviations

1D	: One-dimensional
3D	: Three-dimensional
95PPU	: 95 Percent Prediction Uncertainty
AEP	: Annual Exceedance Probability
ALT	: Active Layer Thickness
AMSL	: Above Mean Sea Level
ANFIS	: Adaptive Neuro-Fuzzy Inference System
ANN	: Artificial Neural Network
AOGCMs	: Atmosphere–Ocean General Circulation Models
ATS	: Arctic Terrestrial Simulator
avg	: Average
CC	: Climate Change
CDF	Cumulative Distribution Function
CDFt	: Cumulative Distribution Function Transformation
CFSR	: Climate Forecast System Reanalysis
CRHM	: Cold Regions Hydrological Model
CryoGrid 3	: A Type of One-Dimensional Land Surface Model in Permafrost-Affected Regions
DEM	: Digital Elevation Model
DMHS	: Deterministic Modelling Hydrological System
ECOMAG	: Ecological Model for Applied Geophysics
EMICs	: Earth System Models of Intermediate Complexity
ESMs	: Earth System Models
ET	: Evapotranspiration
EURO-CORDEX	: Coordinated Downscaling Experiment for Europe
EV1	: Generalized Extreme Value Type I
GA	: Genetic Algorithm
GCM	: Global Climate Model
GEOtop	: A Distributed Hydrological Model with Coupled Water and Energy Balance
GEV	: Generalized Extreme Value
GHG	Greenhouse Gas
GIS	: Geographic Information System
GW_Q	: Ground Water Flow
HBV	: Hydrologiska Byråns Vattenbalansavdelning
HRUs	: Hydrologic Response Units
L95PPU	: Lower Limited of the 95PPU Band
LAT_Q	: Lateral Flow
LH	: Latin Hypercube
M95PPU	: Median Value of the 95PPU Band
MOM	: The Method of Moments, Using for Estimating the Parameters of the Statistical Distribution Model in Flood Frequency Analysis
NNS	Nearest Neighbour Search
NSE	: Nash-Sutcliffe Coefficient of Efficiency
NVE	: The Norwegian Water Resources and Energy Directorate
PERC	: Percolation
PET	: Potential Evapotranspiration
PFLOTRAN-ICE	: Ice Variant of the Existing Massively Parallel Subsurface Flow and Reactive Transport Model
QGIS	: Quantum GIS

RCM	:	Regional Climate Model
RCP	:	Representative Concentration Pathway
RQ	:	Research Question
RSR	:	Root Mean Square Error, Divided by the Standard Deviation
SUFI-2	:	Sequential Uncertainty Fitting Version 2
SUR_Q	:	Surface Runoff
SUTRA-ICE	:	Ice Variant of the Existing Saturated/Unsaturated Transport Model
SVM	:	Support Vector Machine
SWAT	:	Soil and Water Assessment Tool
SWAT_CUP	:	SWAT Calibration Uncertainties Program
TDA	:	Threshold Drainage Area
Topoflow	:	A Type of Spatially Distributed and Process-Based Hydrological Model
U95PPU	:	Upper Limited of the 95PPU Band
USDA	:	United States Department of Agriculture
WaSiM	:	Water Balance Simulation Model
WYLD	:	Water Yield

List of Appended Papers

Paper I

Bui, Minh Tuan; Lu, Jinmei; Nie, Linmei. A review of hydrological models applied in the permafrost-dominated Arctic region. *Geosciences* 2020; Volume 10:401 (10). ISSN 2076-3263.s 1 - 26.s doi: <https://doi.org/10.3390/geosciences10100401>.

The paper was published in the Special Issue, “Hydrological Systems and Models Applied in Permafrost”.

Paper II

Bui, Minh Tuan; Lu, Jinmei; Nie, Linmei. Evaluation of the Climate Forecast System Reanalysis data for hydrological model in the Arctic watershed Målselv. *Journal of Water and Climate Change* 2021. ISSN 2040-2244.s doi: <https://doi.org/10.2166/wcc.2021.346>.

The paper was published in the Special Issue, “Assessment and Adaptation to Climate Change Impacts in Cold Regions”.

Paper III

Bui, Minh Tuan; Lu, Jinmei; Nie, Linmei. Quantify the effects of watershed subdivision scale and spatial density of weather inputs on hydrological simulations in a Norwegian Arctic watershed. *Journal of Water and Climate Change* 2021. ISSN 2040-2244.s doi: <https://doi.org/10.2166/wcc.2021.173>.

The paper was published in the Special Issue “Assessment and Adaptation to Climate Change Impacts in Cold Regions”.

Paper IV

Bui, Minh Tuan; Lu, Jinmei; Nie, Linmei. Projections of future floods in Norwegian Arctic catchments under climate change context (manuscript).

Co-authorship

For **Paper I**, I initiated the idea, planned the scope, collected information and data, structured and produced a draft manuscript and performed revisions. Jinmei Lu supervised the progress, supported ideas and conducted the review and editing. Linmei Nie contributed to the reformulation of the paper structure, HBV hydrological model, language revision and co-supervision of the review and revision processes.

For **Papers II, III and IV**, I gathered all input data, set up the SWAT model, conducted hydrological simulation, calibration, validation, sensitivity and uncertainties analysis. I also collected and processed climate change data from global and regional climate models, established climate change scenarios, performed projections of future daily streamflow under climate change impacts, analysed changes in future flood magnitudes and flood frequencies, visualized and interpreted all the results. Moreover, I wrote draft manuscripts and performed editing. Jinmei Lu supervised the progress and conducted reviews and editing. Linmei Nie co-supervised the processes and conducted reviews and editing.

List of publications/reports not included in the thesis

1. **Bui, Minh Tuan**; Lu, Jinmei; Nie, Linmei. Application of QSWAT model to simulate streamflow variation in Målselv river basin, North of Norway (extended abstract). In Abstract proceedings of 6th IAHR Europe Congress (virtual), 15-18.02.2021, ISBN 978-83-66847-01-9, doi: 10.24425/136660, pp. 393-394. https://iahr2020.pl/wp-content/uploads/2021/03/IAHR_2020_book_of_abstracts_final.pdf.
2. **Bui, Minh Tuan**; Lu, Jinmei; Nie, Linmei. Rainfall-runoff simulation by QSWAT model in Målselv river basin, North of Norway (extended abstract). In Abstract proceedings of 6th IAHR Europe Congress (virtual), 15-18.02.2021, ISBN 978-83-66847-01-9, doi: 10.24425/136660, pp.395-396. https://iahr2020.pl/wp-content/uploads/2021/03/IAHR_2020_book_of_abstracts_final.pdf.
3. Lu, J.; **Bui, M.T.**; Leiviskä, T.; Walder, I.; Dopson, M. Feasibility study of vanadium extraction and recovery from solid and liquid waste streams in the Nordic region. In Abstracts and Proceedings of the Geological Society of Norway. The 34th Nordic Geological Winter Meeting, January 8th-10th 2020, Oslo, Norway, ISBN: 978-82-8347-043-7, pp.129. https://www.geologi.no/images/NGWM20/Abstractvolume_NGWM20.pdf.
4. **Bui, Minh Tuan**; Lu, Jinmei; Nie, Linmei. Evaluating the effects of watershed subdivision on hydrological simulation by SWAT model in an Arctic watershed. IOP Conference Series: Earth and Environmental Science (EES) 2020; Volume 581. ISSN 1755-1307.s 1 - 9.s doi: <http://dx.doi.org/10.1088/1755-1315/581/1/012026>.
5. **Bui, Minh Tuan**; Lu, Jinmei; Nie, Linmei. Sensitivity analysis of the SWAT model to spatial distribution of precipitation in streamflow simulation in an Arctic watershed. IOP Conference Series: Earth and Environmental Science (EES) 2020; Volume 581. ISSN 1755-1307.s 1 - 9.s doi: <http://dx.doi.org/10.1088/1755-1315/581/1/012025>.
6. **Bui, Minh Tuan**; Lu, Jinmei. D8 flow model for pollutants dispersion: A case study at Bogdalen watershed between the Raudfjell and Kvitfjell wind farm, North of Norway. IOP Conference Series: Earth and Environmental Science (EES) 2019; Volume 344 (1). ISSN 1755-1307.s 1 - 9.s doi: <http://dx.doi.org/10.1088/1755-1315/344/1/012036>.
7. Lu, Jinmei; **Bui, Minh Tuan**; Yuan, Fuqing. Evaluation of the water quality at Bogdalen watershed near Kvitfjell and Raudfjell wind farm area. IOP Conference Series: Earth and Environmental Science (EES) 2019; Volume 344 (1). ISSN 1755-1307.s 1 - 7.s doi: <http://dx.doi.org/10.1088/1755-1315/344/1/012022>.
8. **Bui, Minh Tuan**; Kuzovle, Vyacheslav Viktorovich; Zhenikov, Yuri, N.; Füreder, Leopold; Seidel, Jochen; Schletterer, Martin. Water temperatures in the headwaters of the Volga River: Trend analyses, possible future changes, and implications for a pan - European perspective. Rivers Research and Applications: an international journal devoted to river research and management 2018; Volume 34 (6). ISSN 1535-1459.s 495 - 505.s doi: <https://doi.org/10.1002/rra.3275>.

Technical reports

1. **Bui, Minh Tuan**; Lu, Jinmei; Walder, Ingar; Embile, Rodrigo; Dopson, Mark; Zhang, Ruichi; Leiviskä, Tiina. Characteristics of the targeted vanadium resources and liquid waste streams in the Nordic region. VanProd project - Innovation for Enhanced Production of Vanadium from Waste Streams in the Nordic Region, 2020.
2. Lu, Jinmei; **Bui, Minh Tuan**; Yuan, Fuqing. Environmental risk from the deposition of waste in the Nordic region. VanProd project - Innovation for Enhanced Production of Vanadium from Waste Streams in the Nordic Region, 2020.
3. Alakangas, Lena; Salifu, Musah; Rasmussen, Thorkild Maack; Heino, Neea; Hyvönen, Eija; Karlsson, Teemu; Panttila, Hannu; Pietilä, Raija; Tornivaara, Anna; Turunen, Kaisa; Lu, Jinmei; Fu, Shuai; **Bui, Minh Tuan**; Heiderscheidt, Elisangela; Postila, Heini; Leiviskä, Tiina; Ronkanen, Anna-kaisa; Kujala, Katharina; Khan, Uzair; Gogoi, Harshita. Min-North: Development, Evaluation and Optimization of Measures to Reduce the Environmental Impact of Mining Activities in Northern Regions. Luleå University of Technology, 2019.

1 Introduction

1.1 Background of the study

1.1.1 Climate change in the Arctic

Climate change (CC) is more intensified in the Arctic region than in the rest of the world (AMAP 2011, 2017). The annual average temperature has increased at twice the rate of that in the rest of the world since 1980 (AMAP 2011). During the last five decades (1971-2017), the annual mean air temperature in the Arctic increased around 2.7 °C (AMAP 2017). The climate models predicted that the greatest warming will happen in the northern region with high latitudes, especially in wintertime (Dankers 2008). Coinciding with the changes in air temperature, the annual precipitation for the pan-Arctic, in the recent period, has exceeded approx. 5% of the average of the 1950s (AMAP 2011). Many climate models have projected that precipitation will increase across the Arctic over the 21st century, for all emission scenarios. By the end of the 21st century, annual precipitation is projected to have risen by 5-40% (low emission scenario) or by 5-70% (high emission scenario).

1.1.2 Climate change impacts on Arctic's hydrological processes and the associated extreme events

The Arctic environment is dominated by cryospheric features, i.e., snow cover, seasonally frozen soils and permafrost, which are highly sensitive to the changes in air temperature and precipitation (Dankers 2008). The joint changes in air temperature and precipitation are expected to significantly affect the water cycle, as well as hydrological processes, in the Arctic, through changes in snow cover and permafrost. Thus, the integrated changes in snow cover extent and the dynamics of frozen soils, as well as permafrost thaw due to global warming, are expected to alter the hydrological processes in the Arctic.

1.1.2.1 Climate change impacts on Arctic snow cover

Snow is an important and dominant feature of Arctic terrestrial landscapes and present for 8-10 months of the year (Box *et al.* 2019). Snow cover in the Arctic has changed significantly by seasons and regions because of warming and the increase in precipitation (AMAP 2011). Different regional snow cover responses to the extensive warming and increasing winter precipitation have characterized the Arctic climate for the past 40-50 years (Callaghan *et al.* 2011). Projected increases in temperature will decrease the length of time available for the accumulation of a winter snowpack. It is projected that the duration of snow cover will decrease by approx. 10-20% across most of the Arctic area (AMAP 2017). As a result, the magnitude of spring snowmelt, the major hydrological event of the year in most northern systems, will be influenced.

1.1.2.2 Climate change impacts on Arctic permafrost

Permafrost (perennially frozen) is the layer beneath the active layer (seasonally frozen and thawed) and accounts for approx. 24% of the exposed land area in the Northern Hemisphere (Romanovsky *et al.* 2002). Permafrost is highly sensitive to the warming climate (Kong & Wang 2017). Global warming has been observed to cause the degradation of permafrost in many regions across the Arctic (Åkerman & Johansson 2008; Johansson *et al.* 2011; Callaghan *et al.* 2013). The degradation is mainly represented through three variables, i.e., the increase in permafrost temperature, the decrease in the extent of

permafrost and the deepening of the active layer's thickness (Kong & Wang 2017). It is projected that the area of the near-surface permafrost will decrease by approx. 35% under high CC emission by the middle of 21st century (AMAP 2017).

1.1.2.3 The effects of snow cover and soil behaviour on water transfer in the Arctic

Water transfer in the permafrost-dominated Arctic region is controlled by snow cover and soil behaviour through four different stages (seasons) of a year (Fabre *et al.* 2017):

In the first stage of the hydrological process, during the wintertime, the flow is low, and soil is frozen. Snow accumulation in this stage is considered a ground insulation, since snow is a poor heat conductor (Woo 2012b). Snow cover is a source for the recharging of soil moisture, groundwater and the generation of surface runoff at a later stage (Woo 2012b). In addition, because of the uneven distribution of the snow, the ground heat is insulated to different degrees (Woo 2012b), with the ground temperature beneath the thick snow layer being milder and less fluctuant, compared to the ground temperature where the snow layer is thinner (Woo 2012a). Moreover, a deep layer of snow cover can thicken the active layer (Woo 2012a).

The second stage comes in spring. In this stage, snowmelt dominates the hydrological process. This period is considered a transition from the wintertime, with frigid, snow and ice covering, to the summertime of the thawed regime (Woo 2012a). In particular, this stage highlights the transitions: (1) from an enlargement to a reduction of the snow cover; (2) from freezing to thawing of the ground; (3) from an upward trend of soil moisture flux to a downward movement of meltwater in frozen soils; (4) from inactivity to a rise in lateral flows; and (5) from dormancy to germination and bud-burst of vegetation and the increase of evaporation.

The third stage, in summer, witnesses the thawing period of the active layer. Because of the appearance of snow-free areas after the melting period, the active layer starts to thaw when soil heat flux is positive (Woo 2012a). Herein, the thawing rate depends on several factors: (1) the energy balance on the ground surface that strongly impacts the availability of the amount of heat to the ground; (2) the transmission process of heat into the ground; and (3) heat consumption by ground ice melting (Woo 2012a). Noticeably, in summertime, permafrost basins experience greater heat flux into the soil than non-permafrost areas (Woo 2012a). The active layer reaches its maximum depth at this stage (Fabre *et al.* 2017). Moreover, it is stated that the magnitude of surface and subsurface flows is in the same ratio (Fabre *et al.* 2017).

Finally, the last stage is called the freeze-back period. The active layer starts to freeze at the bottom and on the top. However, in cold ground, the freezing only starts when the temperature reaches the freezing point depression or sub-zero temperature. There are several factors influencing the rate of freezing: (1) variation of climate; (2) dissipation of latent heat when ground ice is formed; (3) soil moisture content at the onset of winter; (4) variation of soil types along the vertical profile, including soil material and soil moisture content that contribute to the disruption of the frost rate; (5) the presence of a so-called porous organic surface layer that acts as an insulation layer to delay the penetration of frost; (6) depth of snow cover; and (7) the presence of lateral flow, which limits the freezing of the ground, since heat loss in the vertical direction is compensated for by heat source in the horizontal direction (Woo 2012a). In this stage, snow starts to accumulate and redistribute again, as the primary winter activities, above the ground surface (Woo 2012a). Therefore, only subsurface lateral flow is possible inside the active layer, with a piston effect, leading to the generation of a force or pressure, either upward (tension) or

downward (compression) to the two-sided freezing layers, in this period. However, in this stage, the subsurface lateral flow gradually goes when the two-sided freezing layers meet to totally freeze the active layer. The process ends with the return of permafrost, and the wintertime repeats as in the first stage. Winter is considered the longest season of the year in the permafrost region (Woo 2012a). The time between the freeze-back period and the ground-thawing period varies from 6 months to 9-10 months in the sub-Arctic regions and the Arctic Islands, respectively.

In short, according to the above description, the role of snow cover is very important for the hydrological cycle in the Arctic. Under global warming, rising air temperature would lead to changes in snow cover extent. As a result, subsequent changes in hydrological processes could be projected.

1.1.2.4 The effects of permafrost thaw on the Arctic's hydrological processes

The thawing of perennially frozen permafrost due to warming climate will potentially impact the surface and subsurface hydrology in the Arctic. Figure 1 provides an overview of the impacts of permafrost thaw on hydrological processes under global warming and anthropogenic stressors.

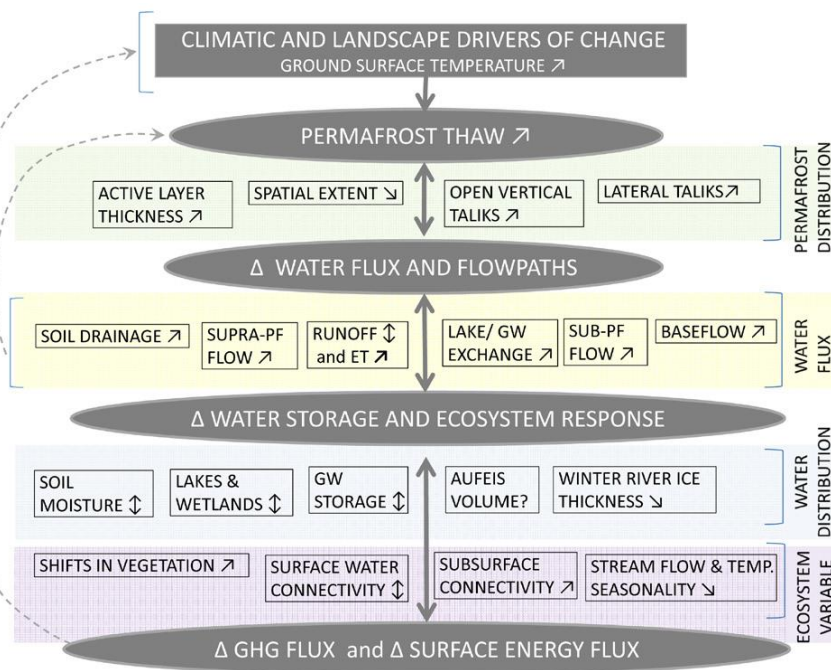


Figure 1 - The impacts and responses of permafrost thaw on water fluxes and distribution (Walvoord & Kurylyk 2016; Bui et al. 2020).

The symbols Δ , \nearrow , \searrow , \updownarrow , and $?$ denote the change, the increase, the decrease, the variation, and the unknown changes of the associated objects, respectively.

1.1.2.5 The effects of climate change on hydrological extreme events in the Arctic

Changes in the hydrological cycle due to CC normally result in changes in extreme events such as floods. Flooding is one of the most destructive natural hazards (Xu et al. 2019b; Engeland et al. 2020), which has a significant impact on human life, infrastructures, the environment, ecosystem, and the socio-economic development of the affected areas (McGrath et al. 2015; Vinet 2017; Quintero et al. 2018; Talbot et al. 2018). Changes in flooding behaviour have been observed/predicted for many Arctic regions. For example, the increase in winter flow or earlier spring floods across large regions of Eurasia have been witnessed (Tan et al. 2011). In contrast, in the northern region of western Siberia, global

warming has increased evaporation and deepened the active layer thickness, reducing the contribution of meltwater to the runoff, e.g., from 70-80% in the early 1990s to only 40-50% in the middle 2000s (Zakharova *et al.* 2011). In Norway, flood regimes are highly heterogeneous and regionally dependent. For example, the flood regimes in Norway are currently dominated by three different types: rainfall-dominated, snowmelt-dominated and mixed rainfall/snowmelt-dominated (Lawrence & Hisdal 2011). By the end of the 21st century, rainfall-dominated flooding is projected to increase its magnitude and frequency of occurrence, while snowmelt-dominated flooding will decrease and occur less often, compared to present climate conditions (Hanssen-Bauer *et al.* 2017). Because of the highly heterogeneous feature of flood regimes in Norway, the impact of CC on flood regimes in this region is expected to be highly complicated (Hanssen-Bauer *et al.* 2017).

1.1.3 The need for a modelling tool

As previously mentioned, CC is more intensified in the Arctic and has a great impact on the hydrological processes and subsequent hydrological extreme events. Thus, an assessment of the CC impacts in this specific region is indeed necessary. There are several ways to investigate the impacts of CC on hydrological processes. The popular method is based on the historical hydro-meteorological records. This is probably the simplest way to track the historical trends in hydrological and meteorological variables (Dye 2002; Huntington *et al.* 2004; Kunkel *et al.* 2016). Based on the relationship between climate factors and hydrological variables in the historical records, valuable visions of how the future hydrological system could response to CC can be provided. However, this approach has its drawbacks, since long-term and reliable records are limited for many reasons, for example, technical errors of the instruments for recording data or gaps in time series data. The Arctic is a sparse-data region, where monitoring networks are usually scattered, especially in the mountainous and remote areas. Therefore, the evaluation of CC impacts at the local level is not possible with the limited/missing records/monitoring networks. Moreover, the historical climate conditions used for the projection of future climate change may be different/change in future conditions. Therefore, applying a modelling tool, e.g., a hydrological model, has been preferred to assess the impacts of CC on hydrology. According to this technique, historical climate data are used as inputs to drive the hydrological model to generate time series data of the hydrological variables of interest, such as surface runoff, water yield, streamflow, etc. The developed hydrological model can be used later to assess the CC impacts at the catchments of interest. However, climate data inputs in the future are not available at present. Such data are normally achieved from the climate models. Thus, coupling the outputs of the climate models and hydrological model is a desirable approach to investigate the CC impacts at the catchment scale.

1.2 Statement of the problems

As discussed in the previous section, there is a demand for a hydrological model to quantify the CC impacts on hydrology, water resources, and the associated consequences. However, challenges exist regarding the applied models' capacities for accurate/reliable simulation of the hydrological processes in the Arctic environment, e.g., the presence of snow cover, seasonally frozen soils and permafrost, as well as the sparse-data feature. Also, uncertainties in the modelling results are usually found in the simulation/projection processes. Thus, this section aims to discuss the challenges of applying the modelling tools in the Arctic conditions.

1.2.1 Challenges for hydrological modelling in the Arctic environment

Hydrological models are state-of-the-art tools for studying the impacts of CC on hydrological processes. Recently, various surface and subsurface hydrological models have been developed and have demonstrated their capacity to simulate hydrology in a permafrost environment. For example, many surface hydrological models are able to simulate the seasonal freezing-thawing process by employing analytical solutions (e.g., using a simple heat transfer equation - Stefan's equation) and numerical solutions (e.g., finite difference, finite element and finite volume methods), while many subsurface hydrological models have the capacity to simulate the three phase changes (i.e., ice, liquid and gas) of water in near-surface soils. In addition, the subsurface hydrological models have coupled a three-dimensional (3D) equation for water flow (e.g., the 3D Richards equation) and a 3D equation for heat transfer. However, with the current structures of the developed modelling tools (both surface and subsurface hydrological models), accurate simulation of the hydrological processes in the permafrost environment remains limited. For example, using only a one-dimensional (1D) (i.e., in a vertical direction) equation for heat transfer, the surface hydrological models are unable to simulate the multidecadal and multidimensional changes associated with the freeze-thaw process of permafrost. In addition, some important processes in the permafrost environment, e.g., heat capacity, thermodynamic equilibrium and the three phase changes of water in near-surface soils, are currently missing in the structures of the surface hydrological models. Furthermore, the subsurface hydrological models do not integrate a land surface scheme in their structure. Such model types require very complex boundary conditions, and it is difficult for non-expert users to apply them. Finally, the Arctic is a data-sparse region and, thus, collecting enough input data to drive the hydrological models in this specific region is also a challenge for the modellers.

1.2.2 Uncertainties in the climate-hydrology modelling chain

As discussed above, coupling climate models and hydrological models is a great approach for investigating CC impacts at the catchment scale. However, the projected results of hydrological CC impacts usually contain uncertainties (Jones 2000; Heal & Kristrom 2002; Collins *et al.* 2006; Ghosh & Mujumdar 2007; Dunn *et al.* 2012; Jung *et al.* 2012), which are an ensemble of various sources, including: (1) assumed future greenhouse gas (GHG) emission scenario and natural variability of the climate system; (2) general climate models (GCM) (e.g., initial condition, boundary conditions, parameterization, process descriptions); (3) downscaling and bias-correction techniques (e.g., using statistical or dynamic methods through the use of regional climate models (RCM)); and (4) hydrological models (e.g., structure and parameterization). Currently, there is no scientific consensus on which uncertainty source is the most significant. For example, one earlier study stated that the major uncertainties could come from the selection of a future GHG emission scenario (Maurer 2007). This assumption was confirmed by the projection cases in Norway (Hanssen-Bauer *et al.* 2017). For example, according to the high emission scenario of the Representative Concentration Pathway (RCP), i.e., the RCP8.5, the median results of CC projection, at the end of the 21st century, indicated that the largest relative changes in rainfall would occur in winter and autumn, while the medium emission scenario RCP4.5 indicated that it would occur in spring and summer (Hanssen-Bauer *et al.* 2017). Other studies argued that the largest uncertainties' source should be from (a) structures of the driven GCMs (Kay *et al.* 2009; Chen *et al.* 2011; Woldemeskel *et al.* 2012), (b) downscaling techniques (Khan *et al.* 2006), or (c) hydrological models (Najafi *et al.* 2011). However, the uncertainties' sources could vary from catchment to catchment and be highly dependent on the catchment's characteristics and the dominant climate conditions (Chen *et al.* 2017; Chen *et al.* 2021).

1.3 Motivation

My background is in water resources engineering and management. Thus, my interest is focused on finding the optimal solutions or advanced technologies for sustainable water resources management, especially under the context of global CC. Previously, I have been involved in numerous research projects where mathematical modelling and GIS (Geographic Information System) technologies have been applied to solve issues associated with water resources and the environment. However, my study areas were mainly in tropical or temperate regions, while the Arctic is really a new area for me. Recently, the Arctic has received much attention from hydrologists and scientists from various disciplines, and I am no exception. Changes in the hydrological system through global warming in the Arctic affect not only the entire Arctic ecosystem but also the region, as well as the whole global climate. Thus, the global effect of Arctic CC is really of high concern. In addition, studying the impacts of CC on hydrology and water resources in the Arctic environment faces numerous challenges and uncertainties, as mentioned in previous sections. Such challenges deserve more studies/research by the scientific community. Thus, this motivated me to conduct research on CC impacts on hydrology and water resources in the Arctic environment. My expectation from this research is to find suitable hydrological models to produce highly reliable simulations of hydrological processes in the Arctic. Also, I would like to examine how hydrology and water resources in the Arctic could change under future climate conditions, by using the current hydrological modelling techniques.

1.4 Research questions

Based on the defined problems and purposes of this research, five research questions (**RQ**) have been proposed as follows:

1. **RQ1:** What are the current capacities and challenges of hydrological modelling in the Arctic environment?
2. **RQ2:** Which types of hydrological model(s) are suitable for the Arctic conditions, and how can their performance in the simulation of hydrological processes in the Arctic catchments be verified?
3. **RQ3:** Considering the sparse data in the Arctic region, can the high-resolution global reanalysis weather data become reliable alternative sources and replace the existing scattered monitoring data, to run a hydrological model in the Arctic catchments?
4. **RQ4:** To what extent do the hydrological models (e.g., structures and parameterizations) and the quality of weather inputs (e.g., spatial resolution) affect hydrological simulations in the Arctic catchments?
5. **RQ5:** How is the projection of CC impacts on hydrology and the associated extreme events (e.g., floods) in the Arctic catchments based on the current hydrological modelling tool? And how is the reliability/uncertainty of the projections quantified?

1.5 Objectives of the study

To fulfil the research questions stated above, the following objectives have been proposed and answered by four scientific papers in this study, as summarized in Table 1.

Table 1 - Summary of research questions and objectives.

Research questions	Objectives	Papers supported
RQ1	Conducting a comprehensive review to figure out suitable hydrological models for Arctic conditions, by taking into account the key factors: (a) the capacities of the models to describe the effects of permafrost on the hydrological processes; and (b) the capacities for wide application of the models with moderate inputs. These impact factors are weighted according to the current status and purposes of each study.	I
RQ2	Using the reviewed results of suitable hydrological models, selecting a model candidate, and running the model to verify its capacities for hydrological simulation/projection in Arctic conditions.	I,II,III,IV
RQ3	Selecting an Arctic catchment and running the hydrological model, using weather inputs from both the existing monitoring network (coarse spatial resolution) and the global reanalysis product (fine spatial resolution). After that, comparing model performances between two options of weather inputs. In the case of the high-resolution global reanalysis weather data being evaluated as having high performance and potentially able to replace the existing scattered monitoring data, conducting further applications of the reanalysis data, as well as investigating performance of the reanalysis data in different Arctic catchments with variations in geographical distributions, characteristics, scales, dominant hydrological regimes, and with different temporal resolutions (e.g., running with monthly and daily time steps).	II,III,IV
RQ4	Running the hydrological model with different options for setting up the model parameters, model structures (e.g., number and size of sub-basins (or sub-catchments), number of Hydrologic Response Units (HRUs)) and different options for weather input (e.g., spatial density), then comparing the simulation results among difference scenarios.	III
RQ5	Defining the future CC scenario and then coupling the climate model simulations with the hydrological model to project future changes in streamflow and, subsequently, floods in various catchments, taking into account the differences in catchments' characteristics, scales, geographical distributions and dominant flood regimes. Performing uncertainties analysis to detect which uncertainties' sources, e.g., from hydrological models or from climate models, are larger or smaller.	IV

1.6 Scope of the study

The scope of this research is hydrological models and their applications for hydrological CC impacts' assessment in the Arctic environment, with the research areas being limited to the Norwegian Arctic catchments. The contents of the research focus mainly on the comprehensive review and verification of suitable hydrological models for accurate/reliable simulation of the hydrological processes in the Arctic conditions. In particular, this study will consider the challenges for the hydrological models in dealing with the specific Arctic features, i.e., the presence of snow cover, seasonally frozen soil and permafrost.

In addition, the models' capability for wide application in the Arctic conditions (e.g., consideration of the sparse-data feature) will also be a criterion for selection of suitable models. Moreover, a suitable model candidate, among other potential models, will be selected and its performance verified to simulate and project the changes in hydrology and water resources and the associated hydrological extreme events (e.g., flooding) in the Arctic catchments under CC impacts. Although both surface and subsurface hydrology are studied in the review, this study is limited to assessing the changes in surface hydrology due to CC. However, the review of the hydrological models from this study aims to benefit a wider range of readers who would prefer either surface or subsurface hydrological models, depending on the purposes of each study. Moreover, uncertainties analysis of the simulation/projection results is another important part of this research. Regarding CC scenarios, this research will focus on the high emission scenario, i.e., the RCP8.5. In addition, considering the highly natural variability, as well as the high uncertainty of the assumed emission scenario in the far future period (e.g., at the end of the 21st century, as many have previously studied), the time frame for the assessment of CC impacts in this research is focused on the near future period, i.e., the 2050s (2041-2070).

1.7 Thesis roadmap

The thesis roadmap and overview are presented in Figure 2.

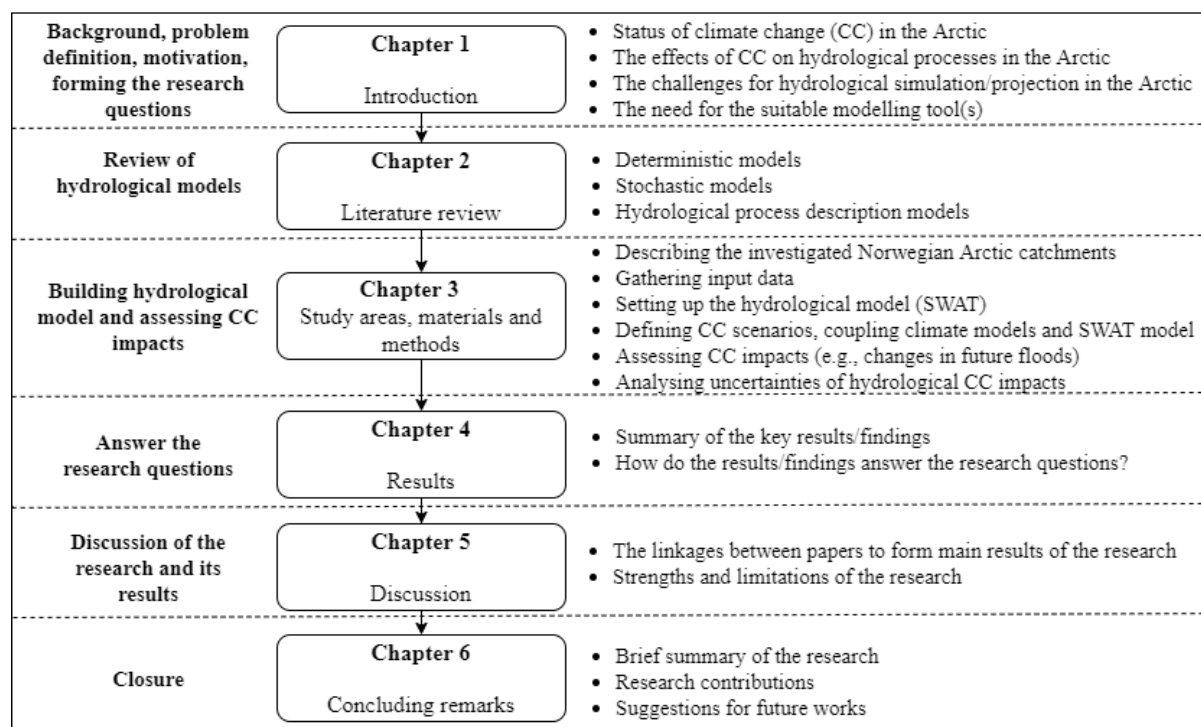


Figure 2 - Thesis roadmap.

2 Literature review on hydrological modelling

Hydrological models are state-of-the-art tools for CC impact assessment at the catchment scales. Recently, numerous models have been developed. Hydrological models are normally classified based on the criteria of interest (Gupta *et al.* 2015). Hydrological models are broadly classified into two main categories: the physical model and the mathematical model (Gupta *et al.* 2015; Jain & Singh 2019). The physical model represents a real system, including scaling and an analogue model. For example, models in the laboratory (Jain & Singh 2019), such as the hydraulic structures including reservoirs, dams or stream networks, are built to a proper scale (Rodda & John 2009) to examine the flow dynamics by such structures in the river system within a catchment. The mathematical model uses a set of mathematical formulas/equations to express the behaviour of a river basin. Generally, the models aim to simulate the interactions of inputs, e.g., climate data, with the system, e.g., a catchment, to generate outputs, e.g., a hydrograph of runoff or river flow. Mathematical models are further classified into three sub-types: theoretical, empirical and conceptual models. These three sub-types are further classified into linear, non-linear, steady, non-steady, lumped, distributed, deterministic and stochastic models. Dwarakish and Ganasri (2015) classified hydrological models based on two main hypotheses: (1) if it is based on the presence of random variables and the temporal-spatial variation of these random variables (Chow *et al.* 1988), it has a deterministic model and a stochastic model; and (2) if the description of hydrological processes is considered, it has a conceptual model, an empirical model and a fully physically based model (Figure 3).

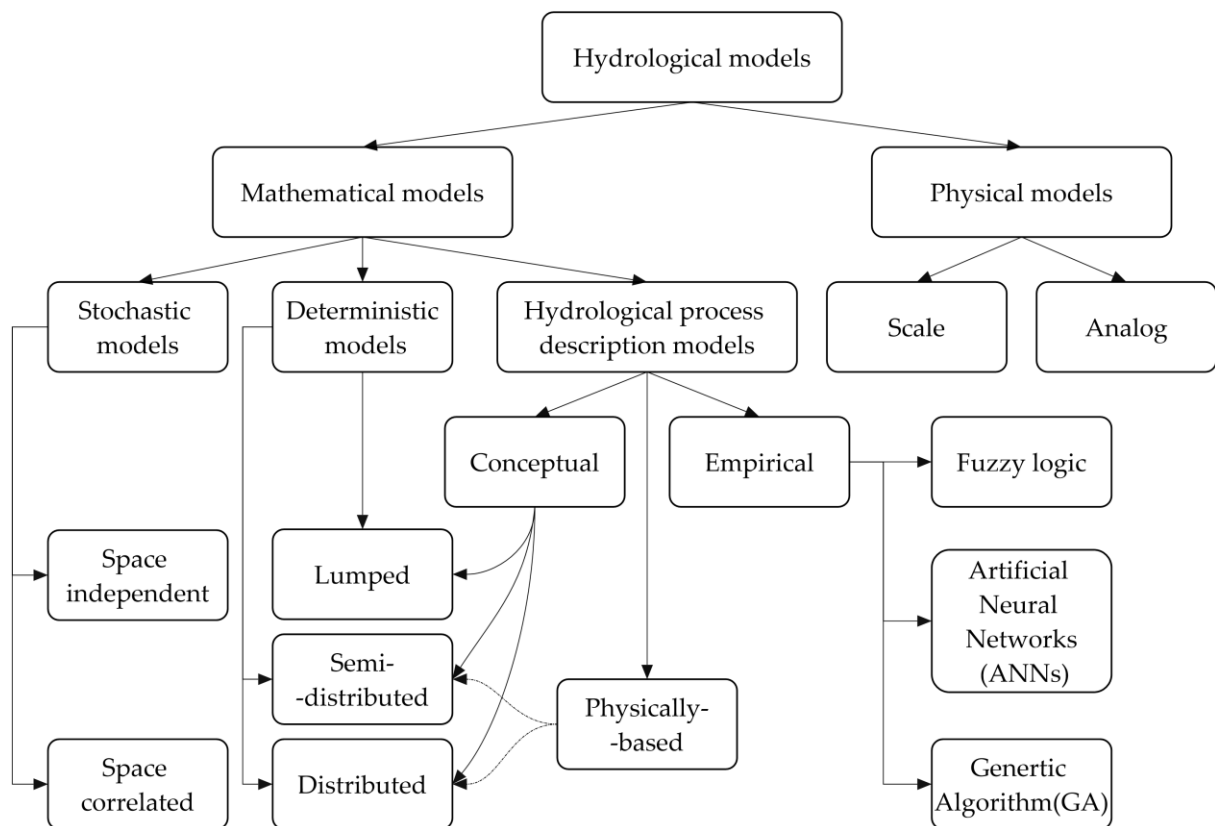


Figure 3 - Classification of hydrological models (Chow *et al.* 1988; Dwarakish & Ganasri 2015; Gupta *et al.* 2015).

2.1 Deterministic models

Deterministic models produce the same output for every run of the model from given input data (Thompson 1999; Dwarakish & Ganasri 2015; Gupta *et al.* 2015). For example, if we use the same input data to estimate evaporation from an open water surface by the Penman equation, we always receive the same output (Thompson 1999). Hence, randomness is not considered in this kind of model. Based on spatial discretization, deterministic models can be further classified into three sub-types, i.e., deterministic lumped model, deterministic semi-distributed model and deterministic distributed model (Dwarakish & Ganasri 2015).

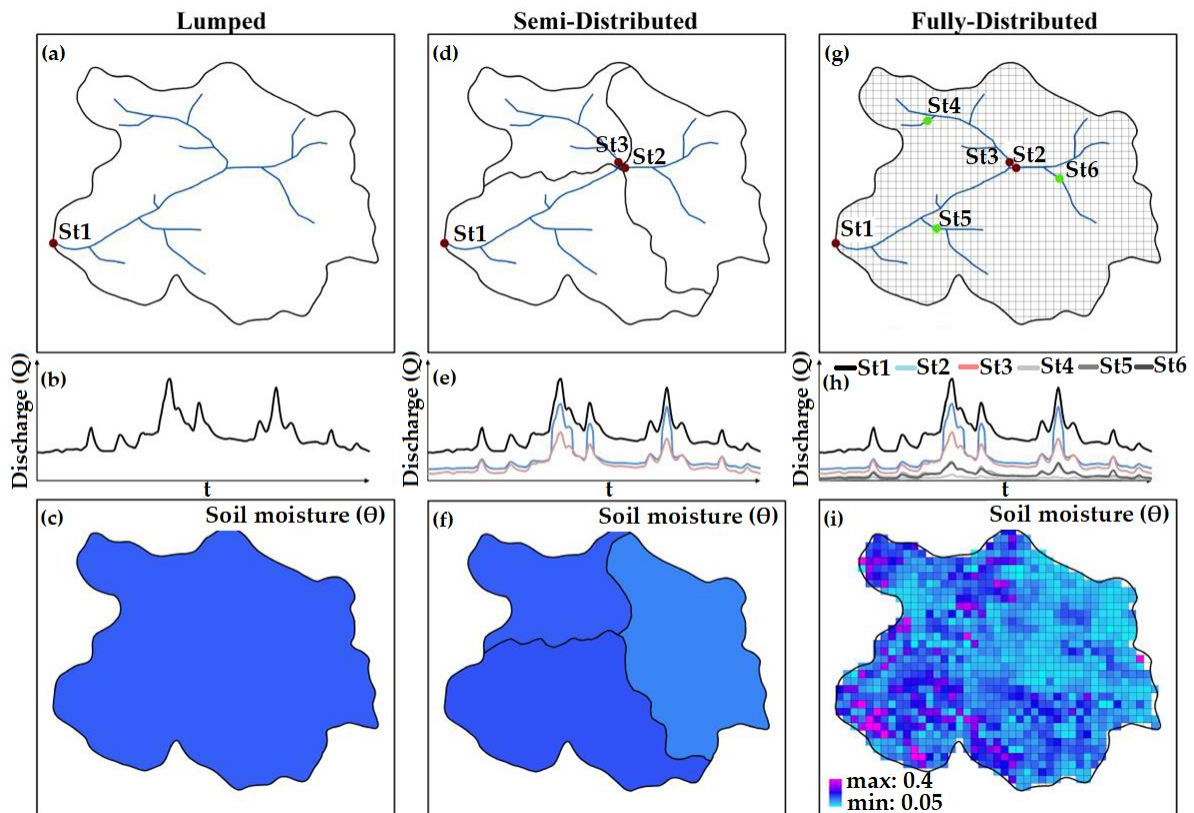


Figure 4 - Classification of deterministic models and use of them to predict discharge (Q) and soil moisture (θ): (a)-(c) lumped model; (d)-(f) semi-distributed model; (g)-(i) fully-distributed model (Koch 2016).

2.1.1 Deterministic lumped model

The hypothesis of a lumped model is that the whole river basin is considered a single system, where spatial variability is disregarded (Devi *et al.* 2015), especially when the river basin has a homogeneous set of parameters, including hydraulic conductivity of soil, roughness of land surface, etc. that govern the hydrological process within the river basin (COMET 2010b). These parameters and variables are averaged over the whole basin (Niel *et al.* 2003; Cheng 2011; Magar & Jothiprakash 2011; Dwarakish & Ganasri 2015). Figure 4a-c provides an example of a lumped model. Figure 4a is a scheme of the whole watershed as a single system. Figure 4b is the hydrograph of discharge (Q) at the basin outlet point, while Figure 4c is the averaged soil moisture, with unique blue colour, for the whole watershed.

2.1.2 Deterministic semi-distributed model

A semi-distributed model divides the river basin into several sub-basins or HRUs (Daofeng *et al.* 2004; Dwarakish & Ganasri 2015), according to land use, land cover, soil property and topographic property. The hydrological process is simulated in each sub-basin or HRU. Figure 4d-f illustrates the semi-

distributed model. Figure 4d shows the discretization scheme with three sub-basins, Figure 4e is the hydrograph of discharge at the outlets of three sub-basins, while Figure 4f provides the averaged soil moisture for each sub-basin.

2.1.3 Deterministic distributed model

A distributed model discretizes the entire catchment into cells of a particular shape and size, such as square or triangulated irregular type (COMET 2010a; Devi *et al.* 2015). The model requires input data and model parameters for each cell, and the hydrological process can be simulated for every cell of the catchment. Therefore, the distributed model can provide a high resolution of model outputs (COMET 2010a). The cell type and cell size will influence the modelling outputs. The advantage of this model is that it can provide results at specific points in the whole river basin. Runoff inside each cell can be estimated, based on the parameters in that cell. Runoff for the whole basin/sub-basin can be estimated based on runoff estimation for the cells inside the basin/sub-basin. Furthermore, runoff for the streamflow can be estimated. One of the main drawbacks of this model is that it requires input data for each cell. In cases where input data are not available, the parameter needs to be estimated, which will lead to model uncertainty (COMET 2010a). Figure 4g-i is an example of a fully distributed model. Figure 4g is the discretization scheme of the watershed. Herein, the whole watershed is divided into several square cells of the same size. Figure 4h is the hydrograph of river discharge at random points from upstream to downstream, while Figure 4i is the soil moisture distribution. The distribution of soil moisture is of much higher spatial resolution, compared to the lumped and semi-distributed models.

2.2 Stochastic models

Unlike deterministic models, stochastic models can produce different outputs for each run of the model from a single set of inputs (Thompson 1999; Gupta *et al.* 2015). It takes into account the spatial-temporal occurrences of the events (Jajarmizadeh *et al.* 2012). Therefore, stochastic models are used to predict values of some variables at non-observed times or at non-observed locations (Bierkens & Geer 2012). The uncertainty of such predictions is also analysed in the stochastic models, unlike deterministic models, since the errors of the model outputs are ignored. Quantification of the errors of the model outputs in stochastic models is usually based on the probability distribution of the errors, which tells us the errors' values in a certain range, based on measured data.

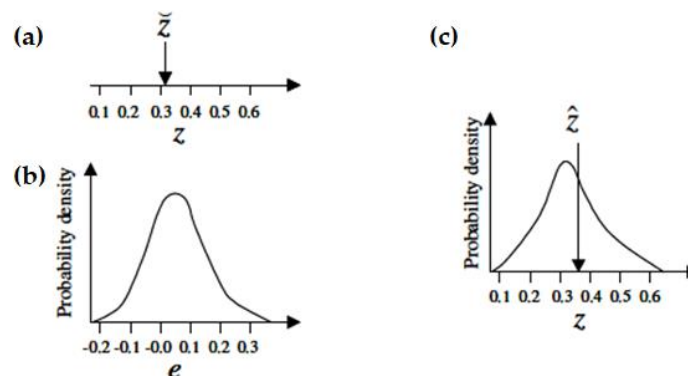


Figure 5 - Example of soil moisture content (z) simulated by stochastic hydrological model: (a) deterministic model outputs (\hat{z}); (b) probability distribution of the modelling errors (e); (c) probability distribution of modelling outputs and the best estimation (\hat{z}) (Bierkens & Geer 2012).

Figure 5 demonstrates simulated soil moisture content and the probability distribution of random errors at some locations and at some times by the stochastic models. From the figure, we can see that the deterministic hydrological models only provide the simulated value, whilst the stochastic hydrological

models yield both simulated value (Figure 5a) and the probability distribution of the random error (Figure 5b). Since errors in modelling outputs are not considered explicitly by most of the approaches used in stochastic hydrological models, an alternative approach is to consider the hydrological variable as a random one. It means that the value of the hydrological variable, e.g., soil moisture content, cannot be known exactly but the probability distribution of such a variable can be calculated (Figure 5c). Figure 5c explains that the value of soil moisture content is not exactly known, but its range is from around 0.2-0.5. It is also possible to achieve the best estimation value with minimum errors. The stochastic model is a combination of deterministic model outputs with a probability distribution of the modelling errors. If there could be a combination of deterministic and stochastic processes, it would generate a perfect hydrological model, since water flow runs on the land phase following the deterministic pathways, while its magnitude, as well as the reaction time of several other processes in the watershed, are controlled by the stochastic processes (Azadi & Zakeri 2010). In practical applications of hydrology, e.g. in flood forecasting, stochastic models are considered a potential tool, since such models consider the chronological results of the hydrological events by examining the occurrences of irregular events (Azadi & Zakeri 2010). Stochastic models can further classified into two sub-categories, i.e., those with spatial independence and those with spatial correlation of random variables (Dwarakish & Ganasri 2015).

2.3 Hydrological process description models

Hydrological models have been developed over several periods from empirical models (black-box), conceptual models (grey-box) to physically based models (white-box) (Xu *et al.* 2019a). Black-box models are the simplest models, while white-box models are the most complicated (Sitterson *et al.* 2017). Grey-box models incorporate both black-box and while-box models (Jajarmizadeh *et al.* 2012; Jain & Singh 2019).

2.3.1 Empirical model (black-box model)

Generally, empirical models, also called black-box models or data-driven models, do not consider any features and hydrological processes in the catchment (Beven 2012; Granata *et al.* 2016; Sitterson *et al.* 2017). Such models are only based on monitoring hydro-meteorological data to build the relationship between inputs and outputs (Sudheer *et al.* 2002; Sarkar & Kumar 2012; Devi *et al.* 2015; Dwarakish & Ganasri 2015). They are particularly suitable for the prediction of rainfall-runoff in a catchment, based on the relationship between rainfall and runoff (Halff *et al.* 1993; Shirke *et al.* 2012; Chen *et al.* 2013; Dwarakish & Ganasri 2015). In this model, statistically based methods, such as regression models and correlation models, are normally used to predict the relationship between rainfall and runoff (Devi *et al.* 2015). Currently, machine learning techniques, such as Artificial Neural Network (ANN), Fuzzy Logic, Genetic Algorithms (GA) etc., are used in the field of hydroinformatics (Devi *et al.* 2015; Dwarakish & Ganasri 2015) to simulate and predict runoff in different river basins (Halff *et al.* 1993; Shirke *et al.* 2012; Chen *et al.* 2013). However, empirical models are not capable of dealing with the practical problems, e.g., simulating the impacts of land use changes on the hydrological regime in the catchment (Dwarakish & Ganasri 2015; Jain & Singh 2019). Figure 6 is an example of the application of an empirical model to predict runoff, while Figure 7 presents runoff modelling by using machine learning techniques.

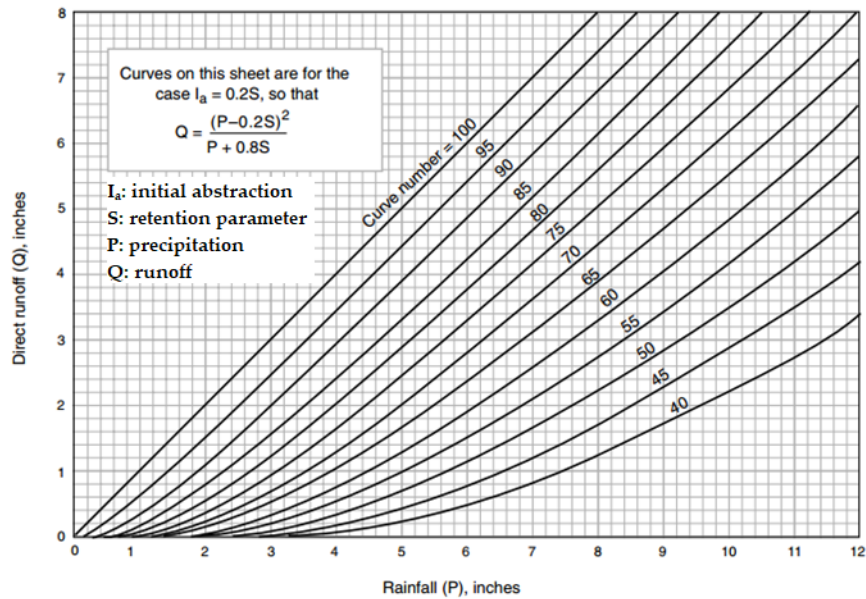


Figure 6 - Application of empirical curve number method to estimate runoff from rainfall (Sitterson et al. 2017).

In Figure 6, the empirical curve number method was used to estimate direct runoff from rainfall. The figure explains the non-linear statistical relationships between rainfall inputs and runoff outputs. Such relationships are described by a mathematical formula as in the top left of the figure. Regarding the machine learning techniques, runoff is simulated by using the most popular methods, such as ANFIS (Adaptive Neuro-Fuzzy Inference System), ANN and SVM (Support Vector Machine), and inputs of rainfall and streamflow (Figure 7).

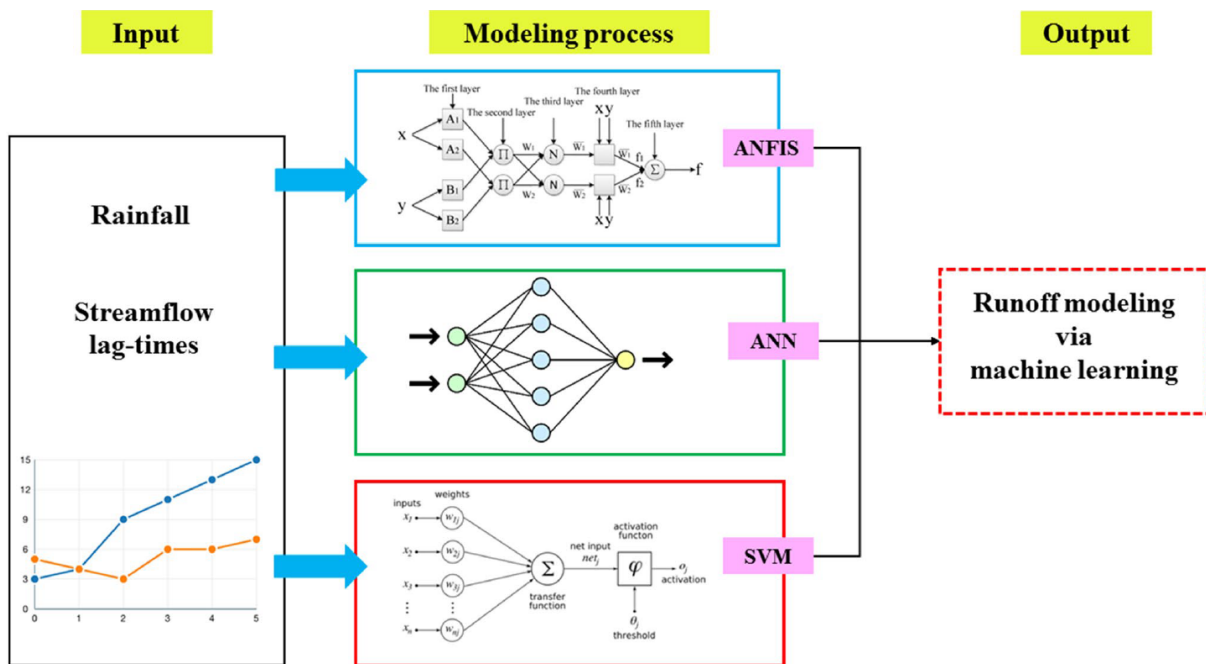


Figure 7 - Application of machine learning technique for runoff modelling (Mohammadi 2021).

2.3.2 Conceptual model (grey-box model)

Conceptual models, also called grey-box models, can simulate all the components of the hydrological process (Devi et al. 2015). A semi-empirical equation is used to describe the hydrological process, based on the observation or assumption of empirical relationships among different hydrological variables

(Devi *et al.* 2015; Dwarakish & Ganasri 2015; Liu *et al.* 2019). In particular, the runoff process in conceptual models is simulated based on the theory of reservoir storage and simplified equations of physical processes in hydrology that provide a conceptual idea of the behaviours occurring within a watershed (Vaze *et al.* 2011; Devi *et al.* 2015; Sitterson *et al.* 2017).

The evaluation of model parameters is based on both field data and the calibration process (Devi *et al.* 2015). Conducting the calibration requires a large amount of hydrometeorological time series data (Devi *et al.* 2015). Moreover, the calibration process involves curve fitting (Devi *et al.* 2015; Jain & Singh 2019), which makes the physical interpretation of modelling results difficult (Devi *et al.* 2015). This will also influence the certainty of the prediction results, especially in the case of it being used in practical problems such as evaluating the impacts of human activities (e.g. land use change) (Devi *et al.* 2015). Additionally, using the curve-fitting method for calibration also indicates that the models may not work well outside the range of calibration data (Jain & Singh 2019). This is a drawback of the conceptual model.

Conceptual models have advantages compared to more complex physically based models, i.e., moderate requirements for input data, as well as shorter running time for models (Seibert & Vis 2012). Noticeably, conceptual models are considered best when the computation time is limited, and there is no need to analyse in detail the catchment features (Sitterson *et al.* 2017). Figure 8 illustrates an example of a schematic structure of a conceptual model HBV (Hydrologiska Byråns Vattenbalansavdelning), including different routines for simulating the rainfall-runoff process and discharge in a watershed, using inputs of daily precipitation, air temperature and estimated monthly long-term potential evaporation.

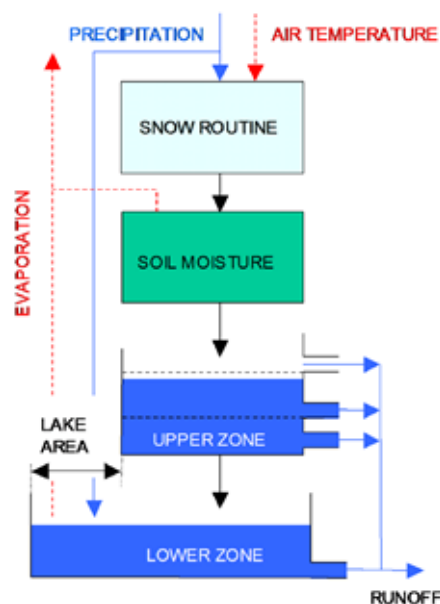


Figure 8 - Conceptual structure of the HBV model (Killingtveit & Sælthun 1995; Bruland & Killingtveit 2002).

2.3.3 Physically based model (white-box model)

Physically based models, also called process-based models or mechanistic models (Sitterson *et al.* 2017), are kinds of white-box models (Xu *et al.* 2019a). Such models represent the real phenomenon of the water cycle in the river basin, by finite difference equations that follow physics laws and principles, including equations of water balance, conservation of mass, energy, momentum and kinematics (Devi *et al.* 2015; Sitterson *et al.* 2017; Jain & Singh 2019). Specifically, surface flow is explained by the Saint

Venant equations, ground water flow is described by the Boussinesq equation, and the Richards equation is used for simulating unsaturated zones, etc. (Jain & Singh 2019).

The main advantage of the physically based model is that it does not require intensive hydrometeorological data for the calibration process (Jain & Singh 2019). However, it requires a large number of parameters to describe the physical features of the river basin (Abbott *et al.* 1986; Devi *et al.* 2015). To set up and run this model, a large amount of input data, such as topography, soil properties, land use and dimensions of the river network, need to be collected. Physically based models overcome the drawbacks of conceptual models and empirical models, since they use parameters with physical meaning (Jain & Singh 2019). In addition, such models can provide a huge amount of information outside the boundary, whereas empirical models are only valid within the boundary (Jain & Singh 2019).

Physically based models have a wide range of applications (Devi *et al.* 2015). For example, the model can simulate the movement and interaction between surface water and ground water, the transportation of sediments, nutrients and pesticides, and the variation of water quality within the watersheds (Devi *et al.* 2015; Jain & Singh 2019). Physically based models can also be applied in a wider range of catchments, since the physics laws used to describe the hydrological processes are the same everywhere, whereas black-box models cannot be applied to all catchments, as many hydrological processes are not taken into account. Figure 9 illustrates the hydrological processes simulated by the physically based SWAT (soil and water assessment tool) model.

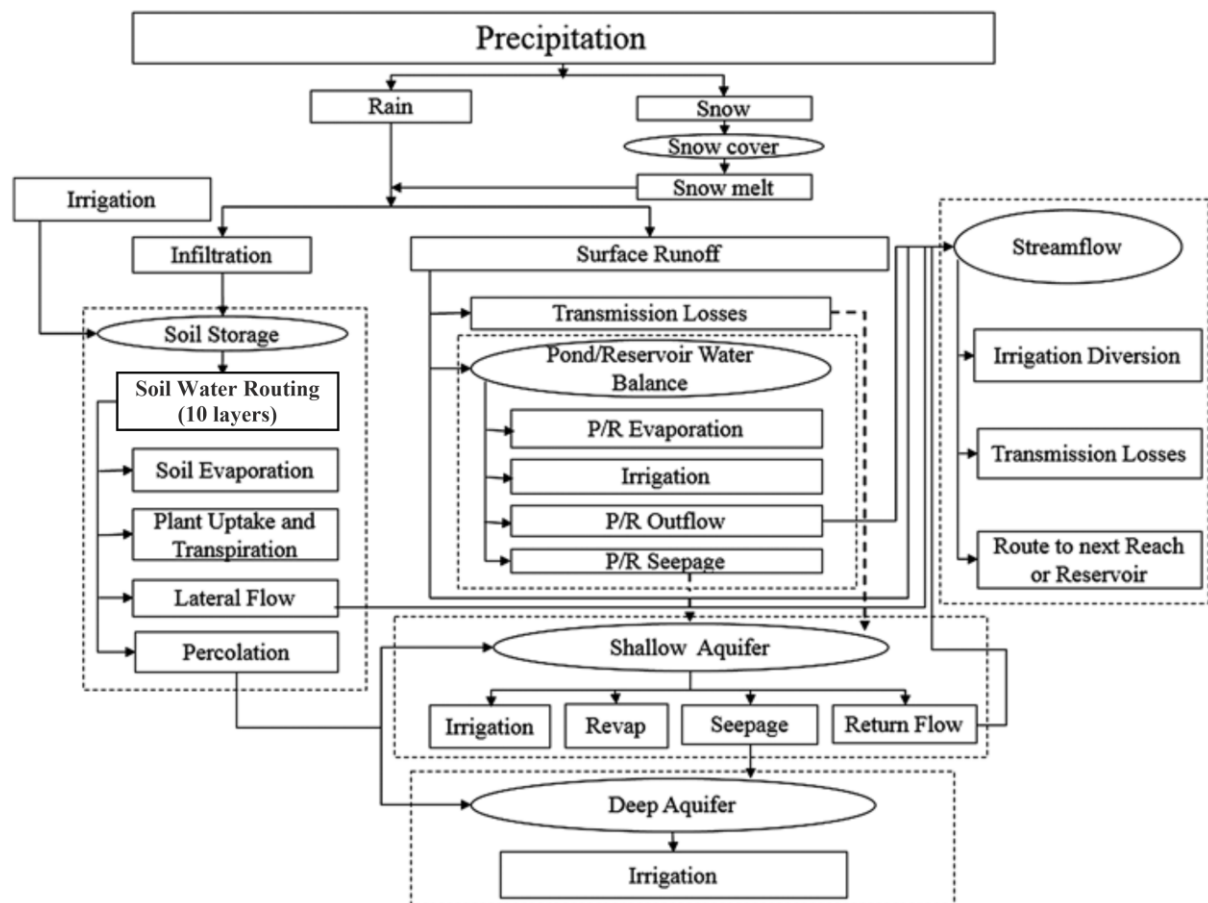


Figure 9 - Overview of the hydrological processes described in the SWAT model (Neitsch *et al.* 2011; Zhang *et al.* 2016).

3 Study areas, materials and methods

3.1 Study areas

The Arctic is distinguished as the area located north of the Arctic Circle (at 66°32'N) (Wilson *et al.* 1998; AMAP 2011). This region is characterized by an extreme climate, with high variations in light and temperature, extensive snow cover and ice in winter, short summers, and the presence of permafrost (Wilson *et al.* 1998). Permafrost, which has significant effects on Arctic hydrological processes, accounts for approximately 24% of the exposed land area in the Northern Hemisphere (Romanovsky *et al.* 2002) (Figure 10, top right subfigure).

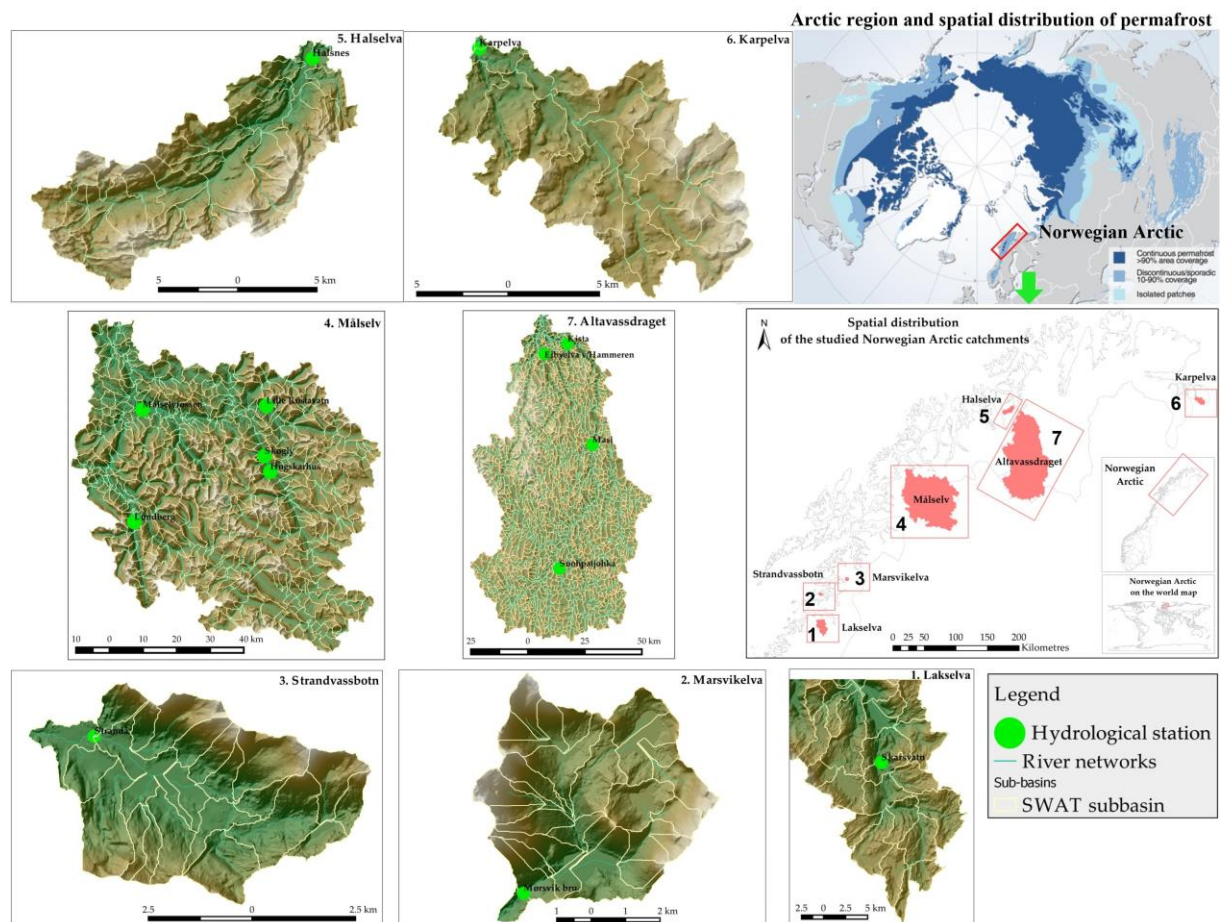


Figure 10 - Map of Arctic region (top right, source: <https://www.nasa.gov/topics/earth/features/earth20130610.html>) and the studied Norwegian Arctic catchments.

Regarding meteorological factors, the Arctic mainland exhibits significant differences in air temperature between winter (e.g., average of -20 to -40°C in January) and summer (e.g., average of 5 to 10°C in July) (Wilson *et al.* 1998). Across the terrestrial Arctic, precipitation is highly heterogeneous in temporal (seasonal) and spatial patterns. The annual precipitation in the Arctic mainland varies from <150 mm to over 1000 mm, of which the higher precipitation is distributed along the Arctic coastal zones (Yang & Kane 2021). Other important factors forming the typical features of the severe Arctic climate and weather are the presence of persistent and extensive stratus cloud cover, extreme fog (e.g., 100 days per year of fog in some parts of the Arctic) and wind (an important factor for snow distribution and the

chilling effect of low temperatures) (Wilson *et al.* 1998). Regarding hydrological characteristics, streamflow regimes differ considerably among Arctic catchments, due to the great variations in climate, permafrost and human activities across the Arctic. Generally, flow regimes in the Arctic catchments are dominated by rainfall, snowmelt and ice melt, of which snowmelt regimes dominate most Arctic rivers. Moreover, some Arctic rivers in the northern regions have proglacial regimes, which occur in summer due to glacial melt. Furthermore, the rivers flowing through the wetlands have a wetland or muskeg regime, with spring snowmelt contributing to the main source of flow (Wilson *et al.* 1998). The Norwegian Arctic is an example of a region presenting highly heterogeneous hydrological regimes. For example, the hydrological regimes in the Norwegian Arctic catchments are categorized into three main types: rainfall-dominated, snowmelt-dominated and mixed rainfall/snowmelt regimes, according to the Norwegian Water Resources and Energy Directorate (NVE) (Lawrence & Hisdal 2011). The subheadings that follow introduce the different Norwegian Arctic catchments where different hydrological regimes are dominant. The selection of those Norwegian Arctic catchments for investigation is based on several criteria: (1) geographical distribution (i.e., from coastal zones to inland areas) and latitude distribution (i.e., from the southern region to the northern region and above the Arctic Circle); (2) catchments' scales (i.e., from small-scale to large-scale); and (3) hydrological regimes (i.e., rainfall, snowmelt and mixed rainfall/snowmelt) (Table 2).

3.1.1 Lakselva catchment

The Lakselva catchment is located in Bodø municipality, in Nordland county, Norway. This catchment is very close to the Arctic Circle (Figure 10, numbered 1). The catchment has a drainage area of approx. 297 km², which consists of forest (44.1%), mountain (35.3%), lake (6.2%), bog (6%), agricultural land (1%) and other types (approx. 7.3%) (Sildre 2020). The elevation of the ground surface is in the range of 0-1112 m (above mean sea level-AMSL). According to long-term observed data (1991-2020), the average annual air temperature and precipitation in this catchment varied from +2 to +8°C and from 750 to 1500mm, respectively. The hydrological regime in the Lakselva catchment is a mixture of rainfall and snowmelt (Table 2).

3.1.2 Strandvassbotn catchment

The small-scale catchment of Strandvassbotn is located in the coastal zone of Bodø municipality, Nordland county, Norway (Figure 10, numbered 2). The catchment has a drainage area of approx. 26 km², which is dominated by forest (30.8%) and mountain (22.1%), followed by bog (10.4%), lake (3.6%), agricultural land (0.2%) and other types (approx. 33%) (Sildre 2020). The elevation of the ground surface is distributed in the range of 0-944 m (AMSL). Long-term monitoring data (1991-2020) revealed that the average annual air temperature and precipitation in this catchment varied from +2 to +10°C and from 1000 to 1500mm, respectively. The hydrological regime in the Strandvassbotn catchment is dominated by rainfall (Table 2).

3.1.3 Marsvikelva catchment

The small-scale catchment Marsvikelva is located in the Sørfold municipality, Nordland county, Norway (Figure 10, numbered 3). The catchment has a drainage area of approx. 32 km². The main land use components consist of forest (52.4%), mountain (28.5%), lake (9.4%), bog (4%) and other types (approx. 5.7%). There is no agricultural activity in this catchment (Sildre 2020). Marsvikelva has its ground surface's elevation in the range of 0-1098 m (AMSL). Long-term monitoring data (1991-2020) revealed that the average annual air temperature and precipitation in this catchment varied from +2 to

+8°C and from 1000 to 1500mm, respectively. Similar to the Strandvassbotn catchment, the hydrological regime in the Strandvassbotn catchment is dominated by rainfall (Table 2).

3.1.4 Målselv catchment

Målselv is a large-scale catchment with a drainage area of approx. 5815 km². The catchment is located in the centre of the Norwegian Arctic, belonging to Målselv municipality in Troms and Finnmark county (Figure 10, numbered 4). Mountain (64.2%) and forest (24.3%) are the dominant land use types in the catchment, but there are other small areas of lake (3.8%), bog (2.1%), glacier (5%), agricultural land (0.7%) and others (approx. 4.3%) (Sildre 2020). The ground surface's elevation varies greatly in this catchment (0-1718m AMSL). The average annual air temperature and precipitation in this catchment varied from -5 to +6°C and from <500 to 1500mm, respectively, based on the long-term monitoring data (1991-2020). Snowmelt is the dominant hydrological regime in this catchment (Table 2).

3.1.5 Altavassdraget catchment

Altavassdraget is another large-scale catchment (approx. 6902 km²), which is located in Alta municipality, Troms and Finnmark county (Figure 10, numbered 7). The land use components in this catchment consist of mountain (43.7%), forest (28.8%), bog (11.1%), lake (7.2%), agricultural land (0.1%) and others (approx. 9.2%) (Sildre 2020). The ground surface's elevation is distributed in the range of 2-973m AMSL. The average annual air temperature and precipitation in this catchment varied from -3 to +6°C and from <500 to 750mm, respectively, based on the long-term monitoring data (1991-2020). Similar to the Målselv catchment, snowmelt is the dominant hydrological regime in this catchment (Table 2).

3.1.6 Halselva catchment

The Halselva catchment (approx. 143 km²) is located in Alta municipality, Troms and Finnmark county (Figure 10, numbered 5). This catchment is very close to the Altavassdraget catchment (in the northwest direction). Both Halselva and Altavassdraget catchments drain into the Alta fjord. Mountains are the dominant land use component in this catchment, at approx. 73.5%, followed by forest (13.9%), bog (1.3%), lake (3.5%), agricultural land (0.2%) and others (approx. 7.7%) (Sildre 2020). Due to its location close to the Altavassdraget catchment, the meteorological characteristics in the Halselva catchment are quite similar to those of the Altavassdraget catchment. For example, the average annual air temperature and precipitation in this catchment varied from -2 to +6°C and from 500 to 750mm, respectively, based on the long-term monitoring data (1991-2020). Snowmelt is the dominant hydrological regime in this catchment (Table 2).

3.1.7 Karpelva catchment

The Karpelva catchment (approx. 129 km²) is located in the uppermost area of the Norwegian Arctic (Figure 10, numbered 6). The catchment is in the Sør-Varanger municipality, Troms and Finnmark county. Forest accounts for approx. 51.3% of total land use, while the remaining components are mountain (12%), lake (5%), agricultural land (0.3%) and other types (approx. 18.9%) (Sildre 2020). According to long-term monitoring data (1991-2020), the average annual air temperature and precipitation in this catchment varied from -1 to +4°C and from 500 to 750mm, respectively. Snowmelt is the dominant hydrological regime in this catchment (Table 2).

3.1.8 Definition of study areas for each scientific paper

In the first paper, the study area was the whole Arctic in general (Figure 10, top right subfigure), while, in the second to the fourth papers, the study area was limited to the Norwegian Arctic. In particular, in the second and third papers, one large-scale catchment in the Norwegian Arctic was selected, i.e., the Målselv catchment (5815 km²) (Figure 10, numbered 4). In the fourth paper, seven Norwegian Arctic catchments (26 - 6902 km²) were employed, to evaluate hydrological modelling performance, as well as to investigate hydrological CC impacts (excluding the Altavassdraget catchment) in the Arctic (Figure 10, numbered 1-7).

Table 2 - General characteristics of the studied Norwegian Arctic catchments.

Region	Catchment	Area (km ²)	No. of sub- basins	No. of HRUs	Glacial cover (%)	Drainage density (km km ⁻²)	Elevation distribution (m)	Average overland sub-basin slope (%)	Average annual precipitation ^a (mm)	Average annual air temperature ^b (°C)	Hydro- gauging stations	Annual		Dominant flood regimes	
												peak flow in March- July (%)	peak flow in August- February (%)		
Nordland	Lakselva	297	24	220	0	0.33	0-1112	20.09	750-1500	+2 to +8	Skarstvatn	57	43	Mixed rainfall/ snowmelt	
	Strandvassbøin	26	22	146	0	0.93	0-944	36.72	1000-1500	+2 to +10	Strandå	27	73	Rainfall	
	Marsvikelva	32	27	168	0	0.85	0-1098	37.14	1000-1500	+2 to +8	Mørsvik bru	20	80	Rainfall	
	Målselv	5815	459	5601	~ 5	0.33	0-1718	25.95	<500-1500	-5 to +6	Lundberg	93	7	Snowmelt	
												Lille Rostavatn	100	0	Snowmelt
												Høgskatthus	100	0	Snowmelt
Troms & Finnmark											Skogly	100	0	Snowmelt	
											Målselvfossen	100	0	Snowmelt	
	Altaavstraget	6902	1376	8320	0	0.55	2-973	6.54	<500-750	-3 to +6	Masi	100	0	Snowmelt	
											Kista	100	0	Snowmelt	
	Halselva	143	35	343	0	0.75	1-1146	26.22	500-750	-2 to +6	Halsnes	100	0	Snowmelt	
	Karpelva	129	27	169	0	0.57	3-404	7.80	500-750	-1 to +4	Karpelva	100	0	Snowmelt	

^{a,b}: averaged based on 30-year observed data (1991-2020) (source: The Norwegian Water Resources and Energy Directorate - NVE).

3.2 Data acquisition

3.2.1 Data acquisition – Paper I

In Paper I, to conduct a comprehensive review of the hydrological models, data from various sources were gathered, as summarized in Table 3 and Figure 11.

Table 3 - Summary of the selected model types used in the review in Paper I.

Model types	Model names	Data sources
Surface hydrological models	Topoflow	Published papers from Google Scholar, Scopus, ResearchGate, electronic books, web pages, etc.
	DMHS	
	HBV	
	SWAT	
	WaSiM	
	ECOMAG	
Subsurface/cryo-hydrogeological model	CRHM	
	ATS	
	CryoGrid 3	
	GEOtop	
	SUTRA-ICE	
	PFLOTRAN-ICE	

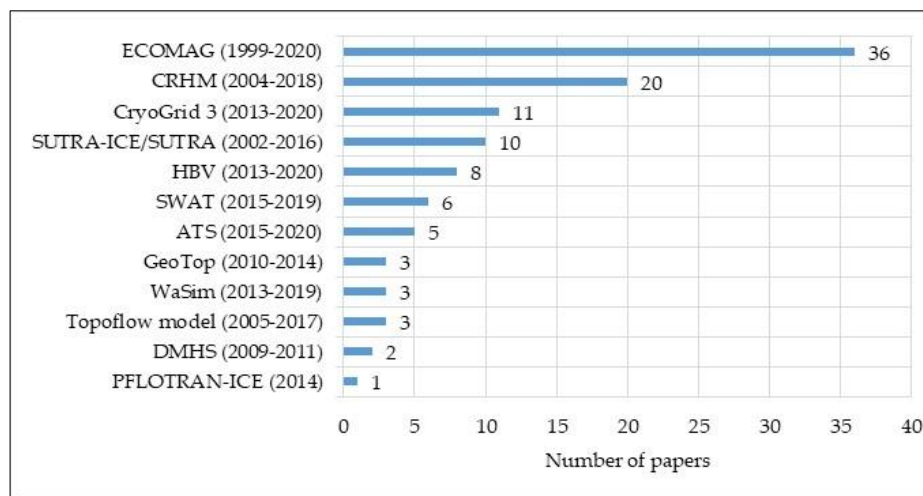


Figure 11 - Number of recent publications related to hydrological models and cryo-hydrogeological models, found via <https://www.scopus.com/>, supporting the review in Paper I.

From Papers II to IV, the hydrological SWAT model was applied. To run the SWAT requires several input data: (a) spatial data (grid) such as Digital Elevation Model (DEM), soil and land use, (b) time series data for precipitation, maximum and minimum air temperature, relative humidity, solar radiation and wind speed. To calibrate and validate the model, time series of observed river discharges are required. Details of data gathering from Papers II to IV are described in the following sections.

3.2.2 Data acquisition – Papers II & III

In Papers II and III, hydrological SWAT models were applied in the same large-scale catchment, the Målselv (approx. 5815 km²). Details of data collection for running the SWAT models are presented in Table 4 and Figure 12.

Table 4 - Data collection for the SWAT models applied in Papers II & III.

Data type	Spatial resolution	Temporal resolution	Source of data
DEM	10 x 10 m		(Geonorge 2013)
Land use	~600 m		(Waterbase 2007a)
Soil	~5000 m		(Waterbase 2007b)
Climate	Ground-based data: 4 stations	Daily	(ECAD 2002)
	CFSR data: 21 grids, ~38 km grid	Daily	(TAMU 2012)
River discharge	5 stations	Monthly	(Sildre 2020)

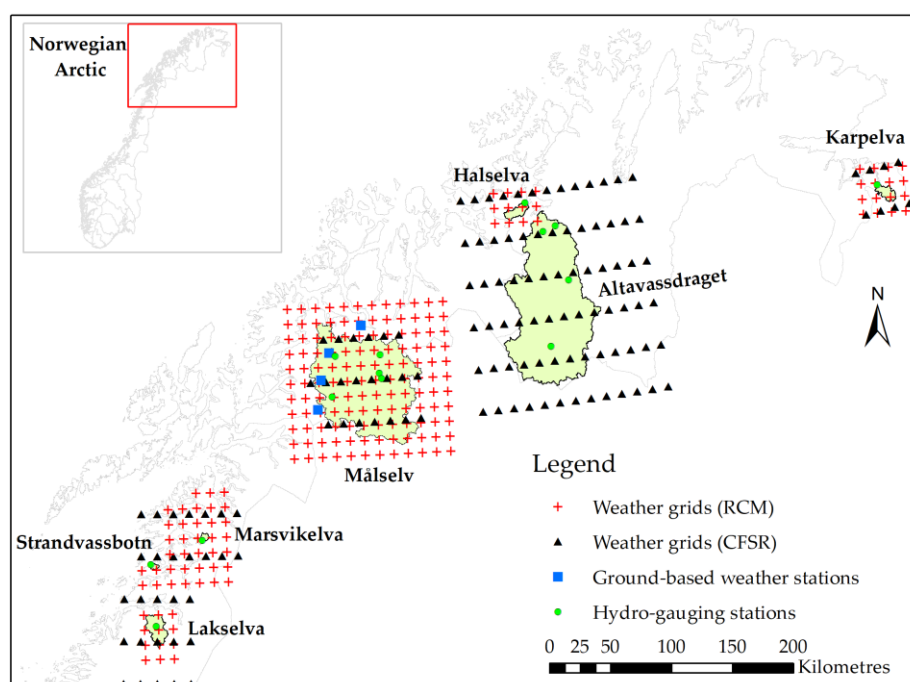


Figure 12 - Spatial resolution of weather inputs (CFSR and RCMs) and hydro-gauging stations in seven Norwegian Arctic catchments.

3.2.3 Data acquisition – Paper IV

In Paper IV, the SWAT models were applied in seven catchments (26–6902 km²). Details of data collection for running the SWAT models are presented in Table 5 and Figure 12.

Table 5 - Data collection for the SWAT models applied in Paper IV.

Data type	Spatial resolution	Temporal resolution	Sources
Spatial data (grid)	DEM	10 x 10 m	(Geonorge 2013)
	Land use	~600 m	(Waterbase 2007a)
	Soil	~5000 m	(Waterbase 2007b)
Temporal data (time series)	Climate data: CFSR	~38 km grid	Daily (TAMU 2012)
	CC data: RCMs	~12.5 km grid	Daily (Jacob <i>et al.</i> 2014)
	River discharge		Daily (Sildre 2020)

3.3 Methods

This section aims to summarize all the main methods applied in four scientific papers to solve the five research questions proposed in the introduction section (Figure 13). A detailed description of each method is presented in the following subheadings.

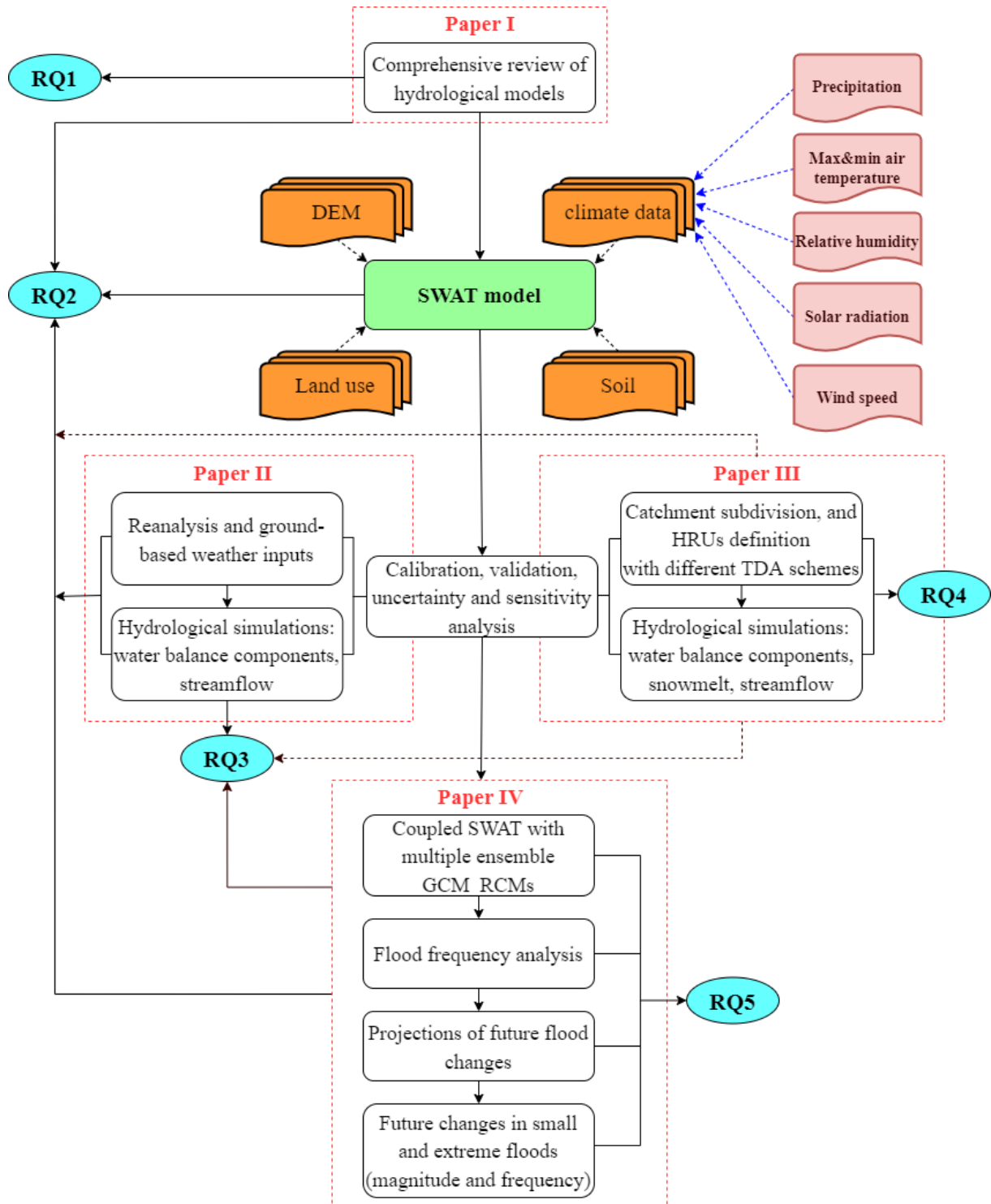


Figure 13 - Summary of all the main methods applied in four scientific papers to solve the five research questions (RQ) of the thesis.

3.3.1 Comprehensive review

In order to select suitable modelling tool(s) for the assessment of hydrological CC impacts in the Arctic, a comprehensive review was conducted, as seen in Paper I. In particular, the idea of the review was formed on the basis of the CC context in the Arctic with complex hydrological processes. Accordingly, a demand for a reliable modelling tool to address hydrological CC impacts in this specific region was defined. Next, twelve well-known hydrological models, including surface hydrological models and cryo-hydrogeological models, were searched for in the literature and gathered based on their applications in previous studies in the Arctic. After that, the capacities and limitations of such models to deal with complex hydrological processes in the Arctic were examined, based on the outcomes of the previous studies. Finally, all the models were compared regarding their capacities, and weighted according to their suitability for different targets of applications. Specifically, the evaluation and selection processes of suitable modelling tools were based on the following criteria:

1. Considering the important processes in permafrost environments, the models should include:
 - Surface energy balance;
 - Snow processes, snow insulation, and snowmelt;
 - Infiltration processes;
 - The dynamics of soil thermal and soil moisture fluxes;
 - Soil heterogeneities;
 - The dynamics (seasonal thawing) of the active layer;
 - Subsidence;
 - A three-phase change of water (ice, liquid, and gas) during the freezing and thawing of near-surface soil.in their models' structures.
2. Consideration of the opportunity for wide application in the Arctic conditions, including:
 - Requirement for input data, i.e., large or small requirement;
 - Requirement for computation processes, i.e., strong or low requirement;
 - Ability to be applied in different sizes of catchments, i.e., small-scale and/or large-scale.
3. Also, suitable model candidates depend on targets and current conditions (e.g., data availability, required timing, and funding) of each study/project.

Although the comprehensive review covered both surface hydrological models and subsurface or cryo-hydrogeological models, the verification of model performances, as well as the assessment of CC impacts (from Paper II to Paper IV), were limited to surface hydrology. Nevertheless, the outcome of the review paper (Paper I) aimed to support a wide range of readers who have different goals for studying the CC impacts.

3.3.2 The selected model candidate SWAT

Based on the review results in Paper I, the surface hydrological SWAT (soil and water assessment tool) model (Figure 14) was selected, among others, for this study. The SWAT model was applied from Paper II to Paper IV, to simulate hydrological processes, as well as to project their changes due to CC in the Norwegian Arctic catchments. The model description, methods for model calibration, validation, sensitivity and uncertainties' analysis are described in the following subsections.

3.3.2.1 Model description

The SWAT is a physically based (or process-based) (Neitsch *et al.* 2009) semi-distributed hydrological model, which was developed by United States Department of Agriculture (USDA)-Agricultural Research Service, USDA-Natural Resources Conservation Service, and Texas A&M University. The model has been widely used around the world (approx. 100 countries). The SWAT is used to simulate the impacts of human activities (Gassman *et al.* 2007) and CC (Dile *et al.* 2013) on water resources and environment in large and complex catchments over a long period. The strengths of the SWAT model are highlighted by its fulfilment of the requirements of the current modelling philosophy, i.e., the transparency of the model (Abbaspour *et al.* 2015). This means the sensitivity and uncertainty analysis of the modelling results are examined in the calibration and validation processes.

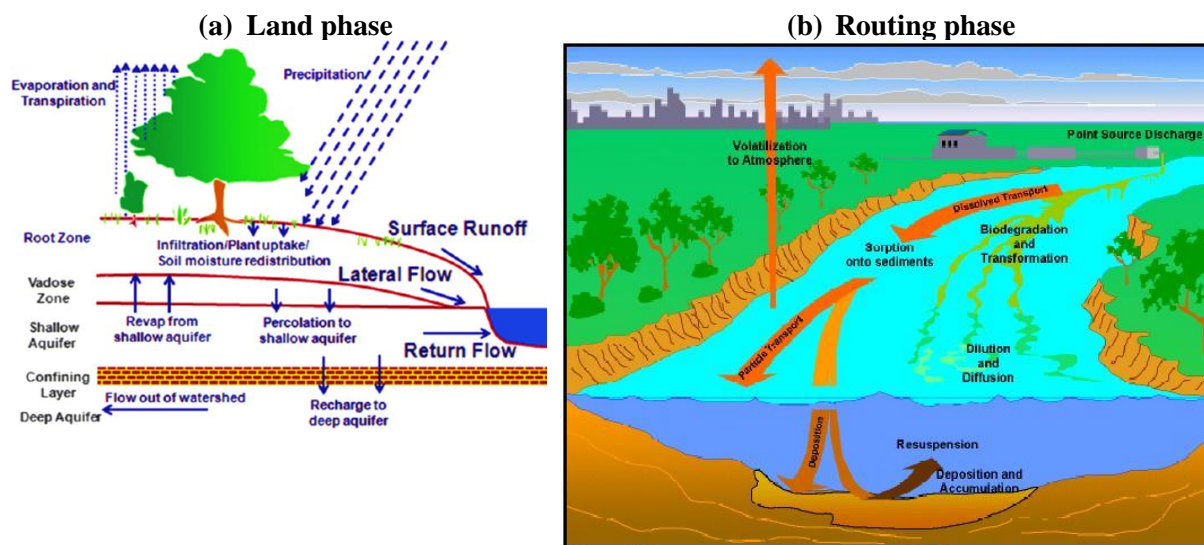


Figure 14 - Description of hydrological simulation in two different phases of the SWAT model (source: <http://www.brc.tamus.edu/swat/>).

Because the SWAT is a type of semi-distributed model, the whole river basin is discretized to smaller sub-basins, to present the spatial heterogeneity over the basin. The number and size of the generated sub-basins are decided by the designed values of the threshold drainage area (TDA). Each sub-basin is then subdivided into hydrologic response units (HRUs), which have homogeneity of topography, land use, soil characteristics and management. Details of the techniques for HRU creation are described in the following section.

3.3.2.2 Methods for HRUs' definition

In the watershed subdivision process, multiple HRUs are generated for each sub-basin, based on a HRU threshold. The inputs to generate HRUs are land use, soil and slope classification. The HRU threshold will decide the percentage of the representative land use/soil/slope for each sub-basin (Figure 15). This threshold is usually from 5-15%, which has been widely used in many previous studies (Sexton *et al.* 2010; Srinivasan *et al.* 2010; Han *et al.* 2012; EPA 2013). In this study, the HRU thresholds for land use/soil/slope were designed as 5/5/5%. Based on this HRU threshold, only types of land use/soil/slope with their areas higher than 5% of the sub-basin area were selected. Furthermore, the terrain slope was classified into five classes: 0-5%, 5-10%, 10-25%, 25-30%, and > 30%.

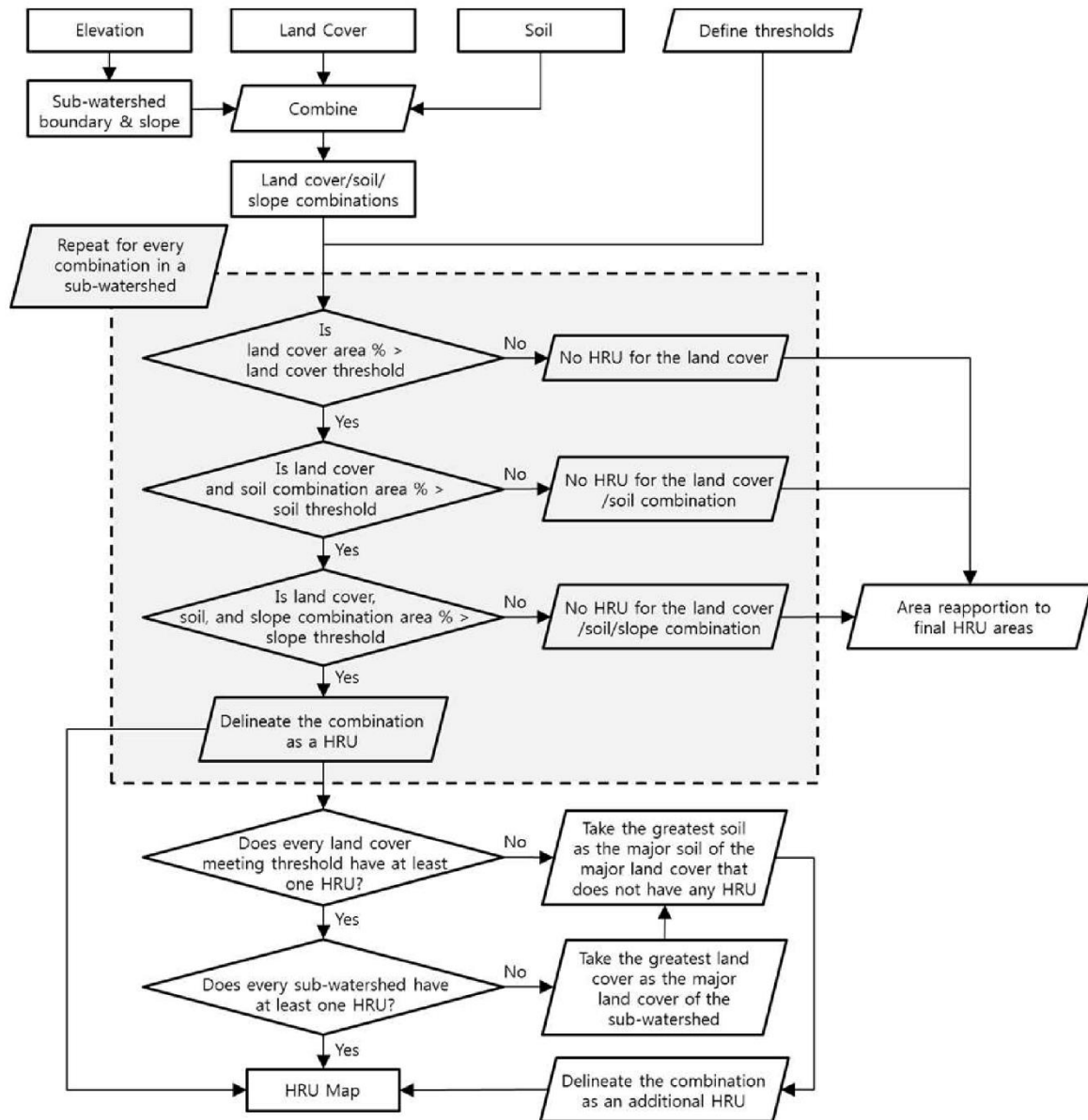


Figure 15 - The algorithm for HRU definition in the SWAT (Her et al. 2015).

3.3.2.3 Hydrological simulation in SWAT model

The hydrological simulation in the SWAT occurs in two main phases, i.e., the land phase and the routing phase (Arnold *et al.* 2012) (Figure 14). The land phase (Figure 14a) works based on the following water balance equation:

$$SW_t = SW_0 + \sum_{i=1}^t (R_i - Q_i - E_i - P_i - QR_i), \quad (1)$$

where

- SW_t is soil water content at time t (mm),
- SW_0 is the initial soil water content (mm),
- R_i is amount of precipitation on day i (mm),
- Q_i is amount of surface runoff on day i (mm),
- E_i is amount of evapotranspiration on day i (mm),

- P_i is amount of percolation on day i (mm), and
- QR_i is amount of return flow on day i (mm).

The loads of water, sediment, nutrients and pesticides from the land phase are then transferred to the streams/ivers, where the routing phase occurs (Figure 14) (Arnold *et al.* 2012). The loads are routed along the streams/ivers and reservoirs (if available). The routing phase simulates several processes in the streams/ivers, such as water movement, mass of flow, chemical processes, flood routing, sediment routing, nutrient routing and pesticide routing. The discharge in the mainstream/river at the outlet of each sub-basin is the contribution of water yield (WYLD) from this sub-basin plus WYLD from upstream sub-basins. The WYLD is the summarization of surface runoff, lateral flow and groundwater, subtracting the transmission loss (Tolera *et al.* 2018).

3.3.2.4 Coupled SWAT and GIS

Several tools have been developed to enhance the application and development of the SWAT model. Of them, the GIS-Geographic Information System has been successfully integrated with the SWAT model to collect, manipulate, visualize and analyse the inputs and outputs (Srinivasan & Arnold 1994). Several versions of GIS, starting from GRASS-GIS to the most recent ArcGIS, have been used to produce input data for the SWAT model (Krysanova & Srinivasan 2015). However, ArcGIS is a commercial version, and obtaining a key licence is very costly. Therefore, an open source GIS, namely QGIS, was developed recently (Chen *et al.* 2010). The QGIS has most functions of the commercial version and has high performance compared to other open sources of GIS. Thus, QGIS has enough necessary functions for water resources management. The following Table 6 presents the different GIS-coupled SWAT interfaces which have been developed.

Table 6 - Summary of GIS-coupled SWAT interfaces.

Coupling model	Description	GIS interface	Source of GIS interface
MW-SWAT	This is an open source; however, it limits capability in large catchments	MW (MapWindow) GIS	https://www.mapwindow.org/
GRASS-SWAT	This is the first GIS-coupled SWAT interfaces that generated and integrated topographic, soil and land use inputs	GRASS (Geographic Resources Analysis Support System) GIS	https://grass.osgeo.org/
ARC-SWAT	This is a commercial source and the most popular version	ArcGIS	http://www.esri.com/software/arcgis
Q-SWAT	This is a new & open source, has capability to merge small sub-basins and has static and dynamic visualizations of outputs which cannot be performed in ArcSWAT	QGIS (Quantum Geographical Information System)	https://qgis.org/en/site/

In this study, the coupling Q-SWAT model was used, due to its upgraded availability and functionality compared to other SWAT interfaces.

3.3.2.5 Model calibration, validation, uncertainty, and sensitivity analysis

This study used the Sequential Uncertainty Fitting Version 2 (SUFI-2) algorithm (Figure 16) in the SWAT Calibration Uncertainties Program (SWAT_CUP) (Abbaspour *et al.* 2007) for model calibration, validation, sensitivity and uncertainties' analysis. Inputs for the SWAT_CUP are outputs from the SWAT model (e.g., discharge). The SWAT_CUP runs several iterations to figure out the optimal model parameters. In each iteration, all the possible simulation outputs are produced and distributed in the so-called 95PPU (95 Percent Prediction Uncertainty) band/envelope (Abbaspour *et al.* 2015). The 95PPU generates all possible estimated values from the lower limit (at 2.5%) to the upper limit (at 97.5%) of the cumulative distribution. This process works based on the Latin hypercube (LH) sampling approach, which is a statistical method to reduce the number of samples from the multiple dimensional distributions (Mckay *et al.* 1979; Özdemir 2016). The 95PPU works to bracket as much of the observed data within the 95PPU envelope as possible.

3.3.2.6 Evaluation of model performance

To quantify the model performance (e.g., the goodness of fit between simulated and observed data) after calibration and validation, this study was based on three main statistical coefficients: (1) the coefficient of determination R^2 (Equation (2)), measuring the fitness of the linear relationship between the simulated and observed values; (2) the Nash-Sutcliffe coefficient of efficiency (NSE) (Equation (3)); and (3) root mean square error, divided by the standard deviation (RSR) (Equation (4)).

$$R^2 = 1 - \frac{\sum_{i=1}^n (Y_i^{obs} - Y_{mean}^{obs})(Y_i^{sim} - Y_{mean}^{sim})}{\left[\sum_{i=1}^n (Y_i^{obs} - Y_{mean}^{obs})^2 \right]^{1/2} \left[\sum_{i=1}^n (Y_i^{sim} - Y_{mean}^{sim})^2 \right]^{1/2}} \quad (2)$$

$$NSE = 1 - \frac{\sum_{i=1}^n (Y_i^{obs} - Y_i^{sim})^2}{\sum_{i=1}^n (Y_i^{obs} - Y_{mean}^{obs})^2} \quad (3)$$

$$RSR = \frac{\left[\sum_{i=1}^n (Y_i^{obs} - Y_i^{sim})^2 \right]^{1/2}}{\left[\sum_{i=1}^n (Y_i^{obs} - Y_{mean}^{obs})^2 \right]^{1/2}} \quad (4)$$

where

- Y_i^{obs} and Y_i^{sim} describe the observed and simulated values at time i ,
- Y_{mean}^{obs} and Y_{mean}^{sim} describe the mean observed and simulated data for the entire evaluation period, and
- n describes the total number of observations/simulations.

The thresholds of three statistical coefficients, R^2 , NSE and RSR, for monthly (in Papers II and III) and daily (in Paper IV) simulations are summarized in Table 7 and Table 8, respectively (Santhi *et al.* 2001; Van Liew *et al.* 2003; Fernandez *et al.* 2005; Moriasi *et al.* 2007; Premanand *et al.* 2018; Koycegiz & Buyukyildiz 2019).

Table 7 - Thresholds of R^2 , NSE and RSR for evaluation of hydrological model's performance (daily simulation).

Model performance	R^2	NSE	RSR
Very good	$0.75 < R^2 \leq 1.00$	$0.75 < NSE \leq 1.00$	$0.00 \leq RSR \leq 0.50$
Good	$0.60 < R^2 \leq 0.75$	$0.60 < NSE \leq 0.75$	$0.50 < RSR \leq 0.60$
Satisfactory	$0.50 < R^2 \leq 0.60$	$0.36 < NSE \leq 0.60$	$0.60 < RSR \leq 0.70$
Unsatisfactory	$0.25 < R^2 \leq 0.50$	$0.00 < NSE \leq 0.36$	$RSR > 0.70$

Table 8 - Thresholds of R^2 , NSE and RSR for evaluation of hydrological model's performance (monthly simulation).

Model performance	R^2	NSE	RSR
Very good	$0.70 \leq R^2 \leq 1.00$	$0.75 < NSE \leq 1.00$	$0.00 \leq RSR \leq 0.50$
Good	$0.60 \leq R^2 < 0.70$	$0.65 < NSE \leq 0.75$	$0.50 < RSR \leq 0.60$
Satisfactory	$0.50 \leq R^2 < 0.60$	$0.50 < NSE \leq 0.65$	$0.60 < RSR \leq 0.70$
Unsatisfactory	$R^2 < 0.50$	$NSE \leq 0.50$	$RSR > 0.70$

3.3.2.7 Uncertainty analysis

The uncertainties between the simulated and observed data were quantified based on two main indicators, i.e., p-factor and r-factor in the SUFI-2 algorithm (Figure 16).

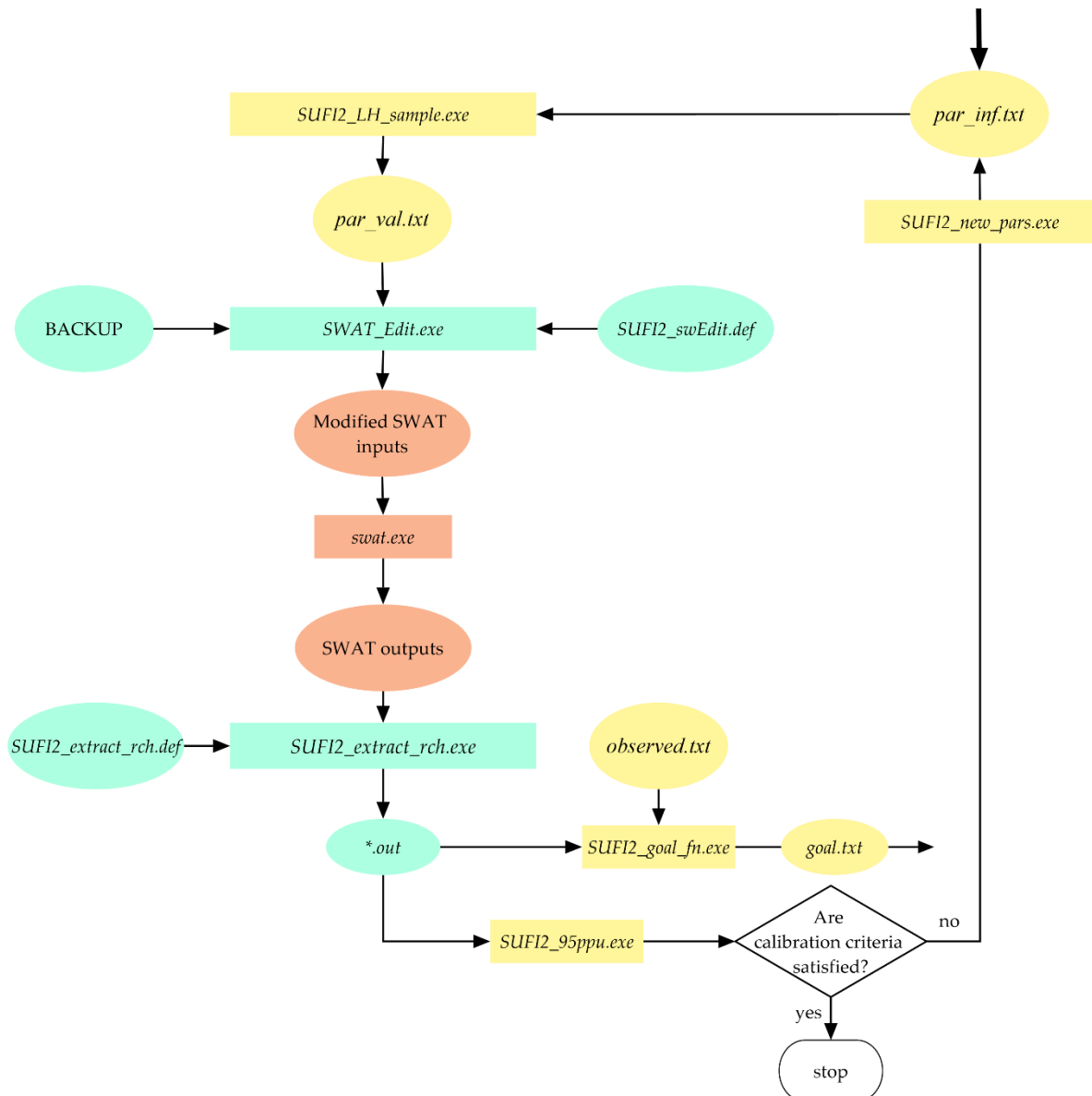


Figure 16 - The SUFI-2 algorithm in SWAT_CUP (Abbaspour 2015).

The first indicator, the p-factor (from 0 to 1), measures the percentage of the observed data which could be bracketed within the 95PPU band. The value of 1 indicates that 100% of the observed data are bracketed in the 95PPU band, or it means that the simulation results are highly accurate. For streamflow simulation, the optimal value of the p-factor is suggested to be higher than 0.70 or 0.75. This threshold depends upon the project scale, quality of input data to run the model, as well as data for calibration.

The second indicator, the r-factor, explains the thickness of the 95PPU band. The narrowness of the 95PPU band indicates the low uncertainty of the simulation results. Thus, the optimal value of the r-factor should be close to zero. For streamflow simulation, the value of the r-factor is recommended to be smaller than 1.5, and this also depends on the study conditions and quality of input data. In short, the simulation results should fulfil the criteria of the two measures of the p-factor and r-factor: the stochastic simulation results should bracket as much of the observed data in the uncertainty envelope as possible, but, at the same time, the uncertainty envelope should be as narrow as possible. When the accepted values of the p-factor and the r-factor are found in the last iteration of the calibration/validation process, the sensitivity of the model parameters are calculated and ranked for the calibrated variables (e.g., discharge). Details of the sensitivity analysis are described in the following section.

3.3.2.8 Sensitivity analysis

In this study, global sensitivity analysis in the SUFI-2 algorithm was applied to figure out the most sensitive model parameters in the calibration process. This technique estimates the average changes of the objective function resulting from the changes of each model parameter, while all other model parameters are changing (Abbaspour 2015). The sensitivities of the model parameters are determined according to the following multiple regression equation (5):

$$g = \alpha + \sum_{i=1}^m \beta_i b_i, \quad (5)$$

where

- g is the objective function for calibration,
- α is the regression constant,
- β_i is the regression coefficient of the calibrated parameter, and
- b_i is the calibrated parameter.

The t-test was employed to identify whether a parameter b_i is significant or not in sensitivity analysis. According to the t-test method, each model parameter is ranked for its sensitivity level, based on the magnitudes of two indicators: t-stat and p-value. The t-stat is the coefficient of a parameter divided by its standard error, while the p-value measures the significance of the sensitivity. The larger the absolute values of the t-stat, and the smaller the p-values, the more sensitive the parameters are. A model parameter is determined to be significant in the sensitivity analysis if the p-value is smaller than 0.05. The t-test ends when the sensitivity levels of all calibrated model parameters are ranked based on the magnitudes of the t-stat and p-value.

3.3.3 Modelling chain for climate change impact assessment

In CC impact assessment, data on the projected climatological variables, e.g., precipitation and air temperature, are required. Such future climate data are usually obtained from climate models, which are described in the following sections.

3.3.3.1 Global climate models (GCMs)

Climate models were developed to investigate the responses of the climate system to numerous forcings. Several types of climate models have been developed for climate research, such as Atmosphere–Ocean General Circulation Models (AOGCMs), Earth System Models (ESMs) and Earth System Models of Intermediate Complexity (EMICs). The horizontal resolutions (grid spacing) of the current GCMs are from approx. 1 to 2 degrees (approx. 111 to 222 km) for the atmospheric component and approx. 1

degree (approx. 111 km) for the ocean component (Flato *et al.* 2013). Because the GCMs have coarse resolutions, they cannot provide detailed information of the changing climate at the regional scale or catchment scale for CC impacts' assessment. Thus, downscaling GCMs is usually carried out prior to transferring the climate simulation into the impact models (e.g., the hydrological models). The downscaling techniques are either statistical or dynamic downscaling. Of them, dynamic downscaling is normally performed through a regional climate model, which is discussed in the next section.

3.3.3.2 Regional climate models (RCMs)

RCMs are usually used for dynamic downscaling of the GCMs to provide more detailed information of the climate pattern in a particular region (Laprise 2008; Rummukainen 2010). While the GCMs provide the climate system for the whole world, the RCMs only present the climate processes for a limited region but with higher temporal-spatial resolution of climate information (Mearns *et al.* 2013). Currently, RCMs have grid spacing of approx. 0.22-0.44 degree (approx. 25-50 km) and six hours of time step (the highest temporal resolution). RCMs have boundary conditions based on GCMs' simulation. Therefore, the dynamic downscaling of the GCMs via the use of RCMs is also known as the nested RCMs approach.

It is noted that, in the scope of this study, downscaling of climate models was not performed, but the downscaling results from the EURO-CORDEX (Coordinated Downscaling Experiment for Europe) initiative project were inherited (Jacob *et al.* 2014). Thus, the above text aims to explain how future climate data are obtained.

3.3.3.3 Coupling climate models and hydrological SWAT model

Although most RCMs produce simulation results of the hydrological components, e.g., surface and subsurface runoff, the simulation results are usually not in agreement with the observed data (Teutschbein & Seibert 2010). As a result, the hydrological simulations yielded from the RCMs might not be used directly for hydrological impacts' assessment at the catchment scales (Bergstrom *et al.* 2001; Graham *et al.* 2007a; Graham *et al.* 2007b). Alternatively, the approach of coupling the RCM and the hydrological model is commonly preferred by scientists for CC impacts' assessment on hydrology and water resources at the catchment scale (Lawrence & Hisdal 2011; Meresa *et al.* 2016). According to this coupling method, the hydrological model is forced by climate inputs obtained from the ensemble RCMs_GCMs simulations. Thus, future change in the climate variables can be transferred to the hydrological model, to produce changes in future hydrological components at the catchment scale.

Figure 17 presents the modelling chain used in this study for hydrological CC impacts' assessment (e.g., projection of changes in future floods under CC). As can be seen in Figure 17, the sub-figures were taken from different sources: the graph of global emissions (van Vuuren *et al.* 2011); GCM (global scale, source: Irene Brox Nilsen, NVE); RCM (regional scale, source: <https://www.euro-cordex.net>); SWAT (source: <http://www.brc.tamus.edu/swat/>). The remaining sub-figures were created by the author.

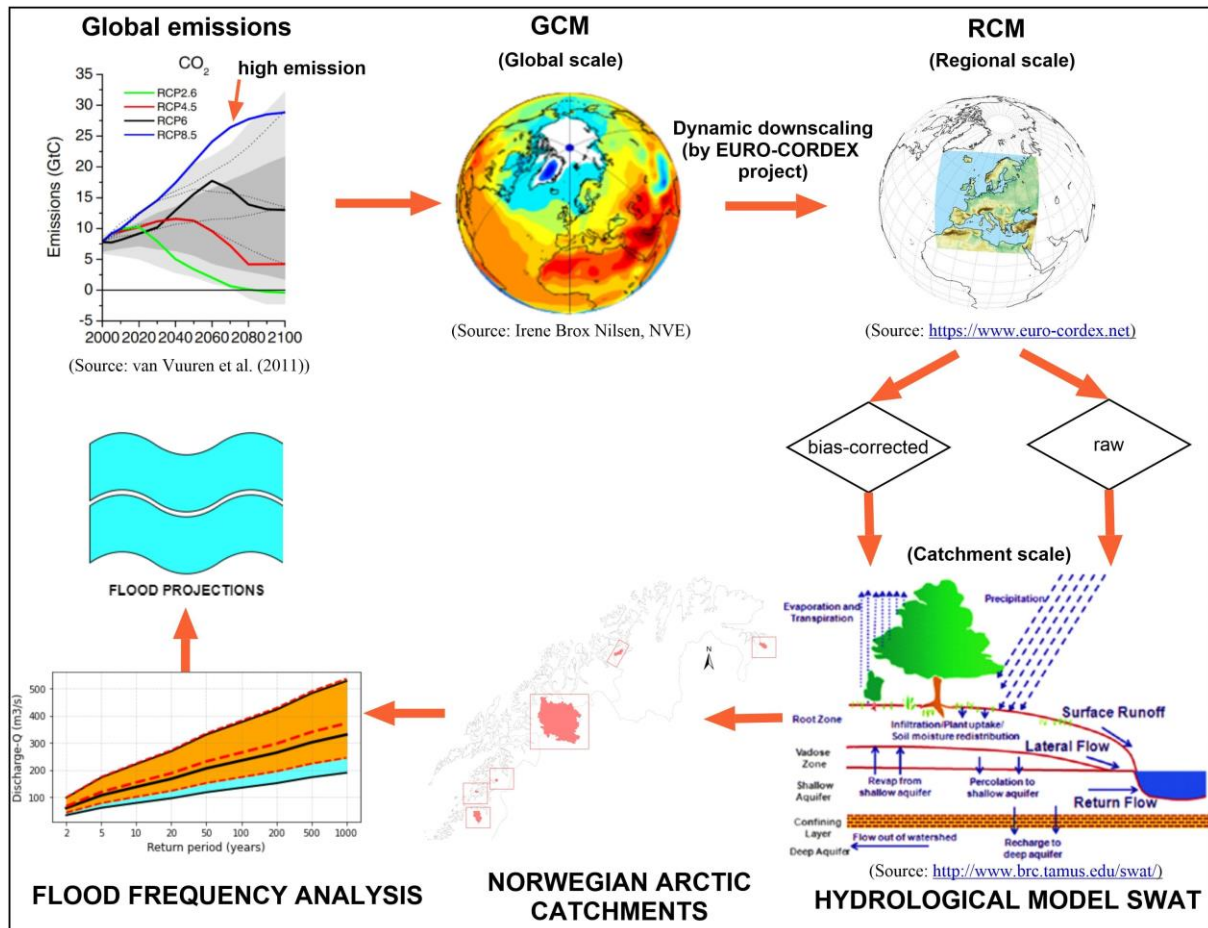


Figure 17 - Modelling chain for flood projections under global CC in the Norwegian Arctic catchments.

3.3.4 Evaluation of climate change impacts on future floods

CC is expected to alter the hydrological processes, especially changing the frequency and intensity of extreme events such as floods. An increase in the magnitude and frequency of floods due to CC has been observed (IPCC 2013; Quintero *et al.* 2018). Floods will cause severe damage to human life, infrastructures, the environment, ecosystem as well as to the socio-economic development of the affected areas (McGrath *et al.* 2015; Vinet 2017; Quintero *et al.* 2018). In order to mitigate the damage of floods, various measures have been developed in many countries, including constructing reservoirs for flood water storage or modifying land use structures in flood-prone areas, etc. (Engeland *et al.* 2020). To design those mitigation structures, it is normally required that the structures have enough capacity to withstand the magnitude of the design floods (or flood sizes, typically in $\text{m}^3 \text{s}^{-1}$) for a specific return period. For example, in Norway, a 200-year flood is commonly aimed at for flood hazard mapping, and the 500-year flood or 1000-year flood is used for dam-safety purposes (Wilson *et al.* 2011). In addition, in water resource management or in risk management, flood frequency analysis is considered a fundamental approach (Zhou *et al.* 2019). Furthermore, in numerous studies, the magnitude and frequency of floods are defined as two important indicators of the flood hazard index in flood risk assessment (Richter *et al.* 1996; Logsdon & Chaubey 2013; Xu *et al.* 2019b). Recently, several international studies stated that the magnitude and frequency of design floods, particularly extremely high floods, are being influenced by CC and land use change, among other impact factors (Rojas *et al.* 2013; Madsen *et al.* 2014; Alfieri *et al.* 2015; Mallakpour & Villarini 2015). Therefore, it is necessary to estimate changes in the future magnitude and frequency of floods under the CC context. In this study,

the impacts of CC on future flood magnitude and frequency are assessed. The results from the study can assist risk managers and water resource managers to design more resistant flood mitigation measures.

3.3.4.1 Flood magnitude and flood frequency analysis

Flood frequency analysis is the estimation of a flood's magnitude according to a given probability of occurrence or return period (Cunnane 1989; Wilson *et al.* 2011). Numerous statistical distribution models have been developed for flood frequency calculation at the specific locations, e.g., Log-normal, Gumbel (Generalized Extreme Value Type I-EV1), Generalized Extreme Value (GEV), Gamma, Log-Pearson, Gaussian Normal, Pareto, Weibull, etc. (Cunnane 1989; Wilson *et al.* 2011). According to practical application in the Norwegian catchments, the proper distribution models are normally either the Gumbel distribution (with two model parameters, i.e., location parameter and scale parameter) or the GEV (with three model parameters, i.e., location parameter, scale parameter and shape parameter) (Midttømme *et al.* 2011; Wilson *et al.* 2011). Nevertheless, for the short river discharge time series data from 30-50 years, the Gumbel distribution is preferred to the GEV distribution (Wilson *et al.* 2011). This is because the GEV distribution model has a high number of model parameters, which results in the high flexibility of the frequency curve (Cunnane 1985; Saelthun & Andersen 1986; Wilson *et al.* 2011). Moreover, it is difficult to estimate the shape parameter of the GEV distribution model because of short time series data. Thus, this could lead to high uncertainty in the estimation of extreme floods with a large return period (Odry & Arnaud 2017). Therefore, this study selected the Gumbel distribution to estimate flood frequency, based on each 30-year time series of the streamflow in the reference period (1976-2005) and the near future period (2041-2070). The procedure for flood frequency analysis in this study consists of the following steps:

1. Assemble and rank the maximum annual peak flows for the 30-year daily time series data, estimated from the SWAT model (using climate inputs of the ensemble GCM_RCMs simulations),
2. Calculate the annual exceedance probability (AEP) for each maximum annual peak flow (event) and its return period T ($T=1/AEP$). The formula for calculating AEP and T depends on the selected plotting position method. In this study, the Weibull method was applied (see Table 9, Equations (6) and (7)),
3. Plot the values of the annual peak flows corresponding to their AEP or T , yielded in step 2, on the graph as points,
4. Apply the statistical distribution model to develop the flood frequency curve to have the best fit with the plotting points of the annual peak flows in step 3. This study used the Gumbel distribution model. Estimation of the two parameters of the Gumbel model was based on the method of moments (MOM) (see Table 9, Equations (8) and (9)),
5. Based on the frequency curve, the values of the interested peak flows for the given return periods were interpolated/extrapolated from the frequency curve. This study examined the estimated peak flows for 2-, 5-, 10-, 20-, 50-, 100-, 200-, 500- and 1000-year return periods,
6. Apply the same procedure for each daily flow dataset in the reference period (1976-2005) and in the near future period (2041-2070), which were driven by five different ensemble GCM_RCMs, and for every six investigated Norwegian Arctic catchments.

Table 9 - Summary of all formulas used for flood frequency analysis.

Tasks	Formulas
	$AEP = \frac{m}{n+1} \quad (6)$
Weibull plotting position (Cunnane 1989; Wilson <i>et al.</i> 2011)	$T = \frac{1}{AEP} = \frac{n+1}{m} \quad (7)$
	where n: number of events m: rank of an event
Gumbel distribution model (Generalized Extreme Value Type I-EV1) (Gumbel 1941; Singh 1998)	
+ cumulative distribution function (CDF) (Singh 1998)	$F(x) = \exp[-e^{-y}] \quad (8)$
	where $y = a(x - b)$: reduced variate x: peak flow data $a > 0$: a concentration parameter $-\infty < b < x$: a parameter for measure of central tendency Parameters a and b were estimated in this study based on the most popular method of moments (MOM) (Lowery & Nash 1970; Landwehr <i>et al.</i> 1979; Singh 1998)
+ estimate the reduced variate y_t for a given return period T	$y_t = -\ln \left\{ \ln \left(\frac{T}{T-1} \right) \right\} \quad (9)$
	where $T = \frac{1}{1-F}$

3.3.4.2 Uncertainties analysis of the flood projection

Quantification of the uncertainties in flood projection is an indispensable procedure to minimize the over-estimated/under-estimated flood scenarios in strategies for flood mitigation measures (Wiltshire 1987; Wilson *et al.* 2011). This study addressed multiple uncertainty sources, which originated from the hydrological SWAT model, as well as the ensemble GCM_RCMs simulations, in the climate-hydrology modelling chain for flood estimations (i.e., magnitudes and frequencies of floods). Therefore, the estimated flood frequencies and magnitudes were provided, together with their uncertainties' envelopes. The SWAT_CUP program generated the estimated daily discharges, which were distributed in the 95PPU band/envelope. The flood frequencies and magnitudes were estimated based on discharge values at the median, lower limited (at 2.5%) and upper limited (at 97.5%) levels within the 95PPU band. Thus, all possible estimated flood values were provided in the 95PPU envelope. The uncertainties of the estimated floods in six Norwegian Arctic catchments with different geographical distributions, latitudes, scales and dominant flood regimes were quantified and compared together.

4 Results

4.1 RQ1 – The current capacities and challenges for hydrological modelling in the Arctic environment

4.1.1 Models' capacities

In Paper I, in total, twelve well-known models, which have recently been applied in the Arctic, were critically reviewed and evaluated regarding their competence to simulate hydrological processes in the Arctic environment. Such models were classified into two main groups: (1) surface hydrological models, i.e., Topoflow, DMHS (deterministic modelling hydrological system), HBV (Hydrologiska Byråns Vattenbalansavdelning), SWAT (soil and water assessment tool), WaSiM (water balance simulation model), ECOMAG (ecological model for applied geophysics) and CRHM (cold regions hydrological model); (2) subsurface hydrological models/groundwater models/cryo-hydrogeological models, i.e., ATS (Arctic terrestrial simulator), CryoGrid 3, GEOtop, SUTRA-ICE (ice variant of the existing saturated/unsaturated transport model) and PFLOTRAN-ICE (ice variant of the existing massively parallel subsurface flow and reactive transport model). As analysed in Paper I, the challenge for hydrological modelling in the Arctic is the models' capacity to deal with permafrost hydrology. In particular, in their structures, the models should be able to describe as many of the important processes in the permafrost environment as possible. According to these criteria, Paper I yielded the results presented in Table 10.

Table 10 - Capacities of each modelling tool to simulate the important processes in permafrost environments (results from Paper I).

Model	Important processes in permafrost environments considered in the model										
	(1)	(2)	(3)	(4)	(5)	(6)	(7)	(8)	(9)	(10)	(11)
Topoflow	✓	n/a	n/a	✓	✓	n/a	✓	✓	✓	n/a	n/a
DMHS	✓	✓	n/a	✓	✓	✓	✓	✓	✓	n/a	✓
HBV	✓	✓	✓	✓	✓	n/a	✓	n/a	✓	n/a	n/a
SWAT	✓	✓	n/a	✓	✓	n/a	✓	✓	✓	n/a	n/a
WaSiM	✓	✓	n/a	✓	✓	✓	✓	✓	✓	n/a	✓
ECOMAG	✓	✓	n/a	✓	✓	✓	✓	✓	✓	n/a	n/a
CRHM	✓	✓	n/a	✓	✓	✓	✓	✓	✓	n/a	n/a
ATS	✓	✓	✓	✓	✓	✓	✓	✓	✓	✓	✓
CryoGrid 3	✓	✓	✓	✓	✓	✓	✓	✓	✓	✓	✓
GEOtop	✓	✓	✓	✓	✓	✓	✓	✓	✓	✓	✓
SUTRA-ICE	n/a	n/a	n/a	n/a	✓	✓	✓	✓	✓	n/a	✓
PFLOTRAN-ICE	n/a	n/a	n/a	n/a	✓	✓	✓	✓	✓	n/a	✓

Note: (1) Surface energy balance; (2) snow process; (3) snow insulation; (4) snowmelt; (5) infiltration; (6) soil thermal; (7) soil moisture; (8) soil heterogeneities; (9) active layer thickness (ALT) dynamics; (10) subsidence; and (11) three-phase change of water during the freezing–thawing process in near-surface soils. The symbol ✓ denotes available, and the abbreviation n/a defines not available, unclear, or no information

4.1.2 Models' challenges

According to the results in Table 10, the lack of some important processes in the permafrost environment in the models' structures is the current challenge for such models to accurately simulate the hydrological processes in the Arctic. For example, many surface hydrological models do not include or do not present well the important processes which control the freezing–thawing process in soil, such as heat capacity,

thermo-dynamic equilibrium, ground surface temperature, and the three phase changes (ice, liquid, and gas) of water in near-surface soils. In addition, most surface hydrological models do not consider the effects of snow insulation on air-soil temperature relationships. The simplification of processes in the models' structures is a further limit. For example, many surface hydrological models use a simple equation (1D vertical direction) for heat transfer, which is not able to simulate the multidecadal and multidimensional changes of the freeze–thaw process. Although most surface hydrological models are able to simulate the ALT dynamics, their performances are still poor, e.g., Topoflow, HBV, SWAT, WaSiM models. The reason is that such models employ relatively simple or empirical methods, while the dynamics of the ALT constitute a complicated process. In brief, the capacity for highly accurate simulation of ground thermal processes, groundwater flow and the freezing–thawing process in soil is the current challenge for many surface hydrological models in the permafrost-dominated Arctic catchments. On the other hand, the cryo-hydrogeological models have a greater capacity to describe subsurface hydrology or the freezing–thawing process (excluding the SUTRA-ICE model) because they consider the three phase changes of water in near-surface soils. However, some cryo-hydrogeological models (e.g., the SUTRA-ICE and PFLOTRAN-ICE models) do not integrate land surface schemes in their model structures. In addition, most cryo-hydrogeological models are only applied in ideal conditions, and their applications are still limited in field conditions. Furthermore, cryo-hydrogeological models have complex boundary conditions, which means it is hard to gather enough inputs in data-spare regions like the Arctic. Lastly, cryo-hydrogeological models are difficult for non-expert users, and intensive computational processes are required.

4.2 RQ2 – Suitable hydrological models and verification of their performance for hydrological simulation/projection in the Arctic catchments

In Paper I, the suitability of each model for different application situations is evaluated, as presented in Table 11. Considering the complex hydrological processes and the data-sparse feature of the Arctic, the selection of suitable models should satisfy two main criteria: (1) the capability of the model to capture the unique permafrost hydrology and (2) the possibility of the models to be applied with moderate input data.

Table 11 - Recommended model candidates for use in the Arctic region (results from Paper I).

Model	Surface hydrology	Subsurface hydrology	ALT dynamics	Catchment sizes		Moderate input requirement
				Small	Large	
Topoflow	✓			✓		
DMHS	✓	✓	✓	✓	✓	
HBV	✓			✓	✓	✓
SWAT	✓			✓	✓	✓
WaSiM	✓	✓		✓	✓	
ECOMAG	✓			✓	✓	
CRHM	✓			✓	✓	✓
ATS	✓	✓	✓	✓	✓	
CryoGrid 3		✓		✓	✓	
GEOtop	✓	✓	✓	✓		
SUTRA-ICE		✓		✓		
PFLOTRAN-ICE		✓	✓	✓		

Firstly, if the goal of a study is to only focus on surface hydrology, Topoflow, HBV, SWAT, ECOMAG, and CRHM could be the options. Of these, the conceptual model, HBV, and the semi-distributed models,

SWAT and CRHM, are more suitable for catchments with a moderate input requirement. On the other hand, the distributed models, Topoflow and ECOMAG, require intensive input data. Secondly, if the high accuracy of subsurface hydrology is weighted, DMHS, WaSiM and the cryo-hydrogeology models are the optimal selections, since they consider the three phase changes of water (i.e., ice, liquid and gas) during the freezing–thawing process of near-surface soils. However, GEOTop, SUTRA-ICE and PFLOTRAN-ICE can only be applied in the small-scale study areas, while ATS and CryoGrid 3 are able to run in large catchments. Thirdly, if accurate simulation of ALT dynamics is required, DMHS, ATS, GEOTop and PFLOTRAN-ICE are highly recommended, compared to other models. Finally, the selection of suitable hydrological models for the Arctic environment still depends on several other factors such as models' ease-of-use, available inputs, the required research period and funding conditions, besides the models' capacity to accurately simulate the hydrological processes in the permafrost environment.

Although, in Paper I, the model candidates for different situations of applications were suggested, from Paper II to Paper IV, the scope of the study was narrowed to surface hydrological models, as the simulation and projection of surface hydrology (including streamflow and floods) are the main targets of those papers. Herein, the SWAT was chosen, among other suitable models, in consideration of its considerable capacity to simulate the hydrological processes in large and complex catchments under anthropogenic and CC impacts. In addition, the SWAT has been demonstrated to be a well-known model with numerous applications around the world. However, applications of the SWAT model are still limited in the Arctic. Thus, further application of the SWAT in this specific region should be conducted, to verify the model's competence. Verification of the SWAT performance (results from Papers II to IV) is discussed in the following sections.

4.2.1 Verification of the model candidate's performances

The SWAT model was selected as a suitable candidate, among others, for hydrological modelling in the Norwegian Arctic catchments in this study. Performance of the SWAT was verified from Papers II to IV, for different Norwegian Arctic catchments with variations in geographical distributions, latitudes, catchments' scales and hydrological regimes. Different temporal resolutions for running the model, such as monthly (in Papers II and III) and daily (in Paper IV), were performed. The model's performance was measured based on the statistical coefficients, which were integrated from Paper II to Paper IV and summarized in Table 12 and Table 13.

Table 12 - Performances of the SWAT for hydrological simulation in the small-scale Norwegian Arctic catchments (results from Paper IV).

Catchments	Gauging stations	Area (km ²)	Hydrological regimes	R ²	NSE	RSR	Performance
							Calibration (1998-2007)
Lakselva	Skarsvatn	297	Mixed rainfall/snowmelt	0.65	0.57	0.66	Satisfactory
Strandvassbotn	Strandå	26	Rainfall	0.60	0.51	0.70	Satisfactory
Marsvikelva	Mørsvik bru	32	Rainfall	0.69	0.65	0.59	Good
Halselva	Halsnes	143	Snowmelt	0.63	0.62	0.61	Good
Karpelva	Karpelva	129	Snowmelt	0.72	0.71	0.54	Good
Validation (1980s-2005)							
Lakselva	Skarsvatn	297	Mixed rainfall/snowmelt	0.67	0.60	0.63	Good (1984-2005)
Strandvassbotn	Strandå	26	Rainfall	0.54	0.42	0.76	Satisfactory (1981-2005)
Marsvikelva	Mørsvik bru	32	Rainfall	0.71	0.66	0.58	Good (1986-2005)
Halselva	Halsnes	143	Snowmelt	0.65	0.63	0.61	Good (1981-2005)
Karpelva	Karpelva	129	Snowmelt	0.73	0.71	0.53	Good (1985-2005)

Table 13 - Performances of the SWAT for hydrological simulation in the large-scale, snowmelt-dominated Norwegian Arctic catchment Målselv (results from Papers II to IV).

Gauging stations	R ²		NSE		RSR		Performance rating	
	Monthly	Daily	Monthly	Daily	Monthly	Daily	Monthly	Daily
Calibration (1998-2007)								
Lundberg	0.73	0.58	0.69	0.55	0.56	0.67	Good	Satisfactory
Lille Rostavatn	0.79	0.76	0.67	0.64	0.58	0.60	Good	Good
Høgskarhus	0.74	0.64	0.65	0.62	0.59	0.62	Good	Good
Skogly	0.77	0.65	0.77	0.50	0.48	0.71	Very good	Satisfactory
Målselvfossen	0.85	0.61	0.82	0.60	0.42	0.63	Very good	Good
Validation (2008-2012)								
Lundberg	0.81	0.45	0.77	0.34	0.48	0.81	Very good	Unsatisfactory
Lille Rostavatn	0.91	0.74	0.66	0.55	0.58	0.67	Good	Satisfactory
Høgskarhus	0.73	0.56	0.59	0.56	0.64	0.67	Satisfactory	Satisfactory
Skogly	0.87	0.67	0.82	0.63	0.42	0.61	Very good	Good
Målselvfossen	0.88	0.70	0.83	0.69	0.41	0.55	Very good	Good
Validation (1981-2005)								
Lundberg		0.58		0.54		0.68		Satisfactory
Lille Rostavatn		0.82		0.74		0.51		Good
Høgskarhus		0.64		0.57		0.66		Satisfactory
Skogly		0.66		0.37		0.79		Satisfactory
Målselvfossen		0.69		0.64		0.60		Good

In general, the SWAT model demonstrated its capacity to simulate surface hydrology in the Arctic environment, but its performance varied from catchment to catchment. Although the statistical coefficients revealed little difference between the model's performance in large-scale and small-scale catchments, the variation in streamflow hydrographs was more clearly captured between simulated and observed data for large-scale catchments than for small-scale catchments (results from Paper IV, supplementary material). This could be because weather inputs from both ground-based weather stations and global reanalysis weather grids were outside the small-scale catchments' boundaries, to some extent. In addition, spatial resolutions of soil and land use were not high for the small-scale catchments and, thus, the catchments' characteristics may not be described well. Considering the different hydrological regimes of the catchments, the SWAT performed better for snowmelt-dominated catchments than for rainfall-dominated catchments. When the effect of the geographical distribution of the catchments is analysed, the performance of the SWAT in catchments near the coastal zone was lower than in the inland catchments. This was explained by the high variation of rainfall and river discharge in the coastal areas, and that the model needed greater efforts to capture such high fluctuations in the natural phenomenon. Furthermore, the model's performance varied among hydro-gauging stations of the large-scale catchment, e.g., Målselv. This demonstrated high fluctuations in local climate features, as well as in characteristics of the Norwegian Arctic catchments. Thus, it is suggested from this study that the requirement for high resolution of weather inputs, as well as other spatial data such as topography, land use and soil, is important for hydrological simulation in the Arctic catchments.

Besides testing the model's performance for individual catchments, the transferability of model parameters between catchments was also examined, particularly in Paper IV. The outcomes from Paper IV revealed the high capacity to exchange model parameters between the donor and the recipient catchments (Table 14). This could open the door to transferring model parameters between gauged and ungauged catchments in the data-sparse Arctic regions. Exceptionally, model performance in the rainfall-dominated catchment (i.e., Strandvassbotn) near the coast was somewhat lower than the satisfactory threshold when it received model parameters from the donor catchment, Marsvikelva. Thus, greater effort is required to calibrate the catchment with the high variation in the rainfall regime.

Table 14 - Transferability of the calibrated model parameters (validation for the period of 2008-2012) in the Norwegian Arctic catchments (results from Paper IV).

Recipient catchments	Gauging stations	Donor catchments	Sub-basin	R ²	NSE	RSR	P-factor	r-factor	Performance rating
Altavassdraget		Målselv							
	Hammeren		1308	0.71	0.69	0.56	0.58	0.72	Good
	Suohpatjohka		1318	0.67	0.65	0.59	0.75	1.05	Good
	Masi		1350	0.69	0.66	0.58	0.77	0.78	Good
	Kista		1370	0.68	0.67	0.58	0.70	0.85	Good
Karpelva	Karpelva	Halselva	26	0.48	0.46	0.73	0.91	0.86	Satisfactory
Halselva	Halsnes	Karpelva	34	0.71	0.69	0.56	0.97	1.45	Good
Marsvikelva	Mørsvik bru	Strandvassbotn	26	0.68	0.65	0.59	0.63	1.22	Good
Strandvassbotn	Strandå	Marsvikelva	21	0.45	0.35	0.81	0.56	0.37	Unsatisfactory

4.2.2 Uncertainties of the modelling results

Uncertainty analysis is an indispensable procedure in the modelling task. SWAT has demonstrated its strength to fulfil the requirement of the current modelling philosophy, i.e., the transparency of the model. This means that uncertainties in the modelling results were analysed during calibration and validation processes. According to this concept, not only are good modelling results based on the measured statistical coefficients, but the reliability of the simulated results is also measured. The results of uncertainty analyses, which were performed from Papers II to IV, are summarized in Table 15 and Table 16. According to Table 15 and Table 16, the capacity of the SWAT model to bracket the observed river flow data inside the 95PPU band was somewhat greater for monthly than daily simulation. In addition, the accuracy of the simulation results in the rainfall-dominated catchments and catchments close to the coast was lower than that of the snowmelt-dominated and inland catchments. Moreover, the thicknesses of the 95PPU bands were quite narrow for most of the investigated catchments. This indicated that the uncertainties of the SWAT models were low or that the modelling results were highly reliable.

Table 15 - Uncertainties analysis of SWAT modelling in the large-scale, snowmelt-dominated Norwegian Arctic catchment Målselv (results from Papers II to IV).

Gauging stations	p-factor			r-factor		
	Monthly	Optimal	Daily	Monthly	Optimal	Daily
Calibration (1998-2007)						
Lundberg	0.88		0.56	1.08		0.70
Lille Rostavatn	0.75		0.69	0.95		0.60
Høgskarhus	0.80	> 0.70	0.56	1.10	< 1.50	0.82
Skogly	0.98		0.73	1.59		1.15
Målselvfossen	0.94		0.69	1.57		0.95
Validation (2008-2012)						
Lundberg	0.90		0.65	1.00		0.71
Lille Rostavatn	0.72		0.75	0.89		0.58
Høgskarhus	0.80	> 0.70	0.64	1.24	< 1.50	0.83
Skogly	0.95		0.81	1.47		1.09
Målselvfossen	0.91		0.80	1.58		1.00
Validation (1981-2005)						
Lundberg			0.52			0.72
Lille Rostavatn			0.74			0.60
Høgskarhus		> 0.70	0.43		< 1.50	0.86
Skogly			0.67			1.15
Målselvfossen			0.66			0.96

Table 16 - Uncertainties analysis of SWAT modelling in the small-scale Norwegian Arctic catchments (results from Paper IV).

Catchments	Gauging stations	p-factor		r-factor		Time slice
		Optimal	Daily	Optimal	Daily	
Calibration						1998-2007
Lakselva	Skarsvatn		0.77		1.71	
Strandvassbotn	Strandå		0.55		0.45	
Marsvikelva	Mørsvik bru	> 0.70	0.79	< 1.50	1.12	
Halselva	Halsnes		0.82		1.26	
Karpelva	Karpelva		0.94		1.08	
Validation						
Lakselva	Skarsvatn		0.77		1.64	1984-2005
Strandvassbotn	Strandå		0.48		0.43	1981-2005
Marsvikelva	Mørsvik bru	> 0.70	0.83	< 1.50	1.22	1986-2005
Halselva	Halsnes		0.89		1.21	1981-2005
Karpelva	Karpelva		0.92		1.08	1985-2005

In brief, outcomes from Papers II to IV demonstrate that the model candidate SWAT has the capacity to simulate well the surface hydrology in the investigated Norwegian Arctic catchments. Moreover, the calibrated model parameters could be exchanged between catchments which have geographical proximity and hydrological similarity. Thus, it could be concluded that the SWAT is a potential candidate for the simulation and projection of surface hydrology in the Arctic environment. However, to achieve reliable simulation results in the Arctic environment, it is suggested that good quality input data should be gathered.

4.3 RQ3 – Potential for using reanalysis climate products to run the hydrological models in the data-sparse Arctic region

In Paper II, the performance of a high-resolution reanalysis climate product, namely, Climate Forecast System Reanalysis (CFSR), was evaluated and compared with the existing scattered ground-based weather data. In particular, the performance of the CFSR data was verified in various ways regarding its capacity to drive the hydrological model SWAT for the simulation of water balance components and streamflow, as well as the reliability/uncertainty of the modelling results. The results showed that CFSR data was a potential source for running the hydrological model in the investigated Målselv catchment in the Norwegian Arctic. The following sections will present in detail the performance of CFSR data for the simulation of water balance components and streamflow, as well as uncertainties in the modelling results.

4.3.1 The simulated water balance components

Rainfall is the major input of water balance components. According to results from Paper II, the CFSR dataset generated higher spatial variation in areal rainfall across the investigated Norwegian Arctic catchment Målselv than the scattered ground-based dataset. The more uniform areal rainfall, presented by the scattered ground-based dataset, may not describe well the high variation in local climate conditions in the Arctic environment. Also, the total rainfall amount from the CFSR dataset was higher (approx. 24%) than that from the ground-based dataset for the investigated catchment. In addition, approx. 88% of the watershed area has a rainfall ratio between ground-based data and CFSR data of less than 1.0 (Figure 18). Thus, the simulation results of some water balance components (i.e., rainfall, actual evapotranspiration (ET), surface runoff (SUR_Q), lateral flow (LAT_Q), percolation (PERC), groundwater flow (GW_Q) and WYLD) obtained from the CFSR data were higher than those obtained from the ground-based data (Table 17).

Table 17 - Comparison of the simulated water balance components.

Weather dataset		Rainfall	ET	SUR_Q	LAT_Q	PERC	GW_Q	WYLD
Ground-based	(mm)	915.2	144.8	286.7	92.5	282.2	255.3	740.8
	(%)	100	15.8	31.3	10.1	30.8	27.9	80.9
CFSR	(mm)	1192	170.8	286.5	391.1	310.5	127.5	834.9
	(%)	100	14.3	24.0	32.8	26.0	10.7	70.0
Ground-based/CFSR difference	(mm)	-276.7	-26.0	0.2	-298.6	-28.3	127.9	-94.1
	(%)	-23.2	-15.2	0.1	-76.4	-9.1	100.3	-11.3

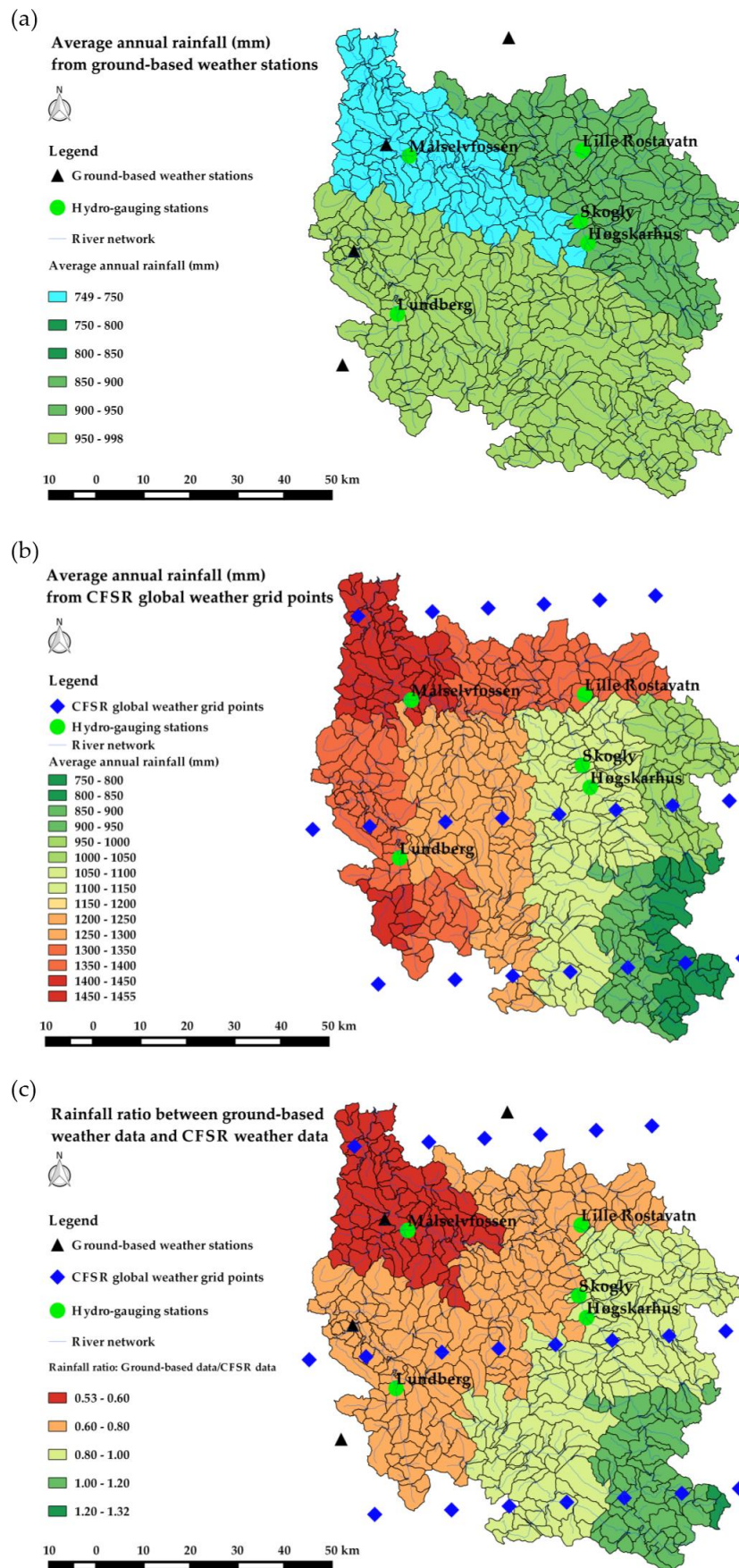


Figure 18 - Deviation between rainfall sources from CFSR and ground-based data for running hydrological model in the Norwegian Arctic catchment Målselv (results from Paper II).

4.3.2 The simulated streamflow

The performance of CFSR data for the simulation of monthly streamflow at the Norwegian Arctic catchment Målselv was examined in Paper II. It was found that the CFSR demonstrated its considerable capacity to replicate the monthly streamflow hydrograph, in terms of the timing and magnitude of peak and low flow (Figure 19), as well as the long-term average monthly streamflow (Figure 20).

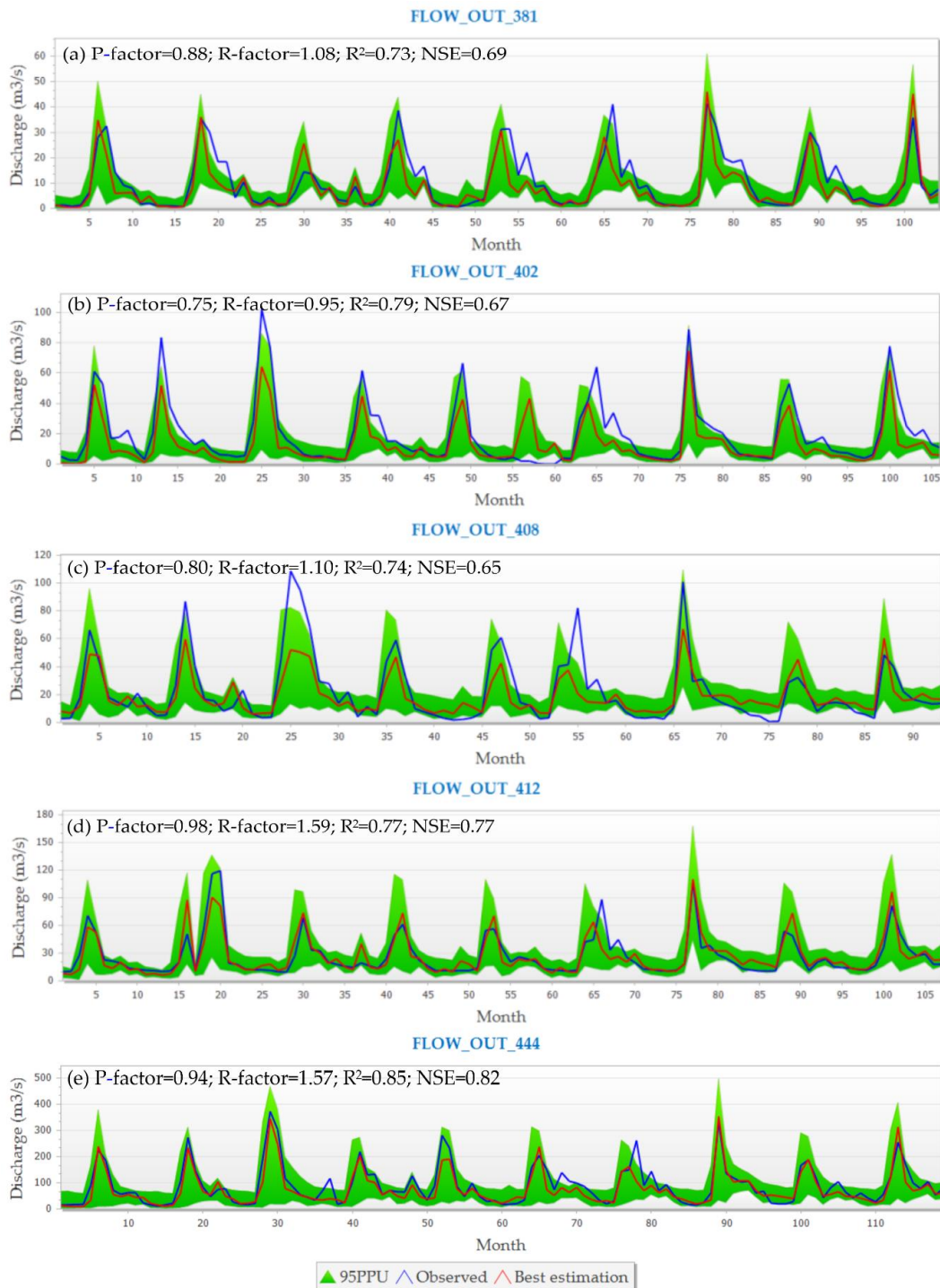


Figure 19 - Monthly streamflow simulation with CFSR data after calibration (1998-2007): (a) at Lundberg; (b) at Lille Rostavatn; (c) at Høgskarhus; (d) at Skogly; and (e) at Målselvfossen hydro-gauging station of Målselv catchment (results from Paper II).

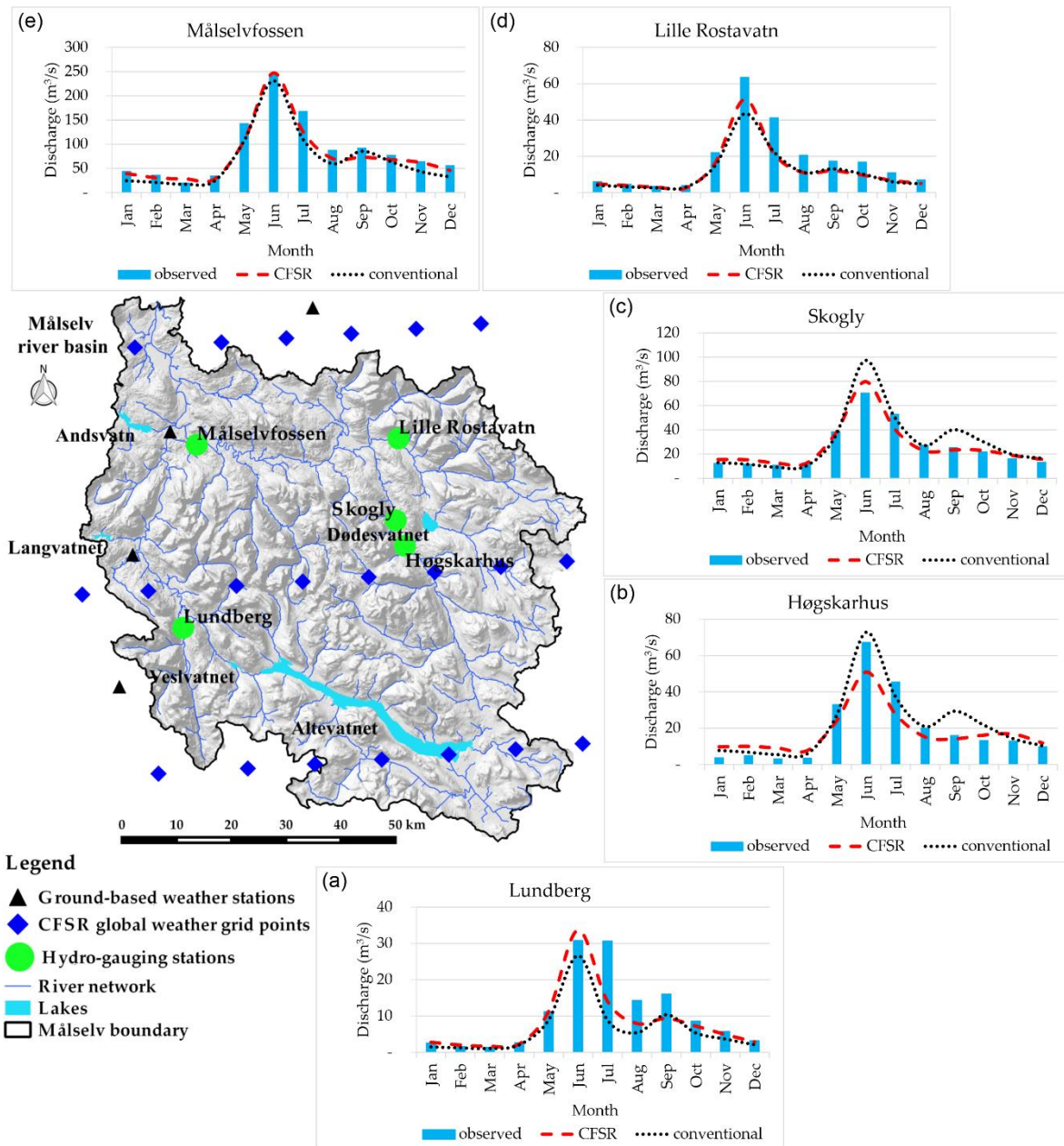


Figure 20 - Long-term average monthly streamflow (in m^3/s) during 1998-2007, generated from observed data and simulation with ground-based weather data and CFSR weather data (results from Paper II).

Moreover, Paper II revealed that the lack of representative ground-based weather stations for the sub-basins around the upstream hydro-gauging stations (e.g., Lundberg, Skogly, and Høgskarhus) resulted in somewhat inconsistent modelling results between the driven ground-based dataset and the CFSR dataset. In contrast, the simulated monthly streamflow in the downstream stations (e.g., Lille Rostavatn and Målselvfossen) was consistent between two driven datasets. This is because ground-based weather stations exist in the downstream sections but are lacking in the upstream sections. Therefore, this explained the limitation of the existing scattered ground-based weather data for running a hydrological model in the Arctic catchments, while the high-resolution CFSR dataset could fill the existing gap in the ground-based dataset. Results from Paper II opened the door to further applications of the CFSR dataset in Papers III and IV.

In Paper III, the CFSR was used to run the SWAT model in the same study area, as well as for the same temporal resolution (i.e., monthly simulation) as in Paper II. According to results from Paper III, the

CFSR demonstrated its performance in driving the SWAT models for monthly hydrological simulations under different scenarios of catchment subdivision scales, while, in Paper IV, the CFSR dataset was used to drive the hydrological SWAT model in different catchments with variations in geographical distributions, latitudes, scales and hydrological regimes. The temporal resolution for running the models was finer, i.e., simulation with daily time steps. The results from Paper IV revealed that the SWAT model performed well in the daily streamflow simulation with the CFSR data inputs (Table 12 and Table 13). However, compared to monthly simulation, the performance of daily simulation (i.e., based on statistical coefficients) was somewhat lower, e.g., the simulation results of the Målselv catchment (Table 13).

4.3.3 Uncertainties of the modelling results

In Paper II, uncertainties of monthly streamflow simulation when using the CFSR data and the existing scattered ground-based data were quantified, based on two statistical measures, i.e., p-factor and r-factor. According to the outcomes of uncertainties' analysis, the accuracy of modelling results (after calibration and validation) when using the high-resolution CFSR data was higher than that when using the existing scattered ground-based data (Figure 21).

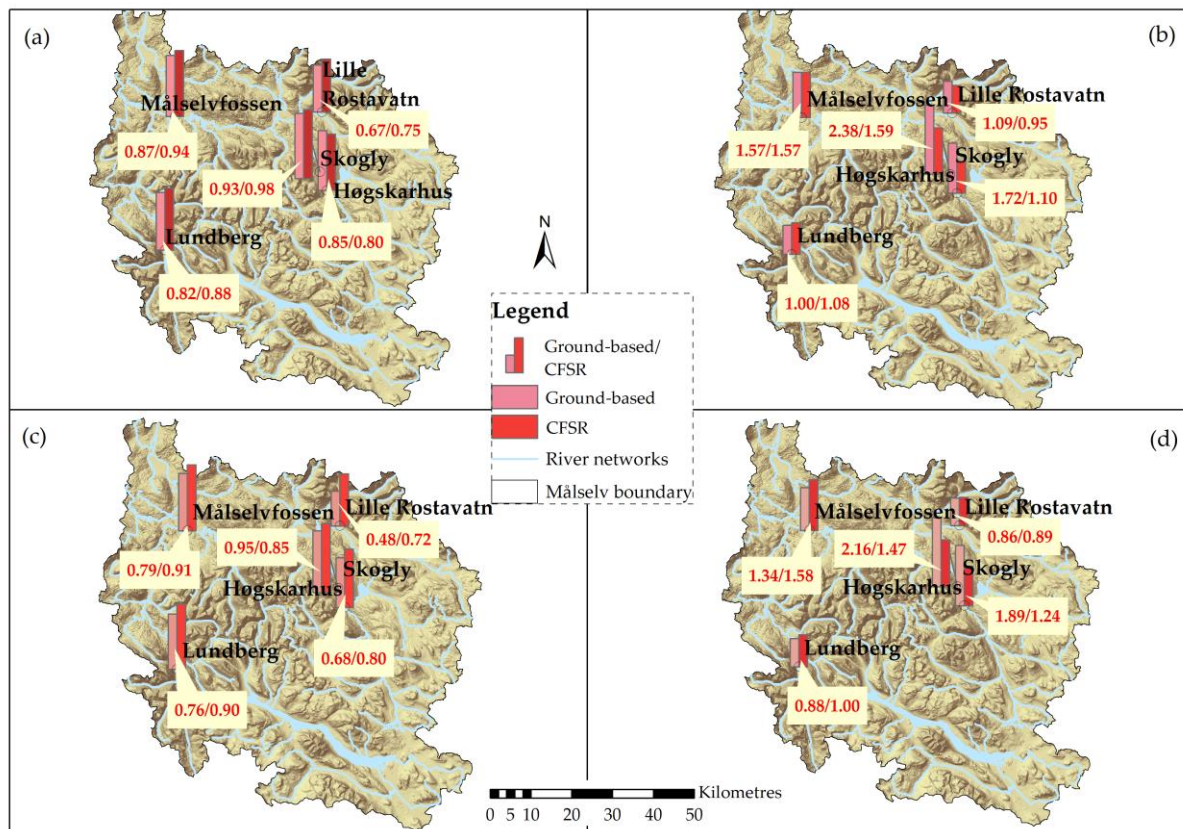


Figure 21 - Uncertainty analysis for monthly streamflow simulation: (a) p-factors for calibration period; (b) r-factors for calibration period; (c) p-factors for validation period; and (d) r-factors for validation period (results from Paper II).

In Paper III, the reliability of using the CFSR to drive the SWAT model was additionally proved. It was found that uncertainties of the monthly simulated streamflow fluctuated among TDA schemes as well as among hydro-gauging stations within the Målselv catchment. However, the CFSR still demonstrated its reliability according to the results of two indicators, i.e., p-factor and r-factor. Furthermore, uncertainties of the daily streamflow simulation when using the CFSR data were further verified in Paper

IV. Noticeably, the accuracy of simulated streamflow at daily time steps was somewhat lower than that at monthly time steps, and the level of uncertainties varied from catchment to catchment (Table 15 and Table 16).

In general, outcomes from Papers II to IV answered RQ3 of this thesis. The reanalysis product, CFSR, was a reliable source to drive the hydrological SWAT model in the investigated Norwegian Arctic catchments. The CFSR data could be an alternative source for running the hydrological model in the case of the monitoring network being scattered and unable to present well the high level of variation in climate conditions in the Arctic catchments.

4.4 RQ4 – The effect of hydrological models (e.g., structures and parameterizations) and quality of weather inputs (e.g., spatial resolution) on the simulation results

Normally, prior to using the hydrological model for impacts' assessment scenarios, e.g., the impacts of CC, the model is firstly set up and well calibrated. The ways to set up the model and the quality of input data could affect the modelling results. Paper III studied such problems by investigating the influences of different solutions for catchment delineation and spatial density of weather input on hydrological simulations such as water balance components, snowmelt runoff volume and streamflow. The SWAT model was applied in the same study area as in Paper II, i.e., the Målselv catchment. The reanalysis weather data, i.e., the CFSR, was further applied in Paper III after its performance was verified in Paper II. The TDA technique for catchment subdivisions was applied in Paper III. In particular, four different TDA schemes, from the finest to the coarsest scheme, i.e., 200 ha, 2000 ha, 5000 ha and 10000 ha, were developed (Figure 22). Discretization of the catchment by using different TDAs resulted in changes in model structure (e.g., number and size of sub-basins, land use components, terrain and topographic attributes) and model parameters (in the calibration process), as well as in the integrated weather grids. As a result, changes in the hydrological simulation results could be expected to be due to such changes.

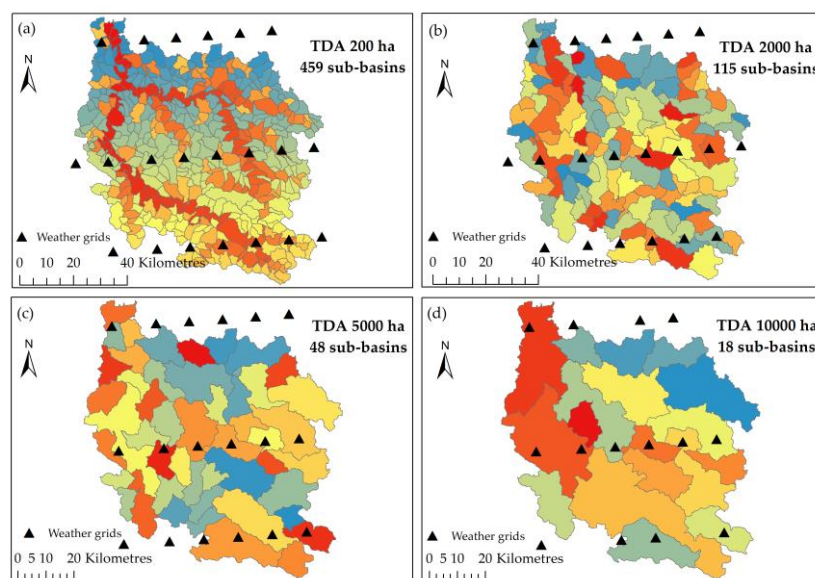


Figure 22 - The changes in number of sub-basins and integrated weather grids by changes in TDA schemes (results from Paper III).

The results from Paper III revealed that complexity of terrain and topographic attributes were significantly altered when TDA schemes changed from the fine level to the coarse level, including: (1)

total stream length ((-47.2%) – (-74.6%)); (2) average stream slope ((-68%) – (-83%)); and (3) drainage density ((-24.2%) – (-51.5%)). Furthermore, using different TDA schemes resulted in different numbers of integrated weather grids. This is because the SWAT model picks up the weather grid point (of the input weather grids), which is representative of each sub-basin, based on the nearest neighbour search (NNS) method. Figure 22 demonstrates that the number of weather grids declined from 21 grids in TDA 200 ha to 20 grids (-5%), 18 grids (-14.3%) and 14 grids (-33.33%) in TDA 2000 ha, 5000 ha and 10000 ha, respectively. The changes in the complex level of terrain and topographic attributes, as well as density of weather input, were expected to influence the results of the hydrological simulations.

4.4.1 The changes in the simulation results of water balance components

According to Paper III, when TDA schemes increased from 200 ha to 10000 ha, the simulation results of water balance components changed. For example, the annual mean rainfall, surface runoff and water yield increased, while PET (potential evapotranspiration), ET and lateral flow decreased. However, the magnitude of the increase/decrease patterns was not significant (Figure 23).

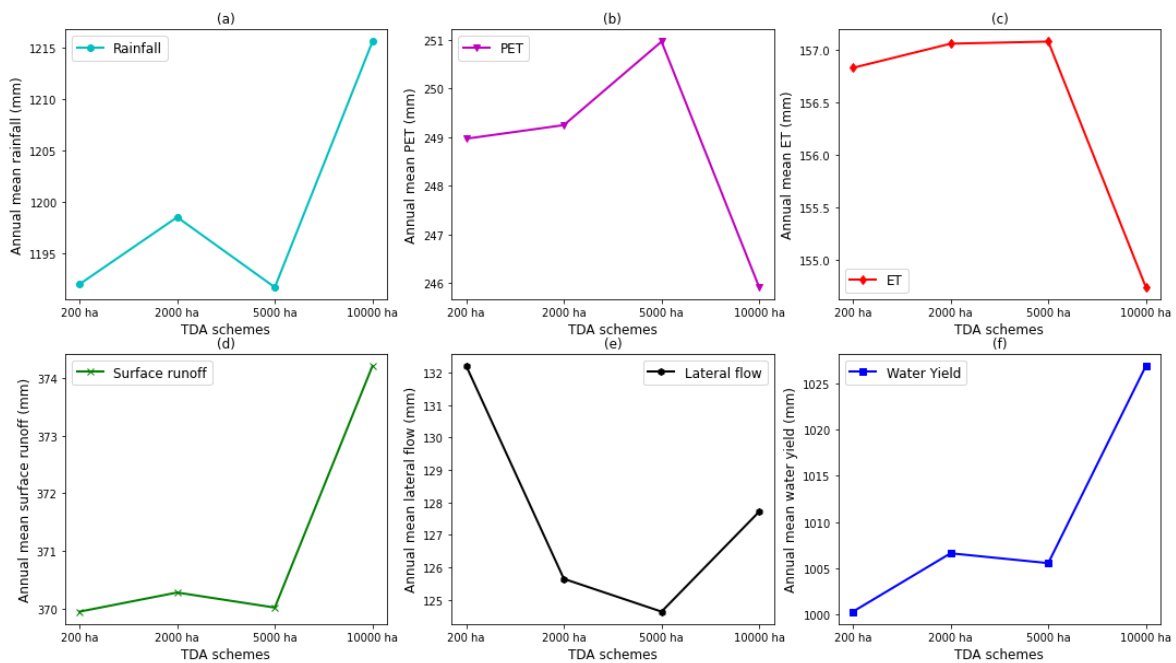


Figure 23 - The changes in annual mean values of some water balance components in Målselv catchment by changes in TDA schemes (results from Paper III).

In addition, the finer TDA schemes generated higher spatial variation of water components across the catchment. Thus, hotspots (e.g., locations with extremely high/low values in comparison to the surrounding areas) of water balance components were identified more clearly in the finer schemes than in the coarser schemes.

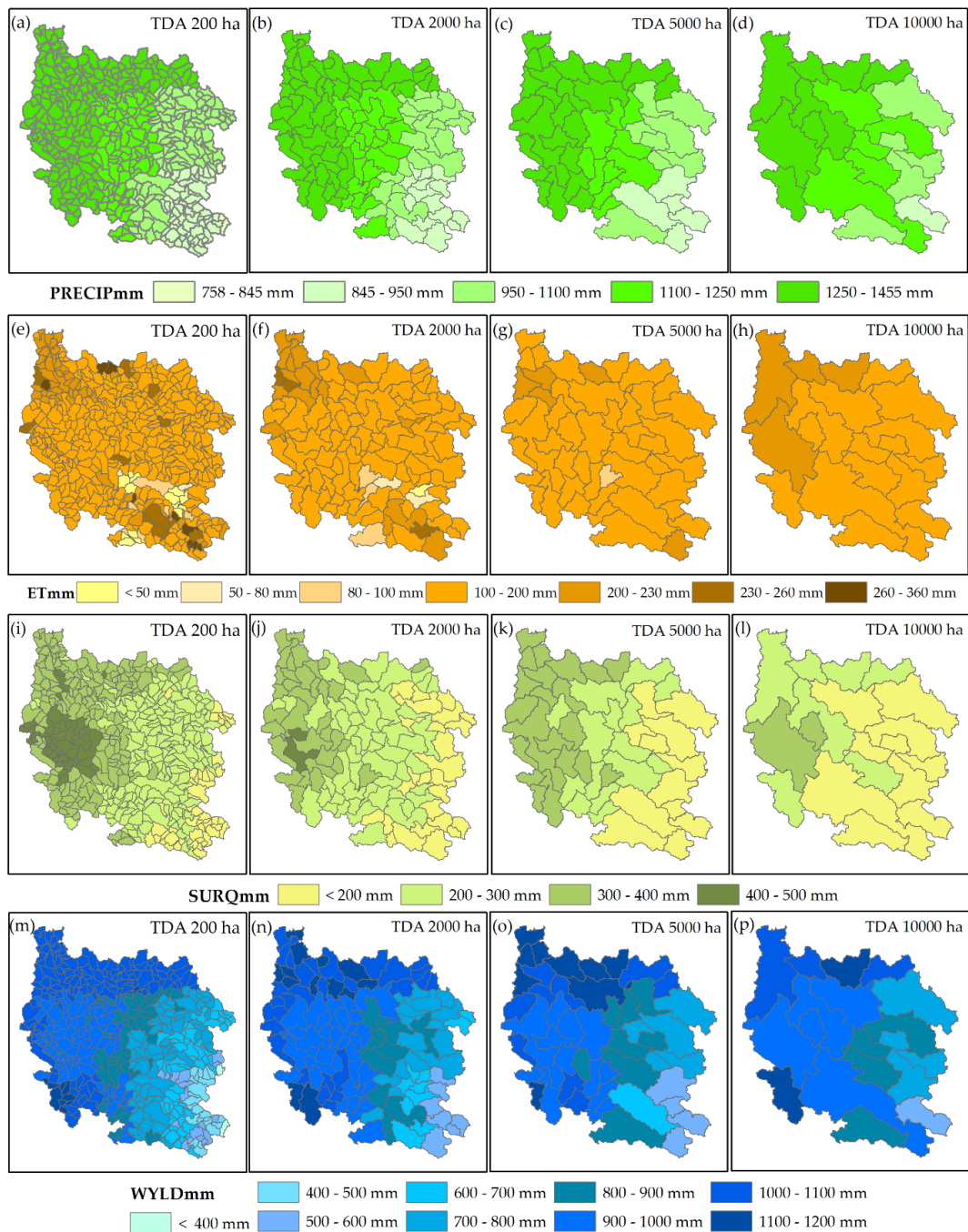


Figure 24 - The changes in spatial variation of annual mean values of some water balance components across the Målselv catchment by changes in TDA schemes: precipitation-*PRECIP* (a-d); actual evapotranspiration-*ET* (e-h); surface runoff-*SURQ* (i-l); and water yield-*WYLD* (m-p) (results from Paper III).

4.4.2 The changes in the simulation results of snowmelt runoff volume

The four different TDA schemes had a consensus in their identification of locations with high or low simulated snowmelt runoff volume across the catchment (Figure 25). However, the maximum/minimum values of the simulated snowmelt runoff volume, as well as the impacted areas due to the simulated snowmelt, differed somewhat among TDA schemes. In general, the fine TDA schemes generated finer and higher ranges of simulated snowmelt runoff volume throughout the catchment.

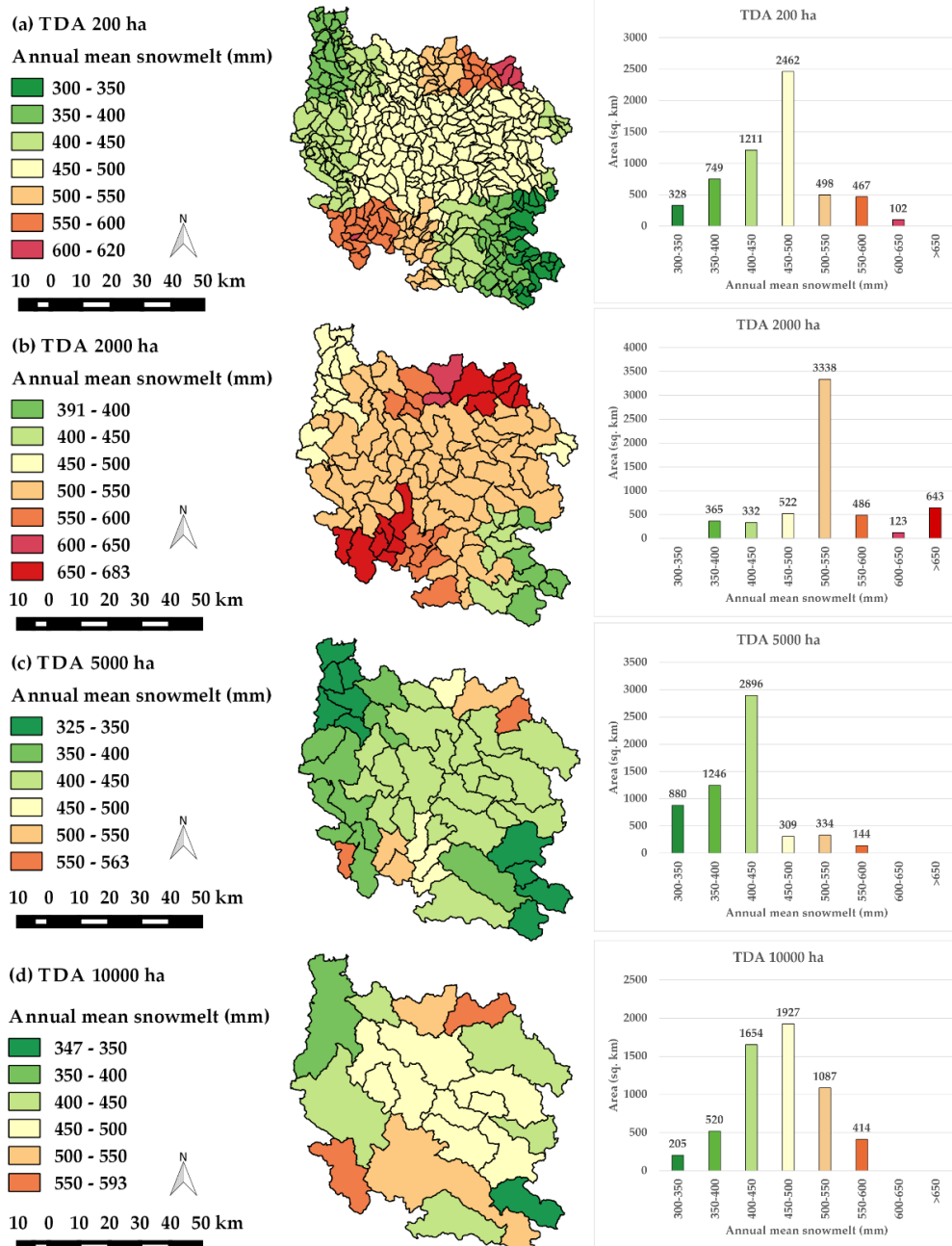


Figure 25 - The changes in spatial variation of simulated annual mean snowmelt runoff volume (1998-2007) across the Målselv catchment by changes in TDA schemes (results from Paper III).

4.4.3 The changes in the simulation results of streamflow

In general, changing the TDA schemes did not significantly impact the capacity of the SWAT model to replicate the observed tendency of the monthly mean streamflow hydrograph at all five hydro-gauging stations within the Målselv catchment. The only differences among the designed TDAs were found in the simulated monthly mean peak flow (Figure 26). Herein, the accuracy of the simulated monthly mean peak flow was heterogeneous among the TDA schemes, as well as among five hydro-gauging stations across the catchment. This explained that factors other than the designed TDAs also affected the simulation streamflow results. Such factors could be the influence of the complexity of hydrological processes and topographic characteristics in the Arctic catchment.

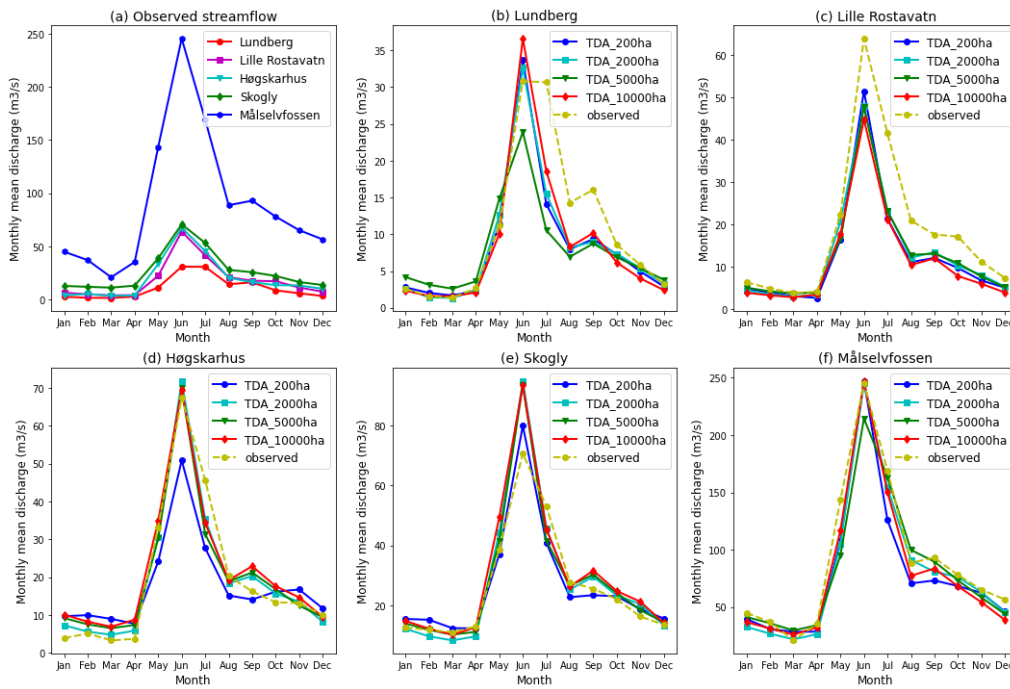


Figure 26 - The changes in monthly mean streamflow (1998-2007) at five hydro-gauging stations within the Målselv catchment by changes in TDA schemes (results from Paper III).

Moreover, applying different resolutions of TDAs resulted in discrepancies in the spatial variation in annual mean streamflows across the catchment (Figure 27).

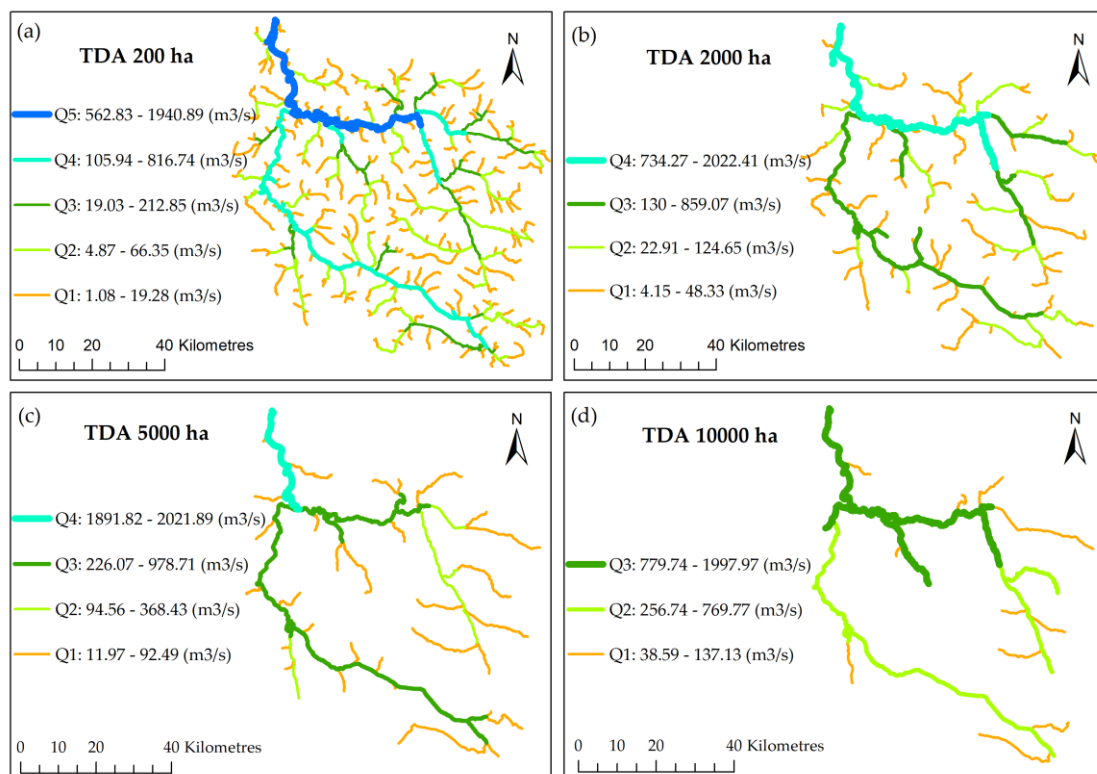


Figure 27 - The changes in stream order levels and spatial variation of annual mean streamflow (1998-2007) in the Målselv catchment by changes in TDA schemes. Q1-Q5 denote streamflows in stream order levels from 1 to 5, respectively (results from Paper III).

The fine TDAs generated higher levels of stream order. Thus, streamflow information could be exposed at minor stream levels under fine TDAs, while the coarse TDAs only presented streamflow data at the major stream levels. Simplification of stream networks may lose some important in-stream processes. Moreover, ignoring minor streams and their flow data may influence flood risk analysis at the sub-basin level. However, the minor stream networks may not be realistic and may not exist on the ground. In short, using different subdivision scales of the catchment might affect water resources management by zones' subdivisions. Depending on the goals of different projects, the designed levels of catchment subdivision might change. Findings from Paper III formed the basis for the selection of TDA schemes in Paper IV. In particular, the fine TDA schemes were used in Paper IV, since accuracy of the simulated peak flow was required in the flood frequency analysis.

4.5 RQ5 – The impacts of climate change on future flood

Paper IV studied the impacts of CC on future floods. To conduct the study, the SWAT model was coupled with five different ensemble GCM_RCMs to project future changes in daily streamflows and subsequent flood frequency and magnitude. The projected climate data of the ensemble GCM_RCMs were generated within the framework of the EURO-CORDEX initiative project. The high emission scenario of the Representative Concentration Pathway (RCP8.5) was applied to investigate changes in floods from the reference period (1976-2005) to the near future (2041-2070). The magnitudes and frequencies of nine flood quantiles, from small to high, i.e., the 2-, 5-, 10-, 20-, 50-, 100-, 200-, 500- and 1000-year floods, were estimated, of which the 200-, 500- and 1000-year floods were defined as extreme floods, while the 2- and 5-year floods were classed as small floods. The projections of future floods were conducted at six Norwegian Arctic catchments, which vary in geographical distributions (e.g., from the coast to inland), latitudes (e.g., from the south to the north and above the Arctic Circle), catchment scales (e.g., from small-scale to large-scale) and dominant flood regimes (e.g., rainfall-dominated, snowmelt-dominated and mixed rainfall/snowmelt). Moreover, uncertainties analysis was performed to detect the sources of uncertainties in the climate-hydrology modelling chain for flood projections. The subsections that follow will present the results from Paper IV.

4.5.1 Projected changes in future climate

Under climate conditions in the near future period (2041-2070), annual rainfall is expected to experience both increase and decrease patterns compared to that in the reference period (1976-2005), while the average annual air temperature would be in an upward trend and more intensified towards the north. In addition, the projected future CC was somewhat dissimilar among the ensemble GCM_RCMs, as well as among catchments. The projected changes in annual rainfall would be in the range of -32.9 to +33.7%, -35.1 to +35.3%, -46.0 to +35.9%, -24.7 to +32.4%, -31.0 to +33.5%, and -33.8 to +35.4% for Lakselva, Strandvassbotn, Marsvikelva, Målselv, Halselva and Karpelva catchments, respectively (Figure 28, middle). The average annual air temperature is expected to increase by 1.2-4.3°C, 1.2-4.4°C, 1.3-4.2°C, 1.4-4.7°C, 1.5-5.0°C and 1.9-5.0°C, at Lakselva, Strandvassbotn, Marsvikelva, Målselv, Halselva and Karpelva catchments, respectively (Figure 28, right). The disagreements in the projections of CC among the ensemble GCM_RCMs were expected to yield uncertainties in the estimated flood frequencies and flood magnitudes.

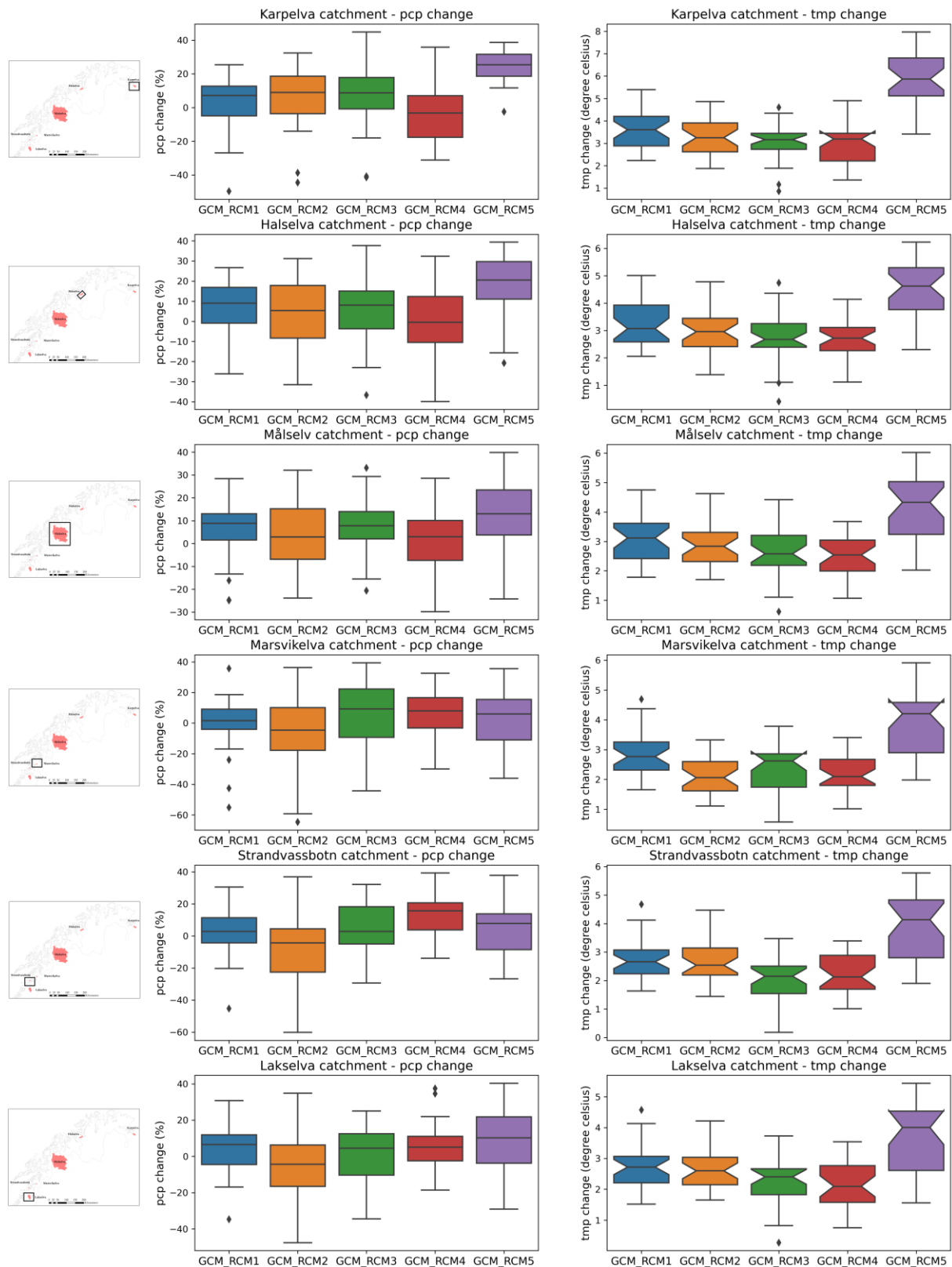


Figure 28 - Deviations in the near future (2041-2070) of annual precipitation-pcp (in %) and annual average air temperature-tmp (in °C) from the reference period (1976-2005), projected from five ensemble GCM_RCMs (results from Paper IV).

4.5.2 Projected changes in flood magnitudes

Figure 29 presents the average (avg) changes in nine flood quantiles from the historical (1976-2005) to the future (2041-2070) in six Norwegian Arctic catchments (numbered 1-6) under a high emission scenario (RCP8.5) of CC. According to Figure 29, the median magnitudes of future floods are expected to increase (e.g., from >1 to <22%) in most snowmelt-dominated catchments (excluding Karpelva (numbered 6)), while they would decrease (e.g., from -25 to <-5%) in the rainfall-dominated catchments. The mixed catchment would experience both decrease (e.g., >-2%, applicable for the small 2-year flood) and increase (e.g., from <4 to <14%) patterns.

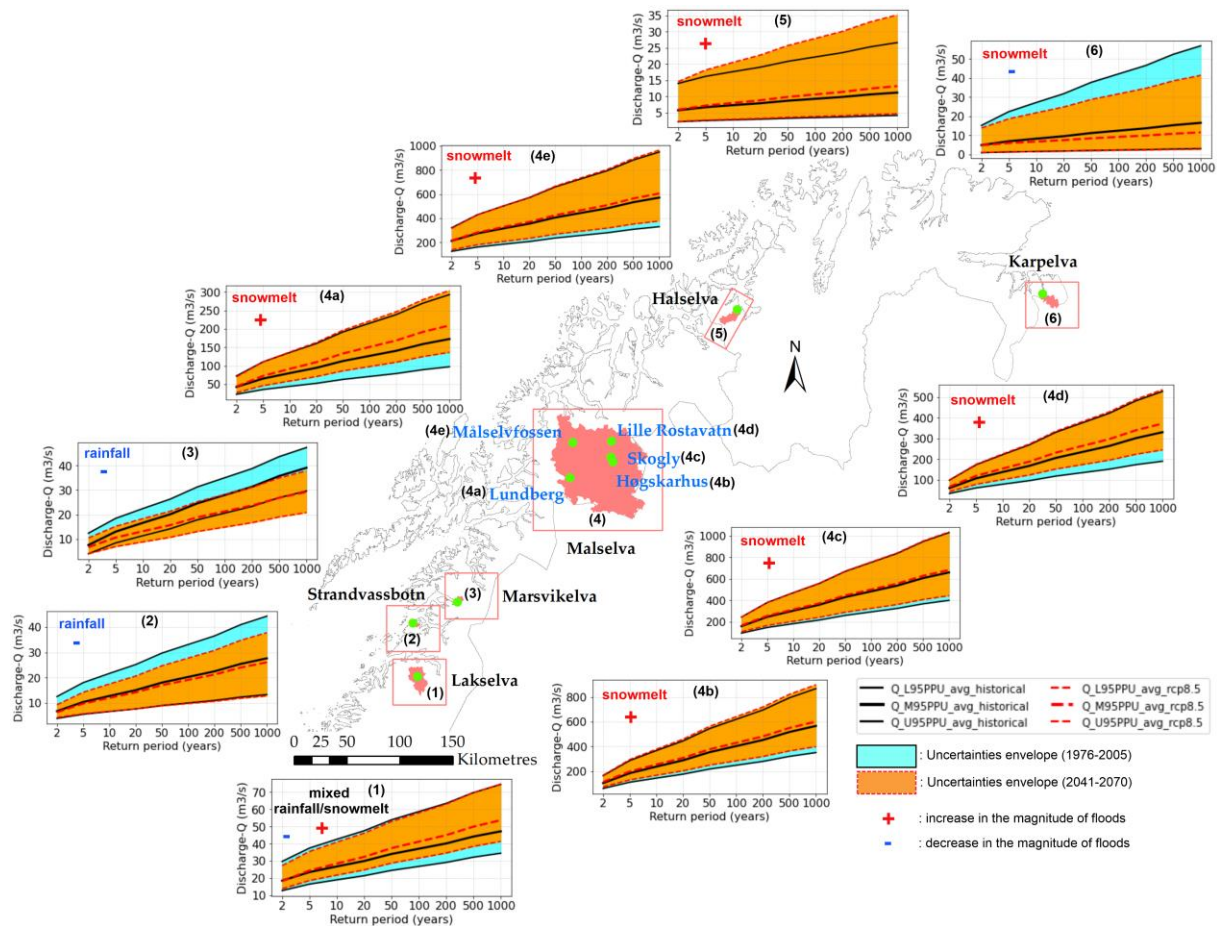


Figure 29 - The average (avg) changes in nine flood quantiles from the historical (1976-2005) to the future (2041-2070) in six Norwegian Arctic catchments under high scenario (RCP8.5) of CC (results from Paper IV). Q_{U95PPU} , Q_{M95PPU} , and Q_{L95PPU} denote the upper limited (at 97.5%), median and lower limited (at 2.5%) curves of the estimated discharges.

4.5.2.1 Projected changes in magnitudes of small floods

According to Paper IV, under climate conditions in the near future (2041-2070), the median magnitude of small floods (i.e., 2-year and 5-year floods) would decrease in the northern catchment (i.e., Karpelva with dominant snowmelt) and the southern catchments (i.e., Marsvikelva and Strandvassbotn (rainfall-dominated)), as well as in the mixed catchment Lakselva (only 2-year flood), whereas an increase in the magnitude of small floods is estimated in the remaining catchments (Table 18).

Table 18 - Median changes in future magnitudes of small and extreme floods (results from Paper IV).

Catchments	Area (km ²)	Flood regimes	Small floods		Extreme floods		
			2-year flood	5-year flood	200-year flood	500-year flood	1000-year flood
Karpeiva	129	Snowmelt	-1.7	-8.8	-27.8	-29.3	-30.3
Halselva	143	Snowmelt	+3.4	+7.6	+15.7	+16.9	+17.8
Målselv	5815	Snowmelt					
at Lundberg		Snowmelt	+3	+11.4	+19.9	+20.7	+21.3
at Lille Rostavatn		Snowmelt	+10.5	+11.6	+12.5	+12.6	+12.7
at Høgskarhus		Snowmelt	+9.1	+7.6	+6.4	+6.3	+6.2
at Skogly		Snowmelt	+4.4	+4.0	+3.6	+3.6	+3.6
at Målselvfossen		Snowmelt	+1.2	+2.9	+5.5	+5.8	+6.0
Marsvikelva	32	Rainfall	-11.4	-18.6	-24.3	-24.8	-25.2
Strandvassbotn	26	Rainfall	-6.4	-6.1	-5.7	-5.7	-5.6
Lakselva	297	Mixed	-1.4	+3.9	+12.0	+13.1	+13.7

4.5.2.2 Projected changes in magnitude of extreme floods

In Norway, 200-year, 500-year and 1000-year floods have been employed for flood risk management (Wilson *et al.* 2011). It was projected from Paper IV that the trends of changes in the future magnitude of extreme floods would be similar to those of small floods. However, the absolute values of changes in the magnitude of extreme floods would be more significant than those of small floods, except at the Høgskarhus and Skogly hydro-gauging stations of the Målselv and Strandvassbotn catchments (Table 18).

4.5.3 Projected changes in likelihood exceedance

The projections of changes in probable future flood events exceeding small floods and extreme floods were conducted for two different scenarios: (1) probable future flood events could exceed small/extreme flood quantiles, which were estimated from discharges of the reference period (1976-2005), and (2) probable future flood events could exceed small/extreme flood quantiles, which were estimated from discharges of the future period (2041-2070).

In general, an overview picture of future floods, drawn from Paper IV, shows that, under future climate conditions (2041-2070), extreme flood events are expected to occur more frequently compared to climate conditions of the reference period (1976-2005). Such changes are projected in the southernmost areas and near the coast, with a rainfall-dominated regime, and in the northernmost areas, with a snowmelt-dominated regime, of the Norwegian Arctic. Meanwhile, in the inland catchments in the central area, with a snowmelt-dominated regime, the frequency of extreme floods is expected to decrease. Moreover, the changes in future extreme flood events are projected to be more complicated in the rainfall-dominated catchment and near the coast, i.e., the Strandvassbotn. For example, extreme flood events would experience both increase (e.g., the 500-year flood) or decrease (e.g., the 200- and 1000-year floods) patterns. This is due to high variation of future rainfall, which is dominating the flood regime in such catchment. The projections of future changes in the frequency of small flood events are found to be totally opposite to those of extreme floods.

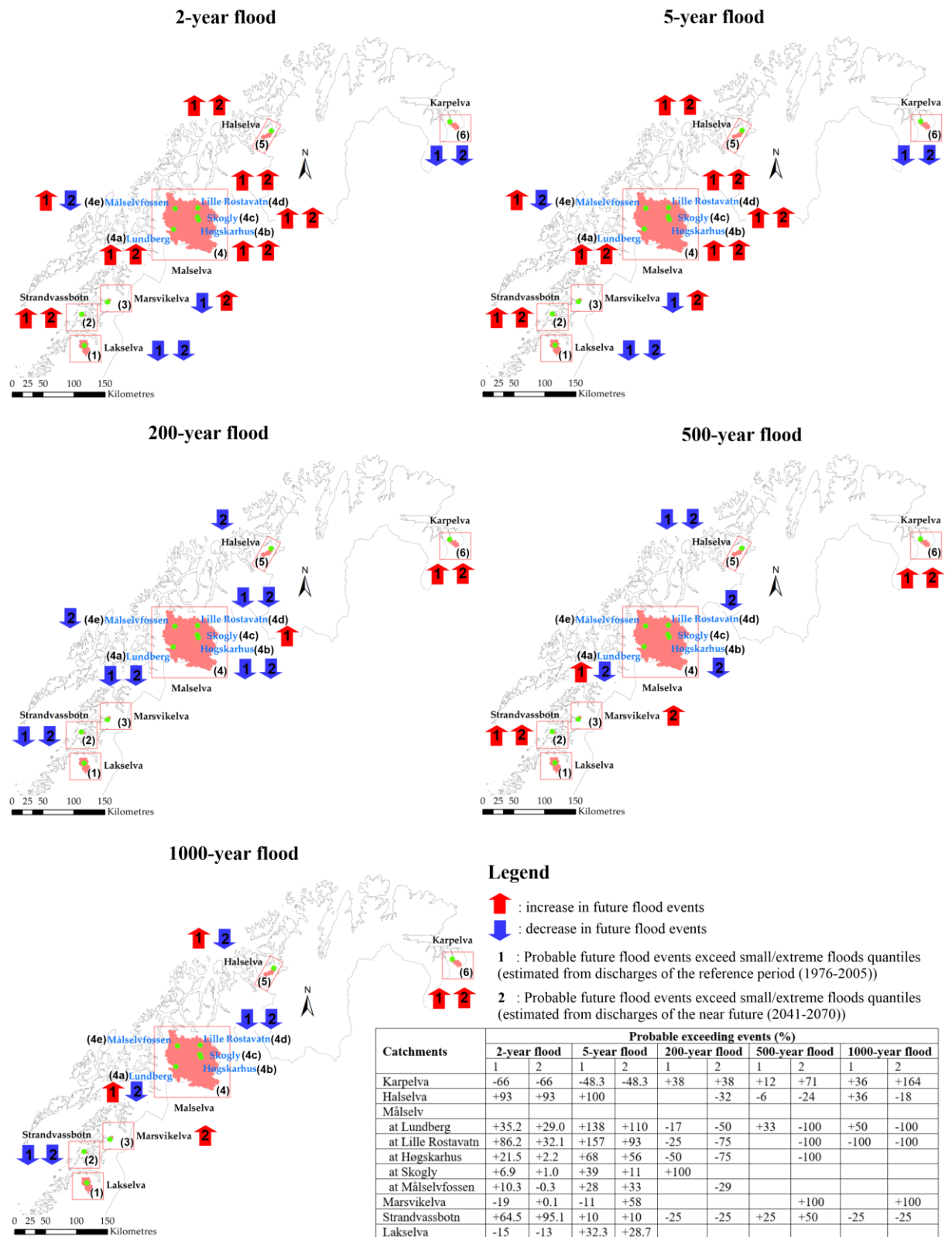


Figure 30 - Projected changes in likelihood exceedance of small and extreme floods, averaged from five ensemble GCM_RCMs inputs.

4.5.4 Uncertainties analysis in the projection of future floods

Uncertainties analysis is an indispensable procedure in flood projections, in order to reduce the overestimation/underestimation of flood scenarios. In Paper IV, uncertainties were detected in the climate-hydrology modelling chain for flood projections. In particular, uncertainties from the hydrological SWAT model were quantified according to two statistical measures, i.e., the p-factor and the r-factor (Table 19). It was revealed that the SWAT model has the capacity to generate relative accuracy in the simulated daily streamflow (based on the p-factor) in the Arctic environment. In addition, the quite narrowness of the uncertainty envelopes (based on the r-factor) explained that the simulated results were highly reliable.

Table 19 - Quantification of uncertainties from the hydrological SWAT model (results from Paper IV).

Catchments	p-factor			r-factor		
	Calibration	Optimal	Validation	Calibration	Optimal	Validation
Karpelva	0.94		0.92	1.08		1.08
Halselva	0.82		0.89	1.26		1.21
Målselv at Lundberg	0.56		0.52	0.70		0.72
Målselv at Lille Rostavatn	0.69		0.74	0.60		0.60
Målselv at Høgskarhus	0.56	> 0.70	0.43	0.82	< 1.5	0.86
Målselv at Skogly	0.73		0.67	1.15		1.15
Målselv at Målselvfossen	0.69		0.66	0.95		0.96
Marsvikelva	0.79		0.83	1.12		1.22
Strandvassbotn	0.55		0.48	0.45		0.43
Lakselva	0.77		0.77	1.71		1.64

It has been claimed by the scientific community that climate models have added further uncertainties in the climate-hydrology modelling chain for the projected hydrology (Kay *et al.* 2009; Chen *et al.* 2011; Woldemeskel *et al.* 2012). Findings from Paper IV verified such statements. In particular, Figure 31 and Figure 32 revealed uncertainties in the flood projections in different catchments through the use of different ensemble GCM_RCM simulations. It was found from Figure 31 and Figure 32 that, by using different ensemble GCM_RCMs inputs, the thicknesses of the uncertainty envelopes of estimated flood frequency in snowmelt-dominated catchments (i.e., Karpelva, Halselva and Målselv) were quite similar, while there was high variation in rainfall-dominated catchments (i.e., Marsvikelva and Strandvassbotn). Moreover, uncertainties from the inputs of climate models were found to be larger than those from the hydrological models in the climate-hydrology modelling chain of flood projection. For example, the calibration and validation results of the hydrological SWAT model in the Karpelva and Halselva catchments were better than those in the remaining catchments, but the uncertainty envelopes of the projected floods in such catchments were broader than those in the remaining catchments. This demonstrated that uncertainties from the ensemble GCM_RCMs inputs were higher in the Karpelva and Halselva catchments, compared to those from the hydrological SWAT model. Furthermore, the magnitudes of estimated floods were not similar when using different ensemble GCM_RCM simulations. This could influence the average/median values of the final results of the projected floods. Therefore, it was suggested that the selection of a suitable ensemble GCM_RCM simulation to drive the hydrological model in flood projection is very important. In addition, using the different time frames of the ensemble GCM_RCM simulation could result in different outcomes of flood projections. Although there is a scientific debate regarding the unreliability of using raw ensemble GCM_RCM simulation for studying CC impacts, findings from Paper IV revealed that using the raw outputs of climate models was

still reliable in some cases. For example, the magnitudes of the projected floods, when using the raw ensemble GCM_RCM simulation, were similar to those when using the bias-corrected ones (e.g., see, in Figure 31, the similar results from the first and third ensemble GCM_RCM inputs in Karpelva catchment or the similar results from all ensemble GCM_RCMs inputs in Lakselva catchment).

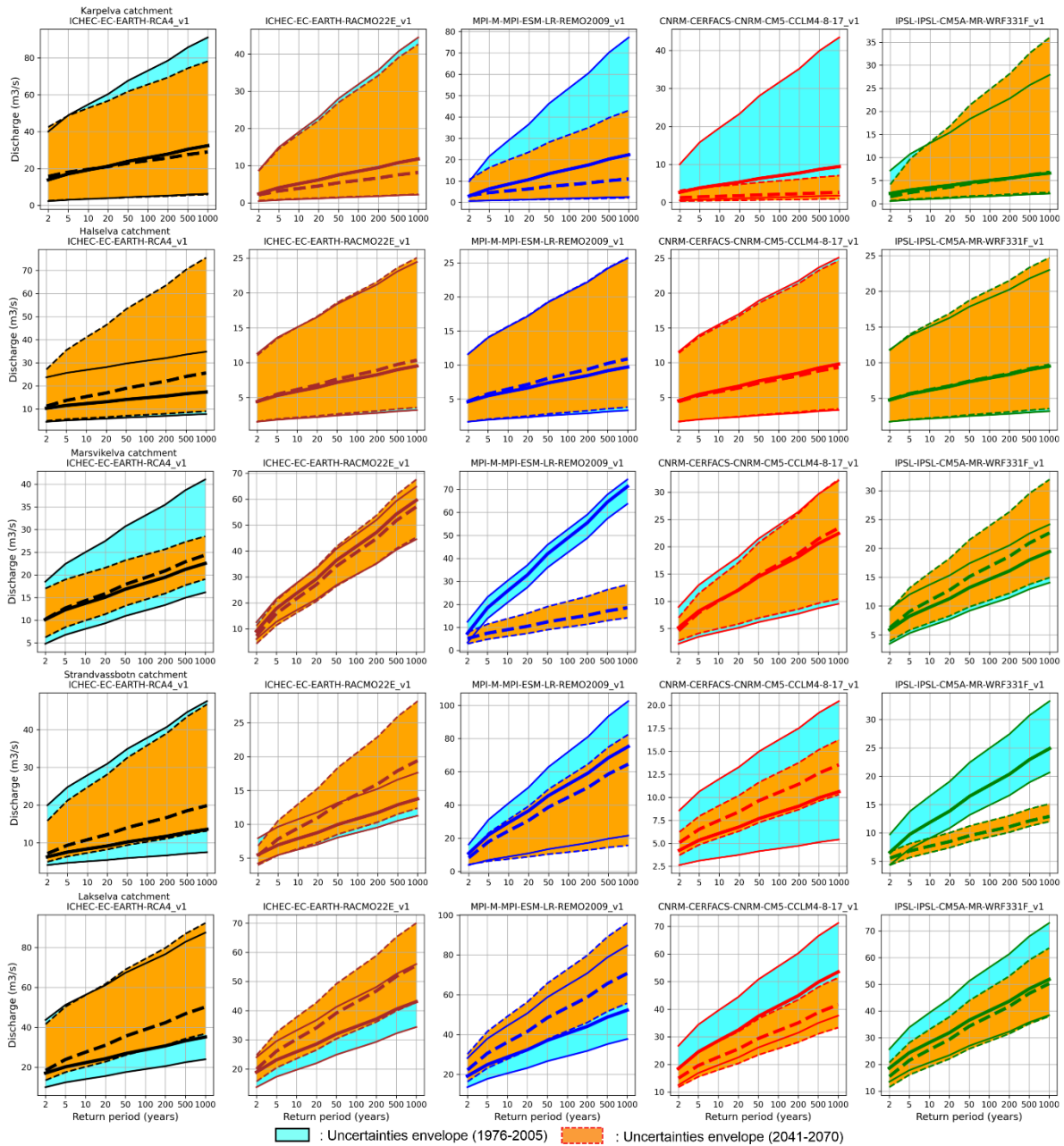


Figure 31 - Uncertainties in the estimation of the probable peak discharges in the reference period (1971-2005) and the future period (2041-2070), in the small-scale Norwegian Arctic catchments (results from Paper IV).

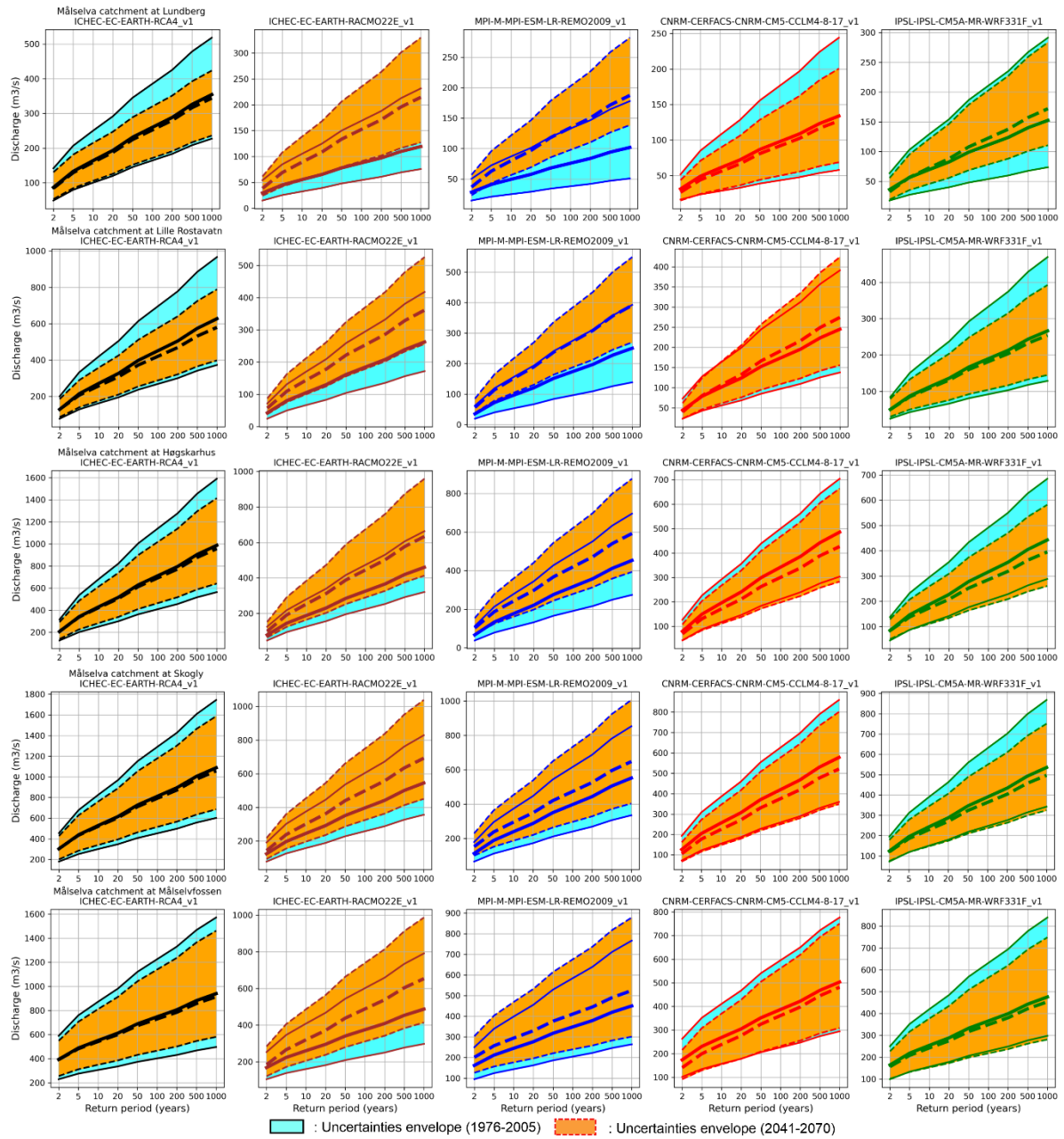


Figure 32 - Uncertainties in the estimation of the probable peak discharges in the reference period (1971-2005) and the future period (2041-2070), in the large-scale Norwegian Arctic catchment Målselv (results from Paper IV).

5 Discussion

5.1 Connection between the papers

As previously mentioned in Table 1, all four papers are built together to form the foundation of this thesis and to answer the five research questions proposed in the introduction. The first paper, supporting **RQ1**, addressed CC issues, their potential impacts on hydrological processes and the associated hydrological extreme events in the Arctic. Also, this paper suggested the need for suitable modelling tools, as well as providing a comprehensive review of different well-known models for studying surface and subsurface hydrology. In Paper II, a model candidate (i.e., SWAT) was selected, among other suitable candidates that were recommended from Paper I, to verify its performance for hydrological simulation in a Norwegian Arctic catchment. After that, the outcome from Paper II was the basis for further applications of the SWAT model in Papers III and IV. Thus, the integrated results from Papers I to IV were used to answer **RQ2** regarding the current performance of hydrological modelling tools applied in the Arctic environment. Moreover, the performance of the reanalysis weather data, i.e., CFSR, to drive the SWAT model was firstly tested in Paper II and then further applied in Papers III and IV. Therefore, the results from Papers II to IV were used to answer **RQ3** regarding the possibility of applying reanalysis weather data in the data-sparse Arctic regions. Paper III, supporting **RQ4**, studied the effects of the structure and parameterization of the SWAT model and the density of weather input, whose performances were tested in Paper II, on hydrological simulations in the Arctic conditions. Finally, Paper IV, supporting **RQ5**, conducted projections of future floods under future CC, using the SWAT model and reanalysis weather data, CFSR, whose performances were verified in Papers II and III.

5.2 Strengths of the work

This study focused on the issue that has received considerable attention among scientists from various disciplines, i.e., CC and its impacts in the Arctic. This is because CC is more intensified in the Arctic than in the rest of the world. Also, changes, caused by global warming, in the hydrological system in the Arctic affect not only the entire Arctic ecosystem but also the whole global climate. This study addressed the capacity, as well as the challenges, of hydrological modelling in the Arctic, by conducting a comprehensive review. In addition, most of the current challenges for hydrological modelling in general and for each model type in particular were critically discussed in the review paper (Paper I). This study performed hydrological modelling in the Arctic region which has complex hydrological processes and sparse data. The state-of-the-art physically based (or processes-based), semi-distributed model (i.e., the SWAT) was successfully run in the Arctic. The SWAT model has demonstrated its capability to fulfil the requirement of modelling philosophy, i.e., transparency of the modelling. This means that calibration, validation, sensitivity and uncertainty analyses are all performed in the modelling processes. Furthermore, the cohesive connection between the papers also constitutes a strength of the work.

5.3 Limitations of the work

One of the limitations of this work is that the performance of only one single surface hydrological model (i.e., the SWAT) is verified, after conducting a comprehensive review of hydrological models applied in the Arctic; however, the testing of multiple models, in order to compare performances among them, was not conducted. Next, the performance of only one reanalysis weather product to drive the SWAT

model in the data-sparse Arctic region is tested. It would be good if multiple reanalysis products were applied and their performances were compared. Also, this study did not perform bias correction of the climate model outputs, but it inherited the bias-corrected products from the EURO-CORDEX project, which applied only one single method, namely, Cumulative Distribution Function transformation (CDFt). Thus, more bias correction methods should be employed to assess the uncertainties of climate model outputs. This is because different bias correction approaches may yield different projection results. Moreover, in the projections of future floods, it is just limited at the projections of future changes in magnitudes and frequencies of floods, but the projections of the changes in flood depths and inundation areas across the catchments are not yet conducted.

6 Concluding remarks

6.1 Conclusion

Considering the severe impacts of CC on hydrological processes, and their consequences in the Arctic environment, there is a real demand for a suitable hydrological modelling tool supporting impacts' assessment, as well as for the sustainable management of water resources, the environment, and ecosystem conservation. Thus, the ideas for this study were developed based on this foundation. Five research questions were proposed, as shown in the introduction section, to form the whole content of this thesis. Four main scientific papers were conducted to answer those research questions. The main conclusions that can be drawn from those papers are as follows:

RQ1 - What are the current capacities and challenges of hydrological modelling in the Arctic environment?

According to the work presented in Paper I, it is concluded that both surface and subsurface hydrological models have capacities as well as limitations regarding simulating the complex hydrological processes in the Arctic. For example, besides the capacity to simulate surface hydrological processes, many surface hydrological models are also able to describe the seasonal freezing–thawing processes in the permafrost environment, by employing analytical (e.g., Stefan's equation for heat transfer) and numerical (e.g., finite difference, finite element and finite volume methods) solutions, while many subsurface hydrological models have considerable capability to simulate water flow and heat transfer in soil through the use of 3D equations. In addition, subsurface hydrological models, particularly cryo-hydrogeological models, are able to simulate quite well the three phase changes (e.g., ice, liquid and gas) of water in near-surface soil.

Challenges for hydrological simulation in the Arctic environment are also drawn from Paper I. Firstly, it is not possible for surface hydrological models to simulate multidecadal and multidimensional changes in the freezing–thawing processes in the permafrost environment by employing the 1D heat transfer equation. In addition, some important processes in permafrost environments, such as heat capacity, thermodynamic equilibrium and the three phase changes (ice, liquid, and gas) of water in near-surface soils, have yet to be developed in surface hydrological models. Subsurface hydrological models do not include land surface schemes in their model structures; they also have complex boundary conditions, and it is hard for non-experts to use them. Moreover, data acquisition is an additional challenge for hydrological modelling in the data-sparse Arctic region.

RQ2 - Which types of hydrological model(s) are suitable for the Arctic conditions, and how can their performance in the simulation of hydrological processes in the Arctic catchments be verified?

Suitable model candidates

It was concluded from Paper I that the selection of suitable hydrological models depends on various factors and targets of each study. Besides the criteria for accurate simulation of hydrological processes in the Arctic environment, other factors, such as available input data, the required research period and funding conditions, could also influence the selection.

For studies that only focus on evaluating surface hydrology, Topoflow, HBV, SWAT, ECOMAG and CRHM could be good candidates. Of these, the semi-distributed models, namely, HBV, SWAT and CRHM, are suitable for catchments with moderate data requirements, while the fully distributed models, namely, Topoflow and ECOMAG, need intensive inputs, as well as model parameters. Application of the CRHM and Topoflow models requires expert knowledge of the catchments, since there are no calibration procedures for such models. In case the need is for highly accurate simulation of subsurface hydrology in permafrost environments, DMHS, WaSiM and the cryo-hydrogeological models are suitable candidates. Furthermore, if the studies aim to simulate active layer dynamics, DMHS, ATS, GEOTop and PFLOTRAN-ICE are good model choices. However, GEOTop, SUTRA-ICE and PFLOTRAN-ICE are only suitable for small-scale case studies, while ATS and CryoGrid 3 could be applied in large-scale catchments.

Verification of model performances

Papers II and IV concluded that the selected model candidate, SWAT, has the capacity to simulate well the surface hydrology in the Norwegian Arctic catchments. However, the results of monthly simulations seem to be somewhat better than those of daily simulations. In addition, model performances based on three statistical coefficients, R^2 , NSE and RSR, and the hydrograph of streamflow vary greatly between catchments and between hydro-gauging stations within a large-scale catchment. The performance of surface hydrological simulation in the snowmelt-dominated catchments is better than that in the rainfall-dominated catchments.

RQ3 - Considering the sparse data in the Arctic region, can the high-resolution global reanalysis weather data become reliable alternative sources and replace the existing scattered monitoring data, to run a hydrological model in the Arctic catchments?

The conclusion was drawn from Papers II and IV that reanalysis weather data (CFSR) is a reliable source for running a hydrological model in the Arctic catchments. The reanalysis weather data could be an alternative in the case of the existing monitoring data being coarse/scattered, and many gaps existing in the time series of observed data.

RQ4 - To what extent do the hydrological models (e.g., structures and parameterizations) and quality of weather inputs (e.g., spatial resolution) affect hydrological simulations in the Arctic catchments?

Paper III concluded that changes in model structures (e.g., number and size of sub-catchments (sub-basins), land use compositions, catchment's characteristics through the catchment delineation process) and model parameterization (e.g., through the calibration process) could affect the results of hydrological simulations. The changes in model structures and model parameterization, as well as in the integrated weather grids, were caused by the designed TDA values. By increasing the value of TDAs (reducing the number of sub-basins), the annual mean values of PET, ET and lateral flow decreased slightly, whereas rainfall, surface runoff and water yield increased slightly. In addition, the estimated peak flow could be overestimated/underestimated by changes in TDA schemes. Moreover, changes in TDAs resulted in changes in model structures that could lead to fluctuation in model parameters' sensitivity rank order in the calibration process. Furthermore, the density of integrated weather grids decreased, together with the increase in TDAs. As a result, this caused discrepancies in the spatial variation of water balance components (e.g., precipitation, ET, PET, surface runoff and water yield),

snowmelt runoff volume and streamflow across the catchment. The fine TDA schemes could produce a higher variation in water balance components, snowmelt runoff volume and streamflow. This would benefit the management of water resources or natural disasters (e.g., flood risk analysis) at sub-basin levels. However, choosing the very fine TDA schemes could influence the time to run or calibrate the model, especially in the large-scale catchments. Thus, it was recommended that, depending on the targets of each study, fine or coarse TDA schemes would be an appropriate choice.

RQ5 - How is the projection of climate change impacts on hydrology and the associated extreme events (e.g., floods) in the Arctic catchments based on the current hydrological modelling tool? And how is the reliability/uncertainty of the projections quantified?

The conclusion was drawn from the work in Paper IV that the physically based, semi-distributed SWAT model demonstrated its considerable capacity to simulate daily streamflow in the Norwegian Arctic catchments. Model performances, which were measured by statistical coefficients, varied from satisfactory to good between catchments, as well as between hydro-gauging stations within a large catchment. In addition, the possibility to transfer calibrated model parameters between catchments was high, and that verified the physical relationship of model parameters. Accordingly, the calibrated SWAT models were evaluated as highly reliable for studying CC impacts. Thus, the SWAT model was coupled with multiple ensemble Global and Regional Model outputs to project future changes in the magnitude and frequency of different flood quantiles, from small floods to extreme floods. It was projected that the median magnitudes of floods in the near future (2041-2070) would increase in most snowmelt-dominated catchments but would decrease in rainfall-dominated catchments, compared to the reference period (1971-2005). The catchment with a mixed rainfall/snowmelt regime would experience both decrease (applicable for the small flood) and increase patterns. In southern catchments (rainfall-dominated), and in northern catchments (snowmelt-dominated), extreme flood events (i.e., 200-, 500- and 1000-year floods) would occur more frequently, but with lower magnitudes. This pattern would be opposite to that of the catchments in the central Norwegian Arctic with a snowmelt-dominated regime. Moreover, the changes in future extreme flood events would be more complicated in the rainfall-dominated catchment and near the coast, e.g., the Strandvassbotn, due to high variation of future rainfall in this area. The future change in likelihood exceedance of small flood events (i.e., 2-year and 5-year floods) would be in the opposite pattern to those of extreme floods.

Moreover, it was concluded that uncertainties regarding the projected floods were heterogeneous between catchments, regarding the dominant flood regimes, catchment's scale and the driven GCM_RCM simulations. For example, a higher variation in the projected floods was found in the rainfall-dominated catchments, when using different ensemble GCM_RCM simulations, compared to those in the snowmelt-dominated catchments. Uncertainty envelopes of the projected floods were larger in the small-scale catchments compared to those in the large-scale catchments. Noticeably, uncertainties from the ensemble GCM_RCMs simulations were larger than those from the hydrological SWAT model in the climate-hydrology modelling chain for flood projections. Furthermore, it was found from Paper IV that using raw climate model output to drive the hydrological SWAT model for flood projection was reliable in certain cases. Therefore, it is suggested that both raw and bias-corrected climate models' outputs are considered in CC impacts' assessment.

6.2 Research contributions

The main contributions of this study are as follows:

- Supporting the scientific community, particularly the modellers, with a comprehensive review of the current capacities and limitations of different hydrological models applied in the Arctic environment,
- Building up and demonstrating the potential applications of a state-of-the-art SWAT model for hydrological simulations and CC impacts' assessment in the Arctic,
- Verifying the possibility of using global reanalysis weather data to drive the hydrological model in the data-sparse Arctic region, and of the reanalysis dataset being an alternative source to replace the existing scattered observed dataset,
- Detecting the factors (e.g., model structure, model parameterization and outputs from climate models) that could affect the simulated/projected results of hydrology,
- Providing projections of future CC impacts on different flood sizes, i.e., from small floods to large floods, in different catchments with variations in geographical distribution (e.g., from coast to inland), latitude (e.g., from southern to northern regions of the Norwegian Arctic), scales (e.g., from small-scale to large-scale) and dominant hydrological regimes (e.g., rainfall-dominated, snowmelt-dominated or mixed rainfall/snowmelt),
- Supporting the scientists, risk managers, planners and decision makers with further knowledge of future flood changes under a CC context, in order to propose proper strategies for flood mitigation and management, as well as contributing to a sustainable environment and ecosystem conservation.

6.3 Suggestions for future works

Based on the outcomes and limitations of the current works in this study, the following suggestions are made for supplementary future works:

- Develop a hydrodynamic model using outputs from the hydrological model to project the changes in water level and inundated areas. This aims to support flood risk assessment under CC,
- Assess/estimate quantitatively the impacts of future flood changes on the environment, and ecosystem.

References

- Abbaspour K. C. 2015 *SWAT-CUP: Swat Calibration and Uncertainty Program - A User Manual*, Eawag: Swiss Federal Institute of Aquatic Science and Technology, Dübendorf, Switzerland.
- Abbaspour K. C., Rouholahnejad E., Vaghefi S., Srinivasan R., Yang H. & Klove B. 2015 A continental-scale hydrology and water quality model for Europe: Calibration and uncertainty of a high-resolution large-scale SWAT model. *Journal of Hydrology*, **524**, 733-52.
- Abbaspour K. C., Yang J., Maximov I., Siber R., Bogner K., Mieleitner J., Zobrist J. & Srinivasan R. 2007 Modelling hydrology and water quality in the pre-alpine/alpine Thur watershed using SWAT. *Journal of Hydrology*, **333**(2-4), 413-30.
- Abbott M. B., Bathurst J. C., Cunge J. A., Oconnell P. E. & Rasmussen J. 1986 An Introduction to the European Hydrological System - Systeme Hydrologique Europeen, She .2. Structure of a Physically-Based, Distributed Modeling System. *Journal of Hydrology*, **87**(1-2), 61-77.
- Åkerman H. J. & Johansson M. 2008 Thawing permafrost and thicker active layers in sub - arctic Sweden. *Permafrost and Periglacial Processes*, **19**(3), 279-92.
- Alfieri L., Burek P., Feyen L. & Forzieri G. 2015 Global warming increases the frequency of river floods in Europe. *Hydrology and Earth System Sciences*, **19**(5), 2247-60.
- AMAP 2011 *Snow, water, ice and permafrost in the Arctic (SWIPA) : climate change and the cryosphere*. AMAP, Oslo.
- AMAP 2017 *Snow, Water, Ice and Permafrost in the Arctic (SWIPA) 2017*. Arctic Monitoring and Assessment Programme.
- Arnold J. G., Moriasi D. N., Gassman P. W., Abbaspour K. C., White M. J., Srinivasan R., Santhi C., Harmel R. D., Griensven A. v., Liew M. W. V., Kannan N. & Jha M. K. 2012 SWAT: model use, calibration, and validation. *American Society of Agricultural and Biological Engineers*, **55**(4), 1491–508.
- Azadi M. & Zakeri Z. 2010 Probabilistic Precipitation Forecasting using a Deterministic Model Output over Iran. *Research journal of environmental sciences*, **4**(2), 138-48.
- Bergstrom S., Carlsson B., Gardelin M., Lindstrom G., Pettersson A. & Rummukainen M. 2001 Climate change impacts on runoff in Sweden - assessments by global climate models, dynamical downscaling and hydrological modelling. *Climate Research*, **16**(2), 101-12.
- Beven K. J. 2012 *Rainfall-runoff modelling : the primer*. In. 2nd ed. edn, Wiley, Hoboken.
- Bierkens M. F. P. & Geer F. V. 2012 GEO4-4420: Stochastic Hydrology. In: *Earth Surface Hydrology*, Department of Physical Geography, Utrecht University, pp. http://www.earthsurfacehydrology.nl/wp-content/uploads/2012/01/Syllabus_Stochastic-Hydrology.pdf.
- Box J. E., Colgan W. T., Christensen T. R., Schmidt N. M., Lund M., Parmentier F. J. W., Brown R., Bhatt U. S., Euskirchen E. S., Romanovsky V. E., Walsh J. E., Overland J. E., Wang M. Y., Corell R. W., Meier W. N., Wouters B., Mernild S., Mard J., Pawlak J. & Olsen M. S. 2019 Key indicators of Arctic climate change: 1971-2017. *Environmental Research Letters*, **14**(4).
- Bruland O. & Killingtveit Å. 2002 Application of the HBV-Model in Arctic catchments - some results from Svalbard. In: *Proceedings of XXII Nordic Hydrological Conference*, Røros, Norway.
- Bui M. T., Lu J. M. & Nie L. M. 2020 A Review of Hydrological Models Applied in the Permafrost-Dominated Arctic Region. *Geosciences*, **10**(10).
- Callaghan T. V., Johansson M., Brown R. D., Groisman P. Y., Labba N., Radionov V., Barry R. G., Bulygina O. N., Essery R. L. H., Frolov D. M., Golubev V. N., Grenfell T. C., Petrushina M. N., Razuvaev V. N., Robinson D. A., Romanov P., Shindell D., Shmakin A. B., Sokratov S. A., Warren S. & Yang D. Q. 2011 The Changing Face of Arctic Snow Cover: A Synthesis of Observed and Projected Changes. *Ambio*, **40**, 17-31.
- Callaghan T. V., Jonasson C., Thierfelder T., Yang Z. L., Hedenas H., Johansson M., Molau U., Van Bogaert R., Michelsen A., Olofsson J., Gwynn-Jones D., Bokhorst S., Phoenix G., Bjerke J. W., Tommervik H., Christensen T. R., Hanna E., Koller E. K. & Sloan V. L. 2013 Ecosystem change and stability over multiple decades in the Swedish subarctic: complex processes and multiple drivers. *Philosophical Transactions of the Royal Society B-Biological Sciences*, **368**(1624).

- Chen D. Y., Shams S., Carmona-Moreno C. & Leone A. 2010 Assessment of open source GIS software for water resources management in developing countries. *Journal of Hydro-Environment Research*, **4**(3), 253-64.
- Chen J., Arsenault R., Brissette F. P. & Zhang S. B. 2021 Climate Change Impact Studies: Should We Bias Correct Climate Model Outputs or Post-Process Impact Model Outputs? *Water Resources Research*, **57**(5).
- Chen J., Brissette F. P., Liu P. & Xia J. 2017 Using raw regional climate model outputs for quantifying climate change impacts on hydrology. *Hydrological Processes*, **31**(24), 4398-413.
- Chen J., Brissette F. P., Poulin A. & Leconte R. 2011 Overall uncertainty study of the hydrological impacts of climate change for a Canadian watershed. *Water Resources Research*, **47**.
- Chen S. M., Wang Y. M. & Tsou I. 2013 Using artificial neural network approach for modelling rainfall-runoff due to typhoon. *Journal of Earth System Science*, **122**(2), 399-405.
- Cheng S. J. 2011 The best relationship between lumped hydrograph parameters and urbanized factors. *Natural Hazards*, **56**(3), 853-67.
- Chow T. V., Maidment R. D. & Mays W. L. 1988 *Applied Hydrology*, New York, USA.
- Collins M., Booth B. B. B., Harris G. R., Murphy J. M., Sexton D. M. H. & Webb M. J. 2006 Towards quantifying uncertainty in transient climate change. *Climate Dynamics*, **27**(2-3), 127-47.
- COMET 2010a Distributed modeling.
http://portal.chmi.cz/files/portal/docs/poboc/CB/runoff_cz/print.htm#page_5.0.0 (accessed 27 October 2018).
- COMET 2010b Lumped modeling.
http://portal.chmi.cz/files/portal/docs/poboc/CB/runoff_cz/print.htm#page_5.0.0 (accessed 27 October 2018).
- Cunnane C. 1985 Factors affecting choice of distribution for flood series. *Hydrological sciences journal*, **30**(1), 25-36.
- Cunnane C. 1989 *Statistical distributions for flood frequency analysis*, WMO Operational hydrology, Geneva, Switzerland.
- Dankers R. 2008 Arctic and Snow Hydrology. In: *Climate and the Hydrological Cycle* Bierkens M, Dolman H and Troch P (eds), IAHS Press, Wallingford (UK), pp. 137-56.
- Daofeng L., Ying T., Changming L. & Fanghua H. 2004 Impact of land-cover and climate changes on runoff of the source regions of the Yellow River. *Journal of Geographical Sciences*, **14**(3), 330-8.
- Devi G. K., Ganasri B. P. & Dwarakish G. S. 2015 A Review on Hydrological Models. *International Conference on Water Resources, Coastal and Ocean Engineering (Icwrcoe'15)*, **4**, 1001-7.
- Dile Y. T., Berndtsson R. & Setegn S. G. 2013 Hydrological Response to Climate Change for Gilgel Abay River, in the Lake Tana Basin - Upper Blue Nile Basin of Ethiopia. *Plos One*, **8**(10).
- Dunn S. M., Brown I., Sample J. & Post H. 2012 Relationships between climate, water resources, land use and diffuse pollution and the significance of uncertainty in climate change. *Journal of Hydrology*, **434**, 19-35.
- Dwarakish G. S. & Ganasri B. P. 2015 Impact of land use change on hydrological systems: A review of current modeling approaches. *Cogent Geoscience*, **1**(1), 1115691.
- Dye D. G. 2002 Variability and trends in the annual snow-cover cycle in Northern Hemisphere land areas, 1972-2000. *Hydrological Processes*, **16**(15), 3065-77.
- ECAD 2002 The European Climate Assessment & Dataset project
<https://www.ecad.eu/dailydata/index.php>.
- Engeland K., Aano A., Steffensen I., Storen E. & Paasche O. 2020 New flood frequency estimates for the largest river in Norway based on the combination of short and long time series. *Hydrology and Earth System Sciences*, **24**(11), 5595-619.
- EPA 2013 *Watershed modeling to assess the sensitivity of streamflow, nutrient, and sediment loads to potential climate change and urban development in 20 U.S. watersheds (final report)*, U.S. Environment Protection Agency, Washington D.C.
- Fabre C., Sauvage S., Tananaev N., Srinivasan R., Teisserenc R. & Perez J. M. S. 2017 Using Modeling Tools to Better Understand Permafrost Hydrology. *Water*, **9**(6).
- Fernandez G. P., Chescheir G. M., Skaggs R. W. & Amatya D. M. 2005 Development and testing of watershed-scale models for poorly drained soils. *Transactions of the Asae*, **48**(2), 639-52.

- Flato G., Marotzke J., Abiodun B., Braconnot P., Chou S. C., Collins W., Cox P., Driouech F., Emori S., Eyring V., Forest C., Gleckler P., Guilyardi E., Jakob C., Kattsov V., Reason C. & Rummukainen M. 2013 Evaluation of Climate Models. In: *Climate Change 2013: The Physical Science Basis. Contribution of Working Group I to the Fifth Assessment Report of the Intergovernmental Panel on Climate Change* Stocker TF, Qin D, Plattner G-K, Tignor M, Allen SK, Boschung J, Nauels A, Xia Y, Bex V and Midgley PM (eds), Cambridge University Press, Cambridge, United Kingdom and New York, NY, USA.
- Gassman P. W., Reyes M. R., Green C. H. & Arnold J. G. 2007 The soil and water assessment tool: Historical development, applications, and future research directions. *Transactions of the Asabe*, **50**(4), 1211-50.
- Geonorge 2013 Height DTM 10. <https://kartkatalog.geonorge.no/metadata/kartverket/dtm-10-terrengmodell-utm33/> (accessed 14 February 2021).
- Ghosh S. & Mujumdar P. P. 2007 Nonparametric methods for modeling GCM and scenario uncertainty in drought assessment. *Water Resources Research*, **43**(7).
- Graham L. P., Andreasson J. & Carlsson B. 2007a Assessing climate change impacts on hydrology from an ensemble of regional climate models, model scales and linking methods - a case study on the Lule River basin. *Climatic Change*, **81**, 293-307.
- Graham L. P., Hagemann S., Jaun S. & Beniston M. 2007b On interpreting hydrological change from regional climate models. *Climatic Change*, **81**, 97-122.
- Granata F., Gargano R. & de Marinis G. 2016 Support Vector Regression for Rainfall-Runoff Modeling in Urban Drainage: A Comparison with the EPA's Storm Water Management Model. *Water*, **8**(3).
- Gumbel E. J. 1941 The return period of flood flows. *Annals of Mathematical Statistics*, **12**, 163-90.
- Gupta S. K., Sharma G., Jethoo A. S., Tyagi J. & Gupta N. K. 2015 A critical review of hydrological models. In: *Proceedings of 20th International Conference on Hydraulics, Water Resources and River Engineering*, IIT Roorkee, India, p. 8.
- Halff A. H., Halff H. M. & Azmoodeh M. 1993 Predicting Runoff from Rainfall Using Neural Networks. *Engineering Hydrology*, 760-5.
- Han E. J., Merwade V. & Heathman G. C. 2012 Implementation of surface soil moisture data assimilation with watershed scale distributed hydrological model. *Journal of Hydrology*, **416**, 98-117.
- Hanssen-Bauer I., Førland E. J., Haddeland I., Hisdal H., Mayer S., Nesje A., Nilsen J. E. Ø., Sandven S., Sandø A. B., Sorteberg A. & Ådlandsvik B. 2017 *Climate in Norway 2100 - a knowledge base for climate adaptation*, Report 1/2017, Norwegian Environment Agency (Miljødirektoratet), Oslo, Norway.
- Heal G. & Kristrom B. 2002 Uncertainty and climate change. *Environmental & Resource Economics*, **22**(1-2), 3-39.
- Her Y., Frankenberger J., Chaubey I. & Srinivasan R. 2015 Threshold Effects in Hru Definition of the Soil and Water Assessment Tool. *Transactions of the Asabe*, **58**(2), 367-78.
- Huntington T. G., Hodgkins G. A., Keim B. D. & Dudley R. W. 2004 Changes in the proportion of precipitation occurring as snow in New England (1949-2000). *Journal of Climate*, **17**(13), 2626-36.
- IPCC 2013 Climate Change 2013: The Physical Science Basis. Working Group I Contribution to the Fifth Assessment Report of the Intergovernmental Panel on Climate Change. In, Cambridge University Press, Cambridge, United Kingdom and New York, NY, USA, p. 1535.
- Jacob D., Petersen J., Eggert B., Alias A., Christensen O. B., Bouwer L. M., Braun A., Colette A., Deque M., Georgievski G., Georgopoulou E., Gobiet A., Menut L., Nikulin G., Haensler A., Hempelmann N., Jones C., Keuler K., Kovats S., Kroner N., Kotlarski S., Kriegsman A., Martin E., van Meijgaard E., Moseley C., Pfeifer S., Preuschmann S., Radermacher C., Radtke K., Rechid D., Rounsevell M., Samuelsson P., Somot S., Soussana J. F., Teichmann C., Valentini R., Vautard R., Weber B. & Yiou P. 2014 EURO-CORDEX: new high-resolution climate change projections for European impact research. *Regional Environmental Change*, **14**(2), 563-78.
- Jain S. K. & Singh V. P. 2019 Hydrological Cycles, Models, and Applications to Forecasting. In, Berlin, Heidelberg: Springer Berlin Heidelberg, Berlin, Heidelberg, pp. 311-39.

- Jajarmizadeh M., Harun S. & Salarpour M. 2012 A Review on Theoretical Consideration and Types of Models in Hydrology. *Environmental Science and Technology*, **5**(5), 249-61.
- Johansson M., Akerman J., Keuper F., Christensen T. R., Lantuit H. & Callaghan T. V. 2011 Past and Present Permafrost Temperatures in the Abisko Area: Redrilling of Boreholes. *Ambio*, **40**(6), 558-65.
- Jones R. N. 2000 Managing uncertainty in climate change projections - Issues for impact assessment - An editorial comment. *Climatic Change*, **45**(3-4), 403-19.
- Jung I. W., Moradkhani H. & Chang H. 2012 Uncertainty assessment of climate change impacts for hydrologically distinct river basins. *Journal of Hydrology*, **466**, 73-87.
- Kay A. L., Davies H. N., Bell V. A. & Jones R. G. 2009 Comparison of uncertainty sources for climate change impacts: flood frequency in England. *Climatic Change*, **92**(1-2), 41-63.
- Khan M. S., Coulibaly P. & Dibike Y. 2006 Uncertainty analysis of statistical downscaling methods using Canadian Global Climate Model predictors. *Hydrological Processes*, **20**(14), 3085-104.
- Killingtveit & Sælthun N. 1995 *Hydrology*. Department of Hydraulic Engineering, Norwegian Institute of Technology, Trondheim, Norway.
- Koch J. 2016 *Evaluating spatial patterns in hydrological modelling*. PhD thesis, Faculty of Science, University of Copenhagen, Denmark.
- Kong Y. & Wang C. H. 2017 Responses and changes in the permafrost and snow water equivalent in the Northern Hemisphere under a scenario of 1.5 degrees C warming. *Advances in Climate Change Research*, **8**(4), 235-44.
- Koycegiz C. & Buyukyildiz M. 2019 Calibration of SWAT and Two Data-Driven Models for a Data-Scarce Mountainous Headwater in Semi-Arid Konya Closed Basin. *Water*, **11**(1).
- Krysanova V. & Srinivasan R. 2015 Assessment of climate and land use change impacts with SWAT. *Regional Environmental Change*, **15**(3), 431-4.
- Kunkel K. E., Robinson D. A., Champion S., Yin X. G., Estilow T. & Frankson R. M. 2016 Trends and Extremes in Northern Hemisphere Snow Characteristics. *Current Climate Change Reports*, **2**(2), 65-73.
- Landwehr J. M., Matalas N. C. & Wallis J. R. 1979 Probability Weighted Moments Compared with Some Traditional Techniques in Estimating Gumbel Parameters and Quantiles. *Water Resources Research*, **15**(5), 1055-64.
- Laprise R. 2008 Regional climate modelling. *Journal of Computational Physics*, **227**(7), 3641-66.
- Lawrence D. & Hisdal H. 2011 *Hydrological projections for floods in Norway under a future climate*, The Norwegian Water Resources and Energy Directorate-NVE, Oslo, Norway.
- Liu Z., Wang Y., Xu Z. & Duan Q. 2019 Conceptual Hydrological Models. In: *Handbook of Hydrometeorological Ensemble Forecasting* Duan Qea (ed.), Springer Berlin Heidelberg, Berlin, Heidelberg, Germany, pp. 341-87.
- Logsdon R. A. & Chaubey I. 2013 A quantitative approach to evaluating ecosystem services. *Ecological Modelling*, **257**, 57-65.
- Lowery M. D. & Nash J. E. 1970 A comparison of methods of fitting the double exponential distribution. *Journal of hydrology (Amsterdam)*, **10**(3), 259-75.
- Madsen H., Lawrence D., Lang M., Martinkova M. & Kjeldsen T. R. 2014 Review of trend analysis and climate change projections of extreme precipitation and floods in Europe. *Journal of Hydrology*, **519**, 3634-50.
- Magar R. B. & Jothiprakash V. 2011 Intermittent reservoir daily-inflow prediction using lumped and distributed data multi-linear regression models. *Journal of Earth System Science*, **120**(6), 1067-84.
- Mallakpour I. & Villarini G. 2015 The changing nature of flooding across the central United States. *Nature Climate Change*, **5**(3), 250-4.
- Maurer E. P. 2007 Uncertainty in hydrologic impacts of climate change in the Sierra Nevada, California, under two emissions scenarios. *Climatic Change*, **82**(3-4), 309-25.
- McGrath H., Stefanakis E. & Nastev M. 2015 Sensitivity analysis of flood damage estimates: A case study in Fredericton, New Brunswick. *International Journal of Disaster Risk Reduction*, **14**, 379-87.

- Mckay M. D., Beckman R. J. & Conover W. J. 1979 A Comparison of Three Methods for Selecting Values of Input Variables in the Analysis of Output from a Computer Code. *Technometrics*, **21**(2), 239-45.
- Mearns L. O., Giorgi F., Whetton P., Pabon D., Hulme M. & Lal M. 2013 Guidelines for use of climate scenarios developed from regional climate model experiments. In, Data Distribution Centre of the Intergovernmental Panel on Climate Change, pp. https://www.ipcc-data.org/guidelines/dgm_no1_v_10-2003.pdf.
- Meresa H. K., Osuch M. & Romanowicz R. 2016 Hydro-Meteorological Drought Projections into the 21-st Century for Selected Polish Catchments. *Water*, **8**(5).
- Midttømme G. H., Petterson L. E., Holmqvist E., Nøtsund Ø., Hisdal H. & Sivertsgård R. 2011 *Retningslinjer for flomberegninger (Guidelines for flood calculations)*, The Norwegian Water Resources and Energy Directorate (NVE), Oslo, Norway.
- Mohammadi B. 2021 A review on the applications of machine learning for runoff modeling. *Sustainable Water Resources Management*, **7**(6).
- Moriassi D. N., Arnold J. G., Van Liew M. W., Bingner R. L., Harmel R. D. & Veith T. L. 2007 Model evaluation guidelines for systematic quantification of accuracy in watershed simulations. *Transactions of the Asabe*, **50**(3), 885-900.
- Najafi M. R., Moradkhani H. & Jung I. W. 2011 Assessing the uncertainties of hydrologic model selection in climate change impact studies. *Hydrological Processes*, **25**(18), 2814-26.
- Neitsch S. L., Arnold J. G., Kiniry J. R. & Williams J. R. 2009 Overview of Soil and Water Assessment Tool (SWAT) Model. In: *Soil and Water Assessment Tool (SWAT): Global Application* Arnold J, Srinivasan R, Neitsch S, George C, Abbaspour K, Gassman P, Fang HH, Griensven Av, Gosain A, Debels P, Kim NW, Somura H, Ella V, Leon L, Jintrawet A, Reyes M and Sombatpanit S (eds), The World Association of Soil and Water Conservation (WASWC), Bangkok, pp. 3-23.
- Neitsch S. L., Arnold J. G., Kiniry J. R. & Williams J. R. 2011 *Soil and Water Assessment Tool Theoretical Documentation Version 2009*. Texas Water Resources Institute, Texas, USA.
- Niel H., Paturel J. E. & Servat E. 2003 Study of parameter stability of a lumped hydrologic model in a context of climatic variability. *Journal of Hydrology*, **278**(1-4), 213-30.
- Odry J. & Arnaud P. 2017 Comparison of Flood Frequency Analysis Methods for Ungauged Catchments in France. *Geosciences*, **7**(3).
- Özdemir A. 2016 *Hierarchical Approach To Semi-Distributed Hydrological Model Calibration*. Doctor of Philosophy, The Graduate School Of Natural And Applied Sciences, Middle East Technical University.
- Premanand B. D., Satishkumar U., Maheshwara Babu B., Parasappa S. K., M. Dandu M., Kaleel I., Rajesh N. L. & Biradar S. A. 2018 QSWAT Model Calibration and Uncertainty Analysis for Stream Flow Simulation in the Patapur Micro-Watershed Using Sequential Uncertainty Fitting Method (SUFI-2). *International journal of current microbiology and applied sciences*, **7**(4), 831-52.
- Quintero F., Mantilla R., Anderson C., Claman D. & Krajewski W. 2018 Assessment of Changes in Flood Frequency Due to the Effects of Climate Change: Implications for Engineering Design. *Hydrology*, **5**(1).
- Richter B. D., Baumgartner J. V., Powell J. & Braun D. P. 1996 A method for assessing hydrologic alteration within ecosystems. *Conservation Biology*, **10**(4), 1163-74.
- Rodda & John C. 2009 *Modelling Of Hydrological Systems*, World Meteorological Organization (WMO), Geneva, Switzerland.
- Rojas R., Feyen L. & Watkiss P. 2013 Climate change and river floods in the European Union: Socio-economic consequences and the costs and benefits of adaptation. *Global Environmental Change-Human and Policy Dimensions*, **23**(6), 1737-51.
- Romanovsky V. E., Burgess M. M., Smith S. L., Yoshikawa K. & Brown J. 2002 Permafrost temperature records: Indicators of climate change. *Eos, Transactions American Geophysical Union*, **83**, 589-94.
- Rummukainen M. 2010 State-of-the-art with regional climate models. *Wiley Interdisciplinary Reviews-Climate Change*, **1**(1), 82-96.

- Saelthun N. R. & Andersen J. H. 1986 New Procedures for Flood Estimation in Norway. *Nordic Hydrology*, **17**(4-5), 217-28.
- Santhi C., Arnold J. G., Williams J. R., Dugas W. A., Srinivasan R. & Hauck L. M. 2001 Validation of the swat model on a large river basin with point and nonpoint sources. *Journal of the American Water Resources Association*, **37**(5), 1169-88.
- Sarkar A. & Kumar R. 2012 Artificial Neural Networks for Event Based Rainfall-Runoff Modeling. *Journal of water resource and protection*, **4**(10), 891-7.
- Seibert J. & Vis M. J. P. 2012 Teaching hydrological modeling with a user-friendly catchment-runoff-model software package. *Hydrology and Earth System Sciences*, **16**(9), 3315-25.
- Sexton A. M., Sadeghi A. M., Zhang X., Srinivasan R. & Shirmohammadi A. 2010 Using Nexrad and Rain Gauge Precipitation Data for Hydrologic Calibration of Swat in a Northeastern Watershed. *Transactions of the Asabe*, **53**(5), 1501-10.
- Shirke Y., Kawitkar R. & Balan S. 2012 Artificial neural network based runoff prediction model for a reservoir. *International Journal of Engineering Research & Technology (IJERT)*, **1**(3), 1-4.
- Sildre 2020 Real-time hydrological data. The Norwegian Water Resources and Energy Directorate (NVE). <http://sildre.nve.no/> (accessed 18 November 2019).
- Singh V. P. 1998 Extreme Value Type 1 Distrffition. In: *Entropy-Based Parameter Estimation in Hydrology*, Springer Science+Business Media Dordrecht, pp. 108-36.
- Sitterson J., Knightes C., Parmar R. & Wolfe K. 2017 *An Overview of Rainfall-Runoff Model Types*. U.S. Environmental Protection Agency, Washington, DC, USA.
- Srinivasan R. & Arnold J. G. 1994 Integration of a Basin-Scale Water-Quality Model with Gis. *Water Resources Bulletin*, **30**(3), 453-62.
- Srinivasan R., Zhang X. & Arnold J. 2010 Swat Ungauged: Hydrological Budget and Crop Yield Predictions in the Upper Mississippi River Basin. *Transactions of the Asabe*, **53**(5), 1533-46.
- Sudheer K. P., Gosain A. K. & Ramasastri K. S. 2002 A data-driven algorithm for constructing artificial neural network rainfall-runoff models. *Hydrological Processes*, **16**(6), 1325-30.
- Talbot C. J., Bennett E. M., Cassell K., Hanes D. M., Minor E. C., Paerl H., Raymond P. A., Vargas R., Vidon P. G., Wollheim W. & Xenopoulos M. A. 2018 The impact of flooding on aquatic ecosystem services. *Biogeochemistry*, **141**(3), 439-61.
- TAMU 2012 CFSR: Global Weather Data for SWAT. <https://globalweather.tamu.edu/> (accessed 05 July 2020).
- Tan A., Adam J. C. & Lettenmaier D. P. 2011 Change in spring snowmelt timing in Eurasian Arctic rivers. *Journal of Geophysical Research-Atmospheres*, **116**.
- Teutschbein C. & Seibert J. 2010 Regional Climate Models for Hydrological Impact Studies at the Catchment Scale: A Review of Recent Modeling Strategies: Regional climate models for hydrological impact studies. *Geography compass*, **4**(7), 834-60.
- Thompson S. 1999 *Hydrology for Water Management*. CRC Press, London, UK.
- Tolera M. B., Chung I. M. & Chang S. W. 2018 Evaluation of the Climate Forecast System Reanalysis Weather Data for Watershed Modeling in Upper Awash Basin, Ethiopia. *Water*, **10**(6).
- Van Liew M. W., Arnold J. G. & Garbrecht J. D. 2003 Hydrologic simulation on agricultural watersheds: Choosing between two models. *Transactions of the Asae*, **46**(6), 1539-51.
- van Vuuren D. P., Edmonds J., Kainuma M., Riahi K., Thomson A., Hibbard K., Hurtt G. C., Kram T., Krey V., Lamarque J. F., Masui T., Meinshausen M., Nakicenovic N., Smith S. J. & Rose S. K. 2011 The representative concentration pathways: an overview. *Climatic Change*, **109**(1-2), 5-31.
- Vaze J., Jordan P. W., Beecham R., Frost A. J. & Summerell G. K. 2011 Guidelines for rainfall-runoff modelling: towards best practice model application. In.
- Vinet F. 2017 Flood Impacts on Loss of Life and Human Health. In: *Floods*, pp. 33-51.
- Walvoord M. A. & Kurylyk B. L. 2016 Hydrologic Impacts of Thawing Permafrost-A Review. *Vadose Zone Journal*, **15**(6).
- Waterbase 2007a Land use. http://www.waterbase.org/download_data.html (accessed 14 February 2021).
- Waterbase 2007b Soil. http://www.waterbase.org/download_data.html (accessed 14 February 2021).

- Wilson D., Fleig A. K., Lawrence D., Hisdal H., Pettersson L.-E. & Holmqvist E. 2011 *A review of NVE's flood frequency estimation procedures*, Norwegian Water Resources and Energy Directorate, Oslo, Norway.
- Wilson S. J., Murray J. L., Huntington H. P., Arctic M. & Assessment P. 1998 *AMAP assessment report : Arctic pollution issues*. Arctic Monitoring and Assessment Programme, Oslo.
- Wiltshire S. E. 1987 *Statistical techniques for regional flood frequency analysis*. Unpublished PhD thesis, Newcastle University.
- Woldemeskel F. M., Sharma A., Sivakumar B. & Mehrotra R. 2012 An error estimation method for precipitation and temperature projections for future climates. *Journal of Geophysical Research-Atmospheres*, **117**.
- Woo M. 2012a Active Layer Dynamics. In: *Permafrost Hydrology* Springer Berlin Heidelberg, Berlin, Heidelberg, Germany, pp. 163-227.
- Woo M. 2012b Snow cover. In: *Permafrost Hydrology* Springer Berlin Heidelberg, Berlin, Heidelberg, Germany, pp. 1-34.
- Xu C.-Y., Xiong L. & Singh V. P. 2019a Black-box hydrological models. In: *Handbook of Hydrometeorological Ensemble Forecasting* Duan Qea (ed.), Springer Berlin Heidelberg, Berlin, Heidelberg, Germany, pp. 341-87.
- Xu X., Wang Y. C., Kalcic M., Muenich R. L., Yang Y. C. E. & Scavia D. 2019b Evaluating the impact of climate change on fluvial flood risk in a mixed-use watershed. *Environmental Modelling & Software*, **122**.
- Yang D. & Kane D. L. 2021 Arctic hydrology, permafrost and ecosystems. In, Springer, Cham, Switzerland.
- Zakharova E. A., Kouraev A. V., Biancamaria S., Kolmakova M. V., Mognard N. M., Zemtsov V. A., Kirpotin S. N. & Decharme B. 2011 Snow Cover and Spring Flood Flow in the Northern Part of Western Siberia (the Poluy, Nadym, Pur, and Taz Rivers). *Journal of Hydrometeorology*, **12**(6), 1498-511.
- Zhang L. H., Jin X., He C. S., Zhang B. Q., Zhang X. F., Li J. L., Zhao C., Tian J. & DeMarchi C. 2016 Comparison of SWAT and DLBRM for Hydrological Modeling of a Mountainous Watershed in Arid Northwest China. *Journal of Hydrologic Engineering*, **21**(5).
- Zhou T., Liu Z. Y., Jin J. L. & Hu H. X. 2019 Assessing the Impacts of Univariate and Bivariate Flood Frequency Approaches to Flood Risk Accounting for Reservoir Operation. *Water*, **11**(3).

Appended Papers

Paper I

Bui, Minh Tuan; Lu, Jinmei; Nie, Linmei. A review of hydrological models applied in the permafrost-dominated Arctic region. *Geosciences* 2020; Volume 10:401 (10). ISSN 2076-3263.s 1 - 26.s doi: <https://doi.org/10.3390/geosciences10100401>.

The paper was published in the Special Issue, “Hydrological Systems and Models Applied in Permafrost”.

Review

A Review of Hydrological Models Applied in the Permafrost-Dominated Arctic Region

Minh Tuan Bui ^{1,*}, Jinmei Lu ¹ and Linmei Nie ²

¹ Department of Technology and Safety, Faculty of Science and Technology, UiT The Arctic University of Norway, 9037 Tromsø, Norway; jinmei.lu@uit.no

² Centre for Sustainable Development and Innovation of Water Technology, Foundation CSDI WaterTech, 0373 Oslo, Norway; linmei.nie@csdi.no

* Correspondence: minh.t.bui@uit.no

Received: 29 June 2020; Accepted: 4 October 2020; Published: 6 October 2020



Abstract: The Arctic region is the most sensitive region to climate change. Hydrological models are fundamental tools for climate change impact assessment. However, due to the extreme weather conditions, specific hydrological process, and data acquisition challenges in the Arctic, it is crucial to select suitable hydrological model(s) for this region. In this paper, a comprehensive review and comparison of different models is conducted based on recently available studies. The functionality, limitations, and suitability of the potential hydrological models for the Arctic hydrological process are analyzed, including: (1) The surface hydrological models Topoflow, DMHS (deterministic modeling hydrological system), HBV (Hydrologiska Byråns Vattenbalansavdelning), SWAT (soil and water assessment tool), WaSiM (water balance simulation model), ECOMAG (ecological model for applied geophysics), and CRHM (cold regions hydrological model); and (2) the cryo-hydrogeological models ATS (arctic terrestrial simulator), CryoGrid 3, GEOtop, SUTRA-ICE (ice variant of the existing saturated/unsaturated transport model), and PFLOTRAN-ICE (ice variant of the existing massively parallel subsurface flow and reactive transport model). The review finds that Topoflow, HBV, SWAT, ECOMAG, and CRHM are suitable for studying surface hydrology rather than other processes in permafrost environments, whereas DMHS, WaSiM, and the cryo-hydrogeological models have higher capacities for subsurface hydrology, since they take into account the three phase changes of water in the near-surface soil. Of the cryo-hydrogeological models reviewed here, GEOtop, SUTRA-ICE, and PFLOTRAN-ICE are found to be suitable for small-scale catchments, whereas ATS and CryoGrid 3 are potentially suitable for large-scale catchments. Especially, ATS and GEOtop are the first tools that couple surface/subsurface permafrost thermal hydrology. If the accuracy of simulating the active layer dynamics is targeted, DMHS, ATS, GEOtop, and PFLOTRAN-ICE are potential tools compared to the other models. Further, data acquisition is a challenging task for cryo-hydrogeological models due to the complex boundary conditions when compared to the surface hydrological models HBV, SWAT, and CRHM, and the cryo-hydrogeological models are more difficult for non-expert users and more expensive to run compared to other models.

Keywords: Arctic region; permafrost; climate change; hydrological model

1. Introduction

1.1. Extreme Global Climate Change in the Arctic Region

Global climate change (GCC) is more intensive in the Arctic region than in other parts of the world [1,2]. The annual average temperature in the Arctic has increased at twice the rate of that in the rest of the world since 1980 [1]. Since 2005, the surface air temperature in the Arctic has been higher

than any recorded five-year period from 1880 [1]. During the 1971–2017 period, the annual mean air temperature in the Arctic increased by around 2.7 °C [2]. It is predicted that the air temperature in autumn and winter in the Arctic region will continue to increase by around 4 °C over the next two decades [2]. Intensive climate change in the Arctic has a significant impact on the hydrological processes in the region.

1.2. The Presence of Permafrost and Its Relation to Hydrological Processes in the Arctic Region

Permafrost accounts for approximately 24% of the exposed land area in the Northern Hemisphere [3]. Permafrost regions have different hydrology and hydrology-related conditions compared to non-permafrost regions [4,5]. Permafrost can affect many hydrological processes in Arctic and sub-Arctic environments [6], for example, surface and subsurface water fluxes [4,7–9]. Especially, permafrost accelerates the initiation of runoff [10] and shortens the time of response to rainfall [4]. Additionally, the evapotranspiration process from vegetation is limited in permafrost environments since permafrost prevents the downward growth of roots and therefore limits the uptake of water for evapotranspiration [4,7]. Other processes, including microclimatology and thermal regimes (related to the evapotranspiration process) [11,12], water storage processes [4,13,14], and energy and water balances [13,14] are also affected by permafrost. The thin soil layer overlying permafrost is the active layer that seasonally freezes and thaws [4,5]. This active layer in the Arctic varies from several centimeters to one or two meters in depth [6] and most of the hydrological and biogeochemical processes occur in this layer [7,15]. The active layer determines the conditions for plant growth, gas fluxes, groundwater flow regimes, and soil formation [13]. While the active layer supports many hydrological and biogeochemical processes, permafrost beneath the active layer limits the amount of soil water percolation and subsurface storage of water [16]. Unlike non-permafrost soils, where a groundwater system is available and deep, the subsurface movement of water in permafrost-affected soil is mostly confined to the shallow active layer [6]. Because of this limitation of the vertical movement of subsurface flow in permafrost soil, subsurface flow in the horizontal direction is therefore important [6,17]. Moreover, the presence of permafrost has influenced the magnitude of the specific base flow in some Arctic basins. According to the study by McNamara et al., the specific base flow in a permafrost basin is lower than that in a non-permafrost basin [10].

1.3. The Impacts of Permafrost Thawing on the Arctic Hydrological Processes

Climate change is expected to alter the hydrological processes in the Arctic [6,18], e.g., through thawing of the permafrost layer, which has been observed from the field measurement data obtained during the last decades [19–24]. Global warming is expected to lead to permafrost degradation through changes in the three-dimensional distribution of permafrost (Figure 1), e.g., via changes in the active layer thickness (ALT) [8,25–28], spatial extent [26], open vertical taliks [29], and lateral taliks [30]. The thawing of permafrost is expected to change both surface and subsurface hydrology in the Arctic [31]. Permafrost thawing leads to alterations in: (1) Water fluxes and flow paths, including increasing soil drainage, increasing suprapermfrost flow (SUPRA-PF) [32], runoff variation [33], increasing evapotranspiration (ET), increasing the exchange of water flow between lakes and groundwater [34], increasing subpermafrost flow (SUB-PF), and increasing baseflow [35–38]; (2) secondly, water storage and ecosystem responses including water distribution, e.g., variation in soil moisture [39], lakes and wetlands [40,41], groundwater (GW) storage [42,43], aufeis (icing) volume [44], decreasing winter river ice thickness [45], and ecosystem variables, e.g., increasing vegetation [46,47], variation in surface water connectivity [48], increasing subsurface connectivity, decreasing streamflow, and temperature seasonality [49]; and (3) also alterations in greenhouse gasses (GHGs) and the surface energy flux [50]. It is projected that, because of permafrost degradation under global climate change, surface water systems will be transferred to more groundwater-based systems in large-scale assessments of the Arctic region [31].

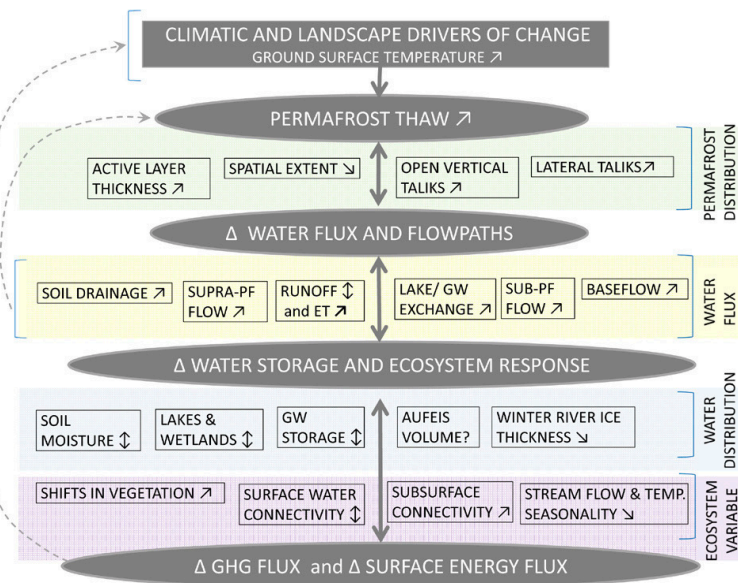


Figure 1. A sketch of impacts and responses of permafrost thawing on water fluxes and distribution. The symbols of Δ , \nearrow , \searrow , \updownarrow , and $?$ denote change, increase, decrease, variation, and unknown changes, respectively. Modified from [25].

1.4. Importance of Choosing the Suitable Modeling Tools for the Arctic Region

It has been demonstrated that the presence of permafrost has a high impact on hydrological processes in the Arctic. The changes of Arctic hydrology (including surface and subsurface hydrology) are expected to be more complicated under the context of global climate change, which causes permafrost degradation and changes in other related processes. Hydrological models are state-of-the-art tools for the investigation of global climate change impacts, and numerous models have been developed in recent decades. Both surface and subsurface hydrological models have demonstrated their capacities to simulate permafrost hydrology. For example, many surface hydrological models have approached analytical solutions (by using a simple heat transfer equation, e.g., Stefan's equation) and numerical solutions (e.g., finite difference, finite element, and finite volume methods) to simulate the seasonal freezing–thawing process. Many subsurface hydrological models have coupled a three-dimensional (3D) equation for water flow (e.g., the 3D Richards equation) and a three-dimensional equation for heat transfer, especially considering the three phase changes of water in near-surface soil. However, both surface and subsurface hydrological models still have their limitations when dealing with permafrost hydrology. For example, one-dimensional (vertical direction) heat transfer, used in surface hydrological models, cannot be used to simulate multidecadal and multidimensional changes. Additionally, surface hydrological models still lack important processes in permafrost environments, such as consideration of heat capacity, thermodynamic equilibrium, and the three phase changes (ice, liquid, and gas) of water in near-surface soils. Subsurface hydrological models do not feature land surface schemes in their structures and have complex boundary conditions, and they are also difficult for non-expert users to use, etc. Moreover, sparse data of the Arctic make it more difficult to collect the necessary input data for the models. Therefore, finding suitable models for the Arctic is a challenge for hydrological modelers. The current paper presents a review and analysis of the functions, advantages, and disadvantages of different hydrological models and evaluates their suitability for simulating hydrological processes in the Arctic region. The selection of suitable models is carried out via answering the following pertinent questions:

1. Do the models consider the important processes in permafrost environments, including the following factors:
 - Surface energy balance;
 - Snow processes, snow insulation, and snow melt;
 - Infiltration processes;
 - The dynamics of soil thermal and soil moisture fluxes;
 - Soil heterogeneities;
 - The dynamics (seasonal thawing) of the active layer;
 - Subsidence;
 - A three-phase change of water (ice, liquid, and gas) during the freezing and thawing of near-surface soil.
2. Can the models be widely applied for Arctic permafrost, particularly considering the following requirements:
 - Requirement for input data, i.e., large or small requirement;
 - Requirement for computation processes, i.e., strong or low requirement;
 - Ability to be applied with different sizes of watersheds, i.e., small-scale and/or large-scale.

2. Some Well-Known Hydrological Models Applied in the Arctic

2.1. Topoflow Model

Topoflow is a spatially distributed and process-based hydrological model that was firstly designed for Arctic and sub-Arctic basins [6]. Topoflow has the capacity to simulate hydrological processes in permafrost environments, including the surface energy balance, snowmelt (using simple degree day or full energy balance methods), infiltration (using Green–Ampt, Smith–Parlange, or 1D Richards' equation with three layers), and volumetric soil moisture content (using Darcian theory with multiple uniform layers). Moreover, Topoflow is able to reasonably simulate the ALT with a relatively simple method. However, such a method should be further improved in order to analyze the dynamics of the active layer more accurately, since the active layer has a high impact on the hydrological processes in permafrost environments [51]. The simulation of subsidence and a three-phase change of water (ice, liquid, and gas) during the freezing–thawing process of the near-surface soil is not mentioned in the Topoflow model.

The Topoflow model was applied in a small-scale watershed in the Arctic, Imnavait Creek, (around 2 km²) in Alaska, United States, which was underlain by continuous permafrost [6]. The results showed that the model has good performance for simulation of the hydrological cycle, including evapotranspiration, snowmelt, infiltration, runoff, and energy balances in the Arctic [6]. The hydrology change of the Imnavait Creek watershed under different climate change scenarios was also simulated [6], including evaluation of the performance of the model. The model has some limitations, such as the spatial variability of the active layer's depth (not presented in the model) and the simplification of the complex soil moisture heterogeneity, etc.

2.2. DMHS Model

The DMHS (deterministic modeling hydrological system) model was developed for both mountainous and flat topographies, including basins with different climate zones, regardless of their scales [52]. This model can be applied to any geographical area in the world [53]. The DMHS model is a kind of physically-based, semi-distributed model for runoff estimation. The model can simulate the important processes in permafrost-affected regions, such as the surface energy balance, snow accumulation, snowmelt, sublimation, infiltration, soil heterogeneity, heat and water dynamics,

and phase changes in soil layers [52–56]. Additionally, DMHS can also simulate the dynamics of the ALT with reliable results [57].

Vinogradov et al. [52] applied the DMHS model to six mountainous watersheds of different sizes, with areas varying from 40 to 2.4 million km² across eastern Siberia and inside the Lena River basin in the Arctic region, showing promising results. However, the DMHS model has limitations regarding the routing scheme, which is especially not applicable to rivers which have a backwater phenomenon [58]. Another limitation of the DMHS model is the difficulty in the acquisition of soil profile properties in a required format for the model [52]. This could be a limiting factor for its wide application in the Arctic, where the available data are usually limited.

2.3. HBV Model

The HBV (Hydrologiska Byråns Vattenbalansavdelning) model is a rainfall–runoff model that was first successfully applied in 1972 [59–63]. The HBV model has developed significantly since then, and nowadays it is considered to be a standard tool for an increasing number of applications, such as flood forecasting, forecasts of inflow to reservoirs of hydropower dams, assessment of the impacts of climate change on water resources, or for the simulation of hazards in designing high hydropower dams, etc. [64–67]. The HBV model can be used as a semi-distributed, conceptual model. The HBV model considers the important processes of permafrost hydrology, such as the surface energy balance, snow routine, snow melt, soil moisture, and infiltration. Especially, the model uses an accumulated degree day coefficient, which is set up based on field measurement, to simulate the ALT [68]. In some case, the HBV model is coupled with other thermal hydrological models, e.g., the CryoGrid model, for simulation of the active layer dynamics [67].

The HBV model has been applied in more than 40 countries with different climate conditions [69]. In Nordic countries, the HBV model is currently used for flood forecasting and several other purposes, such as the simulation of design flood for supporting the design for spillway structures [70], water resource evaluation [71,72], and nutrient load estimates [73]. In Norway, the HBV model has been applied since 1983 [74] and has recently been considered as an important tool for water management by NVE (the Norwegian Water Resources and Energy Directorate). The model has been used for flood forecasting under the impacts of climate change [75].

The advantage of the HBV model is that it requires less input data and computer facilities, which is suitable for the sparse data in the Arctic region. Especially, the model could be a potential tool for hydrological simulation in ungauged river basins. However, obtaining the optimum model parameters for the HBV is not an easy task [64]. In addition, HBV model simplifies the equation for water storage in the catchment. Moreover, the HBV model requires the most basic input data, i.e., only daily precipitation and average daily air temperature, and these data are spatially averaged over the watersheds by Thiessen polygons. However, the Thiessen polygon method does not consider the elevation and temperature gradients in the basin. Hence, the interpolation method used in the HBV model could result in unsatisfactory modeling results.

2.4. SWAT Model

The SWAT (soil and water assessment tool) model [76] is a robust watershed modeling tool which was designed by the USDA (United States Department of Agriculture) Agricultural Research Service, the USDA Natural Resources Conservation Service, and the Texas A&M University. The model is currently used in more than 100 countries around the world. The SWAT is a physically-based, semi-distributed, watershed-scale model which operates on a daily time step [77,78]. The model was developed to simulate the impacts of land use management activities on water resources, sediment, and agricultural chemical yields [79] in large, complex, and ungauged watersheds with variation in soils, land uses, and management conditions over long periods of time [80,81]. Moreover, the model supports the understanding of complex ecosystems, climate change, and agricultural production issues around the world [82–90]. The SWAT model is capable of modeling river basins for thousands

of square miles. Especially, it is able to simulate watersheds without requiring monitoring data. Regarding permafrost hydrology, the SWAT is able to simulate the surface energy balance, snow cover, snow melt, infiltration, soil moisture, soil heterogeneity, and lateral subsurface flow from the soil profile. Additionally, the SWAT takes into account the presence and development of the ALT in the model's structure but only via using the average values [91]. Therefore, further development in the model's structure to obtain a higher resolution for the spatiotemporal variation of the ALT is recommended, or otherwise coupling SWAT with other models to return better modeling results for the active layer dynamics. Moreover, simulation of soil heat transfer, snow insulation effects, and subsidence has not been developed yet for the SWAT model.

The SWAT model has been applied in many river basins in Europe and some regions in the Arctic. For instance, the SWAT model was applied to assess the variation of the hydrological regime and water quality under the impacts of human activities and climate change for the whole European territory [92]. In another study, the SWAT model was coupled with carbon modules to assess organic carbon exportation in an Arctic watershed via examination of the Yenisei River [91]. The advantage of the SWAT model is its capacity to model the temporal and spatial variations of hydrological process in large-scale Arctic watersheds [91]. The NRCS (Natural Resources Conservation Service) runoff curve number method in the SWAT provides a relatively easy way for the model to be adapted to a wide range of hydrological conditions [79].

2.5. WaSiM

The WaSiM (water balance simulation model) is a deterministic, spatially distributed hydrological model that was firstly developed during 1994-1996 by Jörg Schulla [93]. The model was designed to simulate water cycles in both surface and subsurface areas in river basins with variations in the spatial and temporal scales [93]. The WaSiM is able to simulate the hydrological processes for the catchments with sizes varying from <1 up to >100,000 km² [93]. The WaSiM is able to solve several issues in river basins, including assessing the impacts of climate change and land use change on water resources, runoff forecasting, groundwater recharge, soil water, substance transport, etc. [93]. The model runs with time steps from minutes to several days [93]. The WaSiM can be used for both short-term (e.g., floods) and long-term (e.g., water balance) simulations [93]. The WaSiM is able to simulate the important hydrological processes in Arctic permafrost, including snow accumulation, snow melt, infiltration, soil moisture, and soil heterogeneities. Additionally, the model can simulate the ALT dynamics in permafrost regions. However, such simulation is relatively simple and is only based on empirical approaches. Particularly, the WaSiM calculates the thaw depth based on the simple formula given as follows [94]:

$$d_{\text{thaw}} = \alpha \sqrt{n_{\text{sf}}}, \quad (1)$$

where:

- d_{thaw} is the thaw depth (m);
- α is an empirical coefficient (~0.02, . . . , 0.05);
- n_{sf} is the number of snow-free days.

Since the calculation approach in Equation (1) is relatively simple, in order to simulate the freezing–thawing process of the active layer more accurately, a physically-based heat transfer model is recommended [94].

The model is able to deal with soil heat flux. It provides the variations of soil temperatures in three dimensions. In addition, the WaSiM considers phase changes, which allows the model to simulate the freezing and thawing of an active layer in permafrost environments [95]. However, the drawbacks of the WaSiM is its high sensitivity to temporal and spatial resolutions. Therefore, the model is not suitable for transfer to other scales without recalibration. Moreover, the WaSiM requires intensive input data and model parameters for each grid cell of the model domain since it is a fully distributed model. This is considered as a big challenge in light of the scarce data in the Arctic region.

The WaSiM was first applied in the Arctic watershed by Liljedahl [93]. The long-term water balance during 1999–2009 was evaluated and its changes under global climate change in the permafrost-dominated watersheds were projected, such as the two vegetated drained thaw lake basins near Utqiagvik, formerly known as Barrow, in the north of Alaska. In another study, WaSiM was applied to assess the influence of permafrost degradation on the Arctic tundra hydrology [96].

2.6. ECOMAG Model

The ECOMAG (ecological model for applied geophysics) model is a physically-based, distributed hydrological model for the simulation of hydrological cycles and water quality transformation in catchments in cold climate regions [97,98]. The model includes two separate submodels, e.g., a hydrological submodel and a water quality submodel, which operate at a daily time step. The hydrological submodel describes several processes occurring in the catchments, including surface runoff, evapotranspiration, infiltration into soil layers, soil moisture, and subsurface flow. It is able to simulate the hydrothermal processes, which are important in permafrost regions, including the formation of snow cover, snowmelt rate (using the degree day method), ALT dynamics, infiltration of snowmelt into the unfrozen and frozen soils by integrating the governing equations of basic hydrodynamic and thermodynamic of water, heat vertical transfer, horizontal water flow, etc. [99]. The water quality submodel simulates the pollution transformation process from point sources and non-point sources in the catchment, including geochemical processes and the biochemical degradation process of dissolved organic pollutants.

The ECOMAG model was tested for hydrological simulation in numerous river basins in cold climate regions such as Canada, Russia, Norway, and Sweden. The model has been applied in the large Arctic basins, including the Mackenzie River basin in Canada, with satisfactory performance [100], and the Lena River basin in Russia, also with satisfactory performance [101]. Additionally, the ECOMAG was approached to investigate climate change impacts on the water regimes of those river basins [102,103].

2.7. CRHM Model

The CRHM (cold regions hydrological model) is a physically-based, semi-distributed model developed for hydrological cycle simulation over small to medium river basins in cold climate regions [104]. The CRHM is a flexible, object-oriented modeling system with the capacity to simulate a wide range of important permafrost-related processes in the cold regions, including snow processes (e.g., snow redistribution by wind, snow interception, sublimation, snowmelt, and infiltration of snowmelt into unfrozen and frozen soils), glacier melts, actual evaporation and evapotranspiration, radiation exchange, and soil moisture balance, etc. The CRHM is able to simulate the ALT dynamics by approaching Stefan's heat flow equation [105] as follows:

$$\xi = \sqrt{\frac{2kF}{Lw\rho'}} \quad (2)$$

where:

- ξ is the frost/thaw front depth (m);
- k is the thermal conductivity of the soil ($\text{W m}^{-1} \text{K}^{-1}$);
- F is the surface freeze/thaw index ($^{\circ}\text{C degree days}$);
- L is the latent heat of fusion (J kg^{-1});
- w is volumetric water content ($\text{m}^3 \text{m}^{-3}$);
- ρ is the bulk density of the soil (kg m^{-3}).

The CRHM is flexible in terms of its spatial solutions (from lumped to distributed) and model structures (from conceptual to physically-based), depending on the objectives of the studies and available input data for catchments. This is considered as a benefit for use in the Arctic region, which features sparse data. However, there is no required calibration for the model, and the model

parameters are normally obtained based on the expert knowledge of the modeled catchment. Therefore, the modeling results have high uncertainty.

2.8. ATS Model

The ATS (arctic terrestrial simulator) model, which was developed from Amanzi code [106], is an integrated tool of the permafrost-related process model and the physically-based model [107]. The model couples the surface energy balance model [108] and the three-dimensional (3D) subsurface thermal hydrology model [109,110] for multidimensional simulations in permafrost-affected regions. The model employs the diffusion wave equation to simulate the surface hydrology, energy transport, and phase change. However, simulation of the dynamic topography due to the influence of thaw-induced subsidence has not been developed yet.

The ATS model is an open source model and one of the first tools for addressing fully-coupled surface/subsurface permafrost thermal hydrology in multidimensional simulations, which is considered as the existing challenge for hydrological models in permafrost environments. By approaching a novel multiphysics management system [111] to increase the complexity of the model, the ATS model can meet the challenge of operating many numerical models in permafrost regions, i.e., performing nonlinear constitutive modeling, phase change modeling, the coupling of several processes in different spatial domains, the ability for simulating transitions among different states on the land surface, and the possibility for using an unstructured grid according to the given topographical features. Moreover, the ATS model has a fine-scale structure and is suitable for the specific topography of the polygonal Arctic tundra, which requires a high spatial resolution, large spatial model domain, and large grid size because of long-range surface flow. Therefore, the incorporation of the extension ATS code with good parallel scaling of the Amanzi code becomes a potential tool for investigating the responses of small-scale topographic features in permafrost environments in the context of global climate change. Moreover, the ATS is able to simulate comprehensive snow processes, such as an increasing snow density with snow age, snow insulation, and snow thermal conduction [107].

However, the ATS model has limitations regarding (1) solving the convergence of nonlinear systems around the transition between freezing and thawing [112] and (2) simulating topography change by subsurface ice melting requiring the movement of grid/mesh cells but having to maintain the water and energy balance inside the moving grid cells.

2.9. CryoGrid 3 Model

The CryoGrid 3 model is a new, simple, and one-dimensional land surface model developed to simulate ground surface temperatures in permafrost-affected regions. The model was built based on the thermal permafrost model CryoGrid 2 [113] by developing further calculation of the surface energy balance and modifying the snow scheme, which are important factors in permafrost hydrology processes. The CryoGrid 3 model is considered as the upper boundary condition of the CryoGrid 2 model. The surface energy balance describes the processes of energy transfer between the atmosphere and the ground. Such processes include the radiation balance, the exchange of sensible heat, evaporation, etc. [114], as described in the following equation:

$$\frac{\partial E}{\partial t} = S_{in} + S_{out} + L_{in} + L_{out} + Q_h + Q_e + Q_g, \quad (3)$$

where:

- S_{in}, S_{out} are the short-wave radiation input and output, respectively ($W m^{-2}$);
- L_{in}, L_{out} are the long-wave radiation input and output, respectively ($W m^{-2}$);
- Q_h, Q_e, Q_g are the sensible, latent, and ground heat fluxes, respectively ($W m^{-2}$).

The CryoGrid 3 model is able to simulate other important processes in permafrost-affected regions, including subsurface heat transfer (considering the phase change of soil water), energy transfer,

and mass balance of the snowpack. The subsurface thermal scheme is described by the concept of conductive heat transfer via Fourier's law as the following equation:

$$c_{\text{eff}}(z, T) \frac{\partial T}{\partial t} - \frac{\partial}{\partial z} \left(k(z, T) \frac{\partial T}{\partial z} \right) = 0, \quad (4)$$

where:

- $c_{\text{eff}}(z, T)$ is the effective volume capacity ($\text{J m}^{-3} \text{K}^{-1}$);
- $k(z, T)$ is the thermal conductivity ($\text{W m}^{-1} \text{K}^{-1}$).

The energy transfer within the snowpack is conductive heat transfer, which is similar to the soil, as in the following equation:

$$c_{\text{snow}}(z, T) \frac{\partial T^*}{\partial t} - \frac{\partial}{\partial z} \left(k_{\text{snow}}(z, T) \frac{\partial T^*}{\partial z} \right) = 0, \quad (5)$$

where:

- $c_{\text{snow}}(z, T)$ is the snow heat capacity ($\text{J m}^{-3} \text{K}^{-1}$);
- $k_{\text{snow}}(z, T)$ is the thermal conductivity of the snow ($\text{W m}^{-1} \text{K}^{-1}$);
- T^* is the snow temperature ($^{\circ}\text{C}$).

The CryoGrid 3 model is run in the MATLAB programming environment. The model has simple code and is open for modification. Therefore, the CryoGrid 3 model can be considered as a platform to integrate further processes in permafrost environments.

The CryoGrid 3 model has been tested in Arctic conditions with the large Lena River basin and showed satisfactory results to simulate the surface temperature, surface energy balance, ground temperature, ALT, and ground subsidence [115]. However, it is not guaranteed that the model could perform well in other permafrost basins. Instead, further considerations should be made before applying the model to a wider range of permafrost-affected regions. The CryoGrid 3 model has three major challenges [115]: (1) The model considers relatively simple snow processes (e.g., the assumption of a constant density of snowfall); (2) secondly, it is unclear that the model could perform well with the simulation of energy transfer and ground thermal regimes in regions with high vegetation cover; and, finally, (3) the simulation of the water balance needs further improvements, particularly for the simulation of seasonal changes.

2.10. GEOTop Model

The GEOTop model is a physically-based, distributed hydrological model that couples the water and energy balance [116,117]. The model was developed specifically for small catchments and complex mountain terrains. The GEOTop model combines the strengths of both land surface models and flood forecasting models [117]. In the GEOTop model, the interaction of topography with radiation is treated in detail, which is normally not considered in many hydrological models. The model simulates not only the energy balance (e.g., evapotranspiration and heat transfer) but also the water cycle (e.g., cycles of water, snow, and glaciers). The energy and mass balance is calculated based on a 3D Richards equation [118] and a 1D energy equation [112]. Vegetation, which contributes to the turbulent fluxes, is calculated based on a double layer scheme [119]. The snow processes (e.g., snow accumulation and snowmelt) are simulated by a multilayer discretization of the snowpack [120]. Additionally, a blowing snow module [121,122] is also included in the model to calculate the accumulation and blowing of snow because of wind.

The GEOTop model has been applied in a wide range of studies, including studies of soil water content [123], evaporation from soil [124,125], transpiration from vegetation [119], snow in basins [120,126,127], surface temperature [125], the temperature of soil and rock under freezing

conditions [128], the mass balance of glaciers [129], interactions between the ground water table and thaw depth [118], and discharge at basin outlets [116].

The GEOTop model is a fully distributed model and requires intensive inputs, model parameters, field measurements, and experiments, as well as intensive computation. Additionally, modification of the code in the GEOTop model is not allowed, unlike other cryo-hydrogeological models (e.g., CryoGrid 3 or SUTRA-ICE).

2.11. SUTRA-ICE Model

The SUTRA-ICE [130] model was developed by modification of the existing SUTRA (saturated/unsaturated transport) numerical model [131,132] in order to simulate the processes of subsurface ice formation and melting, which is important for heat transport, groundwater, and biological activities in permafrost environments [130]. Basically, the SUTRA model is a finite element numerical model for the simulation of saturated/unsaturated groundwater flow and solute energy transport. Regarding the working mechanisms, the SUTRA model approaches the problem via a two-dimensional hybrid method (e.g., finite element and finite difference methods) to describe two interdependent processes, including: (1) Fluid density-dependent saturated or unsaturated groundwater flow; and (2) the transport of a solute or thermal energy in groundwater flow, as well as in the solid matrix of the aquifer. Especially, the SUTRA model has the capacity to model the thermal regimes, thermal energy storage, and thermal pollution in aquifers, and additionally subsurface heat conductivity, geothermal reservoirs, and natural hydrogeological convection. In addition, the SUTRA model has been applied to investigate the impacts of climate change on permafrost thawing, ALT dynamics, and groundwater flow in cold climate regions [133–138]. Besides the functions existing in the SUTRA version, the modified SUTRA-ICE (with 2-dimensional and 3-dimensional versions) model can deal with the subsurface, saturated/unsaturated freezing processes (including phase changes), latent heat, permeability, heat capacity, thermal conductivity, and liquid porosity [139]. The SUTRA-ICE model has demonstrated its high capacity to simulate the formation and melting of near-surface ice and subsurface temperature distribution in cold climate region in previous studies [140]. The SUTRA-ICE model is a free model (applying for version 3.0) and it allows users to modify the code for further development. This is considered as an advantage of the model. However, the model has some challenges [139]: (1) The boundary conditions are complex; (2) it is still a problem to simulate freezing in unsaturated zones; (3) the model is not accurate for the simulation of active layer dynamics when the pore space is filled with both liquid and ice; (4) intensive computation is required; (5) the model is not able to utilize massive parallel computing hardware [109]; and (6) field verification is needed.

2.12. PFLOTRAN-ICE Model

The PFLOTRAN-ICE is a non-isothermal, single component (water), three-phase (ice, liquid, and gas) numerical model that has been recently developed to simulate subsurface hydrology in permafrost-affected regions [141]. The model calculates the balance of mass and energy for water components in three phases (ice, liquid, and gas) via the following equations [142]:

$$\frac{\partial}{\partial t} [\phi (s_g \eta_g X_w^g + s_l \eta_l + s_i \eta_i)] + \nabla \cdot [v_1 \eta_l] - \nabla \cdot [\phi s_g \tau_g \eta_g D_g \nabla X_w^g] = Q_w, \quad (6)$$

$$\frac{\partial}{\partial t} [\phi (s_l \eta_l U_l + s_g \eta_g U_g + s_i \eta_i U_i) + (1 - \phi) \rho_r c_r T] + \nabla \cdot [v_1 \eta_l H_l] - \nabla \cdot [kVT] = Q_e, \quad (7)$$

$$v_1 = \frac{k_{rl} k}{\mu_l} \nabla [p_l + \rho_l g z], \quad (8)$$

where:

- Subscripts l, g, and i, are the liquid, gas, and ice phases, respectively;
- ϕ is the porosity (-);

- s_l, s_g, s_i (constraint: $s_l + s_g + s_i = 1$) are saturation indices of the liquid, gas, and ice phases, respectively ($\text{m}^3 \text{m}^{-3}$);
- η_l, η_g, η_i are the molar densities of the liquid, gas, and ice phases, respectively (kmol m^{-3});
- X_w^g is the mole fraction of H_2O in the gas phase (-);
- τ_g is tortuosity of the gas phase (-);
- D_g is the diffusion coefficient in the gas phase (-);
- T is the temperature (it is assumed that all the phases and soil are in thermal equilibrium) (K);
- c_r is the heat capacity of the soil (J K^{-1});
- ρ_r is the density of the soil (kg m^{-3});
- U_l, U_g, U_i are the molar internal energies of the liquid, gas, and ice phases, respectively (kJ mol^{-1});
- H_l is the molar enthalpy of the liquid phase (kJ mol^{-1});
- Q_w is the mass source of H_2O ($\text{kmol m}^{-3} \text{s}^{-1}$);
- Q_e is the heat source ($\text{kmol m}^{-3} \text{s}^{-1}$);
- $\nabla()$ is the gradient operator (-);
- $\nabla \cdot ()$ is the divergence operator (-);
- v_l is Darcy velocity of the liquid phase (m s^{-1});
- k_{rl} is the relative permeability of the liquid phase (-);
- k is the absolute permeability (m^2);
- ρ_l is mass density of the liquid phase (kg m^{-3});
- p_l is the partial pressure of the liquid phase (Pa);
- g is acceleration because of gravity (m s^{-2});
- z is the vertical distance from a reference datum (m).

Together with the above balance equations, further requirements for the constitutive relationships (e.g., the mole fraction of water vapor, saturations of the phases, thermal conductivity, relative permeability, and water vapor diffusion coefficient) for the simulation of non-isothermal elements and the multiple phases of water are also described in the PFLOTRAN-ICE model.

The PFLOTRAN-ICE model makes use of the capacity in the PFLOTRAN code [143] for finding highly-scalable, parallel subsurface multiphysics solutions. Therefore, the model can simulate the degradation of ice wedge polygon bogs, which requires elucidation of three-phase change and relatively large model domains [144]. Although the PFLOTRAN-ICE model considers one component (water), the model is able to produce similar results to the more complicated two-component model [142] for the same application. This could be an advantage for the simulation of permafrost hydrology by using fewer demanding components (e.g., a single component of water substance). Moreover, the PFLOTRAN-ICE model is suitable for the large-scale range of model domains (i.e., kilometer scales).

However, the PFLOTRAN-ICE model does not consider surface flows, the surface energy balance, and topography dynamics because of permafrost thawing and the melting of ground ice. Such processes are expected to be coupled with subsurface hydrology for the comprehensive modeling of hydrology in permafrost-dominated regions [144].

2.13. The Present Capacities and Challenges of Hydrological Models to Deal with Permafrost Hydrology in the Arctic

2.13.1. Surface Hydrological Models

Surface hydrological models have demonstrated their capacity to simulate the seasonal freeze–thaw process in soil by approaching analytical and numerical solutions [25]. Regarding the analytical solutions, many physically-based models have incorporated a simple heat transfer equation (e.g., Stefan’s equation [145]) into their structure to deal with the soil freeze–thaw process. Because of the simplification of soil freeze–thaw algorithms, simulation for large-scale basins is an advantage [146,147]. Additionally, Stefan’s equation may be easily modified to include other processes, such as the temporal

variation of soil moisture [148], spatial variation of the moisture content, thermal properties [149], the freezing–thawing process in two directions [150], heat advection [151], and the soil heat capacity [152]. Beside the analytical solutions, some surface hydrological models, especially distributed models [153–156], have approached numerical solutions (e.g., via finite difference, finite element, and finite volume methods) to simulate the ground freezing–thawing process. Such numerical approaches are able to deal with complex conditions (e.g., varying soil heterogeneities and complex temperature boundaries) or complex processes (e.g., coupling heat and water transfer, discontinuous freezing–thawing process, and the temporal variation of thermal factors). Compared to analytical solutions, numerical solutions perform better in the context of the freezing–thawing process in the ground [147]. For example, numerical solutions simulate the freezing and thawing process in soil over a wide range of temperatures, unlike the assumption of sharp change by analytical solutions. Therefore, such a freezing range permits some subsurface water flow at sub-zero temperatures.

However, there are still numerous challenges for surface hydrological models in permafrost environments [25]. First of all, many surface hydrological models coupled with numerical soil freezing models only consider a vertical direction of heat transfer but ignore the lateral direction, which is crucial to the isolated and discontinuous permafrost bodies located in the lowland regions [157,158], as well as in steep and alpine regions [159,160]. Therefore, one-dimensional heat transfer is only suitable for simulating the seasonal freeze–thaw process of permafrost, but not for multidecadal and multidimensional changes. Secondly, many surface hydrological models do not consider the important factors influencing the rate of the freezing–thawing process in soil, such as the heat capacity and soil layering. A lack of those factors could result in an inaccurate calculation of frost, depths of thawing, subsurface water storage, and groundwater routing. Thirdly, many surface hydrological models or numerical models of soil freezing–thawing processes do not represent the thermo-dynamic equilibrium well, particularly the disequilibrium phase change processes occurring during freezing and thawing, as well as disequilibrium pressure during the infiltration of snowmelt into partially frozen soils. Fourthly, surface hydrological models, even complex physically-based models, cannot accurately simulate the ground surface temperature, which controls the seasonal freezing–thawing process of soil under snowpack and snow-free conditions. This is because ground thermal regimes can be highly sensitive to model parameters [140,161,162]. Lastly, in permafrost environments, surface hydrological models are still unable to clearly represent the relationship between the hydraulic conductivity (K) of soil and the ice, liquid, and gas existing in partially frozen and unsaturated soils. For example, it is unclear whether the K factor of partially frozen soils is decreased or not by resistance factors.

2.13.2. Subsurface Hydrological Models/Groundwater Models/Cryo-Hydrogeological Models

Several one-dimensional groundwater models, coupled with energy transport models, have been developed to simulate the freezing and thawing process in soil since the 1970s. However, the simulation is only limited to the vertical direction. In the last decade, many multi-dimensional models have been developed to support groundwater simulation in permafrost environments [109,130,141,163,164]. Such models work by coupling a three-dimensional equation for water flow (the Richards equation) into a three-dimensional equation for heat transfer (e.g., heat conduction, heat advection, and thermal dispersion). Such models are also known as cryo-hydrogeological models, and they take into account the pore water phase change [165] and the impacts of the latent heat of it on the effectiveness of subsurface heat capacity, as well the decreasing hydraulic conductivity of soil because of the formed pore ice. Moreover, cryo-hydrogeological models have been approached in numerous studies of climate change impacts (e.g., the increase of the ALT) on groundwater (e.g., increase of baseflow and the groundwater exchange between supra-permafrost and sub-permafrost aquifers) in permafrost basins [134–138,157,166–170].

Beside the existing achievements, the cryo-hydrogeological models have several limitations. First of all, most of the models have been applied in ideal environmental conditions, except for a few studies conducting investigations under field conditions [108,157,171]. This is due to the lack of

hydrogeological data at high altitude or latitude regions. Secondly, most of the cryo-hydrogeological models do not include the land surface scheme and thermal processes in their structure. Therefore, the boundary conditions for such models must be subsurface conditions, such as the groundwater table, groundwater recharge rate, and soil temperature. However, such input data are limited and they are normally simplified and assumed. Thirdly, the models are limited into two dimensions with simplified structures, only considering small-scale areas. Additionally, the models require a fine grid structure and a small time step for application. Therefore, intensive computational processes are normally expected for the high spatial and temporal resolutions required. Finally, most of cryo-hydrogeological models are difficult for non-expert users to use because of their complexities.

2.14. Model Comparison Regarding the Capacities of the Models to Deal with Permafrost Hydrology in the Arctic

This section aims to summarize and identify the capabilities of the twelve well-known hydrological models for simulating Arctic permafrost hydrology. Permafrost is an important feature affecting hydrological processes in the Arctic. The main factor dominating water storage and transmission in permafrost basins is the ground thermal regime, which has been identified as the typical challenge of hydrological models in permafrost environments [31]. In addition to the ground thermal regime, other important processes related to permafrost hydrology and the Arctic conditions should be considered, such as the surface energy balance, snow process, snow insulation (influencing the air–soil temperature relationships), snowmelt, infiltration, soil heterogeneities, soil moisture regime, the three-phase change of water (ice, liquid, and gas) during the freezing–thawing process of near-surface soil, as well as the dynamics of the ALT. Therefore, the most suitable models for application in permafrost conditions should include as many of the important processes as possible. Table 1 summarizes the important processes for permafrost hydrology that are considered in each model's structure.

Table 1. Model comparison regarding the model's capacities to simulate the important processes in permafrost environments.

Model	Important Processes in Permafrost Environments Considered in the Model										
	(1)	(2)	(3)	(4)	(5)	(6)	(7)	(8)	(9)	(10)	(11)
Topoflow	√	n/a	n/a	√	√	n/a	√	√	√	n/a	n/a
DMHS	√	√	n/a	√	√	√	√	√	√	n/a	√
HBV	√	√	√	√	√	n/a	√	n/a	√	n/a	n/a
SWAT	√	√	n/a	√	√	n/a	√	√	√	n/a	n/a
WaSiM	√	√	n/a	√	√	√	√	√	√	n/a	√
ECOMAG	√	√	n/a	√	√	√	√	√	√	n/a	n/a
CRHM	√	√	n/a	√	√	√	√	√	√	n/a	n/a
ATS	√	√	√	√	√	√	√	√	√	√	√
CryoGrid 3	√	√	√	√	√	√	√	√	√	√	√
GEOtop	√	√	√	√	√	√	√	√	√	√	√
SUTRA-ICE	n/a	n/a	n/a	n/a	√	√	√	√	√	n/a	√
PFLOTRAN-ICE	n/a	n/a	n/a	n/a	√	√	√	√	√	n/a	√

According to Table 1, the important processes in permafrost environments considered in the model include: (1) Surface energy balance; (2) snow process; (3) snow insulation; (4) snowmelt; (5) infiltration; (6) soil thermal; (7) soil moisture; (8) soil heterogeneities; (9) active layer thickness (ALT) dynamics; (10) subsidence; and (11) three-phase change of water during the freezing–thawing process in near-surface soils. Additionally, the symbol of √ denotes available and the abbreviation of n/a defines not available, unclear, or no information.

The twelve hydrological models may be classified into two major groups. The first group are surface hydrological models, including Topoflow, DMHS, HBV, SWAT, WaSiM, ECOMAG, and CRHM. The second group are cryo-hydrogeological models, including ATS, CryoGrid 3, GEOtop, SUTRA-ICE, and PFLOTRAN-ICE. Generally, each model group has its own competences and limitations in dealing

with permafrost hydrology, as addressed in prior sections. The first model group performs well for the simulation of surface hydrology, but the capacities of these models to simulate sophisticated ground thermal processes, groundwater flow, or other processes related to permafrost degradation are low. For instance, most of models in group 1 are not able to take into account the influences of snow insulation on air–soil temperature relationships, as well as a required three-phase change of water in permafrost soil (except for DMHS and WaSiM). Some models exclude the important soil thermal process in their structure, such as Topoflow, HBV, and SWAT. None of the surface hydrological models are able to simulate the subsidence as a result of permafrost thawing. On the contrary, many cryo-hydrogeological models are able to simulate subsurface hydrological processes well.

Most of the cryo-hydrogeological models consider a required three-phase change in permafrost environments. Exceptionally, the SUTRA-ICE and PFLOTRAN-ICE models do not include land surface schemes and only simulate the subsurface hydrology. These two models are also not able to simulate the subsidence. Interestingly, almost all of the twelve models in the two groups have capacities to simulate the dynamics of the ALT. However, the accuracy or reliability of the simulation results are not the same for each model. Topoflow, HBV, SWAT, WaSiM, and SUTRA-ICE have low model performance, since they approach a relatively simple method for the simulation of the active layer dynamics, and they lack consideration of spatiotemporal variation.

2.15. Model(s) Selection for the Arctic

Concerning the specific hydrological processes and the sparse data of the Arctic region, the selection of a suitable model should fulfil two main criteria: (1) The capability of the model to deal with unique permafrost hydrological processes; and (2) the possibility to be applied with moderate amounts of data. Tables 2–5 summarize the main criteria as a basis to choose suitable models for application in the Arctic region. Since the freezing and thawing process of the ALT strongly impacts hydrological processes in the Arctic, the ALT was prioritized among other factors listed in Table 1 for selection of the suitable models for the Arctic.

First of all, if a study aims to only evaluate the surface hydrology process, Topoflow, HBV, SWAT, ECOMAG, and CRHM could be solutions, since they have been verified in many different case studies. Particularly, the conceptual model HBV and the physically-based, semi-distributed SWAT and CRHM models fit best for catchments with moderate data requirements, while the physically-based, distributed models Topoflow and ECOMAG require intensive inputs for every cell of the catchment.

Secondly, if the accuracy of subsurface hydrology simulation is prioritized, DMHS, WaSiM, and the cryo-hydrogeology models are good options, since such models take into account the three phase changes of water, which are important in permafrost environments for analyzing water during the freezing and thawing process of near-surface soils. Other models also have capacities to simulate the subsurface hydrology, but their performances are lower. Further, some cryo-hydrogeology models, e.g., GEOTop, SUTRA-ICE, and PFLOTRAN-ICE, are only suitable for applications in small-scale study areas, while ATS and CryoGrid 3 can be applied to larger basins. Since SUTRA-ICE and PFLOTRAN-ICE do not include a land surface scheme in their structure, these models should be coupled with other land surface models for applications in the Arctic region.

Further, among the five cryo-hydrogeology models, the ATS model has demonstrated its capacity to comprehensively simulate snow processes. It takes into account the snow thermal conductivity, increasing snow density by snow age, and snow insulation. While other models, e.g., CryoGrid 3, have relatively simple snow simulation processes, the ATS and GEOTop models are the first tools that have coupled surface/subsurface permafrost thermal hydrology. Although, such models still have very few applications in the Arctic, so they should be widely tested.

Table 2. Summarization of model comparisons.

Model	Data Requirements	Time Step	Simulating the ALT Dynamics	Study Area (km ²)	Ease-of-Use	Model Availability
Topflow	Spatial data: Digital elevation model (DEM) and soil. Meteorological data: Precipitation, air temperature, air pressure, wind speed, wind direction, relative humidity, solar radiation, and soil temperature.	Seconds to minutes	Using a relatively simple method. Spatial variability of the ALT is not presented.	<250	Simply learned command syntax; no calibration procedure; requires expert knowledge of the given catchment.	Open code
WaSiM	Spatial data: DEM, land use, and soil. Meteorological data: Precipitation, air temperature, wind speed, vapor pressure, and solar radiation.	Minutes to days	Using a relatively simple method only based on empirical parameters.	<1 to >100,000	The model allows various model configurations depending on the targets of studies, available input data, and quality of input data. The model can be operated with various spatial and temporal discretization solutions.	Open software
ECOMAG	Spatial data: DEM, land use, and soil. Meteorological data (for hydrological submodel): Precipitation, air temperature, and humidity.	Daily	Solving the thermodynamic equations and heat vertical transfer.	<250 to >2500	The model structure can be flexibly adjusted according to the available input data.	Requires a licensed ArcView platform

Table 3. Summarization of model comparisons (continued).

Model	Data Requirements	Time Step	Simulating the ALT Dynamics	Study Area (km ²)	Ease-of-Use	Model Availability
DMHS	Spatial data: DEM, land use, and soil. Meteorological data: Precipitation, air temperature, and relative humidity.	Daily/sub-daily	Using a heat transfer analytical solution via considering phase change in the soil profile.	<250 to >2500	Less effort for weather data collection, but difficult for acquisition of the soil profile properties in a suitable format for the model.	n/a
HBV	Spatial data: DEM, land use, and soil. Meteorological data: Precipitation, air temperature, and estimates of potential evapotranspiration.	Daily	Using an accumulated degree field measurement.	<250 to >2500	Requires little time to learn and run the model.	Open software
SWAT	Spatial data: DEM, land use, and soil. Meteorological data: Precipitation, max. and min. air temperature, wind speed, relative humidity, and solar radiation.	Daily	Only using the average values of the ALT.	<250 to >2500	Time consuming for data collection and processing, calibration, and validation.	Requires a licensed ArcGIS platform (applying for ArcSWAT)
CRHM	Spatial data: DEM, land use, and soil. Meteorological data: Precipitation, air temperature, wind speed, relative humidity, and short- and long-wave radiation.	Daily	Solving Stefan's heat flow equation.	<250 to 2500	No calibration procedure, but requires expert knowledge of the catchment.	Open software

Table 4. Summarization of model comparisons (continued).

Model	Data Requirements	Time Step	Simulating the ALT Dynamics	Study Area (km ²)	Ease-of-Use	Model Availability
ATS	Meteorological data: Air temperature, snow precipitation, rain precipitation, wind speed, relative humidity, incoming short-wave and long-wave radiation, and water table elevations.	Daily	Solving equations for the coupled surface (using the diffusion wave equation) and subsurface (using a three phase (ice, liquid, and gas) Richards-like equation), including the energy and flow (using an advection-diffusion equation) and surface energy balance, including snow.	<250 to >2500	Preparing the XML input code is a challenge.	Open code
CryoGrid 3	Meteorological data: Air temperature, relative or absolute humidity, wind speed, incoming short-wave and long-wave radiation, air pressure, and rates of snowfall and rainfall. Spatial data: Elevation (DTM), land use, and soil. Meteorological data: Precipitation intensity, wind velocity, wind direction, relative humidity, air temperature, dew temperature, air pressure, short-wave solar global radiation, short-wave solar direct radiation, short-wave solar diffuse radiation, short-wave solar net radiation, and long-wave incoming radiation.	Daily	Using a simple 1D parameterization.	<250 to >2500	The source code is simple and modifiable.	Open code
GEOtop		Hourly	Solving the energy and mass balance equations dealing with phase change based on the globally convergent Newton scheme.	<250	The source code is modifiable. High effort is required for data acquisition and processing of the hourly forcing data.	Open code

Table 5. Summarization of model comparisons (continued).

Model	Data Requirements	Time Step	Simulating the ALT Dynamics	Study Area (km ²)	Ease-of-Use	Model Availability
SUTRA-ICE	Flow data (specified pressures, specified flows and fluid sources) and energy or solute data (specified temperatures or concentrations, diffusive fluxes of energy, or solute mass at boundaries).	<1 to <12 h	Approaching a two-zone (frozen and thawed) analytical solution to simulate ice forming and melting in porous media, also ignoring a mushy zone containing both ice and water (as considered in the three-zone analytical solution of Lunardini).	Applicable for small-scale study areas (approx. a few hundred square meters).	The source code can be easily modified to add new processes by users.	Open code
PFLOTRAN-ICE	River stage, river chemistry, groundwater recharge, specified infiltration rate, temperature, gas pressure, and infiltration chemistry.	Hours to days	Solving the energy and mass balance equation for soil water in three-phase (ice, liquid, and gas) change.	The size of the study area can be up to a few kilometers.	The source code can be easily modified and further developed by users.	Open code

Although the cryo-hydrogeology models appear to be potential tools for researching permafrost hydrology, they could be difficult for non-expert users because of their complicated model structures. Workshops or training should be helpful for new users. Moreover, it is normally difficult to collect enough input data for subsurface hydrological models in Arctic regions. Thus, coupling surface hydrological models as upper boundary conditions for subsurface hydrological models is recommended as one of the solutions, where the outputs from surface hydrological models would become inputs for the subsurface hydrological models. For example, outputs from the SWAT model, e.g., groundwater recharge, soil deep percolation, and stream stage, etc., could be used as inputs for groundwater models.

Thirdly, if the accuracy of ALT dynamics is targeted, DMHS, ATS, GEOtop, and PFLOTRAN-ICE are desirable choices. The other remaining models are not recommended for the study of ALT dynamics since their approaches are relatively simple, resulting in highly uncertainty for the simulation results.

Fourthly, choosing a proper model also depends on the available input data of the catchments and the study conditions (e.g., funding, etc.). Although the cryo-hydrogeology models have high capacities to simulate permafrost hydrology, they still present challenges in terms of gathering the required input data, especially for information about the subsurface boundary conditions in the Arctic. Therefore, it is very expensive to run such simulations.

Lastly, successful application of a model also depends on the knowledge and experience of the hydrologist users to the given model. For example, although HBV is a kind of conceptual, semi-distributed model, it has been widely used in Nordic regions, i.e., cold climate region. In addition, the ECOMAG and CRHM models are well-known in Russia and Canada, respectively (Figure 2). However, the application of CRHM requires accumulated knowledge and data of the study catchments, since there is no calibration procedure or testing cases for the model. This could present a challenge for non-expert or less experienced users.

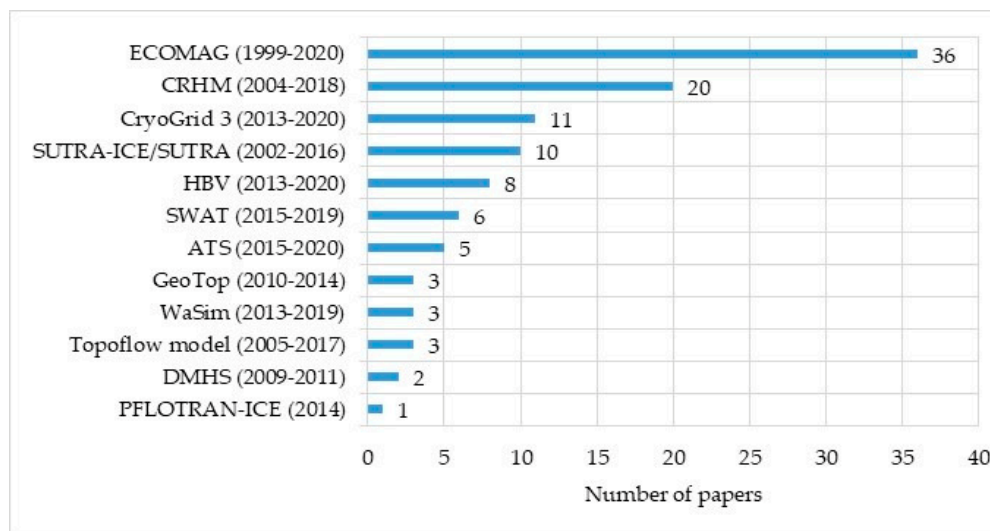


Figure 2. Number of recent publications on applications of hydrological/cryo-hydrogeological models in the Arctic (found via <https://www.scopus.com/>).

3. Conclusions

The hydrological processes in the Arctic are more complicated than in other regions. Finding a suitable hydrological model to simulate and predict changes in the hydrological processes is therefore a challenging task for modelers. This paper has reviewed the functions, structures, operational mechanisms, and performances of twelve hydrological models that have previously been applied or have potential for application in the Arctic. Of them, the DMHS, ATS, GEOtop, and PFLOTRAN-ICE models are desirable options for the simulation of ALT dynamics, which has

strong impacts on surface/subsurface hydrology. The three cryo-hydrogeology models GEOtop, SUTRA-ICE, and PFLOTRAN-ICE are only suitable for small-scale case studies, while the ATS and CryoGrid 3 models could be applied to large-scale catchments. The SUTRA-ICE and PFLOTRAN-ICE models appear to be suitable subsurface hydrological models. However, since they lack land surface schemes in their structures, they should be applied in tandem with other land surface models for the comprehensive simulation of permafrost hydrology. A significant revolution of hydrological modeling is the recently developed ATS and GEOtop models, which are the first tools that couple surface/subsurface permafrost thermal hydrology. It would be valuable to test the new models and to verify their performances in the Arctic condition. In the situation of only studying the surface hydrology, Topoflow, HBV, SWAT, ECOMAG, and CRHM could be good choices. Particularly, the semi-distributed models HBV, SWAT, and CRHM fit best for catchments with moderate data requirements, whereas the fully distributed models Topoflow and ECOMAG require intensive input data and model parameters. It is worth mentioning that since there is no required calibration procedure for the CRHM and Topoflow models, application of these models requires expert knowledge of the catchments, otherwise the modeling results could feature high uncertainty. Further, if the accuracy of simulating the subsurface hydrology in permafrost environments is targeted, DMHS, WaSiM, and the cryo-hydrogeological models are good options, since they consider the three phase changes of water during the freezing and thawing of near-surface soils. Finally, the selection of the suitable models for Arctic permafrost regions should be based on several factors, besides simulating the permafrost hydrology. Other factors, such as data acquisition, the required research period, and funding could influence the model selection and reliability of the results.

Author Contributions: M.T.B. initiated the idea, planned the scope, collected the information and data, structured and produced a draft manuscript, and performed revisions. J.L. supervised the progress, supported the idea, and conducted the review and editing. L.N. contributed to the reformulation of the paper structure, HBV hydrological model, language revision, and co-supervision of the review and revision processes. All authors have read and agreed to the published version of the manuscript.

Funding: This research received no external funding.

Acknowledgments: The authors would like to thank the Department of Technology and Safety, University of Tromsø—The Arctic University of Norway, for their financial support and administration for this study under project number 301184. Additionally, the publication charges for this article have been funded by a grant from the publication fund of UiT The Arctic University of Norway under project 551011. The collaboration with CSDI WaterTech is also highly appreciated. We especially thank the three anonymous reviewers for their constructive comments that helped to reasonably improve our manuscript. Finally, we also thank MDPI for English language editing, especially the English editor Max Kooij.

Conflicts of Interest: The authors declare no conflict of interest.

References

1. *Snow, Water, Ice and Permafrost in the Arctic (SWIPA): Climate Change and the Cryosphere*; Arctic Monitoring and Assessment Programme (AMAP): Oslo, Norway, 2011.
2. *Snow, Water, Ice and Permafrost in the Arctic (SWIPA): Climate Change and the Cryosphere*; Arctic Monitoring and Assessment Programme (AMAP): Oslo, Norway, 2017.
3. Romanovsky, V.; Burgess, M.; Smith, S.; Yoshikawa, K.; Brown, J. Permafrost temperature records: Indicators of climate change. *Eos* **2002**, *83*, 589–594. [[CrossRef](#)]
4. Woo, M.-K. Introduction. In *Permafrost Hydrology*; Springer Science and Business Media LLC: Berlin, Germany, 2012; pp. 1–34.
5. Woo, M.-K. Active Layer Dynamics. In *Permafrost Hydrology*; Springer Science and Business Media LLC: Berlin, Germany, 2012; pp. 163–227.
6. Schramm, I.; Boike, J.; Bolton, W.R.; Hinzman, L.D. Application of TopoFlow, a spatially distributed hydrological model, to the Imnavait Creek watershed, Alaska. *J. Geophys. Res. Space Phys.* **2007**, *112*, 1–14. [[CrossRef](#)]

7. Walsh, J.E.; Anisimov, O.; Hagen, J.O.M.; Jakobsson, T.; Oerlemans, J.; Prowse, T.D.; Romanovsky, V.; Savelieva, N.; Serreze, M.; Shiklomanov, A.; et al. Cryosphere and hydrology, Chapter 6. In *Arctic Climate Impact Assessment*; Cambridge University Press: London, UK, 2005; pp. 184–242.
8. Walvoord, M.A.; Voss, C.I.; Wellman, T.P. Influence of permafrost distribution on groundwater flow in the context of climate-driven permafrost thaw: Example from Yukon Flats Basin, Alaska, United States. *Water Resour. Res.* **2012**, *48*, 1–17. [[CrossRef](#)]
9. Frampton, A.; Destouni, G. Impact of degrading permafrost on subsurface solute transport pathways and travel times. *Water Resour. Res.* **2015**, *51*, 7680–7701. [[CrossRef](#)]
10. McNamara, J.P.; Kane, D.L.; Hinzman, L.D. An analysis of streamflow hydrology in the Kuparuk River Basin, Arctic Alaska: A nested watershed approach. *J. Hydrol.* **1998**, *206*, 39–57. [[CrossRef](#)]
11. Hinzman, L.D.; Kane, D.L.; Benson, C.S.; Everett, K.R. Energy Balance and Hydrological Processes in an Arctic Watershed. In *Ecological Studies*; Springer Science and Business Media LLC: Berlin, Germany, 1996; Volume 120, pp. 131–154.
12. Hinzman, L.D.; Bolton, R.W.; Petrone, K.; Jones, J.; Adams, P. Watershed hydrology and chemistry in the Alaskan boreal forest: The central role of permafrost. In *Alaska's Changing Boreal Forest*; Chapin, F.S., III, Ed.; Oxford University Press: New York, NY, USA, 2006; pp. 269–284.
13. Boike, J.; Roth, K.; Overduin, P.P. Thermal and hydrologic dynamics of the active layer at a continuous permafrost site (Taymyr Peninsula, Siberia). *Water Resour. Res.* **1998**, *34*, 355–363. [[CrossRef](#)]
14. Bowling, L.C.; Kane, D.L.; Gieck, R.E.; Hinzman, L.D.; Lettenmaier, D.P. The role of surface storage in a low-gradient Arctic watershed. *Water Resour. Res.* **2003**, *39*, 1087. [[CrossRef](#)]
15. Kane, D.L.; Hinzman, L.D.; Zarling, J. Thermal response of the active layer in a permafrost environment to climatic warming. *Cold Reg. Sci. Technol.* **1991**, *19*, 111–122. [[CrossRef](#)]
16. Vörösmarty, C.J.; Hinzman, L.D.; Peterson, B.J.; Bromwich, D.H.; Hamilton, L.C.; Morison, J.; Romanovsky, V.E.; Sturm, M.; Webb, R.S. *The Hydrologic Cycle and its Role in the Arctic and Global Environmental Change: A Rationale and Strategy for Synthesis Study*; Arctic Research Consortium of the United States: Fairbanks, AL, USA, 2001; pp. 1–84.
17. Slaughter, C.W.; Kane, D.L. Hydrologic role of shallow organic soils in cold climates. In Proceedings of the Canadian Hydrology Symposium 79: Cold Climate Hydrology, Vancouver, BC, Canada, 10–11 May 1979; pp. 380–389.
18. Hinzman, L.D.; Bettez, N.D.; Bolton, W.R.; Chapin, F.S.; Dyurgerov, M.B.; Fastie, C.L.; Griffith, B.; Hollister, R.D.; Hope, A.; Huntington, H.P.; et al. Evidence and Implications of Recent Climate Change in Northern Alaska and Other Arctic Regions. *Clim. Chang.* **2005**, *72*, 251–298. [[CrossRef](#)]
19. Lachenbruch, A.H.; Marshall, B.V. Changing Climate: Geothermal Evidence from Permafrost in the Alaskan Arctic. *Science* **1986**, *234*, 689–696. [[CrossRef](#)]
20. Osterkamp, T. A thermal history of permafrost in Alaska. In Proceedings of the 8th International Conference on Permafrost, Zurich, Switzerland, 21–25 July 2003; pp. 863–868.
21. Osterkamp, T.E. Characteristics of the recent warming of permafrost in Alaska. *J. Geophys. Res. Space Phys.* **2007**, *112*. [[CrossRef](#)]
22. Wu, Q.; Zhang, T. Recent permafrost warming on the Qinghai-Tibetan Plateau. *J. Geophys. Res. Space Phys.* **2008**, *113*, 13108. [[CrossRef](#)]
23. Batir, J.F.; Hornbach, M.J.; Blackwell, D.D. Ten years of measurements and modeling of soil temperature changes and their effects on permafrost in Northwestern Alaska. *Glob. Planet. Chang.* **2017**, *148*, 55–71. [[CrossRef](#)]
24. Farquharson, L.M.; Romanovsky, V.E.; Cable, W.L.; Walker, D.A.; Kokelj, S.V.; Nicolsky, D. Climate Change Drives Widespread and Rapid Thermokarst Development in Very Cold Permafrost in the Canadian High Arctic. *Geophys. Res. Lett.* **2019**, *46*, 6681–6689. [[CrossRef](#)]
25. Åkerman, H.J.; Johansson, M. Thawing permafrost and thicker active layers in sub-arctic Sweden. *Permafrost. Periglac. Process.* **2008**, *19*, 279–292. [[CrossRef](#)]
26. Mazhitova, G.G.; Malkova, G.; Chestnykh, O.; Zamolodchikov, D. Recent decade thaw depth dynamics in the European Russian Arctic based on the Circumpolar Active Layer Monitoring (CALM) data. In Proceedings of the 9th International Conference on Permafrost, Fairbanks, AL, USA, 29 June–3 July 2008; Institute of Northern Engineering, University of Alaska: Fairbanks, AL, USA, 2008; pp. 1155–1160.

27. Brutsaert, W.; Hiyama, T. The determination of permafrost thawing trends from long-term streamflow measurements with an application in eastern Siberia. *J. Geophys. Res. Space Phys.* **2012**, *117*, 1–10. [[CrossRef](#)]
28. Overeem, I.; Jafarov, E.; Wang, K.; Schaefer, K.; Stewart, S.; Clow, G.; Piper, M.; Elshorbany, Y. A Modeling Toolbox for Permafrost Landscapes. *Eos* **2018**, *99*, 1–11. [[CrossRef](#)]
29. Smith, L.C.; Sheng, Y.; Macdonald, G.M.; Hinzman, L.D. Disappearing Arctic Lakes. *Science* **2005**, *308*, 1429. [[CrossRef](#)]
30. Jepsen, S.M.; Voss, C.I.; Walvoord, M.A.; Minsley, B.J.; Rover, J. Linkages between lake shrinkage/expansion and sublacustrine permafrost distribution determined from remote sensing of interior Alaska, USA. *Geophys. Res. Lett.* **2013**, *40*, 882–887. [[CrossRef](#)]
31. Walvoord, M.A.; Kurylyk, B.L. Hydrologic impacts of thawing permafrost—A review. *J. Vadose Zone* **2016**, *15*, 1–20. [[CrossRef](#)]
32. Lyon, S.W.; Destouni, G. Changes in Catchment-Scale Recession Flow Properties in Response to Permafrost Thawing in the Yukon River Basin. *Int. J. Clim.* **2009**, *30*, 2138–2145. [[CrossRef](#)]
33. Gelfan, A.N. Modelling hydrological consequences of climate change in the permafrost region and assessment of their uncertainty. In *Proceedings of Cold Region Hydrology in a Changing Climate*; Marsh, P., Ed.; IAHS: Wallingford, UK, 2011; Volume 346, pp. 92–97.
34. Fedorov, A.; Gavriliev, P.P.; Konstantinov, P.Y.; Hiyama, T.; Iijima, Y.; Iwahana, G. Estimating the water balance of a thermokarst lake in the middle of the Lena River basin, eastern Siberia. *Ecology* **2013**, *7*, 188–196. [[CrossRef](#)]
35. Smith, L.C.; Pavelsky, T.M.; Macdonald, G.M.; Shiklomanov, A.I.; Lammers, R.B. Rising minimum daily flows in northern Eurasian rivers: A growing influence of groundwater in the high-latitude hydrologic cycle. *J. Geophys. Res. Space Phys.* **2007**, *112*, 1–18. [[CrossRef](#)]
36. Walvoord, M.A.; Striegl, R.G. Increased groundwater to stream discharge from permafrost thawing in the Yukon River basin: Potential impacts on lateral export of carbon and nitrogen. *Geophys. Res. Lett.* **2007**, *34*, 1–6. [[CrossRef](#)]
37. Jacques, J.-M.S.; Sauchyn, D.J. Increasing winter baseflow and mean annual streamflow from possible permafrost thawing in the Northwest Territories, Canada. *Geophys. Res. Lett.* **2009**, *36*, 1–6. [[CrossRef](#)]
38. Rennermalm, A.K.; Wood, E.F.; Troy, T.J. Observed changes in pan-arctic cold-season minimum monthly river discharge. *Clim. Dyn.* **2010**, *35*, 923–939. [[CrossRef](#)]
39. O'Donnell, J.A.; Jorgenson, M.T.; Harden, J.W.; McGuire, A.D.; Kanevskiy, M.Z.; Wickland, K.P. The Effects of Permafrost Thaw on Soil Hydrologic, Thermal, and Carbon Dynamics in an Alaskan Peatland. *Ecosystems* **2011**, *15*, 213–229. [[CrossRef](#)]
40. Labrecque, S.; Lacelle, D.; Duguay, C.R.; Lauriol, B.; Hawkings, J. Contemporary (1951–2001) Evolution of Lakes in the Old Crow Basin, Northern Yukon, Canada: Remote Sensing, Numerical Modeling, and Stable Isotope Analysis. *Arctic* **2009**, *62*, 225–238. [[CrossRef](#)]
41. Rover, J.; Ji, L.; Wylie, B.K.; Tieszen, L.L. Establishing water body areal extent trends in interior Alaska from multi-temporal Landsat data. *Remote. Sens. Lett.* **2011**, *3*, 595–604. [[CrossRef](#)]
42. Muskett, R.R.; Romanovsky, V. Alaskan Permafrost Groundwater Storage Changes Derived from GRACE and Ground Measurements. *Remote. Sens.* **2011**, *3*, 378–397. [[CrossRef](#)]
43. Velicogna, I.; Tong, J.; Zhang, T.; Kimball, J.S. Increasing subsurface water storage in discontinuous permafrost areas of the Lena River basin, Eurasia, detected from GRACE. *Geophys. Res. Lett.* **2012**, *39*, 1–5. [[CrossRef](#)]
44. Yoshikawa, K.; Hinzman, L.D.; Kane, D.L. Spring and aufeis (icing) hydrology in Brooks Range, Alaska. *J. Geophys. Res. Space Phys.* **2007**, *112*, 1–14. [[CrossRef](#)]
45. Beltaos, S.; Prowse, T. River-ice hydrology in a shrinking cryosphere. *Hydrol. Process.* **2009**, *23*, 122–144. [[CrossRef](#)]
46. Chasmer, L.; Hopkinson, C.; Quinton, W. Quantifying errors in discontinuous permafrost plateau change from optical data, Northwest Territories, Canada: 1947–2008. *Can. J. Remote. Sens.* **2010**, *36*, S211–S223. [[CrossRef](#)]
47. Baltzer, J.L.; Veness, T.; Chasmer, L.E.; Sniderhan, A.E.; Quinton, W.L. Forests on thawing permafrost: Fragmentation, edge effects, and net forest loss. *Glob. Chang. Biol.* **2014**, *20*, 824–834. [[CrossRef](#)]
48. Connon, R.F.; Quinton, W.L.; Craig, J.; Hayashi, M. Changing hydrologic connectivity due to permafrost thaw in the lower Liard River valley, NWT, Canada. *Hydrol. Process.* **2014**, *28*, 4163–4178. [[CrossRef](#)]

49. Liu, B.; Yang, D.; Ye, B.; Berezovskaya, S. Long-term open-water season stream temperature variations and changes over Lena River Basin in Siberia. *Glob. Planet. Chang.* **2005**, *48*, 96–111. [[CrossRef](#)]
50. Lawrence, D.M.; Koven, C.D.; Swenson, S.C.; Riley, W.J.; Slater, A.G. Permafrost thaw and resulting soil moisture changes regulate projected high-latitude CO₂ and CH₄ emissions. *Environ. Res. Lett.* **2015**, *10*, 094011. [[CrossRef](#)]
51. Bolton, W.R. Dynamic Modeling of the Hydrologic Processes in Areas of Discontinuous Permafrost. Ph.D. Thesis, University of Alaska Fairbanks, Fairbanks, AL, USA, August 2006.
52. Vinogradov, Y.B.; Semenova, O.M.; Vinogradova, T.A. An approach to the scaling problem in hydrological modelling: The deterministic modelling hydrological system. *Hydrol. Process.* **2010**, *25*, 1055–1073. [[CrossRef](#)]
53. Semenova, O.M.; Vinogradova, T.A. A universal approach to runoff processes modelling: Coping with hydrological predictions in data-scarce regions. In *Proceedings of Symposium HS.2 at the Joint IAHS & IAH Convention*; IAHS: Wallingford, UK, 2009; Volume 333, pp. 11–19.
54. Vinogradov, Y.B. *Mathematical Modelling of Runoff Formation. A Critical Analysis*; Gidrometeoizdat: Leningrad, Russia, 1988. (In Russian)
55. Semenova, O.; Lebedeva, L.; Vinogradov, Y. Simulation of subsurface heat and water dynamics, and runoff generation in mountainous permafrost conditions, in the Upper Kolyma River basin, Russia. *Hydrogeol. J.* **2013**, *21*, 107–119. [[CrossRef](#)]
56. Semenova, O.; Vinogradov, Y.; Vinogradova, T.; Lebedeva, L.; Semenova, O. Simulation of Soil Profile Heat Dynamics and their Integration into Hydrologic Modelling in a Permafrost Zone. *Permafr. Periglac. Process.* **2014**, *25*, 257–269. [[CrossRef](#)]
57. Lebedeva, L.; Semenova, O.; Vinogradova, T. Simulation of Active Layer Dynamics, Upper Kolyma, Russia, using the Hydrograph Hydrological Model. *Permafr. Periglac. Process.* **2014**, *25*, 270–280. [[CrossRef](#)]
58. Finney, D.L.; Blyth, E.; Ellis, R. Improved modelling of Siberian river flow through the use of an alternative frozen soil hydrology scheme in a land surface model. *Cryosphere* **2012**, *6*, 859–870. [[CrossRef](#)]
59. Bergström, S. *Development and Application of a Conceptual Runoff Model for Scandinavian Catchments*; Report RH07; SMHI: Norrköping, Sweden, 1976; pp. 1–134.
60. Bergström, S. *Parametervärden för HBV-Modellen i Sverige (Parameter Values for the HBV Model in Sweden)*; No 28; SMHI Hydrologi: Norrköping, Sweden, 1990; pp. 1–35. (In Swedish)
61. Bergström, S. Principles and Confidence in Hydrological Modelling. *Hydrol. Res.* **1991**, *22*, 123–136. [[CrossRef](#)]
62. Bergström, S.; Harlin, J.; Lindström, G. Spillway design floods in Sweden. I. New guidelines. *Hydrol. Sci. J.* **1992**, *37*, 505–519. [[CrossRef](#)]
63. Bergström, S. *Computer Models of Watershed Hydrology: The HBV Model*; Singh, V.P., Ed.; Water Resources Publications: Highlands Ranch, CO, USA, 1995; pp. 443–476.
64. Bergström, S. Experience from applications of the HBV hydrological model from the perspective of prediction in ungauged basins. *IAHS Public* **2006**, *307*, 97–107.
65. Bøggild, C.E.; Knudby, C.J.; Knudsen, M.B.; Starzer, W. Snowmelt and runoff modelling of an Arctic hydrological basin in west Greenland. *Hydrol. Process.* **1999**, *13*, 1989–2002. [[CrossRef](#)]
66. Wawrzyniak, T.; Osuch, M.; Nawrot, A.; Napiorkowski, J.J. Run-off modelling in an Arctic unglaciated catchment (Fuglebekken, Spitsbergen). *Ann. Glaciol.* **2017**, *58*, 36–46. [[CrossRef](#)]
67. Osuch, M.; Wawrzyniak, T.; Nawrot, A. Diagnosis of the hydrology of a small Arctic permafrost catchment using HBV conceptual rainfall-runoff model. *Hydrol. Res.* **2019**, *50*, 459–478. [[CrossRef](#)]
68. Bruland, O.; Killingtveit, Å. Application of the HBV-Model in Arctic catchments - some results from Svalbard. In *Proceedings of the XXII Nordic Hydrological Conference, Røros, Norway, 4–7 August 2002*.
69. Melesse, A.M. *Nile River Basin: Hydrology, Climate and Water Use*, 1st ed.; Springer: Dordrecht, The Netherlands, 2011.
70. Bergström, S. *The HBV Model, Its Structure and Applications, No. 4*; SMHI-Swedish Meteorological and Hydrological Institute: Norrköping, Sweden, 1992; pp. 1–35.
71. Jutman, T. Production of a New Runoff Map of Sweden. In *The Nordic Hydrological Conference, NHP report No.30*; Østrem, G., Ed.; KOHYNO: Oslo, Norway, 1992; pp. 643–651.
72. Brandt, M.; Bergström, S. Integration of Field Data into Operational Snowmelt-Runoff Models. *Hydrol. Res.* **1994**, *25*, 101–112. [[CrossRef](#)]
73. Arheimer, B. *Riverine Nitrogen—Analysis and Modeling under Nordic Conditions*; Tema, Linköpings Universitet: Linköping, Sweden, 1999; ISBN 91-7219-408-1.

74. Andersen, L.; Hjukse, T.; Roald, L.; Saelthun, N.R. *Hydrologisk Modell for Flomberegninger (A Hydrological Model for Simulation of Floods, in Norwegian)*; Rapport nr 2-83; NVE: Vassdragsdirektoratet, Oslo, Norway, 1983; pp. 1–40.
75. Lawrence, D.; Haddeland, I.; Langsholt, E. *Calibration of HBV Hydrological Models Using PEST Parameter Estimation*; Report No. 1-2009; NVE: Oslo, Norway, 2009; p. 44. ISBN 978-82-410-0680-7.
76. SWAT: Soil and Water Assessment Tool. Available online: <http://swat.tamu.edu/publications/> (accessed on 10 January 2019).
77. Arnold, J.G.; Fohrer, N. SWAT2000: Current capabilities and research opportunities in applied watershed modelling. *Hydrol. Process.* **2005**, *19*, 563–572. [[CrossRef](#)]
78. Srinivasan, R.; Ramanarayanan, T.S.; Arnold, J.G.; Bednarz, S.T. Large Area Hydrologic Modeling and Assessment Part II: Model Application. *JAWRA J. Am. Water Resour. Assoc.* **1998**, *34*, 91–101. [[CrossRef](#)]
79. Gassman, P.W.; Reyes, M.R.; Green, C.H.; Arnold, J.G. The Soil and Water Assessment Tool: Historical Development, Applications, and Future Research Directions. *Trans. ASABE* **2007**, *50*, 1211–1250. [[CrossRef](#)]
80. Arnold, J.G.; Williams, J.R.; Maidment, D.R. Continuous-Time Water and Sediment-Routing Model for Large Basins. *J. Hydraul. Eng.* **1995**, *121*, 171–183. [[CrossRef](#)]
81. Ndomba, P.M.; Mitalo, F.W.; Killingtveit, Å. Developing an Excellent Sediment Rating Curve From One Hydrological Year Sampling Programme Data: Approach. *J. Urban Environ. Eng.* **2008**, *2*, 21–27. [[CrossRef](#)]
82. Dile, Y.T.; Berndtsson, R.; Setegn, S.G. Hydrological Response to Climate Change for Gilgel Abay River, in the Lake Tana Basin—Upper Blue Nile Basin of Ethiopia. *PLoS ONE* **2013**, *8*, e79296. [[CrossRef](#)]
83. Dile, Y.T.; Karlberg, L.; Daggupati, P.; Srinivasan, R.; Wiberg, D.; Rockström, J. Assessing the implications of water harvesting intensification on upstream–downstream ecosystem services: A case study in the Lake Tana basin. *Sci. Total. Environ.* **2016**, *542*, 22–35. [[CrossRef](#)]
84. Krysanova, V.; Hattermann, F.; Wechsung, F. Implications of complexity and uncertainty for integrated modelling and impact assessment in river basins. *Environ. Model. Softw.* **2007**, *22*, 701–709. [[CrossRef](#)]
85. Lautenbach, S.; Volk, M.; Strauch, M.; Whittaker, G.; Seppelt, R. Optimization-based trade-off analysis of biodiesel crop production for managing an agricultural catchment. *Environ. Model. Softw.* **2013**, *48*, 98–112. [[CrossRef](#)]
86. Panagopoulos, Y.; Makropoulos, C.; Mimikou, M. Decision support for diffuse pollution management. *Environ. Model. Softw.* **2012**, *30*, 57–70. [[CrossRef](#)]
87. Schoul, J.; Abbaspour, K.; Srinivasan, R.; Yang, H. Estimation of freshwater availability in the West African sub-continent using the SWAT hydrologic model. *J. Hydrol.* **2008**, *352*, 30–49. [[CrossRef](#)]
88. Schoul, J.; Abbaspour, K.; Yang, H.; Srinivasan, R.; Zehnder, A.J.B. Modeling blue and green water availability in Africa. *Water Resour. Res.* **2008**, *44*, 1–18. [[CrossRef](#)]
89. Srinivasan, M.S.; Veith, T.L.; Gburek, W.J.; Steenhuis, T.S.; Gérard-Marchant, P. Watershed Scale modeling of critical source areas of runoff generation and phosphorus transport. *JAWRA J. Am. Water Resour. Assoc.* **2005**, *41*, 361–377. [[CrossRef](#)]
90. Vandenberghe, V.; Bauwens, W.; Vanrolleghem, P.A. Evaluation of uncertainty propagation into river water quality predictions to guide further monitoring campaigns. *Environ. Model. Softw.* **2007**, *22*, 725–732. [[CrossRef](#)]
91. Fabre, C.; Sauvage, S.; Tananaev, N.; Srinivasan, R.; Teisserenc, R.; Pérez, J.M.S. Using Modeling Tools to Better Understand Permafrost Hydrology. *Water* **2017**, *9*, 418. [[CrossRef](#)]
92. Abbaspour, K.; Rouholahnejad, E.; Vaghefi, S.; Srinivasan, R.; Yang, H.; Kløve, B. A continental-scale hydrology and water quality model for Europe: Calibration and uncertainty of a high-resolution large-scale SWAT model. *J. Hydrol.* **2015**, *524*, 733–752. [[CrossRef](#)]
93. Liljedahl, A.K. The Hydrologic Regime at Sub-Arctic and Arctic Watersheds: Present and Projected. Ph.D. Thesis, University of Alaska Fairbanks, Fairbanks, AL, USA, May 2011.
94. Simple Permafrost Model. Available online: http://www.wasim.ch/en/the_model/feature_permafrost.htm (accessed on 11 August 2020).
95. Model Description WaSiM (Water Balance Simulation Model). Available online: http://www.wasim.ch/downloads/doku/wasim/wasim_2012_ed2_en.pdf (accessed on 15 August 2020).
96. Liljedahl, A.; Boike, J.; Daanen, R.P.; Fedorov, A.N.; Frost, G.V.; Grosse, G.; Hinzman, L.D.; Iijima, Y.; Jorgenson, J.C.; Matveyeva, N.; et al. Pan-Arctic ice-wedge degradation in warming permafrost and its influence on tundra hydrology. *Nat. Geosci.* **2016**, *9*, 312–318. [[CrossRef](#)]

97. Motovilov, Y.G.; Belokurov, A. Modelling the pollution transfer and transformation processes in river basin for the tasks of environmental monitoring. *Proc. Inst. Appl. Geophys.* **1996**, *8*, 32–35. (In Russian)
98. Motovilov, Y. ECOMAG: A distributed model of runoff formation and pollution transformation in river basins. *IAHS Public* **2013**, *361*, 227–234.
99. Motovilov, Y.G.; Gottschalk, L.; Engeland, K.; Belokurov, A. *ECOMAG—Regional Model of Hydrological Cycle. Application to the NOPEX Region*; Report Series no.105; Department of Geophysics, University of Oslo: Oslo, Norway, 1999; ISBN 82-91885-04-4.
100. Motovilov, Y.; Kalugin, A.; Gelfan, A. An ECOMAG-based Regional Hydrological Model for the Mackenzie River basin. *EGUGA* **2017**. Available online: <https://ui.adsabs.harvard.edu/abs/2017EGUGA..19.8064M> (accessed on 29 June 2020).
101. Motovilov, Y. Modeling fields of river runoff (a case study for the Lena River basin). *Russ. Meteorol. Hydrol.* **2017**, *42*, 121–128. [[CrossRef](#)]
102. Gelfan, A.; Gustafsson, D.; Motovilov, Y.; Arheimer, B.; Kalugin, A.; Krylenko, I.; Lavrenov, A. Climate change impact on the water regime of two great Arctic rivers: Modeling and uncertainty issues. *Clim. Chang.* **2016**, *141*, 499–515. [[CrossRef](#)]
103. Krysanova, V.; Vetter, T.; Eisner, S.; Huang, S.; Pechlivanidis, I.; Strauch, M.; Gelfan, A.; Kumar, R.; Aich, V.; Arheimer, B.; et al. Intercomparison of regional-scale hydrological models and climate change impacts projected for 12 large river basins worldwide—A synthesis. *Environ. Res. Lett.* **2017**, *12*, 105002. [[CrossRef](#)]
104. Pomeroy, J.W.; Gray, D.M.; Brown, T.; Hedstrom, N.R.; Quinton, W.L.; Granger, R.J.; Carey, S.K. The cold regions hydrological model: A platform for basing process representation and model structure on physical evidence. *Hydrol. Process.* **2007**, *21*, 2650–2667. [[CrossRef](#)]
105. Krogh, S.A.; Pomeroy, J.W.; Marsh, P. Diagnosis of the hydrology of a small Arctic basin at the tundra-taiga transition using a physically based hydrological model. *J. Hydrol.* **2017**, *550*, 685–703. [[CrossRef](#)]
106. Moulton, J.D.; Berndt, M.; Garimella, R.; Prichett-Sheats, L.; Hammond, G.; Day, M.; Meza, J.C. *High-Level Design of Amanzi, the Multi-Process High Performance Computing Simulator*; ASCEM-HPC-2011-03-1; Office of Environmental Management, U.S. Department of Energy: Washington, DC, USA, 2012.
107. Painter, S.; Coon, E.T.; Atchley, A.; Berndt, M.; Garimella, R.V.; Moulton, D.; Svyatskiy, D.; Wilson, C.J. Integrated surface/subsurface permafrost thermal hydrology: Model formulation and proof-of-concept simulations. *Water Resour. Res.* **2016**, *52*, 6062–6077. [[CrossRef](#)]
108. Atchley, A.L.; Painter, S.L.; Harp, D.R.; Coon, E.T.; Wilson, C.J.; Liljedahl, A.K.; Romanovsky, V.E. Using field observations to inform thermal hydrology models of permafrost dynamics with ATS (v0.83). *Geosci. Model Dev.* **2015**, *8*, 2701–2722. [[CrossRef](#)]
109. Karra, S.; Painter, S.L.; Lichtner, P.C. A three-phase numerical model for subsurface hydrology in permafrost-affected regions (PFLOTRAN-ICE v1.0). *Cryosphere* **2014**, *8*, 1935–1950. [[CrossRef](#)]
110. Painter, S.L.; Karra, S. Constitutive Model for Unfrozen Water Content in Subfreezing Unsaturated Soils. *Vadose Zone J.* **2014**, *13*, 1–8. [[CrossRef](#)]
111. Coon, E.T.; Moulton, J.D.; Painter, S. Managing complexity in simulations of land surface and near-surface processes. *Environ. Model. Softw.* **2016**, *78*, 134–149. [[CrossRef](#)]
112. Dall’Amico, M.; Endrizzi, S.; Gruber, S.; Rigon, R. A robust and energy-conserving model of freezing variably-saturated soil. *Cryosphere* **2011**, *5*, 469–484. [[CrossRef](#)]
113. Westermann, S.; Schuler, T.V.; Gislén, K.; Eitzelmüller, B. Transient thermal modeling of permafrost conditions in Southern Norway. *Cryosphere* **2013**, *7*, 719–739. [[CrossRef](#)]
114. Westermann, S.; Langer, M.; Heikenfeld, M.; Boike, J. CryoGrid 3—A new flexible tool for permafrost modeling. In Proceedings of the CryoFIM Back work shop Svalbard, Longyearbyen, Svalbard, 15–19 April 2013.
115. Westermann, S.; Langer, M.; Boike, J.; Heikenfeld, M.; Peter, M.; Eitzelmüller, B.; Krinner, G. Simulating the thermal regime and thaw processes of ice-rich permafrost ground with the land-surface model CryoGrid 3. *Geosci. Model Dev.* **2016**, *9*, 523–546. [[CrossRef](#)]
116. Rigon, R.; Bertoldi, G.; Over, T.M. GEOTop: A Distributed Hydrological Model with Coupled Water and Energy Budgets. *J. Hydrometeorol.* **2006**, *7*, 371–388. [[CrossRef](#)]
117. GEOTop: A Distributed Hydrological Model with Coupled Water and Energy Balance. Available online: <http://geotopmodel.github.io/geotop/> (accessed on 8 August 2020).
118. Endrizzi, S.; Quinton, W.L.; Marsh, P. Modelling the spatial pattern of ground thaw in a small basin in the arctic tundra. *Cryosphere Discuss.* **2011**, *5*, 367–400. [[CrossRef](#)]

119. Endrizzi, S.; Marsh, P. Observations and modeling of turbulent fluxes during melt at the shrub-tundra transition zone 1: Point scale variations. *Hydrol. Res.* **2010**, *41*, 471–491. [[CrossRef](#)]
120. Endrizzi, S. Snow Cover Modelling at Local and Distributed Scale over Complex Terrain. Ph.D. Thesis, Institute of Civil and Environmental Engineering, Università degli Studi di Trento, Trento, Italy, 2007.
121. Pomeroy, J.; Gray, D.; Landine, P. The Prairie Blowing Snow Model: Characteristics, validation, operation. *J. Hydrol.* **1993**, *144*, 165–192. [[CrossRef](#)]
122. Essery, R.; Li, L.; Pomeroy, J. A distributed model of blowing snow over complex terrain. *Hydrol. Process.* **1999**, *13*, 2423–2438. [[CrossRef](#)]
123. Gebremichael, M.; Rigon, R.; Bertoldi, G.; Over, T.M. On the scaling characteristics of observed and simulated spatial soil moisture fields. *Nonlinear Process. Geophys.* **2009**, *16*, 141–150. [[CrossRef](#)]
124. Bertoldi, G.; Rigon, R.; Over, T.M. Impact of Watershed Geomorphic Characteristics on the Energy and Water Budgets. *J. Hydrometeorol.* **2006**, *7*, 389–403. [[CrossRef](#)]
125. Bertoldi, G.; Notarnicola, C.; Leitingner, G.; Endrizzi, S.; Zebisch, M.; Della Chiesa, S.; Tappeiner, U. Topographical and ecohydrological controls on land surface temperature in an alpine catchment. *Ecohydrology* **2010**, *3*, 189–204. [[CrossRef](#)]
126. Zanotti, F.; Endrizzi, S.; Bertoldi, G.; Rigon, R. The GEOTOP snow module. *Hydrol. Process.* **2004**, *18*, 3667–3679. [[CrossRef](#)]
127. Dall’Amico, M.; Endrizzi, S.; Rigon, R. Snow mapping of an alpine catchment through the hydrological model GEOTop. In Proceedings of the Conference Eaux en Montagne, Lyon, France, 16–17 March 2011; pp. 255–261.
128. Dall’Amico, M. Coupled Water and Heat Transfer in Permafrost Modeling. Ph.D. Thesis, Institute of Civil and Environmental Engineering, Università degli Studi di Trento, Trento, Italy, June 2010. Available online: <http://eprints-phd.biblio.unitn.it/335/> (accessed on 29 June 2020).
129. Noldin, I.; Endrizzi, S.; Rigon, R.; Dall’Amico, M. Sistema di drenaggio di un ghiacciaio alpino: Modello GEOTop. *Nevee Valanghe* **2010**, *69*, 48–54.
130. McKenzie, J.M.; Voss, C.I.; Siegel, D.I. Groundwater flow with energy transport and water–ice phase change: Numerical simulations, benchmarks, and application to freezing in peat bogs. *Adv. Water Resour.* **2007**, *30*, 966–983. [[CrossRef](#)]
131. Voss, C.I.; Provost, A. *SUTRA: A Model for 2D or 3D Saturated-Unsaturated, Variable-Density Ground-Water Flow with Solute or Energy Transport*; United States Geological Survey: Reston, VA, USA, 2002.
132. Voss, C.I. *A Finite-Element Simulation Model for Saturated-Unsaturated, Fluid-Density-Dependent Ground-Water Flow with Energy Transport or Chemically-Reactive Single-Species Solute Transport*, Water Resources Investigations Report 84-4369; United States Geological Survey: Reston, VA, USA, 1984.
133. Kurylyk, B.L.; Hayashi, M.; Quinton, W.L.; McKenzie, J.M.; Voss, C.I. Influence of vertical and lateral heat transfer on permafrost thaw, peatland landscape transition, and groundwater flow. *Water Resour. Res.* **2016**, *52*, 1286–1305. [[CrossRef](#)]
134. Ge, S.; McKenzie, J.; Voss, C.; Wu, Q. Exchange of groundwater and surface-water mediated by permafrost response to seasonal and long term air temperature variation. *Geophys. Res. Lett.* **2011**, *38*, 1–6. [[CrossRef](#)]
135. McKenzie, J.M.; Voss, C.I. Permafrost thaw in a nested groundwater-flow system. *Hydrogeol. J.* **2013**, *21*, 299–316. [[CrossRef](#)]
136. Wellman, T.P.; Voss, C.I.; Walvoord, M.A. Impacts of climate, lake size, and supra- and sub-permafrost groundwater flow on lake-talik evolution, Yukon Flats, Alaska (USA). *Hydrogeol. J.* **2013**, *21*, 281–298. [[CrossRef](#)]
137. Briggs, M.A.; Walvoord, M.A.; McKenzie, J.M.; Voss, C.I.; Day-Lewis, F.D.; Lane, J.W. New permafrost is forming around shrinking Arctic lakes, but will it last? *Geophys. Res. Lett.* **2014**, *41*, 1585–1592. [[CrossRef](#)]
138. Evans, S.G.; Ge, S.; Liang, S. Analysis of groundwater flow in mountainous, headwater catchments with permafrost. *Water Resour. Res.* **2015**, *51*, 9564–9576. [[CrossRef](#)]
139. Cold-Regions Groundwater Modeling Status and Challenges. Available online: http://ccrnetwork.ca/science/workshops/2015-modelling-workshop/Files/McKenzie_CCRN_Presentation.pdf (accessed on 4 August 2020).
140. Wu, M.-S.; Jansson, P.-E.; Tan, X.; Wu, M.-S.; Huang, J. Constraining Parameter Uncertainty in Simulations of Water and Heat Dynamics in Seasonally Frozen Soil Using Limited Observed Data. *Water* **2016**, *8*, 64. [[CrossRef](#)]

141. Endrizzi, S.; Gruber, S.; Dall'Amico, M.; Rigon, R. GEOtop 2.0: Simulating the combined energy and water balance at and below the land surface accounting for soil freezing, snow cover and terrain effects. *Geosci. Model Dev.* **2014**, *7*, 2831–2857. [[CrossRef](#)]
142. Painter, S. Three-phase numerical model of water migration in partially frozen geological media: Model formulation, validation, and applications. *Comput. Geosci.* **2010**, *15*, 69–85. [[CrossRef](#)]
143. Lichtner, P.C.; Hammond, G.E.; Lu, C.; Karra, S.; Bisht, G.; Andre, B.; Mills, R.; Kumar, J. *PFLOTRAN User Manual: A Massively Parallel Reactive Flow and Transport Model for Describing Surface and Subsurface Processes*; Office of Scientific and Technical Information, U.S. Department of Energy: Washington, DC, USA, 2015. [[CrossRef](#)]
144. Painter, S.; Moulton, J.D.; Wilson, C.J. Modeling challenges for predicting hydrologic response to degrading permafrost. *Hydrogeol. J.* **2012**, *21*, 221–224. [[CrossRef](#)]
145. Stefan, J. Über die Theorie der Eisbildung, insbesondere über die Eisbildung im Polarmeere. *Ann. Phys. Chem.* **1891**, *278*, 269–286. [[CrossRef](#)]
146. Riseborough, D.; Shiklomanov, N.; Etzelmüller, B.; Gruber, S.; Marchenko, S. Recent advances in permafrost modelling. *Permafr. Periglac. Process.* **2008**, *19*, 137–156. [[CrossRef](#)]
147. Zhang, Y.; Carey, S.K.; Quinton, W.L. Evaluation of the algorithms and parametrizations for ground thawing and freezing simulation in permafrost regions. *J. Geophys. Res.* **2008**, *113*, D17116. [[CrossRef](#)]
148. Hayashi, M.; Goeller, N.; Quinton, W.L.; Wright, N. A simple heat-conduction method for simulating the frost-table depth in hydrological models. *Hydrol. Process.* **2007**, *21*, 2610–2622. [[CrossRef](#)]
149. Kurylyk, B.L. Discussion of 'A simple thaw-freeze algorithm for a multi-layered soil using the Stefan equation. *Permafr. Periglac. Process* **2015**, *26*, 200–206. [[CrossRef](#)]
150. Woo, M.-K.; Arain, M.A.; Mollinga, M.; Yi, S. A two-directional freeze and thaw algorithm for hydrologic and land surface modelling. *Geophys. Res. Lett.* **2004**, *31*. [[CrossRef](#)]
151. Kurylyk, B.L.; McKenzie, J.M.; MacQuarrie, K.T.; Voss, C.I. Analytical solutions for benchmarking cold regions subsurface water flow and energy transport models: One-dimensional soil thaw with conduction and advection. *Adv. Water Resour.* **2014**, *70*, 172–184. [[CrossRef](#)]
152. Kurylyk, B.L.; Hayashi, M. Improved Stefan Equation Correction Factors to Accommodate Sensible Heat Storage during Soil Freezing or Thawing. *Permafr. Periglac. Process.* **2015**, *27*, 189–203. [[CrossRef](#)]
153. Gouttevin, I.; Krinner, G.; Ciais, P.; Polcher, J.; Legout, C. Multiscale validation of a new soil freezing scheme for a land-surface mode with physically-based hydrology. *Cryosphere* **2012**, *6*, 407–430. [[CrossRef](#)]
154. A Rawlins, M.; Nicolsky, D.J.; McDonald, K.C.; Romanovsky, V. Simulating soil freeze/thaw dynamics with an improved pan-Arctic water balance model. *J. Adv. Model. Earth Syst.* **2013**, *5*, 659–675. [[CrossRef](#)]
155. Zhang, Y.; Cheng, G.; Li, X.; Han, X.; Wang, L.; Li, H.; Chang, X.; Flerchinger, G.N. Coupling of a simultaneous heat and water model with a distributed hydrological model and evaluation of the combined model in a cold region watershed. *Hydrol. Process.* **2012**, *27*, 3762–3776. [[CrossRef](#)]
156. Clark, M.P.; Nijssen, B.; Lundquist, J.D.; Kavetski, D.; Rupp, D.E.; Woods, R.A.; Freer, J.E.; Gutmann, E.D.; Wood, A.W.; Brekke, L.D.; et al. *The Structure for Unifying Multiple Modeling Alternatives (SUMMA), Version 1.0: Technical Description*; Rep. NCAR/TN 514+STR; National Center for Atmospheric Research: Boulder, CO, USA, 2015.
157. McClymont, A.F.; Hayashi, M.; Bentley, L.R.; Christensen, B.S. Geophysical imaging and thermal modeling of subsurface morphology and thaw evolution of discontinuous permafrost. *J. Geophys. Res. Earth Surf.* **2013**, *118*, 1826–1837. [[CrossRef](#)]
158. Sjöberg, Y.; Coon, E.; Sannel, A.B.K.; Pannetier, R.; Harp, D.R.; Frampton, A.; Painter, S.; Lyon, S.W. Thermal effects of groundwater flow through subarctic fens: A case study based on field observations and numerical modeling. *Water Resour. Res.* **2016**, *52*, 1591–1606. [[CrossRef](#)]
159. Noetzli, J.; Gruber, S.; Kohl, T.; Salzmann, N.; Haerberli, W. Three-dimensional distribution and evolution of permafrost temperatures in idealized high-mountain topography. *J. Geophys. Res. Space Phys.* **2007**, *112*, 02–13. [[CrossRef](#)]
160. Noetzli, J.; Gruber, S. Transient thermal effects in Alpine permafrost. *Cryosphere* **2009**, *3*, 85–99. [[CrossRef](#)]
161. Gubler, S.; Endrizzi, S.; Gruber, S.; Purves, R.S. Sensitivities and uncertainties of modeled ground temperatures in mountain environments. *Geosci. Model Dev.* **2013**, *6*, 1319–1336. [[CrossRef](#)]
162. Harp, D.R.; Atchley, A.L.; Painter, S.; Coon, E.T.; Wilson, C.J.; Romanovsky, V.; Rowland, J.C. Effect of soil property uncertainties on permafrost thaw projections: A calibration-constrained analysis. *Cryosphere* **2016**, *10*, 341–358. [[CrossRef](#)]

163. Bense, V.; Kooi, H.; Ferguson, G.; Read, T. Permafrost degradation as a control on hydrogeological regime shifts in a warming climate. *J. Geophys. Res. Space Phys.* **2012**, *117*, 1–18. [[CrossRef](#)]
164. Frederick, J.; Buffett, B.A. Effects of submarine groundwater discharge on the present-day extent of relict submarine permafrost and gas hydrate stability on the Beaufort Sea continental shelf. *J. Geophys. Res. Earth Surf.* **2015**, *120*, 417–432. [[CrossRef](#)]
165. Kurylyk, B.L.; MacQuarrie, K.T.; McKenzie, J.M. Climate change impacts on groundwater and soil temperatures in cold and temperate regions: Implications, mathematical theory, and emerging simulation tools. *Earth-Sci. Rev.* **2014**, *138*, 313–334. [[CrossRef](#)]
166. Bense, V.; Ferguson, G.; Kooi, H. Evolution of shallow groundwater flow systems in areas of degrading permafrost. *Geophys. Res. Lett.* **2009**, *36*, 1–6. [[CrossRef](#)]
167. Frampton, A.; Painter, S.; Lyon, S.W.; Destouni, G. Non-isothermal, three-phase simulations of near-surface flows in a model permafrost system under seasonal variability and climate change. *J. Hydrol.* **2011**, *403*, 352–359. [[CrossRef](#)]
168. Jiang, Y.; Zhuang, Q.; O'Donnell, J.A. Modeling thermal dynamics of active layer soils and near-surface permafrost using a fully coupled water and heat transport model. *J. Geophys. Res. Space Phys.* **2012**, *117*, 1–15. [[CrossRef](#)]
169. Grenier, C.; Régnier, D.; Mouche, E.; Benabderrahmane, H.; Costard, F.; Davy, P. Impact of permafrost development on groundwater flow patterns: A numerical study considering freezing cycles on a two-dimensional vertical cut through a generic river-plain system. *Hydrogeol. J.* **2012**, *21*, 257–270. [[CrossRef](#)]
170. Frampton, A.; Painter, S.; Destouni, G. Permafrost degradation and subsurface-flow changes caused by surface warming trends. *Hydrogeol. J.* **2012**, *21*, 271–280. [[CrossRef](#)]
171. Sjöberg, Y.; Marklund, P.; Pettersson, R.; Lyon, S.W. Geophysical mapping of palsa peatland permafrost. *Cryosphere* **2015**, *9*, 465–478. [[CrossRef](#)]



© 2020 by the authors. Licensee MDPI, Basel, Switzerland. This article is an open access article distributed under the terms and conditions of the Creative Commons Attribution (CC BY) license (<http://creativecommons.org/licenses/by/4.0/>).

Paper II

Bui, Minh Tuan; Lu, Jinmei; Nie, Linmei. Evaluation of the Climate Forecast System Reanalysis data for hydrological model in the Arctic watershed Målselv. Journal of Water and Climate Change 2021. ISSN 2040-2244.s doi: <https://doi.org/10.2166/wcc.2021.346>.

The paper was published in the Special Issue, “Assessment and Adaptation to Climate Change Impacts in Cold Regions”.

ELECTRONIC OFFPRINT

Use of this pdf is subject to the terms described below

Vol 12 | Issue 8 | December 2021



Journal of

Water & Climate Change

Assessment and adaptation to climate change impacts in cold regions



ISSN 2040-2244
E-ISSN 2408-9354
iwaponline.com/jwcc

This paper was originally published by IWA Publishing. It is an Open Access work, and the terms of its use and distribution are defined by the Creative Commons licence selected by the author.

Full details can be found here: <http://iwaponline.com/content/rights-permissions>

Please direct any queries regarding use or permissions to editorial@iwap.co.uk

Evaluation of the Climate Forecast System Reanalysis data for hydrological model in the Arctic watershed Målselv

Minh Tuan Bui, Jinmei Lu and Linmei Nie 

ABSTRACT

The high-resolution Climate Forecast System Reanalysis (CFSR) data have recently become an alternative input for hydrological models in data-sparse regions. However, the quality of CFSR data for running hydrological models in the Arctic is not well studied yet. This paper aims to compare the quality of CFSR data with ground-based data for hydrological modeling in an Arctic watershed, Målselv. The QSWAT model, a coupling of the hydrological model SWAT (soil and water assessment tool) and the QGIS, was applied in this study. The model ran from 1995 to 2012 with a 3-year warm-up period (1995–1997). Calibration (1998–2007), validation (2008–2012), and uncertainty analyses were performed by the Sequential Uncertainty Fitting Version 2 (SUFI-2) algorithm in the SWAT Calibration Uncertainties Program for each dataset at five hydro-gauging stations within the watershed. The objective function Nash–Sutcliffe coefficient of efficiency for calibration is 0.65–0.82 with CFSR data and 0.55–0.74 with ground-based data, which indicate higher performance of the high-resolution CFSR data than the existing scattered ground-based data. The CFSR weather grid points showed higher variation in precipitation than the ground-based weather stations across the whole watershed. The calculated average annual rainfall by CFSR data for the whole watershed is approximately 24% higher than that by ground-based data, which results in some higher water balance components. The CFSR data also demonstrates its high capacities to replicate the streamflow hydrograph, in terms of timing and magnitude of peak and low flow. Through examination of the uncertainty coefficients P -factors (≥ 0.7) and R -factors (≤ 1.5), this study concludes that CFSR data is a reliable source for running hydrological models in the Arctic watershed Målselv.

Key words | Arctic region, Climate Forecast System Reanalysis (CFSR), ground-based weather data, Målselv watershed, QSWAT model, uncertainty analysis


HIGHLIGHTS

- The high-resolution CFSR dataset has higher performance than the existing scattered ground-based dataset in terms of statistical coefficients, R^2 , NSE, and RSR.
- The CFSR dataset has higher simulation results for some water balance components, e.g., actual evapotranspiration, lateral flow, water yield, etc., than the scattered conventional dataset.
- The CFSR demonstrates its high capacities to replicate the streamflow hydrograph.
- Uncertainty analysis reveals that CFSR is a reliable weather input for running hydrological models in the Arctic watershed Målselv.
- The emerging and open-source QSWAT is a valuable tool for the SWAT scientific community because of its upgraded availability and functionality compared to other SWAT interfaces.

This is an Open Access article distributed under the terms of the Creative Commons Attribution Licence (CC BY 4.0), which permits copying, adaptation and redistribution, provided the original work is properly cited (<http://creativecommons.org/licenses/by/4.0/>).

doi: 10.2166/wcc.2021.346

Minh Tuan Bui (corresponding author)
Jinmei Lu
Department of Technology and Safety,
Faculty of Science and Technology,
UiT The Arctic University of Norway,
9037 Tromsø,
Norway
E-mail: minh.t.bui@uit.no

Linmei Nie 
Centre for Sustainable Development and
Innovation of Water Technology,
Foundation CSDI WaterTech,
0373 Oslo,
Norway

INTRODUCTION

A watershed is a basic land unit for studying of hydrological cycle and for water resource management and planning (Edwards *et al.* 2015; Yu & Duffy 2018). It is defined as a land area where most of the precipitation drains to the same places, e.g., water bodies or low land areas (Edwards *et al.* 2015). The development of hydrological models has been a high target of the hydrologists (Ehret *et al.* 2014; Clark *et al.* 2017) in order to improve the understanding of the hydrological processes and supporting for the management of the watershed (Yu & Duffy 2018). However, an existing challenge and time consuming of modeling task is collecting accurately representative weather input data for hydrological models (Mehta *et al.* 2004; Kouwen *et al.* 2005; Fuka *et al.* 2014; Lu *et al.* 2019). Generally, the ground-based weather stations do not always sufficiently represent the weather pattern across the whole watershed (Fuka *et al.* 2014) because (1) the sparse spatial distribution and the far distances of the meteorological stations from the watershed to be modeled (Zhang *et al.* 2016; Tolera *et al.* 2018); (2) time-series data usually contain gaps and errors; (3) up-to-date datasets are not available. Due to these limitations of ground-based data, finding alternative sources of weather inputs for hydrological models is essential. This is especially crucial for the data-sparse Arctic region (Lindsay *et al.* 2014; WMO 2018). An alternative source, which has recently been preferred by scientists, is to use the multiyear globally atmospheric reanalyzed data (Fuka *et al.* 2014).

Basically, the atmospheric reanalyzed data are generated through data assimilation, which is the process of integrating all available information, to estimate as accurately as possible the characteristics of a system (Talagrand 1997), from observed data (e.g., from the ground-based gauges, ships, aircraft, and satellites) and forecasted data (e.g., from numerical modeling of weather prediction) (Parker 2016). Reanalysis provides comprehensive features of climate at regular time steps over a long period usually from years to decades. Therefore, reanalysis data have been used in various fields, such as atmospheric dynamics (Kidston *et al.* 2010), investigation of climate variability (Kravtsov *et al.* 2014), evaluation of climate models (Gleckler *et al.* 2008), studying greenhouse gas fingerprints (Santer *et al.* 2004), and in the study of hydrology and hydrological models

(Lavers *et al.* 2012; Najafi *et al.* 2012; Quadro *et al.* 2013; Smith & Kummerow 2013; Fuka *et al.* 2014; Bressiani *et al.* 2015; Alemayehu *et al.* 2016; Tolera *et al.* 2018). Many atmospheric reanalysis products have been generated recently, and some well-known ones are listed below (Lindsay *et al.* 2014):

1. The National Centers for Environmental Prediction (NCEP)–National Center for Atmospheric Research Reanalysis (NCAR) 1 (NCEP-R1) (Kalnay *et al.* 1996; Kistler *et al.* 2001);
2. The NCEP–U.S. Department of Energy (DOE) Reanalysis 2 (NCEP-R2) (Kanamitsu *et al.* 2002);
3. Climate Forecast System Reanalysis (CFSR) generated by the NCEP (Saha *et al.* 2010);
4. Twentieth-Century Reanalysis (20CR) generated by the National Oceanic and Atmospheric Administration (NOAA) Earth System Research Laboratory (ESRL)–Cooperative Institute for Research in Environmental Sciences (CIRES) (Whitaker *et al.* 2004; Compo *et al.* 2006, 2011);
5. Modern-Era Retrospective Analysis for Research and Applications, Version 2 (MERRA-2) generated by the National Aeronautics and Space Administration (NASA) Global Modeling and Assimilation Office (GMAO) (Gelaro *et al.* 2017; Tao *et al.* 2019);
6. ERA5, the successor of ERA-Interim, generated by European Centre for Medium-Range Weather Forecasts (ECMWF) (Hersbach *et al.* 2020); and
7. Japanese 25-year Reanalysis Project (JRA-25) generated by the Japanese Meteorological Agency (JMA) (Onogi *et al.* 2007).

A comparison on the characteristics of the above seven well-known reanalysis products is shown in Table 1. Of them, the CFSR and ERA5 have the highest spatial resolution with a Gaussian grid (Washington & Parkinson 2005) of approximately 38 km (NCAR 2017) and approximately 31 km (Hersbach *et al.* 2020), respectively. However, CFSR is the only one that covers all required input data (e.g., precipitation, maximum and minimum air temperature, relative humidity, solar radiation, and wind speed) for the hydrological model, the SWAT (soil and water assessment tool) model, used by this study. Therefore,

Table 1 | Characteristics of some well-known reanalysis products (Lindsay *et al.* 2014)

	NCEP-R1	NCEP-R2	CFSR	20CR	MERRA-2	ERA5	JRA-25
Sponsoring agencies	NCEP–NCAR	NCEP–DOE	NCEP	NOAA–ESRL–CIRES	NASA–GMAO	ECMWF	JMA
Temporal coverage	1948–present	1979–present	1979–2017	1871–2012	1980–2017	1950–2019	1979–2004
Temporal resolution	Sub-daily, daily, monthly	Sub-daily, daily, monthly	Sub-daily, monthly	Sub-daily, daily, monthly	Sub-daily, daily, monthly	Sub-daily, daily, monthly	Sub-daily, monthly
Spatial coverage	Global grid	Global grid	Global grid	Global grid	Global grid	Global grid	Global grid
Spatial resolution	210 km	210 km	38 km	210 km	50 km	31 km	120 km
References	Kalnay <i>et al.</i> (1996); Kistler <i>et al.</i> (2001)	Kanamitsu <i>et al.</i> (2002)	Saha <i>et al.</i> (2010)	Whitaker <i>et al.</i> (2004); Compo <i>et al.</i> (2006, 2011)	Gelaro <i>et al.</i> (2017); Tao <i>et al.</i> (2019)	Hersbach <i>et al.</i> (2020)	Onogi <i>et al.</i> (2007)

the CFSR is selected for the evaluation of its performance for running the hydrological model in the Arctic conditions.

The CFSR is the third generation of reanalysis product. This dataset is the cooperation between the National Center for Atmospheric Research (NCAR 2017) and the NCEP (NCEP 2010). A coupling of atmosphere–ocean–land surface–sea ice systems in order to offer the best estimation of the weather pattern of those coupled areas is the great features of the CFSR product. The CFSR data have been verified as weather input for hydrological models in numerous studies at different climate conditions around the world (e.g., temperate, tropical, subtropical, Asian monsoon, and semi-arid) and provided reliable results. First of all, in the temperate climate zone, CFSR performed better than ground-based data for simulation of daily variation of streamflow in four watersheds in the USA, and CFSR could meet the challenge of hydrological simulation in ungauged watersheds (Fuka *et al.* 2014). In another study in the snow-dominated East River basin, Colorado, USA, CFSR was used as forcing data for the prediction of volumetric streamflow and returned good results (Najafi *et al.* 2012). Additionally, in a study of surface and atmospheric water budgets in the Upper Colorado River basin, CFSR showed its high capacity to capture the seasonal cycle of each water budget component (Smith & Kummerow 2013). CFSR was also used as weather input to detect the influences of atmospheric rivers on winter floods in nine river basins along the western coast of Great Britain and showed consistent results with other reanalysis products: the ERA-Interim, the 20CR,

the MERRA, and the NCEP–NCAR (Lavers *et al.* 2012). Secondly, in a tropical climate zone in Ethiopia, CFSR performed better than ground-based data for the prediction of daily streamflow in the Gumera watershed (Fuka *et al.* 2014) and for the prediction of monthly streamflow in the Awash watershed (Tolera *et al.* 2018). It is concluded that CFSR could perform better in large-scale basins (Tolera *et al.* 2018). CFSR also demonstrated its high capacity for predicting potential evapotranspiration in the data-scarce Upper Mara Catchment in Kenya and Tanzania (Alemayehu *et al.* 2016). Thirdly, in a study conducted over South America, with climate characteristics varying from tropical to subtropical zones, CFSR provided the smallest bias in results, compared with other reanalysis products (e.g., MERRA and NCEP-R2), for simulation of the hydrological cycle (Quadro *et al.* 2013). Another study in the semi-arid climate of the Jaguaribe basin, Northeast Brazil, with CFSR as weather input for studying monthly streamflow variation, stated that CFSR's results were good to very good, and had the best performance compared to other weather input datasets (Bressiani *et al.* 2015). Lastly, in the region dominated by the Asian monsoon climate, CFSR demonstrated good performance to simulate monthly streamflow variation in the largest river, the Yangtze River, in China, and was considered an alternative input for the large-scale basins (Lu *et al.* 2019). However, in some case studies, CFSR data performed worse than ground-based data and were not recommended (specifically for those study areas) as an alternative input to replace the high-quality

ground-based data (Dile & Srinivasan 2014; Roth & Lemann 2016). Although the CFSR dataset has demonstrated its performance in hydro-meteorological simulations around the world, this has yet to be verified well in the data-sparse Arctic region. Therefore, to fill this knowledge gap, this paper aims:

1. Investigate the performance of the CFSR in running hydrological models in Arctic conditions, and
2. Examine whether CFSR data could be an alternative for weather input and could replace the limited ground-based data for hydrological models in the data-sparse Arctic region.

STUDY AREA

An Arctic watershed, Målselv, located in northern Norway, was chosen as the study area to investigate the

performance of CFSR (Figure 1). The watershed is distributed at high latitudes from 68°21'N to 69°17'N and approximately 200 km above the Arctic circle (at 66°33'N) calculated from the southernmost point of the watershed. It covers an area of approximately 5,913 km². The elevation distribution of the ground surface is in the range of 0–1,718 m. According to long-term data from the Norwegian Water Resources and Energy Directorate (NVE), the average annual precipitation in the study area varies from approximately 500 to 1,500 mm. The average annual air temperature fluctuates from –5 to 6 °C. The whole watershed has approximately 11 categories of land use, with wooded tundra, mixed tundra, and deciduous broadleaf forest accounting for the highest percentage of total land-use area: 32.38, 23.93, and 22.12% for each type, respectively (Supplementary Material, Table S1). Sandy loam dominates the soil texture of the watershed (Supplementary Material, Table S1).

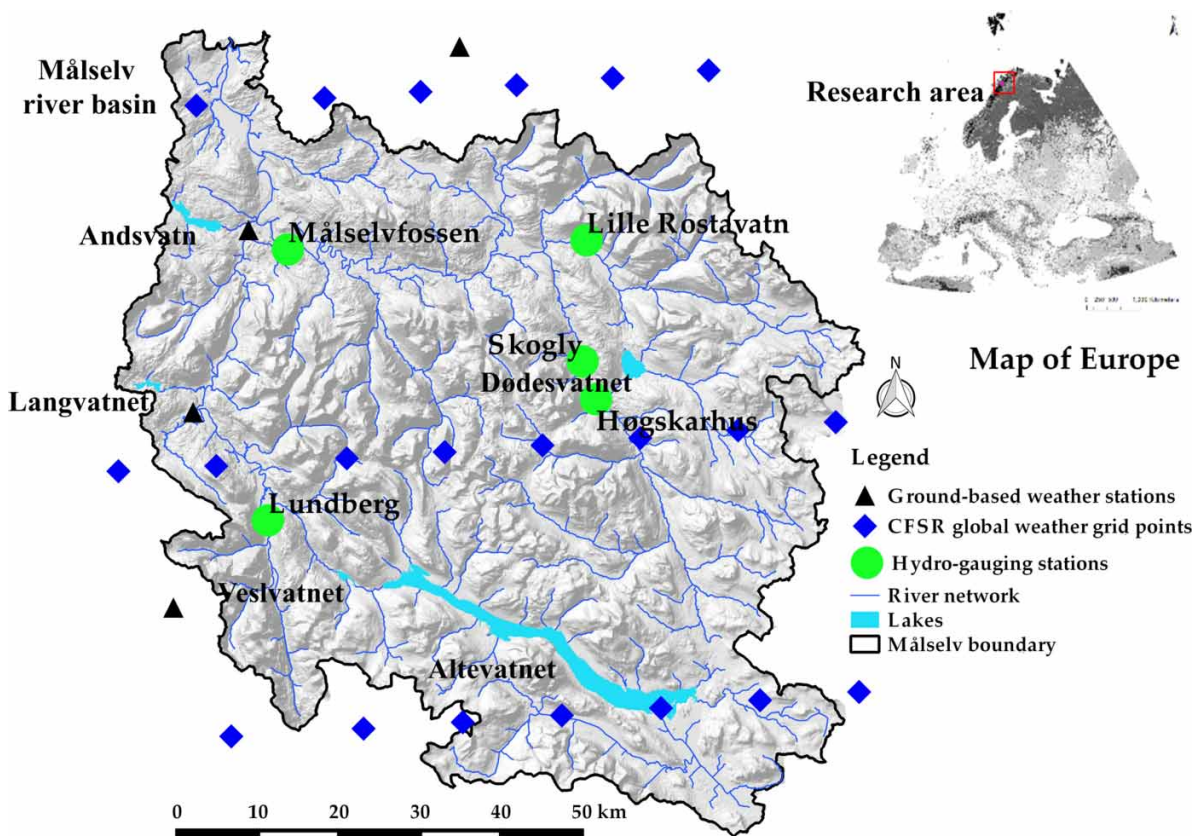


Figure 1 | Map of the study area, Målselv watershed.

MATERIALS AND METHODS

SWAT model

The physically based (or process-based) (Neitsch *et al.* 2009), semi-distributed model SWAT was applied to test the quality of CFSR data. The SWAT was developed to simulate the anthropogenic impacts (Gassman *et al.* 2007) and climate change impacts (Dile *et al.* 2013) on water resources and environmental matters. The model has capacity to simulate the large-scale catchments with complex conditions over a long period. Especially, the SWAT demonstrates its strengths to fulfill the requirements of the current modeling philosophy: transparency of the model (Abbaspour *et al.* 2015). It means that calibration, validation, sensitivity, and uncertainty analyses are performed by the model.

The model has several major components, including weather, hydrology, soil (temperature and properties), plant growth, nutrients, pesticides, bacteria and pathogens, and land management (Arnold *et al.* 2012). The spatial heterogeneity of the study area is presented by discretizing the watershed into smaller sub-basins (Abbaspour *et al.* 2007). Each sub-basin is further subdivided into hydrologic response units (HRUs) that have homogeneous topography, land use, soil characteristics, and management. Hydrological simulation in the SWAT model occurs in two major phases: land phase and routing phase (Arnold *et al.* 2012). The land phase works, based on the water balance formula, as follows:

$$SW_t = SW_0 + \sum_{i=1}^t (R_i - Q_i - E_i - P_i - QR_i), \quad (1)$$

where SW_t is the soil water content at time t (mm), SW_0 is the initial soil water content (mm), R_i is the amount of precipitation on day i (mm), Q_i is the amount of surface runoff on day i (mm), E_i is the amount of evapotranspiration on day i (mm), P_i is the amount of percolation on day i (mm), and QR_i is the amount of return flow on day i (mm).

Specifically, the surface runoff in the SWAT is calculated separately for each HRU, using the Soil Conservation Service's curve number (CN) method, and then transmitted for each sub-basin (Reddy *et al.* 2018). The water balance is mainly controlled by climate factors, such as precipitation, maximum/minimum air temperature, solar radiation, wind

speed, and relative humidity (Arnold *et al.* 2012). In the SWAT, snow is considered, and it is calculated whenever the air temperature falls below the freezing point. Additionally, soil temperature is also calculated, since it influences the water movement in soil (Arnold *et al.* 2012).

The loadings of water and other components, such as sediment, nutrients, and pesticides from the land phase, are transformed into the mainstream, where the second phase (the routing phase) occurs (Arnold *et al.* 2012). In the routing phase, the loadings are routed through the mainstream and reservoirs within the catchment. Particularly, the routing phase describes several processes taking place in the mainstream, including the movement of water, mass flow, chemicals process, flood routing, sediment routing, nutrient routing, and pesticide routing. Streamflow in the mainstream consists of the contributions of water yield (YIELD) from the sub-basins. The YIELD is calculated by summarizing surface runoff, lateral flow, and groundwater, subtracting the transmission loss (Tolera *et al.* 2018). In this study, streamflow and water balance components are main outputs simulated by the SWAT, and these results are used to compare the performances of two weather input datasets.

QSWAT interface

The SWAT model runs on a GIS (Geographical Information System) platform where GIS functions are used to collect, manipulate, visualize, and analyze the inputs and outputs of the model (Srinivasan & Arnold 1994). Several GIS interfaces, e.g., GRASS-GIS (<https://grass.osgeo.org/>), ArcGIS (<http://www.esri.com/software/arcgis>), MapWindow GIS (<https://www.mapwindow.org/>), and the Quantum Geographical Information System QGIS (<https://qgis.org/en/site/>), have been coupled with the SWAT model. Of them, GRASS-SWAT is the first and major interface, while ArcSWAT, MWSWAT, and QSWAT are later developed (Dile *et al.* 2016). ArcSWAT is the most popular interface; it, however, requires a license ArcGIS platform (Winchell *et al.* 2013) and very costly (Dile *et al.* 2016). Additionally, the present version of ArcSWAT does not have an integrated functionality for the visualization of model outputs (Dile *et al.* 2016). MWSWAT has an advantage of being an open source, but it shows limitations to perform in large watersheds and large input datasets (Chen *et al.* 2010). Among

open-source GIS softwares, QGIS is evaluated as an outperformed tool (Chen *et al.* 2010). For example, QGIS could satisfy the desired functionalities for water resource management, and it owns most of functions like a commercial GIS package. Because of the benefits of QGIS, it is highly desired from SWAT users community to couple QGIS with the SWAT model (Dile *et al.* 2016). Therefore, QSWAT is developed from that and it is currently considered as an emerging SWAT interface. QSWAT was firstly tested in a study in the Gumera watershed, Ethiopia and showed a successful performance (Dile *et al.* 2016). To continue that success, the present study applies the new interface QSWAT in order to verify its performance in the Arctic conditions.

Data acquisition

To run the SWAT model, several inputs are required: (1) spatial data, including Digital Elevation Map (DEM), soil, and land use; and (2) time-series data, including climate data and river discharge (Table 2).

A high-resolution DEM (10 × 10 m) is collected from the Norwegian Mapping Authority. The DEM is used to define the catchment topography and generate the catchment boundary, sub-basins, and stream networks. Additionally, other important parameters of the sub-basins, e.g., terrain slope length, slope gradient, slope classes, and channel length, are generated from the DEM. The soil data (scale of 1:5,000,000) and land use (600 m resolution) are collected from the Waterbase organization. The soil and land use are reclassified to represent the specific land use

(Supplementary Material, Table S1) and soil types (Supplementary Material, Table S2) of the catchment based on the SWAT database.

The climate inputs used in this study are from two data sources, which are used to compare their performances: (1) the CFSR weather data (Figure 2(a)) and (2) the ground-based data (Figure 2(b)). The CFSR global weather data cover a 36-year period from 1 January 1979 to 31 July 2014 (TAMU 2012). In total, 21 weather grid points, which are located inside and nearby the catchment, are picked up by the SWAT model with the method of the nearest-neighbor search (NNS). The CFSR time-series data are almost continuous. In contrast, only four ground-based weather stations located within and nearby the study area have continuous time-series data and have the same time window as the CFSR data (regarding the investigation period of this study). Generally, most of the ground-based weather stations locate in the downstream. Of them, two weather stations are inside the watershed, while the other two are outside and close to the watershed's boundary. The ground-based data are collected from the European Climate Assessment & Dataset project (ECAD). It is obvious from Figure 2 that the networks of the available ground-based weather stations (Figure 2(b)) in the Målselv watershed are highly scattered, while the CFSR weather grid points (Figure 2(a)) are denser. Detailed description of the CFSR weather grid points and the ground-based weather stations and their rainfall data are summarized in Table 3.

River discharges, which are used for model calibration and validation, are collected from the Norwegian Water Resources and Energy Directorate. Five datasets from five hydro-gauging stations are gathered, with measurement intervals varying from 30 min to 1 h. The raw dataset is then averaged to a monthly interval dataset, in order to be compatible with the time step format of monthly simulation in the SWAT model. However, there are still some small gaps in the time-series data of river discharges due to technical errors or other reasons.

Model setup

QSWAT version 1.9, a coupling of the hydrological model SWAT version 2012 and the open-source QGIS version 2.6.1, is applied in this study for the evaluation of the CFSR data. Before running the model, two necessary steps

Table 2 | Summarization of inputs and their sources to the SWAT model

Data type	Resolution	Source of data
DEM	10 × 10 m	Geonorge (2013)
Land use	approximately 600 m	Waterbase (2007a)
Soil	approximately 5,000 m	Waterbase (2007b)
Climate	Ground-based data: four stations	ECAD (2002)
	CFSR data: 21 grid points, approximately 38 km grid	TAMU (2012)
River discharge	Five stations	Sildre (2020)

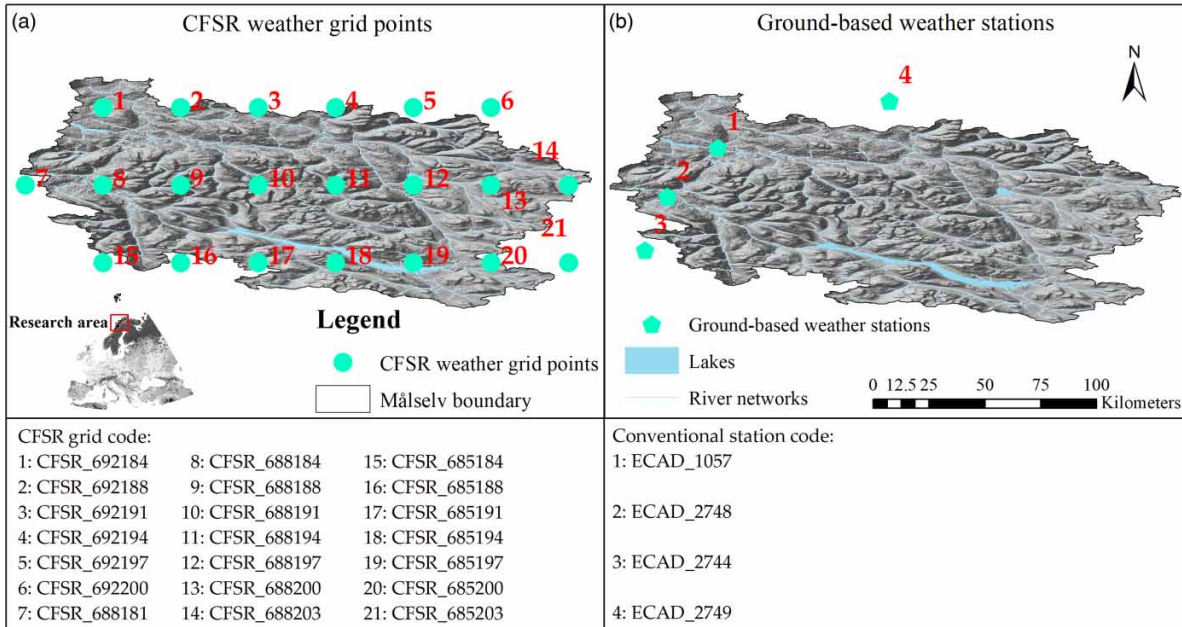


Figure 2 | CFSR weather grid points (a) versus ground-based weather stations (b).

Table 3 | Description of the ground-based weather stations and the CFSR weather stations and their rainfall information (1995–2012) in the Målselv watershed

Weather data	Station	Latitude	Longitude	Elevation (m)	Average annual rainfall (mm)
Ground-based	ECAD_1057	69.1	18.5	76	711
	ECAD_2749	69.2	19.2	27	852
	ECAD_2748	68.9	18.3	114	903
	ECAD_2744	68.6	18.2	230	967
CFSR	CFSR_692184	69.2	18.4	156	1,413
	CFSR_692188	69.2	18.8	516	1,382
	CFSR_692191	69.2	19.1	194	1,350
	CFSR_692194	69.2	19.4	954	1,329
	CFSR_692200	69.2	20	440	1,303
	CFSR_692197	69.2	19.7	970	1,314
	CFSR_688197	68.8	19.7	587	1,059
	CFSR_688200	68.8	20	1,140	1,005
	CFSR_688188	68.8	18.8	1,000	1,267
	CFSR_688194	68.8	19.4	1,040	1,119
	CFSR_688191	68.8	19.1	800	1,192
	CFSR_688184	68.8	18.4	267	1,320
	CFSR_688181	68.8	18.1	175	1,366
	CFSR_688203	68.8	20.3	760	957
	CFSR_685203	68.5	20.3	686	750
	CFSR_685200	68.5	20	708	826
	CFSR_685188	68.5	18.8	837	1,345
	CFSR_685194	68.5	19.4	1,290	1,039
	CFSR_685184	68.5	18.4	1,041	1,437
	CFSR_685197	68.5	19.7	668	925
CFSR_685191	68.5	19.1	880	1,192	

including watershed delineation and HRUs creation are performed (Dile *et al.* 2016). The watershed delineation step is carried out by using the input of DEM. In this step, the sub-basins and their parameters are generated based on the stream networks and locations of sub-basin outlets, as well as watershed outlets. The second step, HRUs creation, is to divide each sub-basin into smaller units with specific soil types, land uses, and terrain slopes' distribution. The HRUs were generated from the inputs of the land-use map, the soil map, and slope classification. In this study, five slope classes are defined: 0–5, 5–10, 10–25, 25–30,

and >30% (Supplementary Material, Table S3). Totally, 459 sub-basins, including 5,601 HRUs, are generated. The sizes of sub-basins vary from 205 to 7,075 hectares (ha). The QSWAT is run with monthly time steps from 1995 to 2012, including a 3-year warming-up period to let the model reach the optimal stage from the estimated initial condition (Arnold *et al.* 2012; Kim *et al.* 2018). A 10-year period, 1998–2007, is used for model calibration, and the remaining 5 years from 2008 to 2012 are for model validation. Figure 3 illustrates the overview of methodologies used in this study.

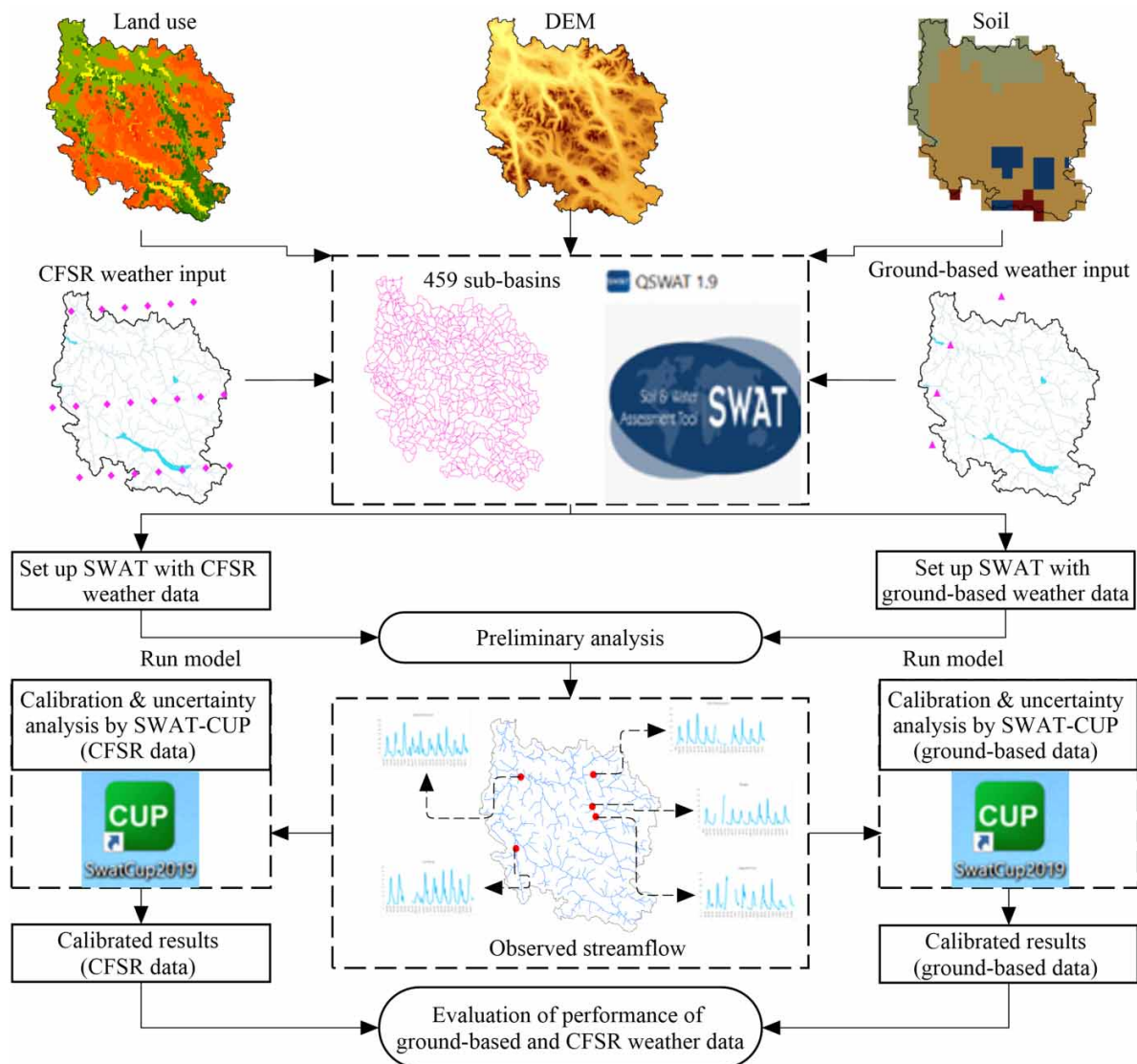


Figure 3 | Schematic diagram of methodologies used in the present study.

Model calibration, validation, and uncertainty analyses

Model calibration, validation, and uncertainty analyses are performed with the Sequential Uncertainty Fitting Version 2 (SUF2) algorithm (Figure 4) in the SWAT Calibration Uncertainties Program (SWAT_CUP) (Abbaspour *et al.* 2007). Outputs from the SWAT model are imported into SWAT-CUP for analyses. For each weather input, five iterations were performed, with 500 simulations for each,

totally 2500 simulations, in order to find the best fit between observed data and simulated data. In each iteration, the SUFI-2 algorithm produces all the possible simulation outputs in a distribution or range, which is called the 95% prediction uncertainty (95PPU) range (Abbaspour *et al.* 2015). Principally, the 95PPU calculates the possible estimated values, which are in the range from the lowest level of 2.5% up to the highest level of 97.5% of the cumulative distribution, by the method of Latin hypercube (LH)



Figure 4 | Flow chart of the SUFI-2 algorithm used in SWAT-CUP (Abbaspour 2015).

sampling, a statistical method which is used to reduce the number of samples from the multiple dimensional distributions (Mckay *et al.* 1979; Özdemir 2016). The 95PPU attempts to capture as many of the observed values within the 95PPU's range as possible.

Furthermore, the SUFI-2 algorithm uses two main indicators, *P*-factor and *R*-factor, in order to measure the goodness of fit between measured data and simulated data (Abbaspour *et al.* 2004, 2015). The first indicator, *P*-factor, is the percent of observed data bracketed in the 95PPU band. The values of *P*-factor range from 0 to 1, in which the value of 1 presents the high accuracy of the simulation results, or it means that 100% of observed data are bracketed in the 95PPU band. For river discharge, the value of *P*-factor is recommended to be higher than a value of 0.7 or 0.75, depending on the project scale, quality of input data to run the model, as well as data for calibration. The second indicator, *R*-factor, presents the thickness of the 95PPU band and is calculated by the ratio between the average width of the 95PPU band and the standard deviation of the observed variable. Ideally, the *R*-factor should be close to zero. For river discharge, the value of *R*-factor is recommended to be smaller than a threshold of 1.5, to indicate a highly accurate simulation result. This threshold also depends on the study conditions and quality of input data. Whenever acceptable values of *P*-factor and *R*-factor are achieved in the last iteration, sensitive statistical parameters are then calculated for the calibrated variables. The ranges of every model parameter obtained in the last iteration are the calibrated parameters for the model. Table 4 provides a list of a total of 18 model parameters including their ranges for calibration and the best-fitted values after calibration. Such model parameters are recommended as the sensitive ones for river discharge calibration (Abbaspour *et al.* 2007, 2015).

Evaluation of model performance

The simulated results are compared with the observed data using the statistical coefficients, including (1) the coefficient of determination – R^2 (Equation (2)), measuring the fitness of the relationship between the simulated and observed values; (2) the Nash–Sutcliffe coefficient of efficiency – NSE (Equation (3)); and (3) root mean square error, divided

by the standard deviation – RSR (Equation (4)).

$$R^2 = 1 - \frac{\sum_{i=1}^n (Y_i^{\text{obs}} - Y_{\text{mean}}^{\text{obs}}) (Y_i^{\text{sim}} - Y_{\text{mean}}^{\text{sim}})}{\left[\sum_{i=1}^n (Y_i^{\text{obs}} - Y_{\text{mean}}^{\text{obs}})^2 \right]^{1/2} \left[\sum_{i=1}^n (Y_i^{\text{sim}} - Y_{\text{mean}}^{\text{sim}})^2 \right]^{1/2}} \quad (2)$$

$$\text{NSE} = 1 - \frac{\sum_{i=1}^n (Y_i^{\text{obs}} - Y_i^{\text{sim}})^2}{\sum_{i=1}^n (Y_i^{\text{obs}} - Y_{\text{mean}}^{\text{obs}})^2} \quad (3)$$

$$\text{RSR} = \frac{\left[\sum_{i=1}^n (Y_i^{\text{obs}} - Y_i^{\text{sim}})^2 \right]^{1/2}}{\left[\sum_{i=1}^n (Y_i^{\text{obs}} - Y_{\text{mean}}^{\text{obs}})^2 \right]^{1/2}} \quad (4)$$

where Y_i^{obs} and Y_i^{sim} are the observed and simulated values at time i , $Y_{\text{mean}}^{\text{obs}}$ and $Y_{\text{mean}}^{\text{sim}}$ are mean observed and simulated data for the entire evaluation period, and n is the total number of observations/simulations.

Table 5 provides the threshold values of every statistical coefficient, R^2 , NSE, and RSR (Santhi *et al.* 2001; Van Liew *et al.* 2003; Moriasi *et al.* 2007; Premanand *et al.* 2018).

Moreover, for the additional evaluation of the performance of the CFSR weather data and the ground-based weather data, the simulation results of two major hydrology components are considered in this study: (1) the annual average water balance components, e.g., the total areal rainfall (PCP), actual evapotranspiration (ET), surface runoff (SUR_Q), lateral runoff (LAT_Q), groundwater recharge amount (PERCO), groundwater contribution to streamflow (GW_Q), and water yield (YIELD = SUR_Q + LAT_Q + GW_Q – Transmission losses) contributing to streamflow and (2) the long-term average monthly streamflow. The results are discussed in the following section.

Table 4 | Model parameters and their ranges for calibration

Parameters	Description (unit)	Range		Fitted value
		Minimum	Maximum	
r_CN2.mgt	Runoff CN (-)	-0.225	0.051	-0.14
v_ESCO.hru	Soil evaporation compensation factor (-)	0.067	0.202	0.14
r_SOL_AWC.sol	Available water capacity of the soil layer (mmH ₂ O/mm soil)	-1	-0.581	-0.72
v_ALPHA_BF.gw	Baseflow alpha factor (days)	0	0.12	0.09
v_GW_DELAY.gw	Groundwater delay (days)	260.05	321.81	313.35
v_GW_REVAP.gw	Groundwater 'revap' coefficient (-)	0.117	0.19	0.19
v_GWQMN.gw	Threshold depth of water in the shallow aquifer required for return flow to occur (mm)	2,215	3,318	3,285
v_REVAPMN.gw	Threshold depth of water in the shallow aquifer for 'revap' to occur (mm)	252.18	382.86	353.45
v_SFTMP.bsn	Snowfall temperature (°C)	-2.72	0.99	-1.48
v_SMFMN.bsn	Minimum melt rate for snow during the year (occurs on winter solstice) (mmH ₂ O °C ⁻¹ d ⁻¹)	1.767	6.47	5.33
v_SFMX.bsn	Maximum melt rate for snow during year (occurs on summer solstice) (mmH ₂ O °C ⁻¹ d ⁻¹)	1.914	5.744	2.91
v_SMTMP.bsn	Snow melt base temperature (°C)	-3.189	2.557	-0.56
v_TIMP.bsn	Snowpack temperature lag factor (-)	0.145	0.309	0.15
a_CH_N2.rte	Manning's 'n' value for the main channel (-)	0.145	0.227	0.21
a_CH_K2.rte	Effective hydraulic conductivity in main channel alluvium (mm/h)	-0.01	70.781	22.01
r_SOL_K.sol	Saturated hydraulic conductivity (mm h ⁻¹)	4.482	7.977	7.30
r_SOL_BD.sol	Moist bulk density (g cm ⁻³)	0.403	0.635	0.53
a_CANMX.hru	Maximum canopy storage (mmH ₂ O)	4.016	12.056	4.49

Note:

- The term 'a_' explains that a given value is added to the existing parameter value.
- The term 'r_' explains that an existing parameter value is multiplied by (1+ a given value).
- The term 'v_' explains that the existing parameter value is replaced by a given value.

RESULTS AND DISCUSSION

Comparison of precipitation input between ground-based weather data and CFSR weather data

Monthly precipitation, during the period of 1995–2012, from the ground-based dataset and the CFSR dataset are averaged for all stations across the whole watershed, and the results are plotted as boxplots, where the general trend of the long-term seasonal variation of precipitation, as well as the variation of precipitation in each month for both weather dataset, is displayed (Figure 5).

Generally, precipitation from the ground-based dataset and the CFSR dataset have similar seasonal trends. March, July, September, October, and November showed higher variations in precipitation compared with the remaining

months. Magnitudes of monthly precipitation from the CFSR dataset are higher approximately 11–46% than that from the ground-based dataset, except September. The highest differences are observed in April–June when

Table 5 | Thresholds of R^2 , NSE, and RSR for the evaluation of the hydrological model's performance

Model performance	R^2	NSE	RSR
Very good	$0.70 \leq R^2 \leq 1.00$	$0.75 < NSE \leq 1.00$	$0.00 \leq RSR \leq 0.50$
Good	$0.60 \leq R^2 < 0.70$	$0.65 < NSE \leq 0.75$	$0.50 < RSR \leq 0.60$
Satisfactory	$0.50 \leq R^2 < 0.60$	$0.50 < NSE \leq 0.65$	$0.60 < RSR \leq 0.70$
Unsatisfactory	$R^2 < 0.50$	$NSE \leq 0.50$	$RSR > 0.70$

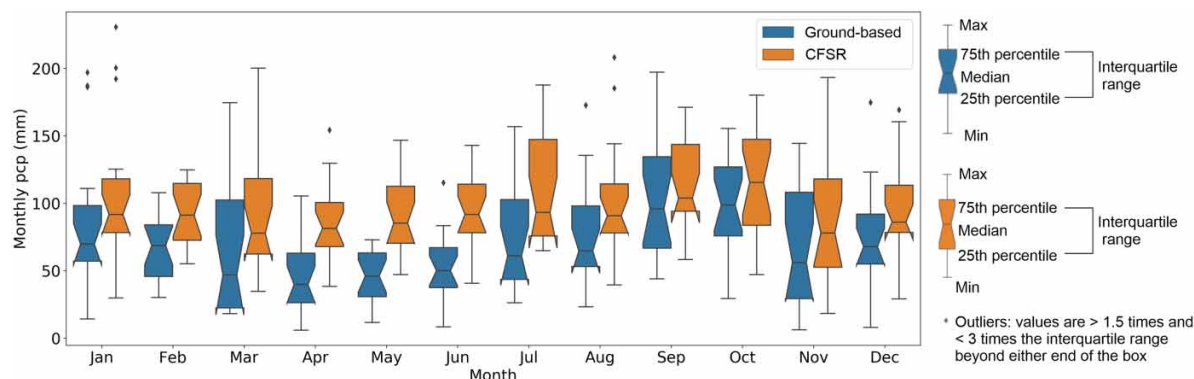


Figure 5 | Ground-based and CFSR average monthly precipitation (1995–2012) for the entire watershed.

precipitation from the CFSR data is much higher approximately 45–46% than that from the ground-based data. In previous studies in upper Awash catchment, Ethiopia (Tolera *et al.* 2018) and in mountainous Black Sea catchment (Cuceloglu & Ozturk 2019), they also demonstrated that CFSR data were able to capture the seasonal trend of precipitation in ground-based data. Similar to findings from our study, the higher in magnitudes of monthly precipitation from the CFSR dataset compared with that from the ground-based dataset were also detected in those studies. However, in the tropical region (the study in upper Awash catchment, Ethiopia), the significant differences of monthly precipitation between the CFSR data and the ground-based data were mostly observed in summer time (July–August), while these were in wet seasons (December to April) in the temperate climate zone in the Black Sea catchment. In contrast, our study found the differences in monthly precipitation between two weather data sources from middle spring to beginning of summer (April to June).

The seasonal variation of precipitation (1995–2012 periods) is locally investigated at four co-located points (the points are closest together) between the ground-based weather stations and the CFSR weather grid points (Figure 6). Of them, two co-located points are inside and the other two are outside of the watershed. As shown in Figure 6, the seasonal trends of precipitation of the CFSR data and ground-based data are almost similar at all the co-located points. However, the magnitude of precipitation from CFSR data is overestimated than that from the ground-based data. Especially, one co-located point locating inside the watershed (as in Figure 6(a)) has 8 months of a

year, e.g., January, February, April–June, September, October, and December, when precipitation from the CFSR data is overestimated precipitation from the ground-based data. At other co-located points, the significant differences of precipitation between the CFSR data and the ground-based data are observed in the months of January, April–June, and December for co-located point 2 (Figure 6(b)), and in February, April, June, and December for co-located point 3 (Figure 6(c)), and in February, April–June, September, and December for co-located point 4 (Figure 6(d)). In brief, the significant differences of monthly precipitation between the CFSR data and the ground-based data at the co-located points mostly occur in winter, from middle spring to the beginning of summer, and from the beginning to middle autumn.

Figure 7 describes the boxplots of variation of total annual precipitation at four pairs of co-located points between ground-based weather stations and CFSR weather grid points. In general, at each pair of co-located points, the values of annual rainfall from the CFSR weather grid point are higher than that from the ground-based weather station. For example, the average annual rainfall from the CFSR data are higher approximately 49.70% (Figure 7(a)), 32.70% (Figure 7(b)), 31.60% (Figure 7(c)), and 36.90% (Figure 7(d)) compared with that from the gauge-based data.

It is obvious that precipitation from the high-resolution CFSR data is higher than that from the scattered ground-based data. Therefore, it is estimated that simulation results, e.g., streamflow or water balance components, would be higher by using the CFSR weather input compared with that by using the ground-based weather input.

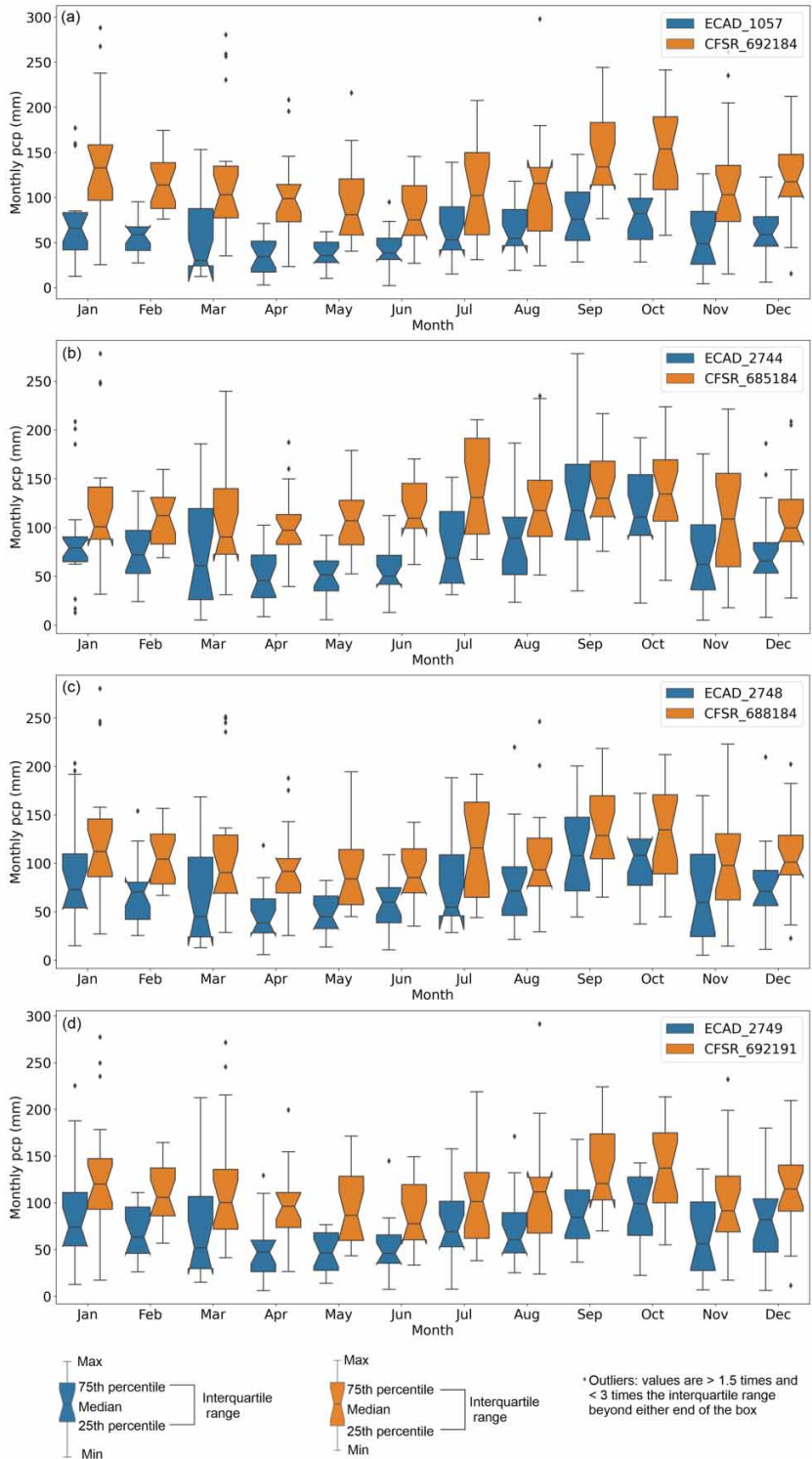


Figure 6 | Ground-based and CFSR average monthly precipitation (1995–2012) at four co-located points.

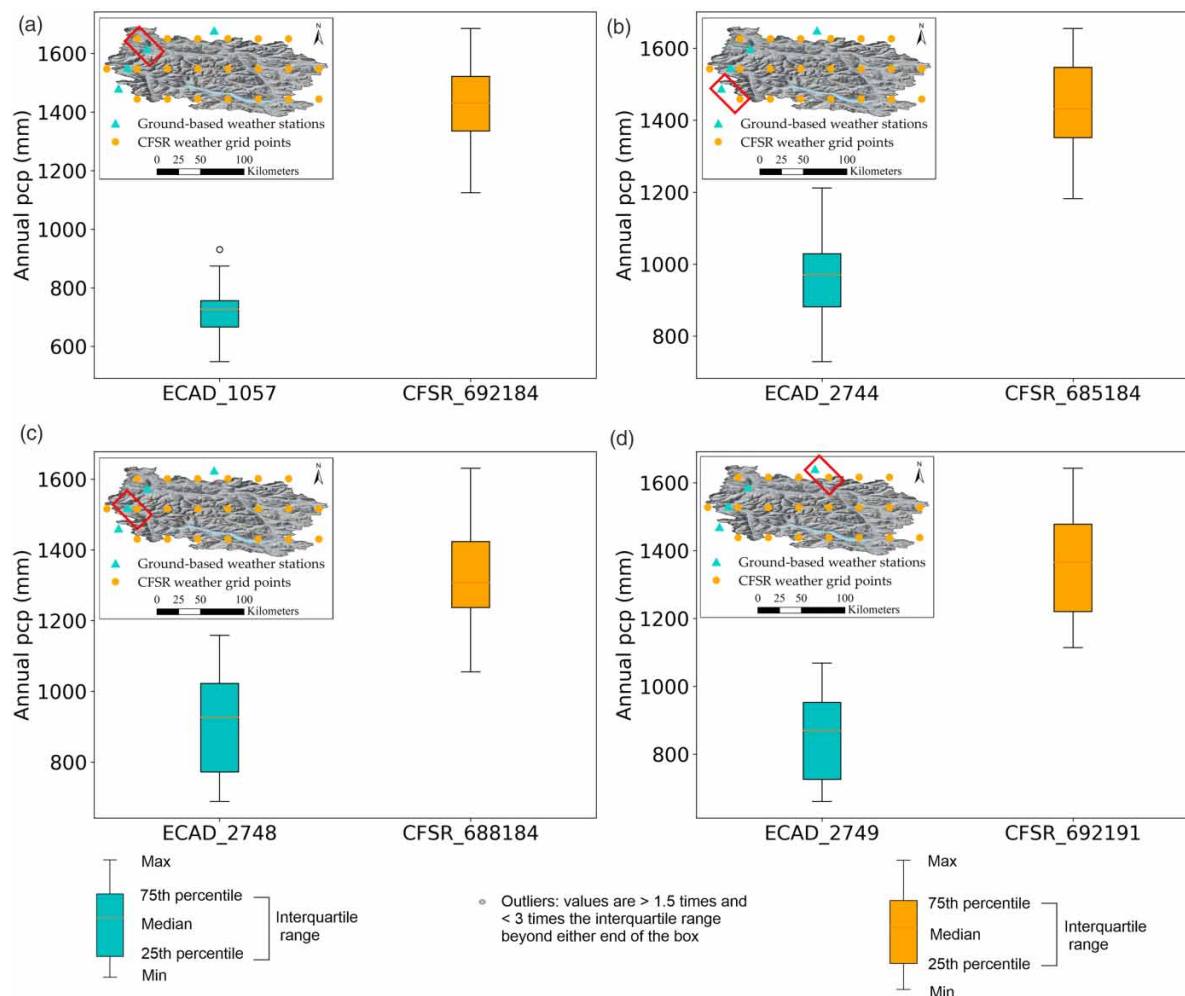


Figure 7 | Ground-based and CFSR total annual precipitation data for the period, 1995–2012.

Comparison of model performance based on the statistical coefficients R^2 , NSE, and RSR

The model performances for the calibration period are shown in Table 6. Generally, the high-resolution CFSR dataset demonstrated higher performance than the existing limited ground-based dataset after calibration. However, model performances are heterogeneous among five hydro-gauging stations within the watershed (Table 6). According to the performance rating from three statistical coefficients, R^2 , NSE, and RSR, ground-based weather data performed well at Høgskarhus and Målselvossen stations and satisfactorily at three remaining stations: Lundberg, Lille Rostavatn, and Skogly. On the contrary, CFSR weather

data performed very well at two stations, Skogly and Målselvossen, and well at Lundberg, Lille Rostavatn, and Høgskarhus. Høgskarhus and Målselvossen are the two stations where performance does not significantly differ between ground-based data and CFSR data, and both have good performances. A very good value of R^2 achieved at all five hydro-gauging stations, from using both weather datasets, demonstrates a high correlation between observation and simulation (Table 6 and Supplementary Material, Figure S1). In addition, the R^2 values explain a good agreement between measured data and estimated results, in terms of timing for the runoff process occurring in the sub-basins, as well as the hydrograph of streamflow (Malago *et al.* 2015).

Table 6 | Model performances for the calibration period (1998–2007)

Station	Sub-basin	Weather input	R^2	NSE	RSR	Performance rating
Lundberg	381	Ground-based	0.71	0.55	0.67	Satisfactory
		CFSR	0.73	0.69	0.56	Good
Lille Rostavatn	402	Ground-based	0.72	0.55	0.67	Satisfactory
		CFSR	0.79	0.67	0.58	Good
Høgskarhus	408	Ground-based	0.73	0.71	0.54	Good
		CFSR	0.74	0.65	0.59	Good
Skogly	412	Ground-based	0.77	0.60	0.63	Satisfactory
		CFSR	0.77	0.77	0.48	Very good
Målselvfossen	444	Ground-based	0.82	0.74	0.51	Good
		CFSR	0.85	0.82	0.42	Very good

According to model validation results, the high-resolution CFSR data (Table 7 and Supplementary Material, Figure S6) also demonstrate its higher performance than the scattered ground-based data (Table 7 and Supplementary Material, Figure S5). For example, CFSR performed very well at Lundberg and Skogly, and well at Lille Rostavatn, where the performance of ground-based data is only satisfactory. Additionally, model performance is good at Målselvfossen, through the use of ground-based data, whereas it is very good through the use of CFSR data. Noticeably, simulation results at the Høgskarhus station in the validation period are worse than those in the calibration period for both weather datasets. This could be partly because of gaps in the time-series data of river discharge used for validation (Supplementary Material, Figure S6c). However, the relatively good values of R^2 (Table 7 and Supplementary Material, Figure S2) achieved in the validation period indicate that the simulated results have high correlation with the observed data.

The performance of the CFSR data in the present study, which is based on an evaluation of the statistical coefficients, is in agreement with the performance of the CFSR data in the previous studies, such as the studies conducted in the temperate climate zone (Najafi *et al.* 2012; Fuka *et al.* 2014), the study in the tropical climate zone (Fuka *et al.* 2014), the study in the Asian monsoon climate zone (Lu *et al.* 2019), and the study in the semi-arid climate zone (Bressiani *et al.* 2015). Such studies concluded that the CFSR data were the potential sources for weather inputs to run the hydrological models in ungauged and large-scale catchments. According to outcomes from the present study, it could be concluded that the CFSR data not only perform well in temperate, tropical, semi-arid, and Asian monsoon climate zones, but also in Arctic conditions. However, findings from the present study also contradict findings from other studies (Dile & Srinivasan 2014; Roth & Lemann 2016), which stated that CFSR could not replace

Table 7 | Model performances for the validation period (2008–2012)

Station	Sub-basin	Weather input	R^2	NSE	RSR	Performance rating
Lundberg	381	Ground-based	0.82	0.64	0.60	Satisfactory
		CFSR	0.81	0.77	0.48	Very good
Lille Rostavatn	402	Ground-based	0.87	0.52	0.69	Satisfactory
		CFSR	0.91	0.66	0.58	Good
Høgskarhus	408	Ground-based	0.66	0.46	0.73	Unsatisfactory
		CFSR	0.73	0.59	0.64	Satisfactory
Skogly	412	Ground-based	0.78	0.55	0.67	Satisfactory
		CFSR	0.87	0.82	0.42	Very good
Målselvfossen	444	Ground-based	0.86	0.72	0.52	Good
		CFSR	0.88	0.83	0.41	Very good

the high-quality ground-based data. However, in the data-sparse regions like the Arctic, reanalysis data, e.g., the CFSR, could be an alternative source, since there are not enough representative meteorological stations for the large catchment, or observed data often contain gaps or errors.

Comparison of the simulated streamflow hydrograph

According to the simulation results of the streamflow hydrograph, a good agreement between observed data and simulated results is achieved from both ground-based weather data (Supplementary Material, Figure S3 for calibration and Supplementary Material, Figure S5 for validation) and CFSR data (Supplementary Material, Figure S4 for calibration and Supplementary Material, Figure S6 for validation). A relatively high level of accuracy, in terms of the timing of the streamflow hydrograph, between observed data and simulated results is obtained. Therefore, lag time is not detected in the simulation. This finding is similar to findings in the previous study in Upper Awash Basin, Ethiopia (Tolera *et al.* 2018). Regarding the calibration period, the magnitude of peak flow is almost captured at Skogly and Målselvossen for both weather datasets. However, at Høgskarhus, peak flow is captured by using the ground-based data, but it is slightly underestimated by using the CFSR data. This could be explained by the fact that some sub-basins upstream of Høgskarhus have higher areal precipitation achieving from the ground-based data than from the CFSR data. On the contrary, most values of peak flow at the Lundberg station are captured by using CFSR data, but those are somewhat underestimated by using ground-based data. At the Lille Rostavatn station, both weather datasets slightly underestimate the magnitude of peak flow.

Regarding the validation period, the peak flows are almost captured at Skogly and Målselvossen, but they are underestimated at Lille Rostavatn, for both weather datasets. The differences in model performance between the two weather datasets are observed at Høgskarhus and Lundberg. For instance, the model performs well in peak flow at Høgskarhus, but it performs worse at Lundberg from using the ground-based dataset, whereas the model performance at those stations shows the opposite behaviors through the use of the CFSR weather data.

In terms of low-flow simulation, a relatively good fitness between simulation and observation is achieved from the calibration and validation period by using both weather datasets. This finding is somewhat better than the finding from the study in Upper Awash Basin, Ethiopia (Tolera *et al.* 2018), since they concluded that simulation of low flow was underestimated/overestimated by using the CFSR data.

Comparison of the simulated water balance components

Rainfall is one of the major inputs of water balance components. In the SWAT, areal rainfall is calculated separately for every sub-basin. In particular, each sub-basin collects rainfall for itself from the stations (e.g., the ground-based weather stations or the CFSR grid points) that are closest to the centroid of the sub-basin by the method of the NNS. The results of spatial variation of areal rainfall calculated for every sub-basin, obtained from ground-based weather data and CFSR weather data, are displayed as in Figure 8. Generally, the total rainfall amount calculated for the whole watershed by CFSR data is approximately 24% higher than that by the ground-based data. Approximately 88% of the watershed area has a rainfall ratio between ground-based data and CFSR data (rainfall ratio (Figure 8(c)) = rainfall amount from ground-based data (Figure 8(a))/rainfall amount from CFSR data (Figure 8(b))) smaller than 1.0, of which 42% of areas in the downstream sections have a rainfall ratio varying from 0.53 to 0.75, while 45.5% of areas in the middle sections have a rainfall ratio varying from 0.75 to 1.0. Exceptionally, approximately 12% of the watershed in the uppermost areas have a rainfall ratio higher than 1.0 which varies from 1.0 to 1.32. This indicates that rainfall in some parts in the upstream calculated from the CFSR dataset is lower than that from the ground-based dataset.

The higher rainfall amount from the CFSR dataset than from the ground-based dataset results in higher simulation results of some water balance components (Table 8). This finding is in agreement with findings from the previous studies in the tropical climate zone (Dile & Srinivasan 2014; Tolera *et al.* 2018). For example, in this study, water yield (WYLD) contributing to streamflow from the CFSR

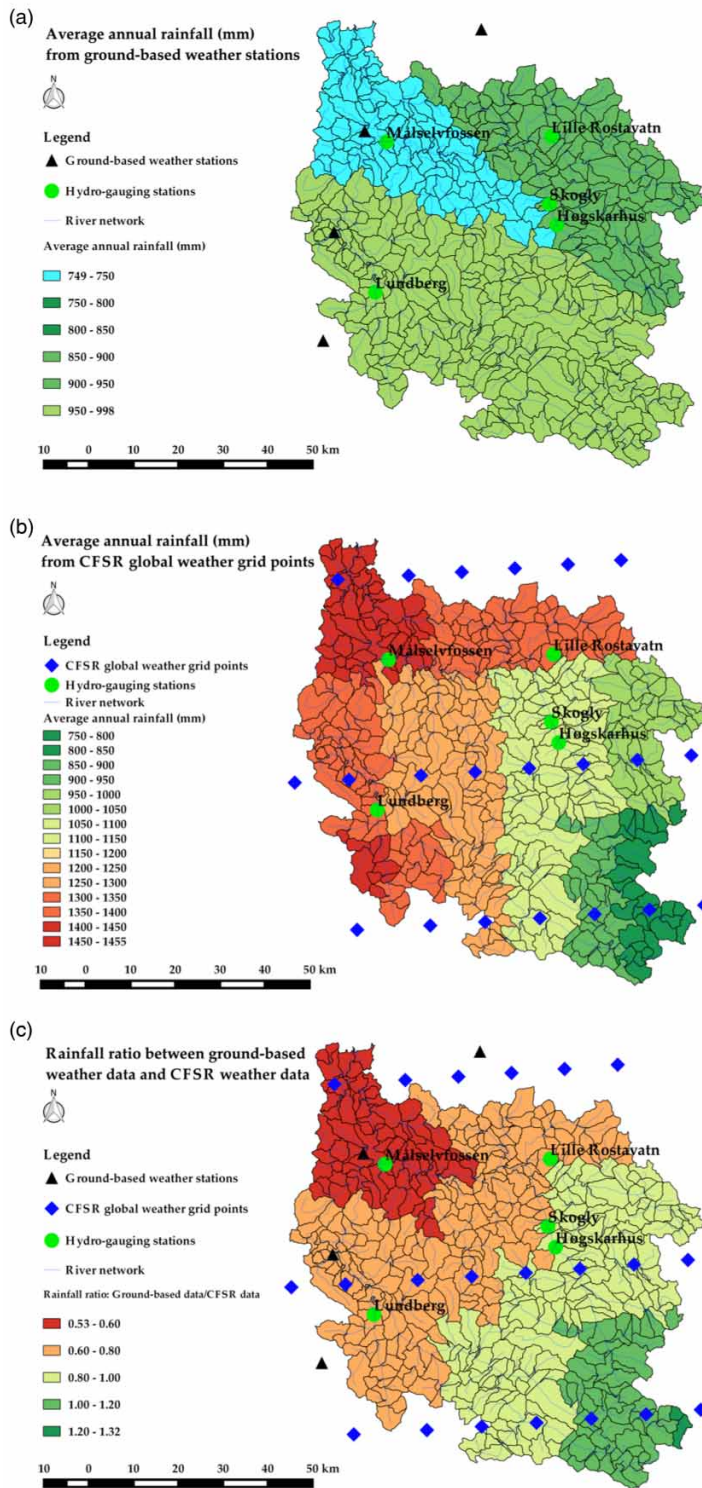


Figure 8 | Spatial variation in the ratio of average annual rainfall (1998–2007) between the ground-based weather data and the CFSR global weather data.

Table 8 | Comparison of the simulated water balance components

Weather dataset		Rainfall	ET	SUR_Q	LAT_Q	PERC	GW_Q	WYLD
Ground-based	(mm)	915.2	144.8	286.7	92.5	282.2	255.3	740.8
	(%)	100	15.8	31.3	10.1	30.8	27.9	80.9
CFSR	(mm)	1192	170.8	286.5	391.1	310.5	127.5	834.9
	(%)	100	14.3	24.0	32.8	26.0	10.7	70.0
Ground-based/CFSR difference	(mm)	-276.7	-26.0	0.2	-298.6	-28.3	127.9	-94.1
	(%)	-23.2	-15.2	0.1	-76.4	-9.1	100.3	-11.3

data is around 11% higher than that from the ground-based data. Actual ET, lateral flow (LAT_Q), and amount of groundwater recharge (PERC) generated from the CFSR data are also higher than from the ground-based weather data. However, the groundwater amount (GW_Q) produced from the ground-based data is higher than that from CFSR data. Noticeably, the surface runoff component generated from the two weather datasets is almost similar.

Comparison of the simulation results of long-term average monthly streamflow

The simulated monthly streamflows, which are generated from ground-based data and CFSR data, are averaged for a 10-year period, 1998–2007, and the results are compared with the averaged values of observed data and shown in Figure 9. According to the graphs in Figure 9, both weather datasets simulate quite well the low value of the average monthly flow, except that slight overestimations are observed in September at Høgskarhus (Figure 9(b)) and Skogly (Figure 9(c)) from the ground-based data. However, the simulation of peak value of the average monthly flow differs somewhat between two weather datasets. For example, the CFSR replicates the peak flow at Lundberg (Figure 9(a)) and Skogly better than the ground-based data. In contrast, the ground-based data replicate the peak flow at Høgskarhus better than CFSR data. The ground-based data generated higher peak flows at Høgskarhus and Skogly than the CFSR data. This could be because of the contribution of higher areal rainfall in upstream sub-basins from the ground-based data, compared with that from the CFSR data. Interestingly, the graphs of long-term average monthly streamflows at Lille Rostavatn (Figure 9(d)) and Målselvossen (Figure 9(e)) generated from both weather datasets are

almost similar, excluding a slightly higher peak flow at Lille Rostavatn achieved from the CFSR data compared with the ground-based data. The graphs of long-term average monthly streamflow at the downstream station, Målselvossen, demonstrate that a fairly good model performance was achieved from both weather datasets.

In brief, a relatively good model performance in terms of simulation of the long-term average monthly streamflow, as well as the consistency of modeling results between the ground-based dataset and the CFSR dataset, achieved at Lille Rostavatn and Målselvossen compared with other hydro-gauging stations, have demonstrated the influences of the representativeness of ground-based weather stations across the Målselv watershed. Since the representative ground-based weather stations are missing for the upstream sub-basins at hydro-gauging stations Lundberg, Skogly, and Høgskarhus, areal rainfall calculated for those sub-basins are from the ground-based weather stations in the downstream and outside of the watershed. However, such weather stations might not be the representative weather stations for the upstream sub-basins. As a result, the simulation results of long-term average monthly streamflow at Lundberg, Skogly, and Høgskarhus stations are not consistent between two weather datasets. In contrast, the hydrographs of the long-term average monthly streamflow at Lille Rostavatn and Målselvossen are almost consistent between two weather datasets. The reason could be because these sub-basins receive correct rainfall from the representative weather stations.

Uncertainty analysis of the modeling results from the two weather inputs

Values of *P*-factors, calculated at all five hydro-gauging stations, from both weather input datasets, in the calibration

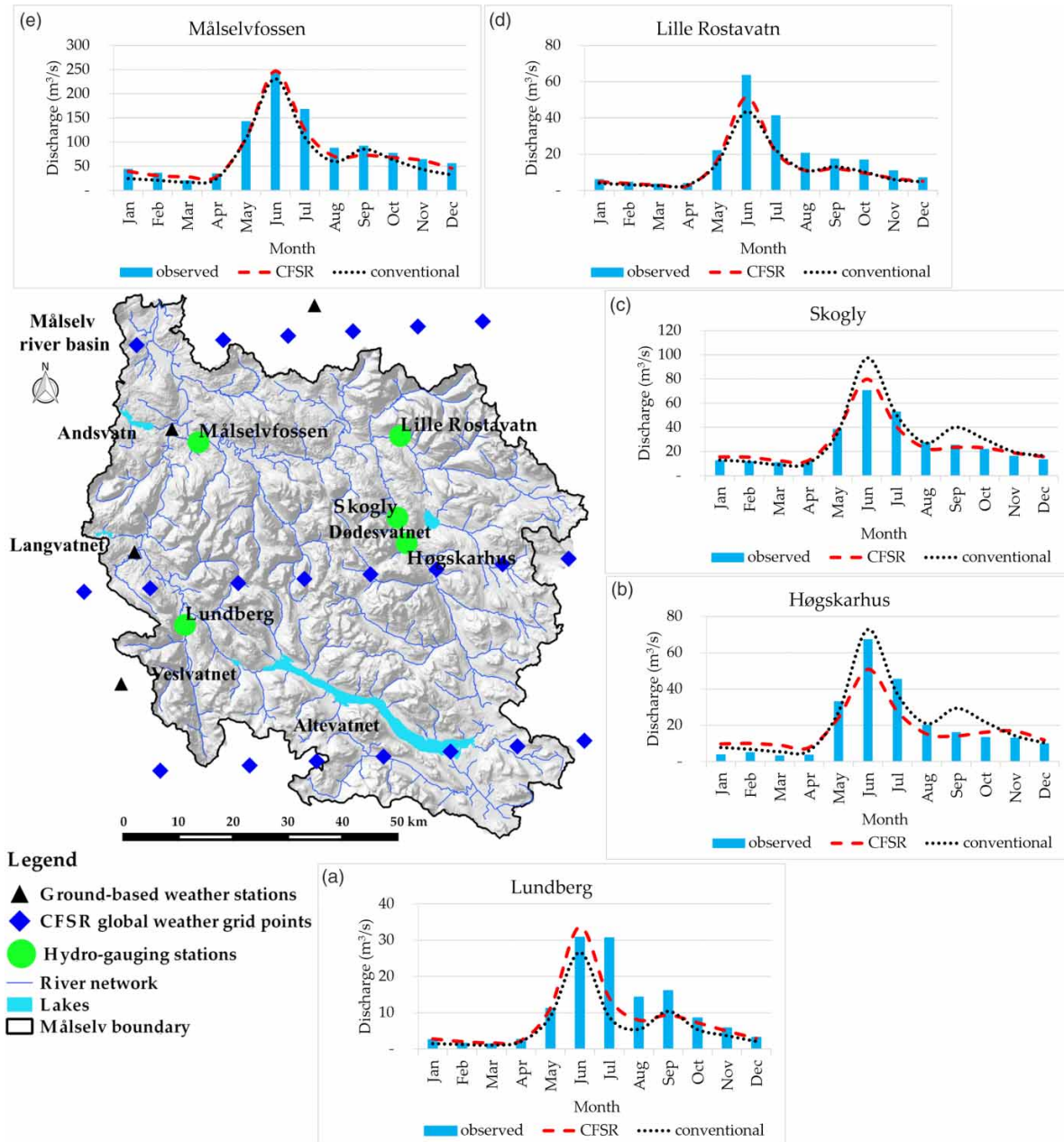


Figure 9 | Average monthly streamflow (in m³/s) during 1998–2007, generated from observed data and simulation with ground-based weather data and CFSR weather data.

period, are ≥ 0.75 , except that the value of P -factor at the Lille Rostavatn station calculated from the ground-based dataset is slightly under 0.70 (Figure 10(a)). Regarding the validation period, values of P -factors at most hydro-gauging stations, from both weather input datasets, are higher than 0.70, excluding the results at Skogly and Lille Rostavatn from the

ground-based dataset (Figure 10(c)). The good values of P -factors achieved from the uncertainty analyses indicate that the measured river discharge is simulated well by the model, or the modeling error is low. The accuracy of modeling results by using the high-resolution CFSR dataset is higher than that by using the existing scattered ground-based dataset.

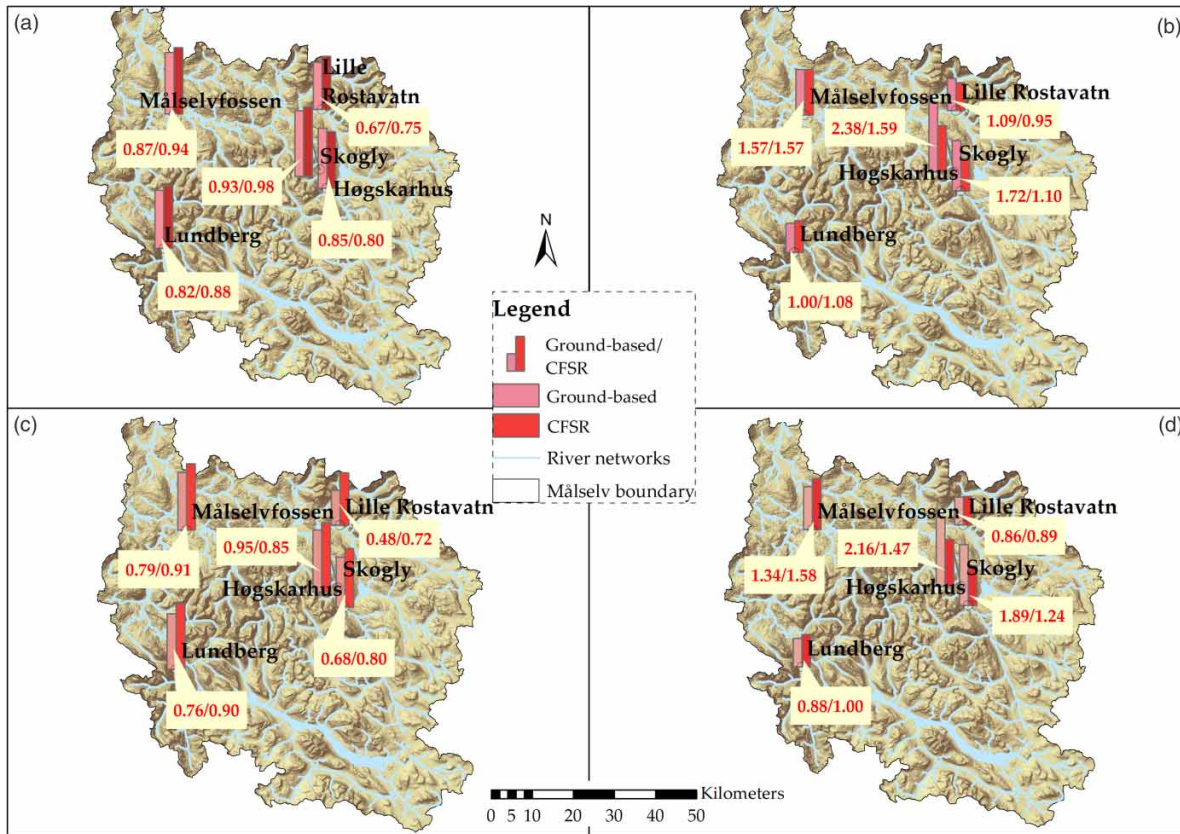


Figure 10 | Uncertainty analysis for streamflow simulation: (a) *P*-factors for the calibration period; (b) *R*-factors for the calibration period; (c) *P*-factors for the validation period; and (d) *R*-factors for the validation period.

Values of *R*-factors obtained from both weather input datasets are ≤ 1.50 for both calibration and the validation periods, except that *R*-factors at Høgskarhus and Skogly, which are obtained from the ground-based dataset, are higher than 1.50 (Figure 10(b) and 10(d)). Therefore, based on the analyzed results of *R*-factors, it could be concluded that using the high-resolution CFSR weather input to simulate river discharge in the Målselv watershed could produce a high certainty of modeling results. In contrast, using the available scattered ground-based data to simulate river discharge may produce uncertain results in upstream sections of the watershed, particularly the areas close to Høgskarhus and Skogly stations. This is because most of the available ground-based stations are located in the downstream of the watershed, and there is a lack of representative stations in the middle, as well as in the upstream, sections.

In brief, according to the above analyses of the statistical coefficients of model performance (e.g., R^2 , NSE, and RSR),

the uncertainty measures (*P*-factor and *R*-factor), the simulation results of water balance components, monthly streamflow hydrograph, and long-term average monthly streamflow, the present study demonstrates that using the high-resolution CFSR weather input to run the SWAT model produces better modeling results than using the existing limited ground-based weather input, in the Arctic watershed, Målselv. It could be interpreted that one of the underlying reasons leading to lower model performance by using the ground-based weather input in this study area is that most of the available meteorological stations are located in the downstream sections, and there is a lack of representative stations in the middle, as well as in the upstream, sections. The Målselv watershed has characteristics of mountainous topography, where rainfall is high variant in space and time. Therefore, the scattered ground-based networks could not represent well the rainfall feature of the whole large watershed, unlike the denser grid points of the

global reanalysis weather data CFSR distributed across the whole watershed. Furthermore, the SWAT model used the NNS method to calculate the areal rainfall for every sub-basin. This approach could result in uncertain outputs when the local meteorological data are recognized to be representative of larger areas. To our knowledge, the CFSR dataset has been used for the first time to run the QSWAT model in the Arctic watershed Målselv by this study. Since the available ground-based weather data are limited in this study area, the CFSR dataset is evaluated as a reliable alternative source. Also, performances and certainties of the CFSR data are verified in this study via the evaluation of multiple factors and criteria. It could be, therefore, highly reliable to apply the CFSR dataset for running hydrological models in Målselv watershed. According to the performance of the CFSR input dataset in this case study, it is expected that CFSR weather data could be a potential source to be widely applied in other Arctic watersheds.

CONCLUSIONS

Collecting enough weather input data to run hydrological models in the data-sparse Arctic region is a challenge for all modelers. In this study, the possibility of using the high-resolution global reanalysis weather data, CFSR, as an alternative data input for the hydrological models was investigated in an Arctic watershed Målselv. The performance of CFSR data is compared with the ground-based (gauged) data through running the hydrological model QSWAT. Model performance with the high-resolution CFSR data is higher than that with the existing scattered ground-based data via the evaluation of the statistical coefficients. The NSE coefficient is in the range of 0.65–0.82 (good to very good) with the CFSR weather input, whereas it is in the range of 0.55–0.74 (satisfactory to good) with the ground-based weather input. The simulation results also demonstrate the high capacity of CFSR data to replicate the monthly average streamflow, in terms of monthly average hydrograph, peak and low-flow values, during a 10-year period, 1998–2007. In contrast, the ground-based weather data showed lower performance than the CFSR data because the network of the ground-based weather station is scattered with only

two stations inside and two stations outside the watershed. In addition, most of the ground-based weather stations locate in the downstream. The representativeness of weather stations in the middle and upstream is missing. The higher rainfall amount and its spatial variation from the CFSR dataset than that from the ground-based dataset leads to higher simulation results of some water balance components, in terms of actual evapotranspiration, lateral flow, groundwater recharge, and water yield contributing to streamflow. By evaluating the uncertainty measures, *P*-factors (with results ≥ 0.70) and *R*-factors (with results ≤ 1.5), CFSR data demonstrated its capacity to produce a high certainty of modeling results in the Målselv watershed. The promising results from this study will open the chances for hydrological applications of the CFSR data in other watersheds in the Arctic region.

ACKNOWLEDGEMENTS

The authors would like to acknowledge the Department of Technology and Safety, University of Tromsø – The Arctic University of Norway, for their financial support for this study. Additionally, we would like to acknowledge the support from The Research Council Project – Dissemination of climate change research outcomes in cold climate regions (project no. 321305).

DATA AVAILABILITY STATEMENT

All relevant data are included in the paper or its Supplementary Information.

REFERENCES

- Abbaspour, K. C. 2015 *SWAT-CUP: Swat Calibration and Uncertainty Program – A User Manual*. Eawag: Swiss Federal Institute of Aquatic Science and Technology, Dübendorf, Switzerland.
- Abbaspour, K. C., Johnson, C. A. & van Genuchten, M. T. 2004 [Estimating uncertain flow and transport parameters using a sequential uncertainty fitting procedure](#). *Vadose Zone Journal* 3 (4), 1340–1352.

- Abbaspour, K. C., Yang, J., Maximov, I., Siber, R., Bogner, K., Mieleitner, J., Zobrist, J. & Srinivasan, R. 2007 Modelling hydrology and water quality in the pre-alpine/alpine Thur watershed using SWAT. *Journal of Hydrology* **333** (2–4), 413–430.
- Abbaspour, K. C., Rouholahnejad, E., Vaghefi, S., Srinivasan, R., Yang, H. & Klove, B. 2015 A continental-scale hydrology and water quality model for Europe: calibration and uncertainty of a high-resolution large-scale SWAT model. *Journal of Hydrology* **524**, 733–752.
- Alemayehu, T., van Griensven, A. & Bauwens, W. 2016 Evaluating CFSR and WATCH data as input to SWAT for the estimation of the potential evapotranspiration in a data-scarce Eastern-African catchment. *Journal of Hydrologic Engineering* **21** (3), 1–16.
- Arnold, J. G., Moriasi, D. N., Gassman, P. W., Abbaspour, K. C., White, M. J., Srinivasan, R., Santhi, C., Harmel, R. D., Griensven, A. v., Liew, M. W. V., Kannan, N. & Jha, M. K. 2012 SWAT: model use, calibration, and validation. *American Society of Agricultural and Biological Engineers* **55** (4), 1491–1508.
- Bressiani, D. D., Srinivasan, R., Jones, C. A. & Mendiondo, E. M. 2015 Effects of spatial and temporal weather data resolutions on streamflow modeling of a semi-arid basin, Northeast Brazil. *International Journal of Agricultural and Biological Engineering* **8** (3), 125–139.
- Chen, D. Y., Shams, S., Carmona-Moreno, C. & Leone, A. 2010 Assessment of open source GIS software for water resources management in developing countries. *Journal of Hydro-Environment Research* **4** (3), 253–264.
- Clark, M. P., Bierkens, M. F. P., Samaniego, L., Woods, R. A., Uijlenhoet, R., Bennett, K. E., Pauwels, V. R. N., Cai, X. T., Wood, A. W. & Peters-Lidard, C. D. 2017 The evolution of process-based hydrologic models: historical challenges and the collective quest for physical realism. *Hydrology and Earth System Sciences* **21** (7), 3427–3440.
- Compo, G. P., Whitaker, J. S. & Sardeshmukh, P. D. 2006 Feasibility of a 100-year reanalysis using only surface pressure data. *Bulletin of the American Meteorological Society* **87** (2), 175.
- Compo, G. P., Whitaker, J. S., Sardeshmukh, P. D., Matsui, N., Allan, R. J., Yin, X., Gleason, B. E., Vose, R. S., Rutledge, G., Bessemoulin, P., Bronnimann, S., Brunet, M., Crouthamel, R. I., Grant, A. N., Groisman, P. Y., Jones, P. D., Kruk, M. C., Kruger, A. C., Marshall, G. J., Maugeri, M., Mok, H. Y., Nordli, O., Ross, T. F., Trigo, R. M., Wang, X. L., Woodruff, S. D. & Worley, S. J. 2011 The twentieth century reanalysis project. *Quarterly Journal of the Royal Meteorological Society* **137** (654), 1–28.
- Cuceloglu, G. & Ozturk, I. 2019 Assessing the impact of CFSR and local climate datasets on hydrological modeling performance in the mountainous Black sea catchment. *Water* **11** (11), 1–20.
- Dile, Y. T. & Srinivasan, R. 2014 Evaluation of CFSR climate data for hydrologic prediction in data-scarce watersheds: an application in the Blue Nile River Basin. *Journal of the American Water Resources Association* **50** (5), 1226–1241.
- Dile, Y. T., Berndtsson, R. & Setegn, S. G. 2013 Hydrological response to climate change for Gilgel Abay River, in the Lake Tana Basin – upper blue Nile Basin of Ethiopia. *PLoS One* **8** (10), 1–13.
- Dile, Y. T., Daggupati, P., George, C., Srinivasan, R. & Arnold, J. 2016 Introducing a new open source GIS user interface for the SWAT model. *Environmental Modelling & Software* **85**, 129–138.
- ECAD 2002 *The European Climate Assessment & Dataset Project*. Available from: <https://www.ecad.eu/dailydata/index.php>.
- Edwards, P. J., Williard, K. W. J. & Schoonover, J. E. 2015 Fundamentals of watershed hydrology. *Journal of Contemporary Water Research & Education* **154** (1), 3–20.
- Ehret, U., Gupta, H. V., Sivapalan, M., Weijis, S. V., Schymanski, S. J., Blöschl, G., Gelfan, A. N., Harman, C., Kleidon, A., Bogaard, T. A., Wang, D., Wagener, T., Scherer, U., Zehe, E., Bierkens, M. F. P., Di Baldassarre, G., Parajka, J., van Beek, L. P. H., van Griensven, A., Westhoff, M. C. & Winsemius, H. C. 2014 Advancing catchment hydrology to deal with predictions under change. *Hydrology and Earth System Sciences* **18** (2), 649–671.
- Fuka, D. R., Walter, M. T., MacAlister, C., Degaetano, A. T., Steenhuis, T. S. & Easton, Z. M. 2014 Using the climate forecast system reanalysis as weather input data for watershed models. *Hydrological Processes* **28** (22), 5613–5623.
- Gassman, P. W., Reyes, M. R., Green, C. H. & Arnold, J. G. 2007 The soil and water assessment tool: historical development, applications, and future research directions. *Transactions of the ASABE* **50** (4), 1211–1250.
- Gelaro, R., McCarty, W., Suarez, M. J., Todling, R., Molod, A., Takacs, L., Randles, C. A., Darmenov, A., Bosilovich, M. G., Reichle, R., Wargan, K., Coy, L., Cullather, R., Draper, C., Akella, S., Buchard, V., Conaty, A., da Silva, A. M., Gu, W., Kim, G. K., Koster, R., Lucchesi, R., Merkova, D., Nielsen, J. E., Partyka, G., Pawson, S., Putman, W., Rienecker, M., Schubert, S. D., Sienkiewicz, M. & Zhao, B. 2017 The Modern-Era Retrospective Analysis for Research and Applications, Version 2 (MERRA-2). *Journal of Climate* **30** (14), 5419–5454.
- Geonorge 2013 *Height DTM 10*. Available from: <https://kartkatalog.geonorge.no/metadata/kartverket/dtm-10-terrengmodell-utm33/>.
- Gleckler, P. J., Taylor, K. E. & Doutriaux, C. 2008 Performance metrics for climate models. *Journal of Geophysical Research-Atmospheres* **113** (D6), 1–20.
- Hersbach, H., Bell, B., Berrisford, P., Hirahara, S., Horanyi, A., Muñoz-Sabater, J., Nicolas, J., Peubey, C., Radu, R., Schepers, D., Simmons, A., Soci, C., Abdalla, S., Abellan, X., Balsamo, G., Bechtold, P., Biavati, G., Bidlot, J., Bonavita, M., De Chiara, G., Dahlgren, P., Dee, D., Diamantakis, M., Dragani, R., Flemming, J., Forbes, R., Fuentes, M., Geer, A., Haimberger, L., Healy, S., Hogan, R. J., Holm, E., Janiskova,

- M., Keeley, S., Laloyaux, P., Lopez, P., Lupu, C., Radnoti, G., de Rosnay, P., Rozum, I., Vamborg, F., Villaume, S. & Thepaut, J. N. 2020 [The ERA5 global reanalysis](#). *Quarterly Journal of the Royal Meteorological Society* **146** (730), 1999–2049.
- Kalnay, E., Kanamitsu, M., Kistler, R., Collins, W., Deaven, D., Gandin, L., Iredell, M., Saha, S., White, G., Woollen, J., Zhu, Y., Chelliah, M., Ebisuzaki, W., Higgins, W., Janowiak, J., Mo, K. C., Ropelewski, C., Wang, J., Leetmaa, A., Reynolds, R., Jenne, R. & Joseph, D. 1996 [The NCEP/NCAR 40-year reanalysis project](#). *Bulletin of the American Meteorological Society* **77** (3), 437–471.
- Kanamitsu, M., Ebisuzaki, W., Woollen, J., Yang, S. K., Hnilo, J. J., Fiorino, M. & Potter, G. L. 2002 [NCEP-DOE AMIP-II reanalysis \(R-2\)](#). *Bulletin of the American Meteorological Society* **83** (11), 1631–1643.
- Kidston, J., Frierson, D. M. W., Renwick, J. A. & Vallis, G. K. 2010 [Observations, simulations, and dynamics of jet stream variability and annular modes](#). *Journal of Climate* **23** (23), 6186–6199.
- Kim, K. B., Kwon, H. H. & Han, D. W. 2018 [Exploration of warm-up period in conceptual hydrological modelling](#). *Journal of Hydrology* **556**, 194–210.
- Kistler, R., Kalnay, E., Collins, W., Saha, S., White, G., Woollen, J., Chelliah, M., Ebisuzaki, W., Kanamitsu, M., Kousky, V., van den Dool, H., Jenne, R. & Fiorino, M. 2001 [The NCEP-NCAR 50-year reanalysis: monthly means CD-ROM and documentation](#). *Bulletin of the American Meteorological Society* **82** (2), 247–267.
- Kouwen, N., Danard, M., Bingeman, A., Lu, W., Seglenieks, F. R. & Soulis, E. D. 2005 [Case study: watershed modeling with distributed weather model data](#). *Journal of Hydrologic Engineering* **10** (1), 23–38.
- Kravtsov, S., Wyatt, M. G., Curry, J. A. & Tsonis, A. A. 2014 [Two contrasting views of multidecadal climate variability in the twentieth century](#). *Geophysical Research Letters* **41** (19), 6881–6888.
- Lavers, D. A., Villarini, G., Allan, R. P., Wood, E. F. & Wade, A. J. 2012 [The detection of atmospheric rivers in atmospheric reanalyses and their links to British winter floods and the large-scale climatic circulation](#). *Journal of Geophysical Research-Atmospheres* **117**, 1–13.
- Lindsay, R., Wenshanan, M., Schweiger, A. & Zhang, J. 2014 [Evaluation of seven different atmospheric reanalysis products in the Arctic](#). *Journal of Climate* **27** (7), 2588–2606.
- Lu, J. Z., Zhang, L., Cui, X. L., Zhang, P., Chen, X. L., Sauvage, S. & Sanchez-Perez, J. M. 2019 [Assessing the climate forecast system reanalysis weather data driven hydrological model for the Yangtze River Basin in China](#). *Applied Ecology and Environmental Research* **17** (2), 3615–3632.
- Malago, A., Pagliero, L., Bouraoui, F. & Franchini, M. 2015 [Comparing calibrated parameter sets of the SWAT model for the Scandinavian and Iberian peninsulas](#). *Hydrological Sciences Journal-Journal Des Sciences Hydrologiques* **60** (5), 949–967.
- Mckay, M. D., Beckman, R. J. & Conover, W. J. 1979 [A comparison of three methods for selecting values of input variables in the analysis of output from a computer code](#). *Technometrics* **21** (2), 239–245.
- Mehta, V. K., Walter, M. T., Brooks, E. S., Steenhuis, T. S., Walter, M. F., Johnson, M., Boll, J. & Thongs, D. 2004 [Application of SMR to modeling watersheds in the Catskill Mountains](#). *Environmental Modeling & Assessment* **9** (2), 77–89.
- Moriyas, D. N., Arnold, J. G., Van Liew, M. W., Bingner, R. L., Harmel, R. D. & Veith, T. L. 2007 [Model evaluation guidelines for systematic quantification of accuracy in watershed simulations](#). *Transactions of the ASABE* **50** (3), 885–900.
- Najafi, M. R., Moradkhani, H. & Piechota, T. C. 2012 [Ensemble streamflow prediction: climate signal weighting methods vs. climate forecast system reanalysis](#). *Journal of Hydrology* **442**, 105–116.
- NCAR 2017 [The Climate Data Guide: Climate Forecast System Reanalysis \(CFSR\)](#). Available from: <https://climatedataguide.ucar.edu/climate-data/climate-forecast-system-reanalysis-cfsr> (accessed 05 July 2020).
- NCEP 2010 [CFSR: Products and Notes](#). Available from: <https://www.cpc.ncep.noaa.gov/products/wesley/cfsr/index.html> (accessed 05 July 2020).
- Neitsch, S. L., Arnold, J. G., Kiniry, J. R. & Williams, J. R. 2009 [Overview of Soil and Water Assessment Tool \(SWAT\) model](#). In: *Soil and Water Assessment Tool (SWAT): Global Application* (J. Arnold, R. Srinivasan, S. Neitsch, C. George, K. Abbaspour, P. Gassman, H. H. Fang, G. Av, A. Gosain, P. Debels, N. W. Kim, H. Somura, V. Ella, L. Leon, A. Jintrawet, M. Reyes & S. Sombatpanit, eds). The World Association of Soil and Water Conservation (WASWC), Bangkok, pp. 3–23.
- Onogi, K., Tslltsui, J., Koide, H., Sakamoto, M., Kobayashi, S., Hatsushika, H., Matsumoto, T., Yamazaki, N., Kaalhor, H., Takahashi, K., Kadokura, S., Wada, K., Kato, K., Oyama, R., Ose, T., Mannoji, N. & Taira, R. 2007 [The JRA-25 reanalysis](#). *Journal of the Meteorological Society of Japan* **85** (3), 369–432.
- Özdemir, A. 2016 [Hierarchical Approach To Semi-Distributed Hydrological Model Calibration](#). Doctor of Philosophy, The Graduate School Of Natural And Applied Sciences, Middle East Technical University.
- Parker, W. S. 2016 [Reanalyses and observations: what's the difference?](#) *Bulletin of the American Meteorological Society* **97** (9), 1565–1572.
- Premanand, B. D., Satishkumar, U., Maheshwara Babu, B., Parasappa, S. K., Dandu M, M., Kaleel, I., Rajesh, N. L. & Biradar, S. A. 2018 [QSWAT model calibration and uncertainty analysis for stream flow simulation in the Patapur micro-watershed using sequential uncertainty fitting method \(SUFI-2\)](#). *International Journal of Current Microbiology and Applied Sciences* **7** (4), 831–852.
- Quadro, M. F. L., Berbery, E. H., Dias, M. A. F. S., Herdies, D. L. & Goncalves, L. G. G. 2013 [The atmospheric water cycle over South America as seen in the new generation of global](#)

- reanalyses. *Radiation Processes in the Atmosphere and Ocean* **1531**, 732–735.
- Reddy, N. N., Reddy, K. V., Vani, J. S. L. S., Daggupati, P. & Srinivasan, R. 2018 *Climate change impact analysis on watershed using QSWAT*. *Spatial Information Research* **26** (3), 253–259.
- Roth, V. & Lemann, T. 2016 *Comparing CFSR and conventional weather data for discharge and soil loss modelling with SWAT in small catchments in the Ethiopian Highlands*. *Hydrology and Earth System Sciences* **20** (2), 921–934.
- Saha, S., Moorthi, S., Pan, H. L., Wu, X. R., Wang, J. D., Nadiga, S., Tripp, P., Kistler, R., Woollen, J., Behringer, D., Liu, H. X., Stokes, D., Grumbine, R., Gayno, G., Wang, J., Hou, Y. T., Chuang, H. Y., Juang, H. M. H., Sela, J., Iredell, M., Treadon, R., Kleist, D., Van Delst, P., Keyser, D., Derber, J., Ek, M., Meng, J., Wei, H. L., Yang, R. Q., Lord, S., Van den Dool, H., Kumar, A., Wang, W. Q., Long, C., Chelliah, M., Xue, Y., Huang, B. Y., Schemm, J. K., Ebisuzaki, W., Lin, R., Xie, P. P., Chen, M. Y., Zhou, S. T., Higgins, W., Zou, C. Z., Liu, Q. H., Chen, Y., Han, Y., Cucurull, L., Reynolds, R. W., Rutledge, G. & Goldberg, M. 2010 *The Ncep climate forecast system reanalysis*. *Bulletin of the American Meteorological Society* **91** (8), 1015–1057.
- Santer, B. D., Wigley, T. M. L., Simmons, A. J., Kallberg, P. W., Kelly, G. A., Uppala, S. M., Ammann, C., Boyle, J. S., Bruggemann, W., Doutriaux, C., Fiorino, M., Mears, C., Meehl, G. A., Sausen, R., Taylor, K. E., Washington, W. M., Wehner, M. F. & Wentz, F. J. 2004 *Identification of anthropogenic climate change using a second-generation reanalysis*. *Journal of Geophysical Research-Atmospheres* **109** (D21), 1–19.
- Santhi, C., Arnold, J. G., Williams, J. R., Dugas, W. A., Srinivasan, R. & Hauck, L. M. 2001 *Validation of the swat model on a large river basin with point and nonpoint sources*. *Journal of the American Water Resources Association* **37** (5), 1169–1188.
- Sildre 2020 *Real-time Hydrological Data*. The Norwegian Water Resources and Energy Directorate (NVE). Available from: <http://sildre.nve.no/> (accessed 18 November 2019).
- Smith, R. A. & Kummerow, C. D. 2013 *A comparison of in situ, reanalysis, and satellite water budgets over the Upper Colorado River Basin*. *Journal of Hydrometeorology* **14** (3), 888–905.
- Srinivasan, R. & Arnold, J. G. 1994 *Integration of a basin-scale water-quality model with GIS*. *Water Resources Bulletin* **30** (3), 453–462.
- Talagrand, O. 1997 *Assimilation of observations, an introduction*. *Journal of the Meteorological Society of Japan* **75** (1b), 191–209.
- TAMU 2012 *CFSR: Global Weather Data for SWAT*. Available from: <https://globalweather.tamu.edu/> (accessed 05 July 2020).
- Tao, J., Koster, R. D., Reichle, R. H., Forman, B. A., Xue, Y., Chen, R. H. & Moghaddam, M. 2019 *Permafrost variability over the Northern Hemisphere based on the MERRA-2 reanalysis*. *Cryosphere* **13** (8), 2087–2110.
- Tolera, M. B., Chung, I. M. & Chang, S. W. 2018 *Evaluation of the climate forecast system reanalysis weather data for watershed modeling in upper Awash Basin, Ethiopia*. *Water* **10** (6), 1–17.
- Van Liew, M. W., Arnold, J. G. & Garbrecht, J. D. 2003 *Hydrologic simulation on agricultural watersheds: choosing between two models*. *Transactions of the ASAE* **46** (6), 1539–1551.
- Washington, W. M. & Parkinson, C. L. 2005 *An Introduction to Three-Dimensional Climate Modeling*. University Science Books, Sausalito, CA.
- Waterbase 2007a *Land use*. Available from: http://www.waterbase.org/download_data.html (accessed 14 February 2021).
- Waterbase 2007b *Soil*. Available from: http://www.waterbase.org/download_data.html (accessed 14 February 2021).
- Whitaker, J. S., Compo, G. P., Wei, X. & Hamill, T. M. 2004 *Reanalysis without radiosondes using ensemble data assimilation*. *Monthly Weather Review* **132** (5), 1190–1200.
- Winchell, M., Srinivasan, R., Di Luzio, M. & Arnold, J. G. 2013 *Arcswat Interface for SWAT2012: User's Guide*. Blackland Research Center, Texas AgriLife Research, College Station.
- WMO 2018 *WMO Addresses Arctic Science Ministerial*. Available from: <https://public.wmo.int/en/media/news/wmo-addresses-arctic-science-ministerial#:~:text=The%20Arctic%20represents%20about%204,the%20world%2C%20said%20Mr%20Taalas> (accessed 05 July 2020).
- Yu, X. & Duffy, C. J. 2018 *Watershed hydrology: scientific advances and environmental assessments*. *Water* **10** (3), 1–6.
- Zhang, L., Nan, Z. T., Xu, Y. & Li, S. 2016 *Hydrological impacts of land use change and climate variability in the headwater region of the Heihe River Basin, Northwest China*. *PLoS One* **11** (6), 1–25.

Supplementary material

Table S1. Land use classification in SWAT model.

Land use code	Area (ha)	%Watershed	Crop name
GRAS	33046.05	5.68	grassland
SHRB	50757.53	8.73	shrubland
FODB	128666.06	22.12	deciduous broadleaf forest
FOEN	730.48	0.13	evergreen needleleaf forest
FOMI	9126.23	1.57	mixed forest
WATR	23924.18	4.11	water
WEWO	1535.38	0.26	wooded wetland
BSVG	3658.14	0.63	barren or sparsely vegetated
TUWO	188328.17	32.38	wooded tundra
TUMI	139179.82	23.93	mixed tundra
TUBG	2591.84	0.45	bare ground tundra

Table S2. Soil classification in SWAT model.

Soil code	Area (ha)	%Watershed	Texture
Po35-1b-6611	115250.66	19.82	sandy loam
I-Re-Rx-1-3125	409375.91	70.39	sandy loam
I-Po-Od-1-3118	15540.66	2.67	sandy loam
WATER-6997	41376.65	7.11	water

Table S3. Slope classification in SWAT model.

% of slope	Area (ha)	%Watershed
0-5.0	107394.5	18.47
5.0-10.0	78841.49	13.56
10.0-25.0	191854.09	32.99
25.0-30.0	39609.69	6.81
> 30.0	163844.11	28.17

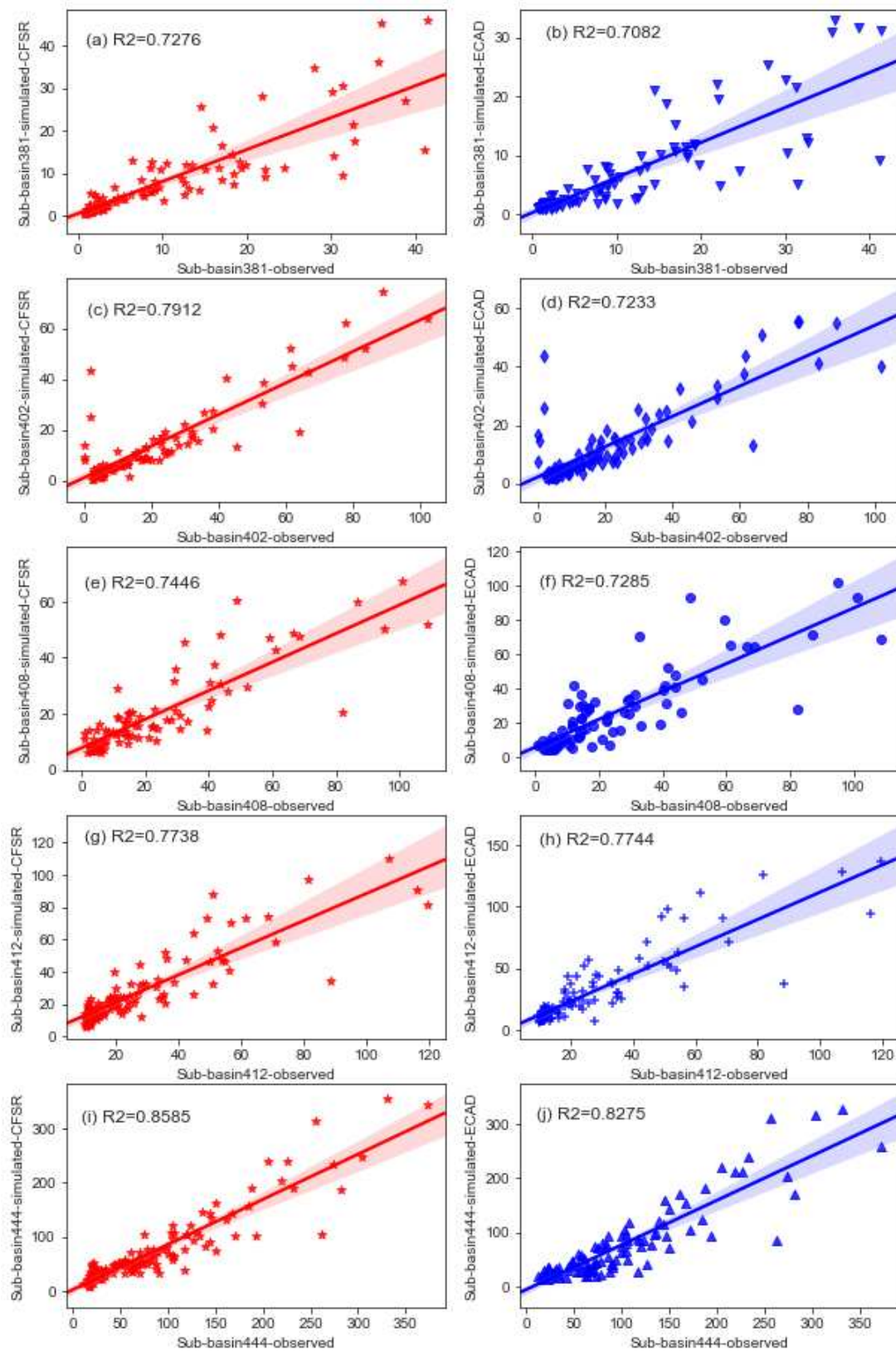


Figure S1. Scatter plots of observed and simulated streamflow from using CFSR data and ground-based data (ECAD) for the calibration period (1998-2007): (a,b) at Lundberg; (c,d) at Lille Rostavatn; (e,f) at Høgskarhus; (g,h) at Skogly; and (i,j) at Målselvfossen.

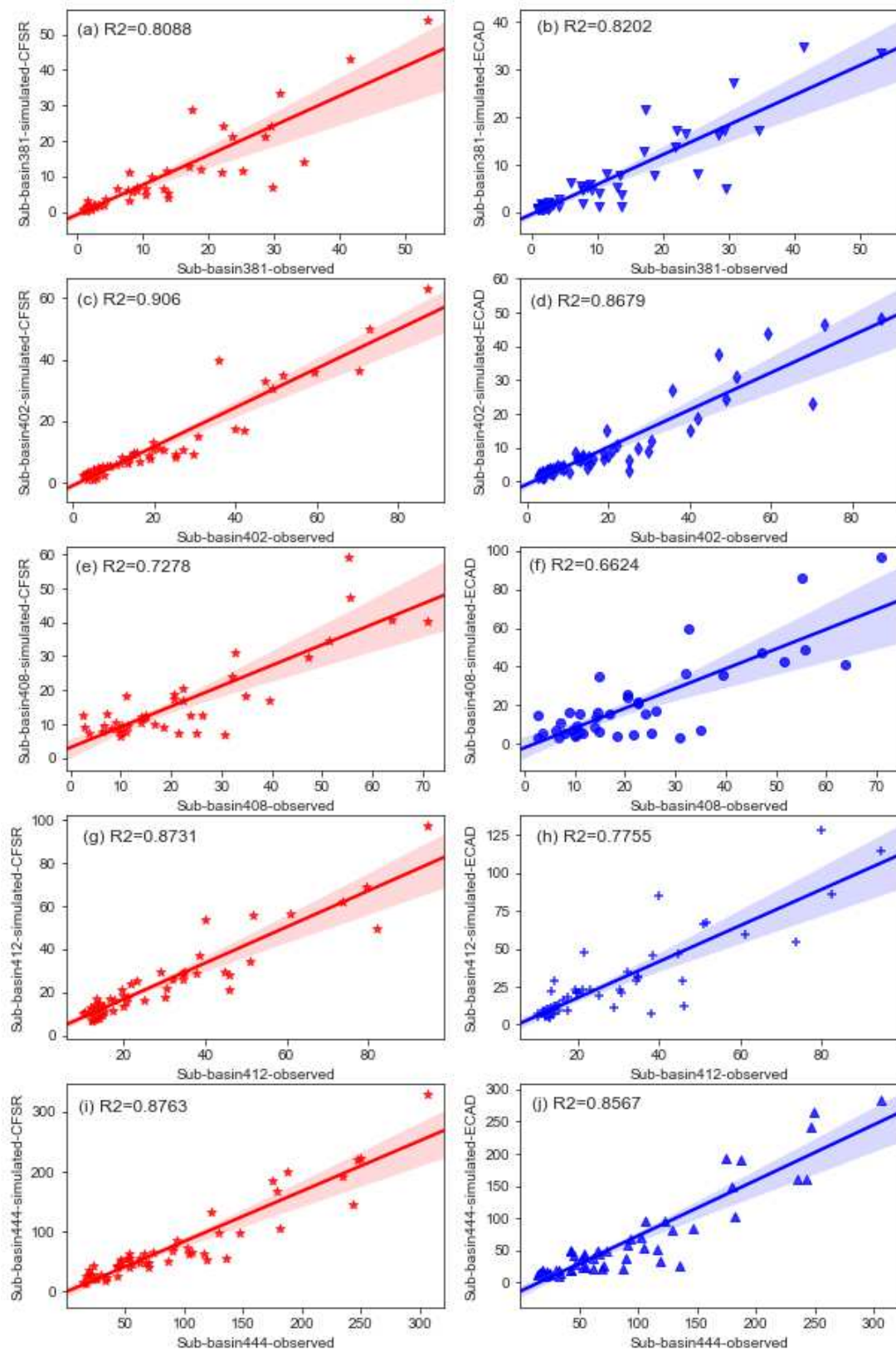


Figure S2. Scatter plots of observed and simulated streamflow from using CFSR data and ground-based data (ECAD) for the validation period (2008-2012): (a,b) at Lundberg; (c,d) at Lille Rostavatn; (e,f) at Høgskarhus; (g,h) at Skogly; and (i,j) at Målselvfossen.

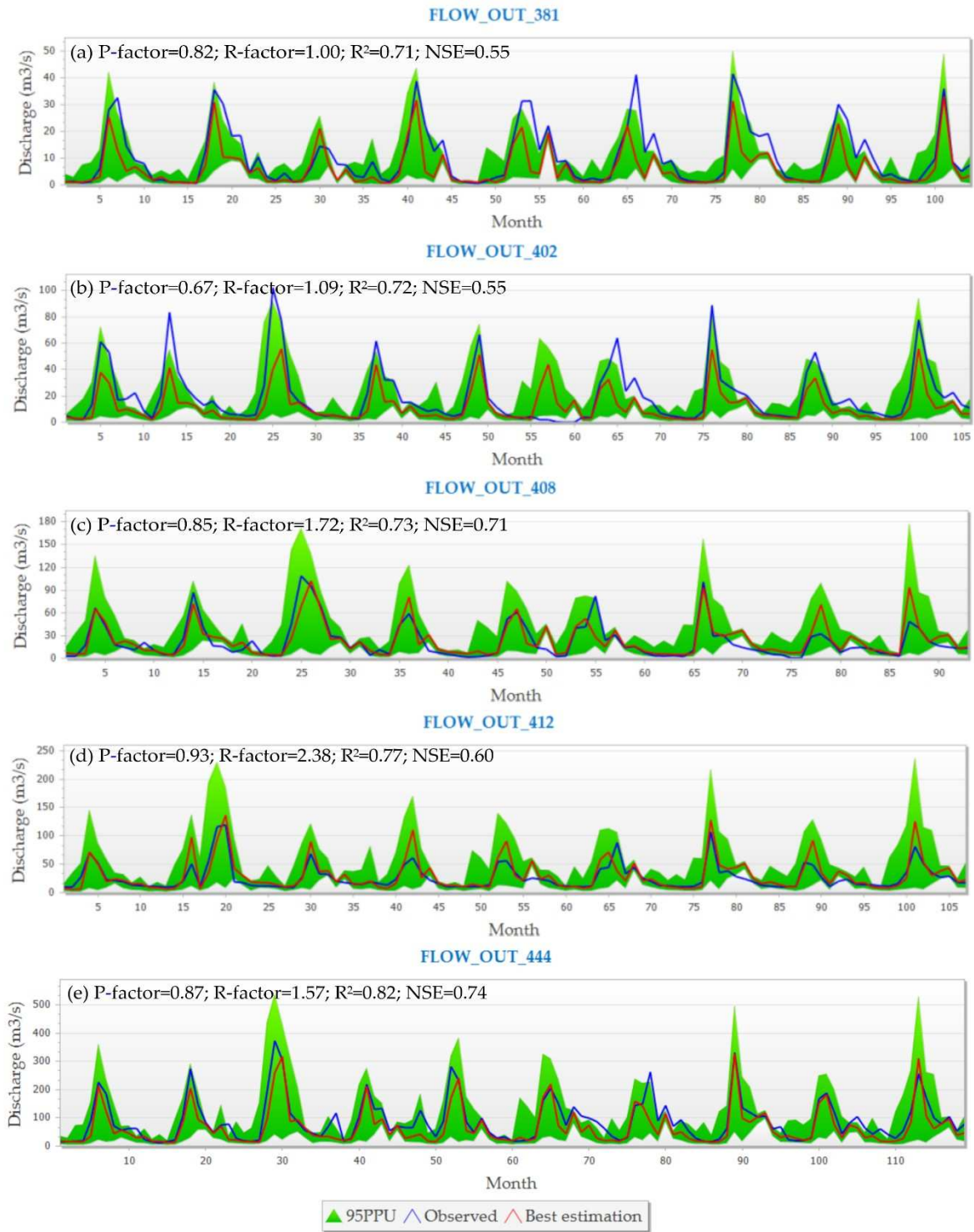


Figure S3. Calibration results for the period 1998-2007 by monthly simulation with ground-based weather data: (a) at Lundberg; (b) at Lille Rostavatn; (c) at Høgskarhus; (d) at Skogly; and (e) at Målselvfossen.

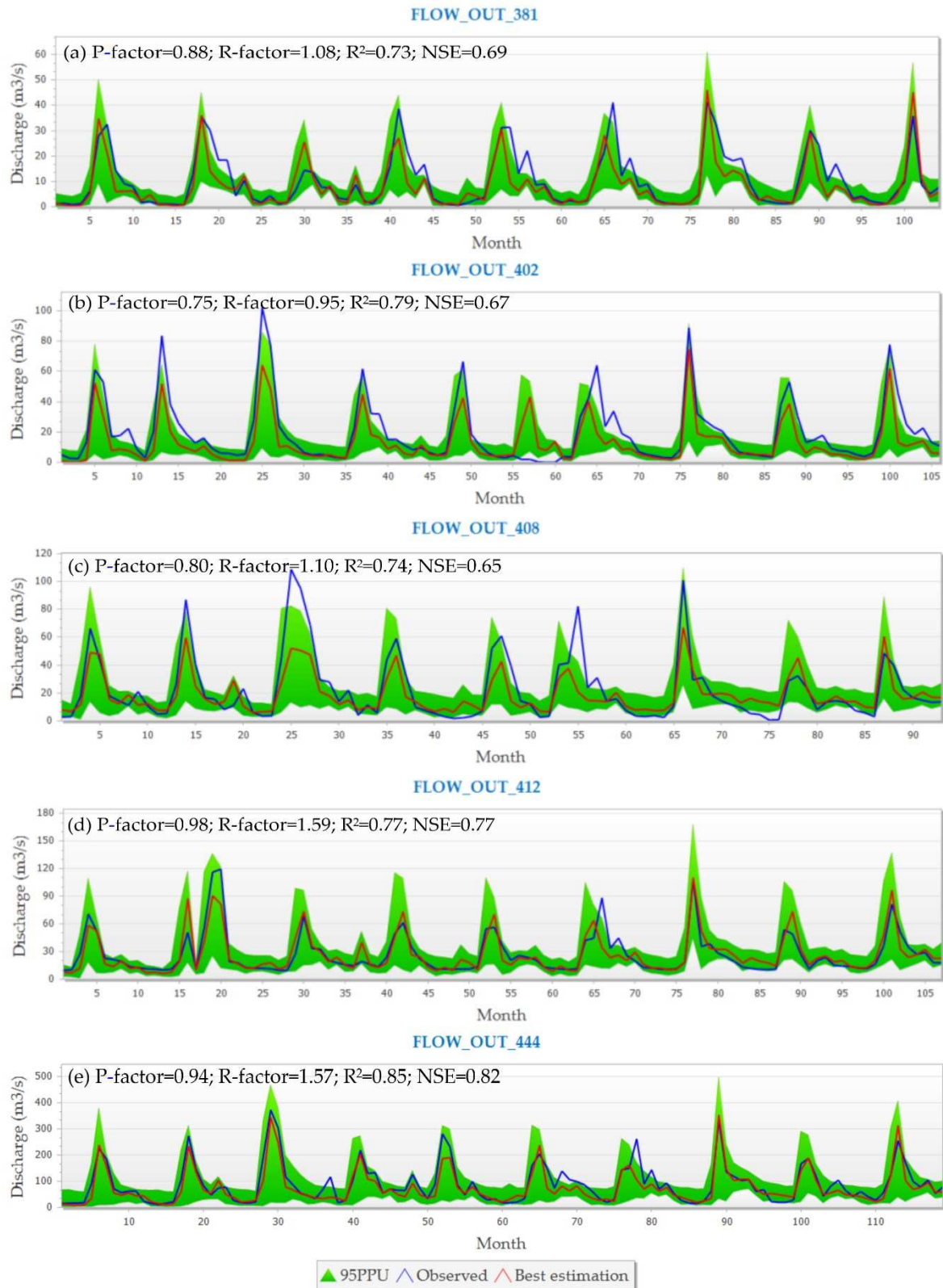


Figure S4. Calibration results for the period 1998-2007 by monthly simulation with CFSR global weather data: (a) at Lundberg; (b) at Lille Rostavatn; (c) at Høgskarhus; (d) at Skogly; and (e) at Målselvossen.

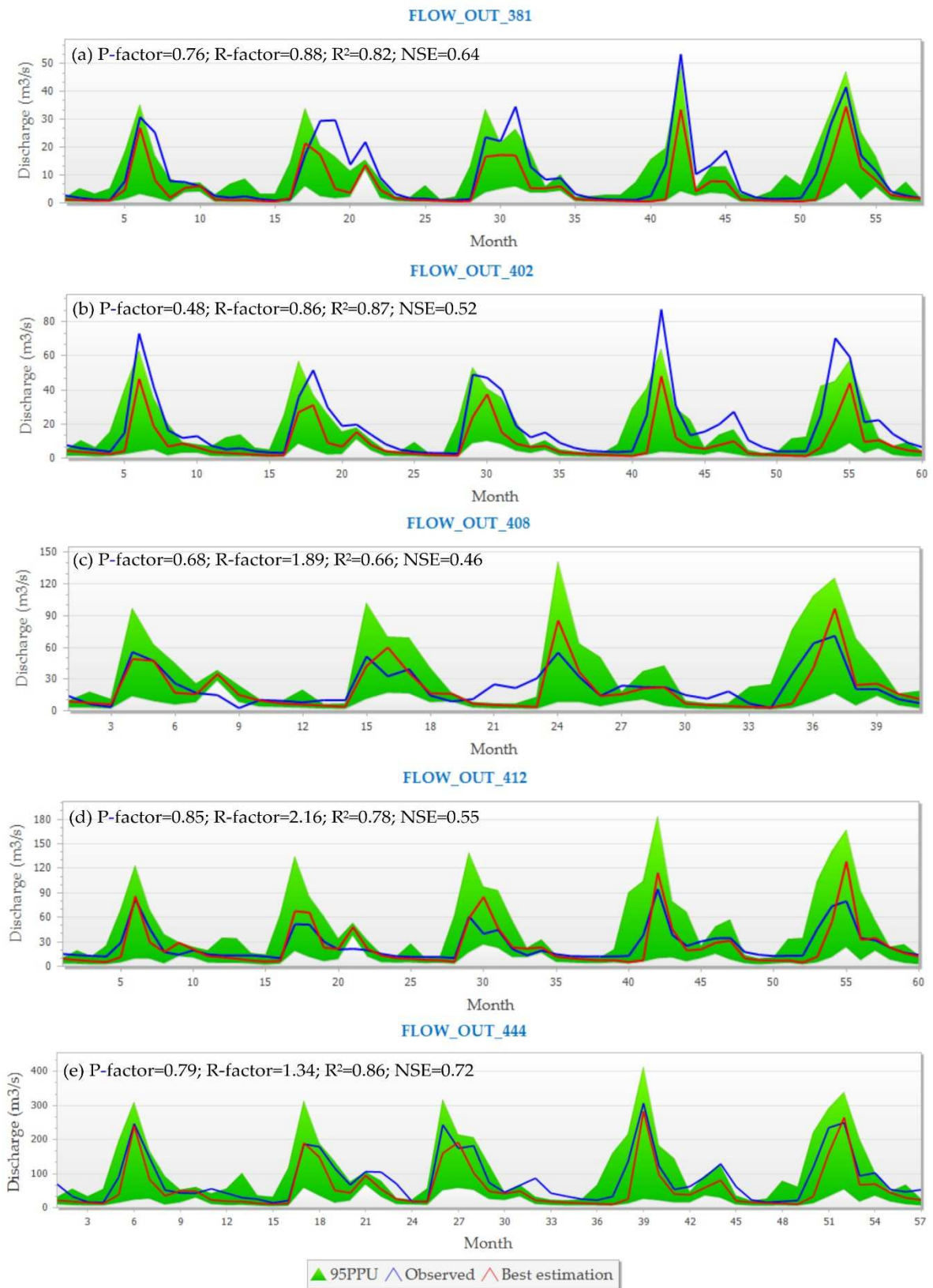


Figure S5. Model validation for the period 2008-2012 by monthly simulation with ground-based weather data: (a) at Lundberg; (b) at Lille Rostavatn; (c) at Høgskarhus; (d) at Skogly; and (e) at Målselvossen.

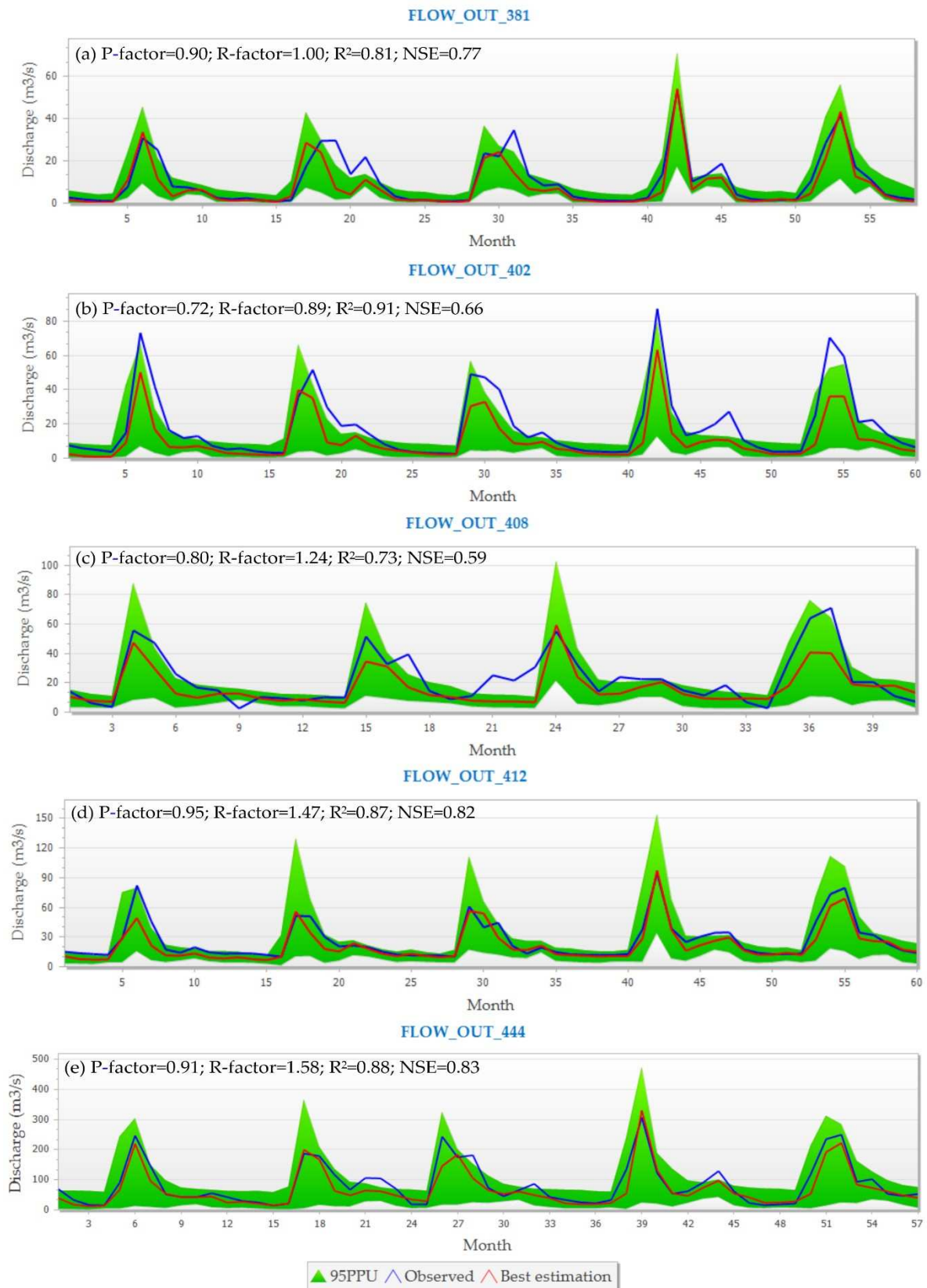


Figure S6. Model validation for the period 2008-2012 by monthly simulation with CFSR global weather data: (a) at Lundberg; (b) at Lille Rostavatn; (c) at Høgskarhus; (d) at Skogly; and (e) at Målselvfossen.

Paper III

Bui, Minh Tuan; Lu, Jinmei; Nie, Linmei. Quantify the effects of watershed subdivision scale and spatial density of weather inputs on hydrological simulations in a Norwegian Arctic watershed. *Journal of Water and Climate Change* 2021. ISSN 2040-2244.s doi: <https://doi.org/10.2166/wcc.2021.173>.

The paper was published in the Special Issue “Assessment and Adaptation to Climate Change Impacts in Cold Regions”.

Quantifying the effects of watershed subdivision scale and spatial density of weather inputs on hydrological simulations in a Norwegian Arctic watershed

Minh Tuan Bui ^{a,*}, Jinmei Lu^a and Linmei Nie ^b

^a Department of Technology and Safety, Faculty of Science and Technology, UIt The Arctic University of Norway, Tromsø 9037, Norway

^b Centre for Sustainable Development and Innovation of Water Technology, Foundation CSDI WaterTech, Oslo 0373, Norway

*Corresponding author. E-mail: minh.t.bui@uit.no

 MTB, 0000-0001-6793-1238

ABSTRACT

The effects of watershed subdivisions on hydrological simulations have not been evaluated in Arctic conditions yet. This study applied the Soil and Water Assessment Tool and the threshold drainage area (TDA) technique to evaluate the impacts of watershed subdivision on hydrological simulations at a 5,913-km² Arctic watershed, Målselv. The watershed was discretized according to four TDA scheme scales including 200, 2,000, 5,000, and 10,000 ha. The impacts of different TDA schemes on hydrological simulations in water balance components, snowmelt runoff, and streamflow were investigated. The study revealed that the complexity of terrain and topographic attributes altered significantly in the coarse discretizations: (1) total stream length (−47.2 to −74.6%); (2) average stream slope (−68 to −83%); and (3) drainage density (−24.2 to −51.5%). The spatial density of weather grid integration reduced from −5 to −33.33% in the coarse schemes. The annual mean potential evapotranspiration, evapotranspiration, and lateral flow slightly decreased, while areal rainfall, surface runoff, and water yield slightly increased with the increases of TDAs. It was concluded that the fine TDAs produced finer and higher ranges of snowmelt runoff volume across the watershed. All TDAs had similar capacities to replicate the observed tendency of monthly mean streamflow hydrograph, except overestimated/underestimated peak flows. Spatial variation of streamflow was well analyzed in the fine schemes with high density of stream networks, while the coarse schemes simplified this. Watershed subdivisions affected model performances, in the way of decreasing the accuracy of monthly streamflow simulation, at 60% of investigated hydro-gauging stations (3/5 stations) and in the upstream. Furthermore, watershed subdivisions strongly affected the calibration process regarding the changes in sensitivity ranking of 18 calibrated model parameters and time it took to calibrate.

Key words: Arctic watershed Målselv, hydrological simulations, snowmelt runoff, SWAT, threshold drainage area (TDA), watershed subdivisions

HIGHLIGHTS

- The annual mean PET, ET, and lateral flow slightly decreased, while rainfall, surface runoff and water yield slightly increased with the increase of TDAs.
- The fine TDAs produced finer and higher ranges of snowmelt runoff volume across the watershed.
- All TDAs had similar capacities to replicate the observed tendency of monthly mean streamflow hydrograph, except overestimated/underestimated peak flows.
- Spatial variation of streamflow was well analysed in the fine schemes compared to the coarse ones.
- The scales of watershed subdivisions affected model performances, and sensitivity ranking of 18 calibrated model parameters in five hydrological subgroup processes (e.g. surface runoff, lateral flow, snowmelt, channel water routing, and groundwater) and time taking for calibration.

INTRODUCTION

The semi-distributed model SWAT (Soil And Water Assessment Tool) (Neitsch *et al.* 2009) was developed to predict the impacts of human activities (Gassman *et al.* 2007) and climate change (Dile *et al.* 2013) on environment and water resources in large complex watersheds. Lumped models consider the entire watershed/basin as a single system (Devi *et al.* 2015); on the other hand, the semi-distributed models like SWAT divide the whole watershed/basin into smaller sub-watersheds/sub-basins (Daofeng *et al.* 2004; Dwarakish & Ganasri 2015). It is assumed that each sub-basin is a homogeneous unit with representative parameters for the entire sub-basin (Bingner *et al.* 1997). Choosing the size for the sub-basins also influences the

This is an Open Access article distributed under the terms of the Creative Commons Attribution Licence (CC BY 4.0), which permits copying, adaptation and redistribution, provided the original work is properly cited (<http://creativecommons.org/licenses/by/4.0/>).

homogeneous assumption because the larger the sizes of the sub-basins, the higher variable conditions the sub-basins have (Bingner *et al.* 1997). When the sizes of sub-basins are reduced and the number of sub-basins are increased, it significantly influences the amounts of required input data and model parameters, the computational process (Bingner *et al.* 1997), as well as the calibration effort since the large number of sub-basins may require more adjusted model parameters needed to optimize the simulation results and more iterations needed for running the calibration (Rouhani *et al.* 2009).

Watershed delineation is considered as an important preliminary step since the accuracies of the modeling results, e.g., runoff (Rouhani *et al.* 2009; Gong *et al.* 2010; Chaplot 2014), streamflow (Norris & Haan 1993; Rouhani *et al.* 2009), and soil erosion and pollution (Gong *et al.* 2010) may be influenced by the delineation resolutions, beside the quality of input data (Chaplot *et al.* 2005; Ning *et al.* 2015; Nazari-Sharabian *et al.* 2020). For example, the accuracy of runoff simulation results decreases at the coarse levels of watershed discretization due to the effects of the changes in the distribution of runoff curve numbers over the entire watershed, particularly in the SWAT model (Rouhani *et al.* 2009). Increasing or decreasing numbers of sub-watersheds also influences the accuracy of simulation of peak flows or extreme flows (Rouhani *et al.* 2009). In particular, the deviation between observed and simulated peak flows/extreme flows increases when the number of sub-watershed increases. This is because higher numbers of sub-watersheds lead to higher variation of the runoff values that contribute to streamflow. In addition, the values of runoff curve numbers are automatically updated according to the variation of soil moisture condition in each sub-watershed. Therefore, when the runoff curve numbers have high fluctuation, then the values of runoff contributing to streamflow also highly fluctuate. As a result, the accuracy of simulated peak flows/extreme flows is influenced (Rouhani *et al.* 2009). Moreover, delay in the travel time of runoff occurring in the watersheds with large numbers of sub-watersheds may result in lower values of simulated peak flows compared to that with small numbers of sub-watersheds. The reason is because runoff from the upper sub-watersheds could reach to the outlet of the watershed only after runoff from the lower sub-watersheds has been already discharged (Rouhani *et al.* 2009). Furthermore, increasing the number of sub-watersheds leads to increasing channel slope and drainage density that result in higher simulation results of some water balance components (Chen *et al.* 2021). Also, the change in drainage density also influences the accuracy of runoff prediction (Goodrich 1992). Finally, the automated computational processes of morphological and hydrological parameters of the watershed are strongly influenced by the chosen numbers and sizes of sub-watersheds (Munoth & Goyal 2019b).

The most natural subdivision method is dividing a watershed into its natural sub-watersheds based on topography data, which are extracted from a digital elevation model (DEM). Such watershed subdivision also aims to preserve the watershed's natural boundaries, flowpaths, as well as channels for realistic flow routing (Zhang *et al.* 2004). With the development of GIS (geographic information system) technologies, several watershed subdivision approaches have been developed to investigate the impacts of watershed subdivision on modeling outputs (Savvidou *et al.* 2014), including (1) critical source area (CSA) (Thieken *et al.* 1999; FitzHugh & Mackay 2000; Kalin *et al.* 2003; Di Luzio & Arnold 2004; Arabi *et al.* 2006); (2) threshold drainage area (TDA) (Nour *et al.* 2008); (3) aggregated simulation area (Lacroix 1999); (4) representative elementary areas (Wood *et al.* 1988); (5) representative elementary watershed (Reggiani & Rientjes 2005); (6) hydrologic similar units (Karvonen *et al.* 1999); (7) functional units (Argent *et al.* 2006); and (8) hydrologic response units (HRUs) (Flugel 1995, 1997). In the SWAT model, watershed subdivision is basically based on the TDA, which is the minimum upstream drainage area for a channel to originate (Aouissi *et al.* 2013), or as a percentage of total catchment area (Di Luzio & Arnold 2004; Kumar & Merwade 2009). Each sub-basin in SWAT is further subdivided into smaller HRUs.

Many previous studies around the world applied the SWAT model to investigate the impacts of watershed subdivision on the results of hydrological simulations, including runoff (Norris & Haan 1993; Bingner *et al.* 1997; Jha *et al.* 2004; Arabi *et al.* 2006; Rouhani *et al.* 2009; Chaplot 2014; Munoth & Goyal 2019a), water balance components (Tripathi *et al.* 2006; Chaplot 2014; Chen *et al.* 2021), and streamflow (Mamillapalli *et al.* 1996; FitzHugh & Mackay 2000; Haverkamp *et al.* 2002; Jha *et al.* 2004; Muleta *et al.* 2007; Rouhani *et al.* 2009; Aouissi *et al.* 2013, 2018; Chiang & Yuan 2015; Ozdemir *et al.* 2017; Pignotti *et al.* 2017; Chen *et al.* 2021). Regarding the studies on runoff, there was inconsistency among previous findings. For example, in a study in the 21.3-km² Goodwin Creek Watershed, in northern Mississippi, USA, it was found that values of runoff volume generated from 10 different levels of watershed subdivision based on different values of the CSA were not significantly impacted by the chosen number and size of sub-watersheds (Bingner *et al.* 1997). For example, the simulation of total annual runoff volume varied less than 5% among 10 watershed subdivision schemes (Bingner *et al.* 1997). In contrast, little variation in the total simulated surface runoff among 12 sub-watershed delineation schemes was detected in a study in four Iowa watersheds, USA, with the areas varying from 2,000 to 18,000 km² (Jha *et al.* 2004). However, the variation in the total simulated surface runoff was not clearly quantitative in such a study (Jha *et al.* 2004). Also, changes

in runoff simulation were found in a study in the 384-km² Grote Nete River catchment, in Flanders, Belgium (Rouhani *et al.* 2009). They pointed out that the larger number of sub-watersheds in the watershed delineation schemes resulted in higher variation of runoff that led to higher fluctuation in the values of simulated extreme flows (Rouhani *et al.* 2009). Nevertheless, the deviation of simulated peak flow among watershed delineation schemes was not clearly quantified (Rouhani *et al.* 2009). Another study in the 65,145-km² Tapi River, in India, concluded that surface runoff decreased (approximately 35%) when TDA increased (from 25 to 400 km²) (Munoth & Goyal 2019a). In contrast, a study in a 26.12-km² flat watershed, the Walnut Creek watershed, in central Iowa, USA, found that surface runoff increased (approximately 15%) when TDA increased (from 23 to 654 ha) (Chaplot 2014). However, the larger relative errors, between observed and simulated results, were also detected for the coarse watershed subdivision schemes with higher TDA values (Chaplot 2014). For example, the relative error for estimated runoff from TDA 654 ha was approximately 15%, while it was 0% from TDA 23 ha or approximately 8% from TDA 100 ha (Chaplot 2014). Therefore, it was learned from that study that using the coarse watershed subdivision schemes could produce higher values of surface runoff volume, but at the same time, the simulated results were more uncertain compared to those by using the fine schemes.

Similar to the studies in runoff, the changes in the results of streamflow simulations under different watershed delineation schemes were also inconsistent among previous studies. For example, it was found in a study in the four Iowa watersheds, USA, that streamflow components were increased only less than 7% when the number of sub-watersheds increased (from 5 to 53) for a 1,929-km² watershed, which indicated quite insensitive streamflow to the number of sub-watersheds (Jha *et al.* 2004). In other studies, the changes in watershed subdivision schemes had slight impacts on the results of streamflow simulation (FitzHugh & Mackay 2000; Aouissi *et al.* 2013; Chiang & Yuan 2015). For example, the simulated annual and monthly streamflow, in a 62-km² Pheasant Branch watershed, Dane County, Wisconsin, USA, slightly increased (approximately 12%) from the coarse schemes to the fine schemes (FitzHugh & Mackay 2000). In a study in the 418-km² Joumine watershed, northern Tunisia, the simulated annual and monthly streamflow were only few percentage of variation among watershed delineation schemes (Aouissi *et al.* 2013). In a study in the large-scale watershed, the Kaskaskia River watershed in Illinois, USA, with 11,350 km², the simulated average annual streamflow increased by less than 2% from the finest scheme to the coarsest scheme (Chiang & Yuan 2015). However, a study in a small-scale watershed, the 26.12-km² Walnut Creek watershed, in central Iowa, USA, found significant increase of mean streamflow (approximately 62%) when TDA increased from 23 to 654 ha (Chaplot 2014). However, that study also pointed out that simulation of streamflow by using the coarse watershed subdivision solution produced higher uncertain results than by using the finer watershed subdivision solution (Chaplot 2014). For example, the relative error between observed data and simulated results of mean streamflow was 163% for TDA 654 ha, while it was less than 6% for TDAs 23, 100, and 261 ha (Chaplot 2014). Another study in the 4,297-km² Bosque River watershed, Texas, USA, found the positive effects of changes in watershed subdivision schemes on the accuracy of streamflow prediction (Mamillapalli *et al.* 1996). Such study revealed that the accuracy of streamflow prediction was improved by increasing the number of sub-watersheds and/or the number of HURs (Mamillapalli *et al.* 1996). This finding was also similar to findings from other studies in the Weiherbach (6.3 km²) and Dietzhoelze (81.7 km²) watersheds, Germany, and the Bosque River watershed (4,297 km²) in Texas, USA (Haverkamp *et al.* 2002; Muleta *et al.* 2007). In contrast, the accuracy of peak flow prediction was concluded to be decreased (approximately 20%) when numbers of sub-watersheds increased in a study in the 384-km² Grote Nete River catchment, in Flanders, Belgium (Rouhani *et al.* 2009). Recently, a study in the 491,700-km² Upper Mississippi River Basin, USA, found that the fine schemes of watershed delineation (12-digit sub-basin scenario) yielded higher values of streamflow simulation (approximately 1.79–7.17%) compared to the coarser schemes (8-digit sub-basin scenario), since the fine schemes are able to capture a sophisticated level of the spatial variation of watershed features including variation of rainfall regime (Chen *et al.* 2021). This finding agreed with the finding of a previous study in the 152.29-km² Little Washita watershed, near Chickasha, Oklahoma, USA, since they pointed out that the number of sub-watersheds strongly impacted the simulated streamflow hydrograph (Norris & Haan 1993). In particular, the estimated peak flow increased approximately 30% when the number of sub-watersheds increased from 1 and 2 sub-watersheds up to 15 sub-watersheds (Norris & Haan 1993).

Regarding studying water balance components, a previous study in the 90.23-km² Nagwan watershed in India revealed that the size and number of sub-watersheds had significant impacts on the simulation results of evapotranspiration (ET), percolation, and soil water (SW) content, with the exception of surface runoff (Tripathi *et al.* 2006). For example, increasing the number of sub-watersheds (from a single watershed to the discretization of 12 and 22 sub-watersheds) resulted in increasing approximately 0.28–61.4% ET, 4.48–26.7% percolation, and 17.7–22.3% SW content (Tripathi *et al.* 2006). A study in a

26.12-km² flat watershed, the Walnut Creek watershed, in central Iowa, USA, found that decreasing sizes of sub-watersheds (from 654 ha down to 23 ha) or increasing numbers of sub-watersheds (from 1–4 to 96–115) resulted in increased ET (4.6%), decreased SW (5.1%), decreased percolation (2.8%), decreased surface runoff (15.1%), and decreased groundwater (2.4%) (Chaplot 2014). In this case, the trends of changes were not consistent for every water balance component, particularly in ET (Chaplot 2014). Another study in the 4,91,700-km² Upper Mississippi River Basin, USA, found that the simulation results of surface runoff, lateral flow, groundwater flow, and water yield (WYLD) increased approximately 0.98, 92, 2.73, and 2.07%, respectively, when the number of sub-watersheds and HRUs increased (Chen *et al.* 2021).

However, the fine watershed delineation does not always yield higher model performances compared to the coarse schemes (Boyle *et al.* 2001; Reed *et al.* 2004; Rouhani *et al.* 2009). For example, some previous studies stated that the modeling results are better when using the semi-lumped and semi-distributed model structures compared to those using the distributed models (Ogden & Julien 1994; Smith *et al.* 2004; Das *et al.* 2008). The reason is that the capacities to capture the important features of the watersheds and variation of rainfall regime of the coarse watershed delineation are better than those of the fine one. This argument is somewhat against the argument in the study in the Upper Mississippi River Basin, USA (Chen *et al.* 2021).

In another method of assessment, a study in two small-scale watersheds, the Dreisbach (6,23 km²) and the Smith Fry (7,30 km²) watersheds, in Maumee River Basin, Allen County, Indiana, USA, demonstrated the importance of manner of watershed subdivision on the efficiency of different best management practices (BMPs) for controlling the fate and transport of nutrients (e.g., total nitrogen and total phosphorus) and sediment within the watersheds (Arabi *et al.* 2006). Herein, nutrients and sediments are transported into the channels by surface runoff and lateral subsurface flow (Arabi *et al.* 2006). Therefore, the changes in these water balance components because of different watershed subdivision solutions could potentially affect the estimation of nutrient and sediment outputs. Besides that, the study found that watershed subdivisions caused discrepancies in watershed characteristics, e.g., drainage density, channel networks which affected nutrient and sediment yields (Arabi *et al.* 2006). In particular, it was expected from the study that more studies in future should be focused on the larger watersheds to verify the impacts of watershed subdivision scales on BMPs of the watersheds, since the larger watersheds may reveal different trends of changes compared to the smaller watersheds (Arabi *et al.* 2006). Also, it was highly expected from the study that the impacts of watershed subdivision should deserve more attention in future than those carried out in the past because of uncertainties resulting from different spatial resolutions (Arabi *et al.* 2006).

Beside the impacts of watershed delineation, density and spatial distribution of weather data input are also the important factors that may affect the modeling results (Chaubey *et al.* 1999; Bardossy & Das 2008; Aouissi *et al.* 2013, 2018; Chaplot 2014; Chen *et al.* 2021). For example, the high uncertainty in the estimated model parameters in the hydrological models results from using spatial homogeneity of rainfall and does not consider the refined variation of rainfall input (Chaubey *et al.* 1999). In addition, the performances of the hydrological models significantly decline when the density of integrated rain gauges is reduced (Bardossy & Das 2008). Also, the accuracy of streamflow simulation is significantly impacted by the spatial distribution of rain-gauge networks (Aouissi *et al.* 2013, 2018). It was found from a study in the 26.12-km² Walnut Creek watershed, in central Iowa, USA, that spatial resolution of rain-gauge networks significantly impacted water balance components in different manners (Chaplot 2014). For example, when increasing the number of rain gauges from 1 to 13, ET decreased approximately 17.7%, SW content increased approximately 41.3%, percolation increased approximately 66.67%, surface runoff decreased approximately 40.9%, and groundwater decreased approximately 42.1% (Chaplot 2014). Furthermore, it was learned from a study in the 491,700-km² Upper Mississippi River Basin, USA, that higher values of streamflow prediction were yielded from the denser weather networks compared to those from the scatter networks (Chen *et al.* 2021). For example, the simulated average monthly streamflow increased approximately 6.30–8.32% by using the denser climate dataset compared to using the sparser dataset in a large-scale watershed (Chen *et al.* 2021). However, the influences of weather networks density on hydrological simulations might vary from region to region and might depend upon the environmental characteristics or conditions of the investigated watersheds, where the differences in rainfall types (e.g., convective or advective), rainfall seasonality, the importance of snow accumulation and snowmelt processes, topographic features, and land use are identified (Bardossy & Das 2008; Chaplot 2014). The regions with complex hydrological processes might require high density of rain-gauge networks (Bardossy & Das 2008). Therefore, more studies are necessary to verify the effects of density and spatial distribution of weather data on hydrological simulations.

Obviously, the impacts of watershed subdivision and spatial resolution of weather networks on hydrological simulations were significantly investigated in numerous regions around the world, where there are differences in climate conditions,

topography, land-use, and hydrological regimes. This contributed valuable knowledge for the scientific community; however, a consensus has not yet been obtained among outcomes under different environmental conditions (Mulungu & Munishi 2007; Chaplot 2014). For example, using the fine watershed delineation schemes could result in both positive and negative effects on the accuracy of hydrological simulations compared to those by using the coarse schemes. Similarly, the impacts of weather network density on hydrological simulations also varied regionally and could depend upon different environmental characteristics or conditions (Mulungu & Munishi 2007; Chaplot 2014). Therefore, the consequences of watershed subdivision and spatial density of weather networks on hydrological simulations are still a controversial issue. In addition, most of the previous studies were conducted in tropical/sub-tropical or temperate climate zones. However, studies in the Arctic region, with complex hydrological processes and sparse weather data, are still limited. Moreover, snowmelt runoff is an important component in the Arctic hydrology, since it contributes approximately 75% of the total annual flow in many Arctic watersheds (Woo 1980). Nevertheless, studies on the effects of watershed subdivision and weather network density on snowmelt runoff have not been addressed in previous studies. Also, many studies assessed the changes in streamflow, because of watershed subdivisions, mostly at the basin outlet or at certain hydro-gauging stations. However, the spatial variation of streamflow in each sub-basin, which is important for the case of flood hotspots analysis because of watershed delineation solutions, has not been well investigated. Therefore, to fill the existing knowledge gaps as well as to satisfy the expectation of previous studies, this paper conducted a study in the Arctic conditions to investigate the combined effects of watershed subdivision scale and weather network density on the results of hydrological simulations. In particular, outcomes of the present study aim to answer the following pertinent questions:

1. How much discrepancies in watershed characteristics and land-use composition could change?
2. How much model performance (in terms of statistical indicators) could be influenced?
3. How much snowmelt runoff volume and water balance components could vary spatially across the watershed?
4. How much streamflow could vary in temporal-spatial patterns across the watershed?
5. How much the sensitivity of model parameters under the Arctic conditions could be influenced?

STUDY AREA

Målselv watershed in northern Norway, distributing from 68°21'N to 69°17'N, was selected as the study area (Figure 1). This is a large-scale watershed with an area of approximately 5,913 km². Målselv has the features of mountainous terrain with the ground surface elevation ranges from 0 to 1,718 m. This area is located in the cold climate zone with the average annual air temperature varying from -5 to 6 °C. Rainfall regime is also highly variant across the watershed. The long-term average annual rainfall in this area fluctuates from ~500 to 1,500 mm.

MATERIALS AND METHODS

SWAT model

The physically based, semi-distributed SWAT model (Neitsch *et al.* 2009) was used. The SWAT includes two important phases in its structure such as land phase and routing phase (Du *et al.* 2013) to describe the water cycle in the watershed. The land phase works based on a water balance equation as follows:

$$SW_t = SW_0 + \sum_{i=1}^t (R_i - Q_i - E_i - P_i - QR_i) \quad (1)$$

where SW_t is the SW content at time t (mm), SW_0 is the initial SW content (mm), R_i is the amount of precipitation on day i (mm), Q_i is the amount of surface runoff on day i (mm), E_i is the amount of ET on day i (mm), P_i is the amount of percolation on day i (mm), and QR_i is the amount of return flow on day i (mm).

The routing phase describes several processes occurring in the stream including movement of water, sediments, flow mass in the channel, and transformation of chemicals in the stream and streambed.

The QSWAT interface, version 1.9, was used in this study. This is a coupling product of the hydrological model SWAT version 2012 and the open-source QGIS version 2.6.1.

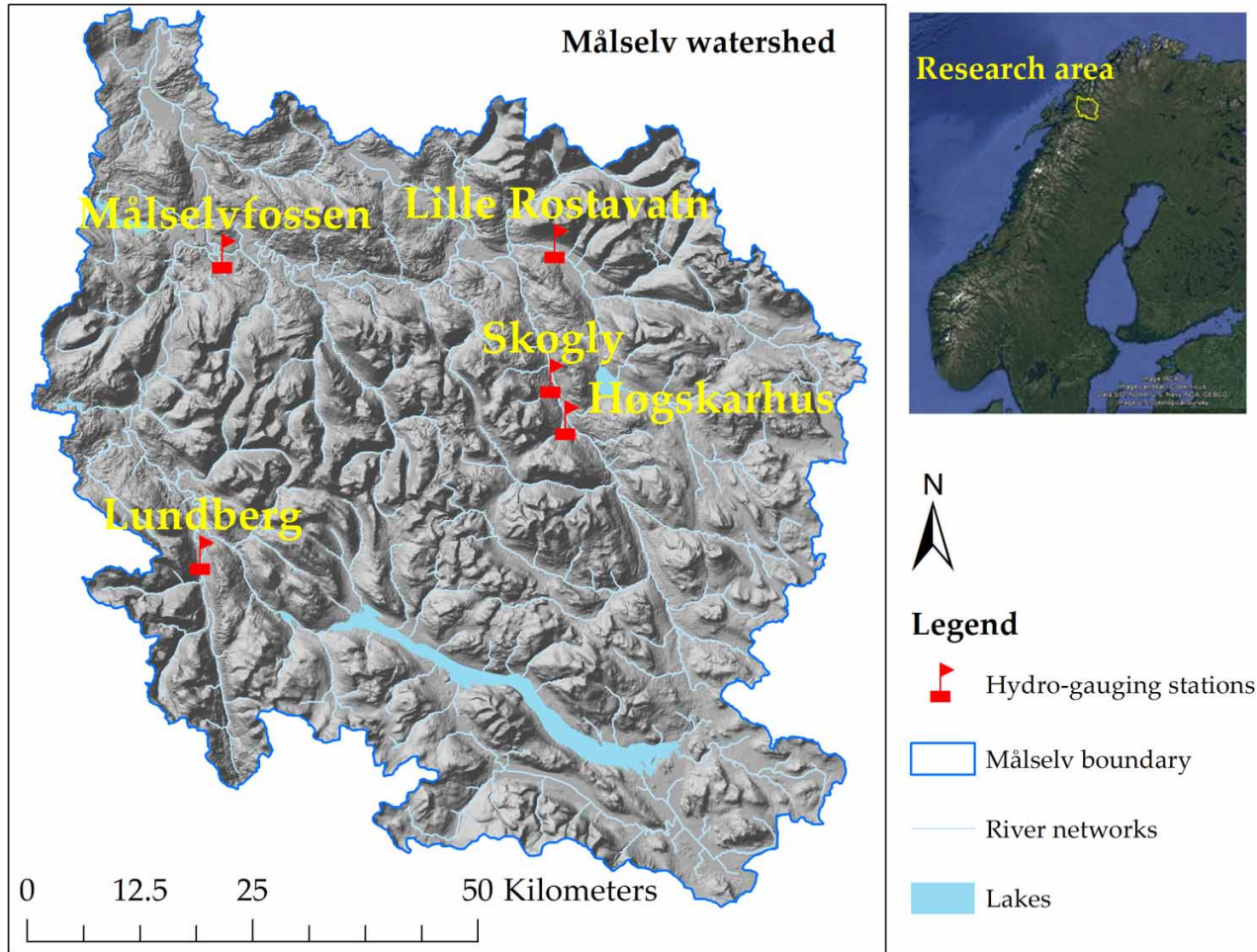


Figure 1 | Map of study area: Målselv watershed.

Data acquisition

In order to run the SWAT model, several temporal-spatial input data including time series of climate data such as precipitation, maximum and minimum air temperature, wind speed, relative humidity, solar radiation, and spatial (grid) data such as land use, soil, and topography (e.g., DEM) were required. In addition, time series of river discharge were needed for model calibration and validation. These data were collected from several sources. Details of data types, data resolution, and sources of data are summarized in [Table 1](#).

Methods for development of the TDA schemes

The technique of watershed subdivisions in the SWAT model is based on the values of the TDA. Four different TDA schemes, using TDA values of 200, 2,000, 5,000, and 10,000 ha, were developed in this study.

Table 1 | Summary of data inputs and their sources using the SWAT model

Data type		Resolution	Sources
Spatial data (grid)	DEM	10 × 10 m	Geonorge (2013)
	Land use	~600 m	Waterbase (2007a)
	Soil	~5,000 m	Waterbase (2007b)
Temporal data (time series)	Climate data: climate forecast system reanalysis	~38 km grid	TAMU (2012)
	River discharge	Five stations	Sildre (2020)

Methods for HRU creation

Watershed subdivision and HRU creation were performed for each option of TDA values. Multiple HRUs were generated for each sub-basin, from the inputs of land use, soil, and slope classes, based on an HRU threshold (Figure 2). This threshold considers the percentage of the representative land use/soil/slope for each sub-basin. The HRU thresholds from 5 to 15% were widely used in many studies (Sexton *et al.* 2010; Srinivasan *et al.* 2010; Han *et al.* 2012; EPA 2013). In this study, the designed HRU thresholds for land use, soil, and slope were 5% for each. According to this threshold, only types of land use, soil, and slope, which are higher than 5% of the sub-basin area, were considered. In addition, the terrain slope was classified into five classes such as 0–5, 5–10, 10–25, 25–30, and >30%.

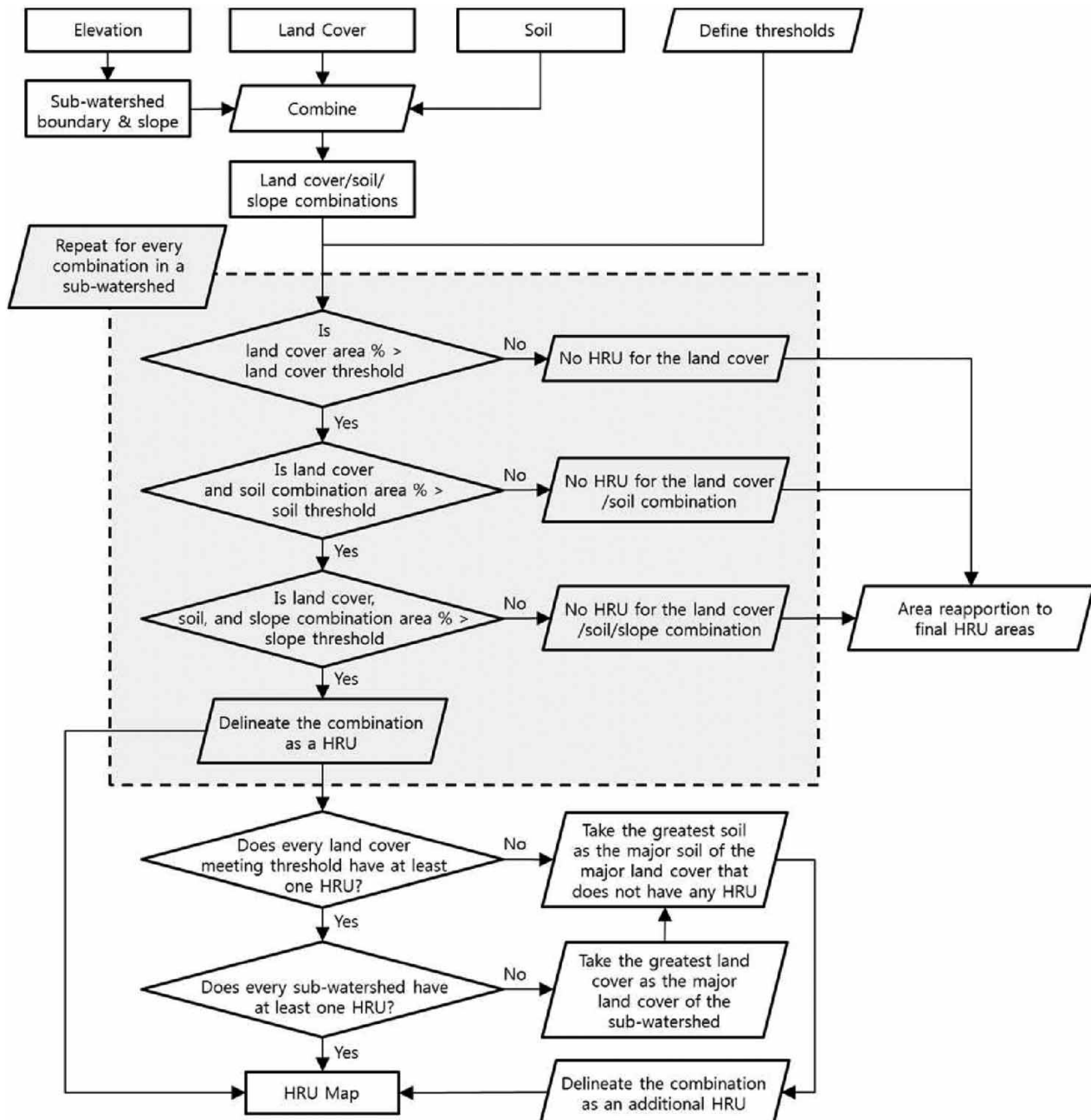


Figure 2 | The algorithm for HRU definition in SWAT (Her *et al.* 2015).

Model running, calibration, validation, sensitivity, and uncertainty analysis

For each level of watershed subdivision, the model ran on a monthly time step from 1995 to 2012, including a 3-year warming up period (1995–1997). The 10-year period, from 1998 to 2007, was used for model calibration, and the remaining 5 years, from 2008 to 2012, were used for model validation.

The Sequential Uncertainty Fitting Version 2 (SUFI-2) algorithm in the SWAT Calibration Uncertainties Program (SWAT_CUP) (Abbaspour *et al.* 2007) was used for model calibration, model validation, parameters sensitivity, and uncertainty analyses. Each SWAT model corresponding to each watershed subdivision scheme was calibrated separately. A total of 18 model parameters, which were recommended as the most sensitive parameters for streamflow calibration (Abbaspour *et al.* 2007, 2015), were used in calibration and validation processes. Those model parameters are classified into five different subgroup processes of hydrological cycle, including (1) surface runoff (e.g., CN2.mgt and CANMX.hru); (2) lateral flow (e.g., ESCO.hru, SOL_AWC.sol, SOL_BD.sol, and SOL_K.sol); (3) snowmelt (e.g., SMTMP.bsn, Timp.bsn, SMFMN.bsn, SMFMX.bsn, and SFTMP.bsn); (4) channel water routing (e.g., CH_K2.rte and CH_N2.rte); and (5) ground-water (e.g., ALPHA_BF.gw, GW_REVAP.gw, GWQMN.gw, REVAPMN.gw, and GW_DELAY.gw). The finest scheme used a total of 2,500 simulations to detect the optimal model parameters, while each of the other coarser schemes used a total of 2,000 simulations. In addition, cross-validation was approached to test whether or not the calibrated model parameters achieved from the finest watershed subdivision scheme could also perform well in other coarser schemes. All the possible results, which are found during the calibration process, are distributed in the so-called 95PPU band. The two statistical indicators, such as P-factor and R-factor, were used to measure the uncertainty of the calibration results. Herein, the values of P-factor range from 0 to 1, of which a threshold of 0.7 or 0.75 is suggested for river discharge calibration. The optimal values of R-factor, which presents the thickness of the 95PPU band, should be close to zero. For river discharge calibration, the value of R-factor is suggested to be smaller than 1.5. When the thickness of the 95PPU band is large, it means that the possibility of the model to capture most of the observed data is high; however, the model uncertainty is also high.

Global sensitivity analysis in the SUFI-2 algorithm was approached to detect the most sensitive model parameters used for calibration. The concept of global sensitivity analysis is to estimate the average changes of the objective function as the results of the changes of each parameter, whereas all other parameters are changing (Abbaspour 2015). In particular, the parameter sensitivities are determined based on the multiple regression formula as follows:

$$g = \alpha + \sum_{i=1}^m \beta_i b_i \quad (2)$$

where g is the objective function for calibration, α is the regression constant, β_i is the regression coefficient of calibrated parameter, and b_i is the calibrated parameter.

To identify whether or not a parameter b_i is significant in sensitivity analysis, a t -test was used. This method uses two indicators, namely p -value and t -stat, to measure and rank the sensitive level of each calibrated model parameter. The hypothesis of the t -test method is that the larger the absolute values of t -stat, and the smaller the p -values, the more sensitive the parameters are determined. In addition, a parameter is considered significant in sensitivity analysis if the p -value calculated for that parameter is smaller than a value of 0.05. Finally, all calibrated model parameters are ranked for their sensitivity levels according to the magnitudes of t -stat and p -value.

Evaluation of model performance

The three statistical coefficients were used to measure the good fit between the simulation and observation, including (1) the coefficient of determination – R^2 (Equation (3)), measuring the fitness of the relationship between the simulated and observed values; (2) the Nash–Sutcliffe coefficient of efficiency – NSE (Equation (4)); and (3) root-mean-square error, divided by the standard deviation – RSR (Equation (5)).

$$R^2 = 1 - \frac{\sum_{i=1}^n (Y_i^{\text{obs}} - Y_{\text{mean}}^{\text{obs}})(Y_i^{\text{sim}} - Y_{\text{mean}}^{\text{sim}})}{\left[\sum_{i=1}^n (Y_i^{\text{obs}} - Y_{\text{mean}}^{\text{obs}})^2 \right]^{\frac{1}{2}} \left[\sum_{i=1}^n (Y_i^{\text{sim}} - Y_{\text{mean}}^{\text{sim}})^2 \right]^{\frac{1}{2}}}, \quad (3)$$

$$\text{NSE} = 1 - \frac{\sum_{i=1}^n (Y_i^{\text{obs}} - Y_i^{\text{sim}})^2}{\sum_{i=1}^n (Y_i^{\text{obs}} - Y_{\text{mean}}^{\text{obs}})^2}, \quad (4)$$

$$\text{RSR} = \frac{\left[\sum_{i=1}^n (Y_i^{\text{obs}} - Y_i^{\text{sim}})^2 \right]^{\frac{1}{2}}}{\left[\sum_{i=1}^n (Y_i^{\text{obs}} - Y_{\text{mean}}^{\text{obs}})^2 \right]^{\frac{1}{2}}}, \quad (5)$$

where Y_i^{obs} and Y_i^{sim} are the observed and simulated values at time i , $Y_{\text{mean}}^{\text{obs}}$ and $Y_{\text{mean}}^{\text{sim}}$ are the mean observed and simulated data for the entire evaluation period, and n is the total number of observations/simulations.

The threshold values of the statistical coefficient R^2 , NSE, and RSR for monthly simulation are shown in Table 2 (Santhi *et al.* 2001; Van Liew *et al.* 2003; Moriasi *et al.* 2007; Premanand *et al.* 2018).

Evaluation of the hydrological simulations

To investigate the effects of watershed subdivisions on the hydrological simulations, the present study focused on the evaluation of the simulation results of water balance components and streamflow. Regarding water balance components, the annual mean values of total areal rainfall (PCP), actual ET, surface runoff (SUR_Q), snowmelt runoff, lateral runoff (LAT_Q), groundwater recharge amount (PERCO), groundwater contribution to streamflow (GW_Q), and WYLD (YIELD = SUR_Q + LAT_Q + GW_Q - Transmission losses) contributing to streamflow were calculated. In addition, to compare the spatial variation of such water balance components across the entire watershed among different TDA schemes, the GIS maps were produced. Furthermore, the long-term monthly average streamflow at five different hydro-gauging stations was analyzed. Also, the GIS maps of the spatial variation of the long-term annual mean streamflow were produced. The ArcGIS software version 10.6.1 was used in this study for generating the GIS maps and for spatial analysis. The results are discussed in the following section.

RESULTS AND DISCUSSION

Discrepancies in watershed characteristics and land-use composition resulting from different TDA schemes

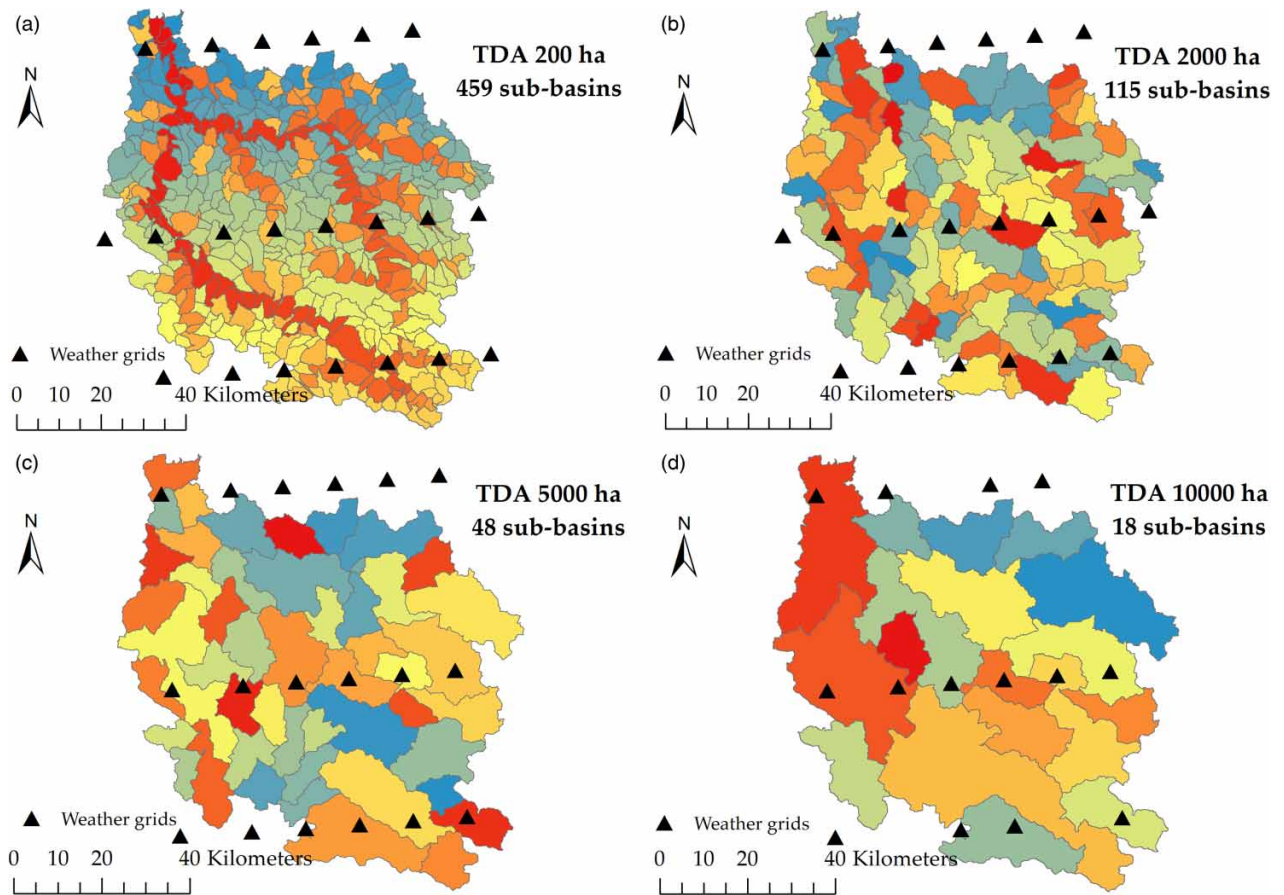
The methods of watershed delineation have significant impacts on the levels of terrain complexity as well as the topographic attributes. The number of sub-basins declined 75, 90, and 96% in the coarse TDAs 2,000 ha (115 sub-basins), 5,000 ha (48 sub-basins), and 10,000 ha (18 sub-basins), respectively, compared to the finest TDA 200 ha (459 sub-basins) (Table 3; Figure 3). When numbers of sub-basins increase and the sub-basin sizes decrease, the accurate level of the representative land uses for the watershed will be high. For example, the TDAs 200 ha (with 459 sub-basins) and 2,000 ha (with 115 sub-basins) presented a total of 11 main land-use groups for the entire watershed, while other coarser schemes such as TDAs 5,000 and 10,000 ha lost two and four land-use groups, respectively. In addition, the areas of each land-use group varied as the number of sub-basins declined, of which some land-use groups decreased in their areas while others increased, but the magnitudes of decreasing were greater than those of increasing (Table 4). For example, land-use groups of barren or sparsely vegetated, mixed forest, grassland, shrubland, bare ground tundra, water, and wooded wetland had declining trends, whereas the remainder had slight increasing trends. In particular, under TDA scheme 2,000 ha, the area of wooded wetland decreased approximately 70% compared to the finest scheme 200 ha, and this was the highest ratio among the decreased land-use

Table 2 | Thresholds of R^2 , NSE, and RSR for evaluation of the hydrological model's performance

Model performance	R^2	NSE	RSR
Very good	$0.70 \leq R^2 \leq 1.00$	$0.75 < \text{NSE} \leq 1.00$	$0.00 \leq \text{RSR} \leq 0.50$
Good	$0.60 \leq R^2 < 0.70$	$0.65 < \text{NSE} \leq 0.75$	$0.50 < \text{RSR} \leq 0.60$
Satisfactory	$0.50 \leq R^2 < 0.60$	$0.50 < \text{NSE} \leq 0.65$	$0.60 < \text{RSR} \leq 0.70$
Unsatisfactory	$R^2 < 0.50$	$\text{NSE} \leq 0.50$	$\text{RSR} > 0.70$

Table 3 | Summary of watershed and sub-watershed features under different TDA schemes

	TDA 200 ha	TDA 2,000 ha	TDA 5,000 ha	TDA 10,000 ha
Number of sub-basins	459	115	48	18
Number of HRUs	5,601	2,102	1,098	518
Total drainage area (km ²)	5,815.44	5,805.54	5,805.54	5,805.54
Maximum sub-basin area (km ²)	70.75	166.68	345.26	881.19
Minimum sub-basin area (km ²)	2.05	20.04	52.53	116.68
Average sub-basin area (km ²)	12.67	50.48	120.95	322.53
Average sub-basin elevation (m)	637.81	664	629.66	671.69
Average overland sub-basin slope (%)	25.95	24.05	23.85	25.18
Total stream length (km)	1,921.76	1,014.65	688.19	487.97
Average stream slope (%)	7.32	2.35	1.46	1.22
Levels of stream order	5.00	4.00	4.00	3.00
Drainage density (km km ⁻²)	0.33	0.17	0.12	0.08
Number of weather grid points integration	21	20	18	14

**Figure 3** | Number of sub-watersheds generated by four different TDA schemes.

groups. Regarding TDA scheme 5,000 ha, the highest percentage of decreasing area (approximately 75%) was in the group of barren or sparsely vegetated. For the coarsest scheme 10,000 ha, mixed forest had the highest percentage of declined area with approximately 55%. Noticeably, two land-use groups, evergreen needleleaf forest and wooded wetland, disappeared

Table 4 | Changes of land use and HRUs (in ha and in %) under four different TDA schemes

Landuse code	Name	Area								% change compared to the finest TDA 200ha					
		Original (ha)	%	TDA 200ha (ha)	%	TDA 2,000ha (ha)	%	TDA 5,000ha (ha)	%	TDA 10,000ha (ha)	%	TDA 200ha	TDA 2,000ha	TDA 5,000ha	TDA 10,000ha
BSVG	Barren or sparsely vegetated	3,287	0.56	3,194	0.55	2,360	0.41	806	0.14	0.00	-	-26.12	-74.78	-100	
FODB	Deciduous broadleaf forest	130,406	22.05	129,336	22.24	131,648	22.68	130,604	22.50	132,182	22.77	-	1.79	0.98	2.20
FOEN	Evergreen needleleaf forest	723	0.12	514	0.09	535	0.09	0.00	0.00	-	4.03	-100	-100		
FOMI	Mixed forest	8,917	1.51	8,839	1.52	7,279	1.25	6,324	1.09	4,024	0.69	-	-17.64	-28.45	-54.47
GRAS	Grassland	32,417	5.48	31,232	5.37	28,570	4.92	28,453	4.90	21,997	3.79	-	-8.52	-8.90	-29.57
SHRB	Shrubland	51,261	8.67	50,004	8.60	48,567	8.37	48,697	8.39	49,204	8.48	-	-2.87	-2.61	-1.60
TUBG	Bare ground tundra	2,475	0.42	2,205	0.38	1,625	0.28	1,342	0.23	0.00	-	-26.31	-39.16	-100	
TUMI	Mixed tundra	144,020	24.36	141,146	24.27	142,793	24.60	146,306	25.20	149,767	25.80	-	1.17	3.66	6.11
TUWO	Wooded tundra	192,078	32.48	190,960	32.84	193,793	33.38	198,012	34.11	203,387	35.03	-	1.48	3.69	6.51
WATR	Water	24,434	4.13	23,344	4.01	23,155	3.99	20,009	3.45	19,994	3.44	-	-0.81	-14.29	-14.35
WEWO	Wooded wetland	1,275	0.22	771	0.13	228	0.04	0.00	0.00	-	-70.44	-100	-100		
Sum		591,294	100	581,544	100	580,554	100	580,554	100	580,554	100				
% change compared to TDA 200ha (total)				-		-0.17		-0.17		-0.17					

under TDA scheme 5,000 ha, while TDA scheme 10,000 ha lost four land-use groups, namely barren or sparsely vegetated, evergreen needleleaf forest, bare ground tundra, and wooded wetland. In contrast, other land-use groups including deciduous broadleaf forest, evergreen needleleaf forest (excluding TDA 5,000 ha and TDA 10,000 ha), mixed tundra, and wooded tundra slightly decreased in their areas compared to the finest scheme 200 ha. For land-use groups with increased areas, the highest percentage of increasing was only 6.5% and this was for the group of wooded tundra under TDA 10,000 ha. Obviously, land-use groups with small areas significantly decreased, even disappeared in the coarse schemes. This is because the threshold for the HRU definition in the present study was 5% for land-use/soil/slope. Therefore, the land uses with their areas smaller than 5% of the sub-basin areas were not defined, since they were regrouped into the major land-use groups. The decrease in the areas of the minor land-use groups in the coarse watershed subdivision schemes was also validated in some previous studies in the USA (Bingner *et al.* 1997; Chiang & Yuan 2015; Chen *et al.* 2021). Table 3 provides the summary of the discrepancies in watershed characteristics resulting from the changes in TDA schemes.

In addition to the changes in the presence of land uses over the watershed resulting from the changes (decreasing) in the number of sub-watersheds, other topographic attributes were also changed. For example, the increases of sub-basins' sizes resulted in the changes in the average elevation and average overland slope of the sub-basins, which may affect the surface runoff process (Table 3). The finest TDA 200 ha had the highest average sub-basin slope compared to other coarse schemes. Such an increase in the overland slope could result from a better representation of spatial variation of surface elevation by discretization to smaller sub-watershed. In addition, the finest TDA scheme generated denser stream networks. For example, the TDA 200 ha produced approximately 1,922 km total stream length with 5 levels of stream order, while other coarser schemes 2,000, 5,000 and 10,000 ha produced approximately 1,015 km stream length (-47%) with 4 levels of stream order, 688 km stream length (-64%) with 4 levels of stream order, and 488 km stream length (-75%) with 3 levels of stream order, respectively (Figure 4). The decrease in stream length could affect some important in-stream processes. However, generating more sub-channels may not be realistic, since the channels from a very detailed level of sub-watershed description may only represent the low-lying areas in nature but they may not be existing/real channels. Moreover, the average stream slope remarkably declined (approximately 68–83%) from the finest scheme to the coarsest scheme. Drainage density dropped from 0.33 km km⁻² (TDA 200 ha) to 0.17 km km⁻² (TDA 2,000 ha), 0.12 km km⁻² (TDA 5,000 ha), and 0.08 km km⁻² (TDA 10,000 ha). The decrease in drainage density of the coarse TDAs may affect the accuracy of runoff simulation. However, one of the advantages of using the coarse watershed subdivisions is requiring less inputs, computation time (e.g., for running the model, calibration, and validation), as well as computer resources (e.g., reducing storage space). For example, in this study, in order to run 500 simulations for one iteration in the calibration process, it took around 56 h for the TDA 200 ha, while it was only 19.1, 7, and 3.2 h for TDA 2,000, TDA 5,000, and TDA 10,000 ha, respectively. Therefore, using a lower number of sub-watersheds could benefit some users in the cases of limitations in time and the available

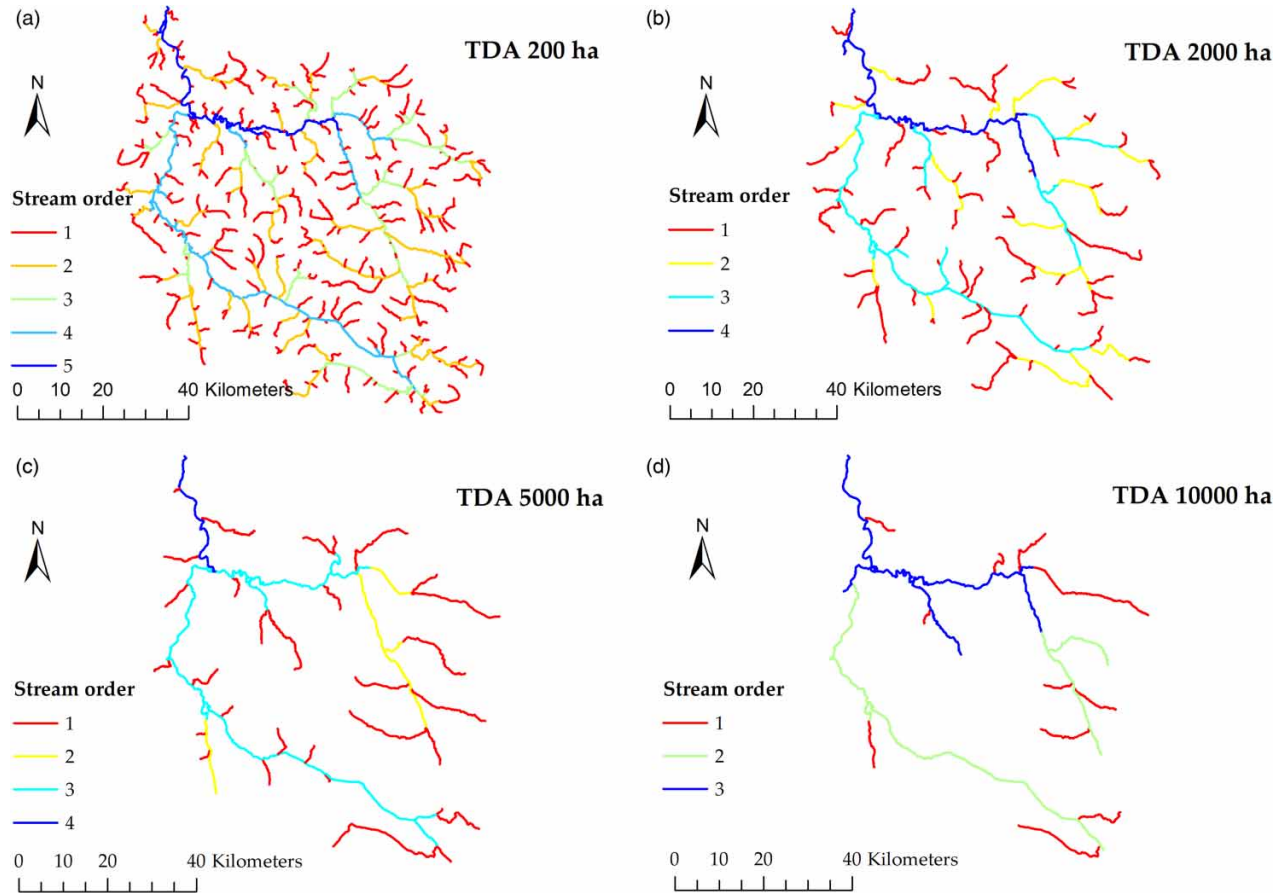


Figure 4 | Density and order of stream networks generated by four different TDA schemes.

resources. However, for the watersheds with high variation of land uses, it may require a detailed analysis of sub-watersheds for sophisticated description of the important features of the watersheds. The decreases in drainage density, total stream length, stream order level, average sub-watershed slope, and average stream slope in the coarse schemes compared to those in the fine schemes in the present study also agreed with findings from previous studies, but the level of declines depended upon the drainage area of the study area as well as the designed TDA values (Bingner *et al.* 1997; Jha *et al.* 2004; Chiang & Yuan 2015; Munoth & Goyal 2019a; Chen *et al.* 2021).

The influences of watershed subdivisions on model performance in terms of statistical indicators

During the calibration period, at Lille Rostavatn and Målselvossen hydro-gauging stations, model performances were relatively stable under the changes of number of sub-watersheds. Although the number of integrated weather grids decreased due to the decrease of numbers of sub-watersheds, the selected weather grid points may be the correct representatives for the watershed as well as for the sub-watersheds surrounding these two hydro-gauging stations. The negligible impact of watershed subdivision on model performance was also validated in previous studies (Aouissi *et al.* 2013, 2018). In contrast, model performances at three remaining stations fluctuated under different watershed subdivisions. For example, at Høgskarhus station, model performance increased from TDAs 200 to 2,000 ha, then slightly decreased when numbers of sub-watersheds decreased. At Skogly station, model performance declined gradually when numbers of sub-watersheds decreased. At Lundberg, model performance highly fluctuated. For instance, it was stable from TDAs 200 to 2,000 ha, then decreased with TDA 5,000 ha, and afterward increased with TDA 10,000 ha. The decreases in model performances in the coarse schemes in the present study agreed with conclusions from the previous studies (Mamillapalli *et al.* 1996; Haverkamp *et al.* 2002; Tegegne *et al.* 2019). Obviously, model performances were heterogeneous among hydro-gauging stations under the changes

of TDA schemes (Figure 5(a)). The reasons could be the complexity of hydrological processes as well as topographic characteristics in the Arctic.

The general tendencies of the changes in model performances in the validation period were repeated to those in the calibration period at Målselvossen, Lundberg, and Høgskarhus, except at Skogly and Lille Rostavatn (Figure 5(b)). Details of the statistical coefficients for calibration and validation at all five hydro-gauging stations under different TDA schemes are presented in Tables 5–9.

The influences of watershed subdivisions on water balance components

Rainfall is one of the main inputs of water balance components. It was observed from the present study that the annual mean values of areal rainfall increased with the decreases in the number of sub-watersheds (Figure 6(a)). However, the magnitudes of deviations in annual mean values of areal rainfall were not significant among the TDA schemes. For example, the gap in the annual mean values of areal rainfall was only 24 mm between TDAs 200 and 10,000 ha. It could be interpreted that the coarse scheme had higher rainfall input than the finer scheme because fewer weather grid points in the coarse scheme generated more uniform rainfall across the watershed. In particular, the average and minimum values of annual rainfall from 14 weather grids in the TDA 10,000 ha were 1,207 and 826 mm, respectively, which were higher than those from 21 weather grids in the TDA 200 ha, with 1,185 and 750 mm, respectively. Therefore, the integrated rainfall amount from the coarse scheme was higher than that from the fine scheme, although the number of integrated weather grids from the coarse scheme was less than that from the fine scheme. Also, the denser weather grid points of the fine TDA scheme produced lower rainfall amount, since rainfall had high variation among weather grids. This could be true for the mountainous watershed, since rainfall is usually high variation. Figure 7(a)–7(d) illustrates the spatial variation of areal rainfall resulting from different resolutions of watershed discretizations. Obviously, the higher number of sub-watersheds produced finer variation of areal rainfall across the watershed. The finest scheme was able to display some

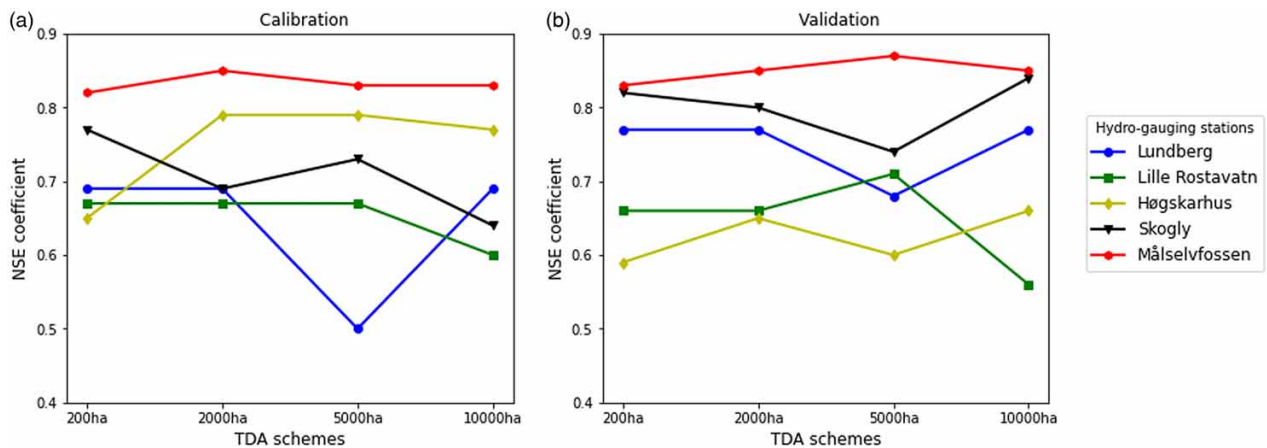


Figure 5 | Model performances for calibration and validation under four different TDA schemes.

Table 5 | Comparison of model performance at Lundberg

TDA (ha)	Sub-basin	Calibration					Validation				
		p -factor	r -factor	R^2	NSE	RSR	p -factor	r -factor	R^2	NSE	RSR
200	381	0.88	1.08	0.73	0.69	0.56	0.90	1.00	0.81	0.77	0.48
2,000	87	0.80	0.76	0.73	0.69	0.55	0.78	0.67	0.84	0.77	0.48
5,000	32	0.58	0.64	0.57	0.50	0.71	0.72	0.59	0.76	0.68	0.56
10,000	10	0.75	0.84	0.73	0.69	0.56	0.81	0.73	0.82	0.77	0.48

Table 6 | Comparison of model performance at Lille Rostavatn

TDA (ha)	Sub-basin	Calibration					Validation				
		p-factor	r-factor	R ²	NSE	RSR	p-factor	r-factor	R ²	NSE	RSR
200	402	0.75	0.95	0.79	0.67	0.58	0.72	0.89	0.91	0.66	0.58
2,000	92	0.63	0.69	0.78	0.67	0.58	0.47	0.62	0.91	0.66	0.59
5,000	34	0.58	0.66	0.81	0.67	0.57	0.43	0.59	0.91	0.71	0.54
10,000	4	0.50	0.60	0.78	0.60	0.63	0.33	0.52	0.89	0.56	0.66

Table 7 | Comparison of model performance at Høgskarhus

TDA (ha)	Sub-basin	Calibration					Validation				
		p-factor	r-factor	R ²	NSE	RSR	p-factor	r-factor	R ²	NSE	RSR
200	408	0.80	1.10	0.74	0.65	0.59	0.80	1.24	0.73	0.59	0.64
2,000	94	0.71	0.94	0.79	0.79	0.46	0.61	1.10	0.75	0.65	0.59
5,000	35	0.72	0.87	0.79	0.79	0.46	0.59	0.97	0.74	0.60	0.63
10,000	14	0.71	0.95	0.77	0.77	0.48	0.66	1.11	0.72	0.66	0.58

Table 8 | Comparison of model performance at Skogly

TDA (ha)	Sub-basin	Calibration					Validation				
		p-factor	r-factor	R ²	NSE	RSR	p-factor	r-factor	R ²	NSE	RSR
200	412	0.98	1.59	0.77	0.77	0.48	0.95	1.47	0.87	0.82	0.42
2,000	95	0.80	1.21	0.81	0.69	0.56	0.60	1.17	0.88	0.80	0.44
5,000	37	0.83	1.15	0.8	0.73	0.52	0.63	1.06	0.89	0.74	0.51
10,000	16	0.91	1.30	0.77	0.64	0.60	0.90	1.32	0.88	0.84	0.40

Table 9 | Comparison of model performance at Målselvossen

TDA (ha)	Sub-basin	Calibration					Validation				
		p-factor	r-factor	R ²	NSE	RSR	p-factor	r-factor	R ²	NSE	RSR
200	444	0.94	1.57	0.85	0.82	0.42	0.91	1.58	0.88	0.83	0.41
2,000	108	0.82	1.10	0.86	0.85	0.39	0.77	1.08	0.88	0.85	0.38
5,000	43	0.86	1.09	0.85	0.83	0.41	0.86	1.08	0.89	0.87	0.36
10,000	13	0.82	1.06	0.85	0.83	0.41	0.86	1.07	0.87	0.85	0.39

locations in the watershed with low rainfall amount. For example, based on [Figure 7\(a\)](#), the minimum value of annual mean rainfall in some sub-basins in the upstream, from the finest TDA scheme 200 ha, was 758 mm which was lower at 87 mm compared to that from other coarser schemes.

Annual mean potential ET (PET) ([Figure 6\(b\)](#)) and actual ET ([Figure 6\(c\)](#)) slightly increased from TDAs 200 to 5,000 ha, then slightly decreased to TDA 10,000 ha. This could be because the coarse scheme 10,000 ha simplified the land-use and cropland variations that resulted in lower ET amount. For example, the coarse scheme 10,000 ha lost 4 land-use groups compared to 11 land-use groups in the fine scheme 200 ha ([Table 4](#)). In contrast, annual mean lateral flow (LATQ) dropped from

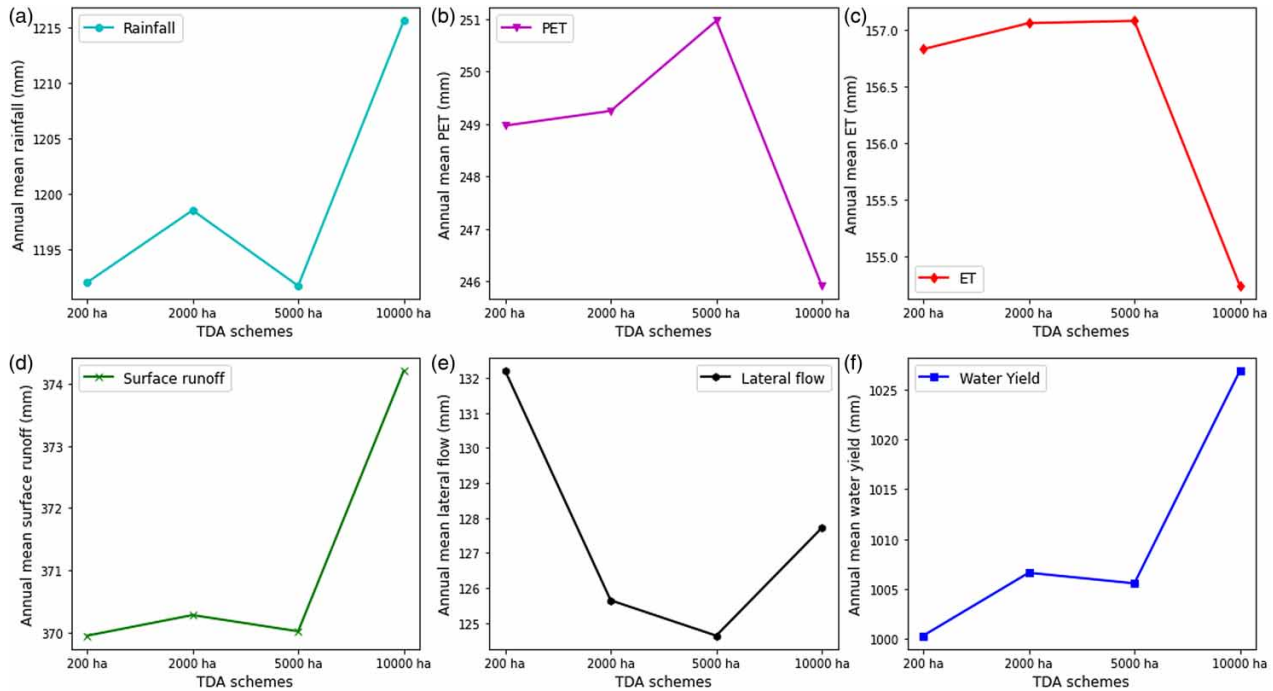


Figure 6 | The changes in annual mean values of some water balance components under different TDAs.

TDAs 200 to 5,000 ha, after which it went up to TDA 10,000 ha (Figure 6(e)). The annual mean surface runoff (SURFQ) (Figure 6(d)) and WYLD (Figure 6(f)) had similar trends. In general, SURFQ and WYLD had an upward trend from TDAs 200 to 10,000 ha, but the trend dropped down to TDA 5,000 ha. Therefore, this could reveal that the TDA 5,000 ha could be a threshold which sketched the line of the discrepancies between watershed subdivision schemes. The water balance components could increase/decrease if the number of sub-watersheds was lower/higher than this threshold.

Although the annual mean values of PET and ET decreased, and surface runoff and WYLD increased when TDA increased, the magnitudes of these changes were not significant. The trends of changes in such water balance components from the present study agreed with findings from the previous studies in the 21.3-km² Goodwin Creek Watershed, in northern Mississippi, USA (Bingner *et al.* 1997), the four Iowa watersheds (2,000–18,000 km²), USA (Jha *et al.* 2004), and the 26.12-km² Walnut Creek watershed, in central Iowa, USA (Chaplot 2014). The slight increase in surface runoff and WYLD in the present study could suggest that rainfall amount had a slight increasing trend, and PET and ET had a slight decreasing trend when the number of sub-watersheds decreased. Therefore, additional water was more than water loss. However, the findings from the present study also contradicted the findings in the study at the 65,145-km² Tapi River, India, since they concluded that surface runoff decreased when TDA increased (Munoth & Goyal 2019a). They stated that reduction in the number of streams was the reason for decreasing runoff in the coarse schemes. However, loss of streams could affect sediment yield more than runoff volume (Bingner *et al.* 1997), since stream loss would result in loss of deposition process in streams (Jha *et al.* 2004).

According to the GIS maps of the spatial variation of ET (Figure 7(e)–7(h)), SURQ (Figure 7(i)–7(l)), and WYLD (Figure 7(m)–7(p)), the higher number of sub-watersheds produced finer variation of water balance components. This was in agreement with the study in the 384-km² Grote Nete River catchment, in Flanders, Belgium (Rouhani *et al.* 2009). In addition, hotspots (e.g., the places with extremely high/low values of water balance components in comparison to their surroundings) were presented more clearly in the finer schemes than those in the coarser ones.

The influences of watershed subdivisions on spatial variation of snowmelt runoff

Snowmelt is the main source of spring runoff in the Arctic. Determining the vulnerable locations due to high snowmelt runoff volume is highly important for risk management, e.g., flash flood, erosion, and landslide. In general, four different TDA schemes produced similar locations with high or low snowmelt volume across the watershed (Figure 8).

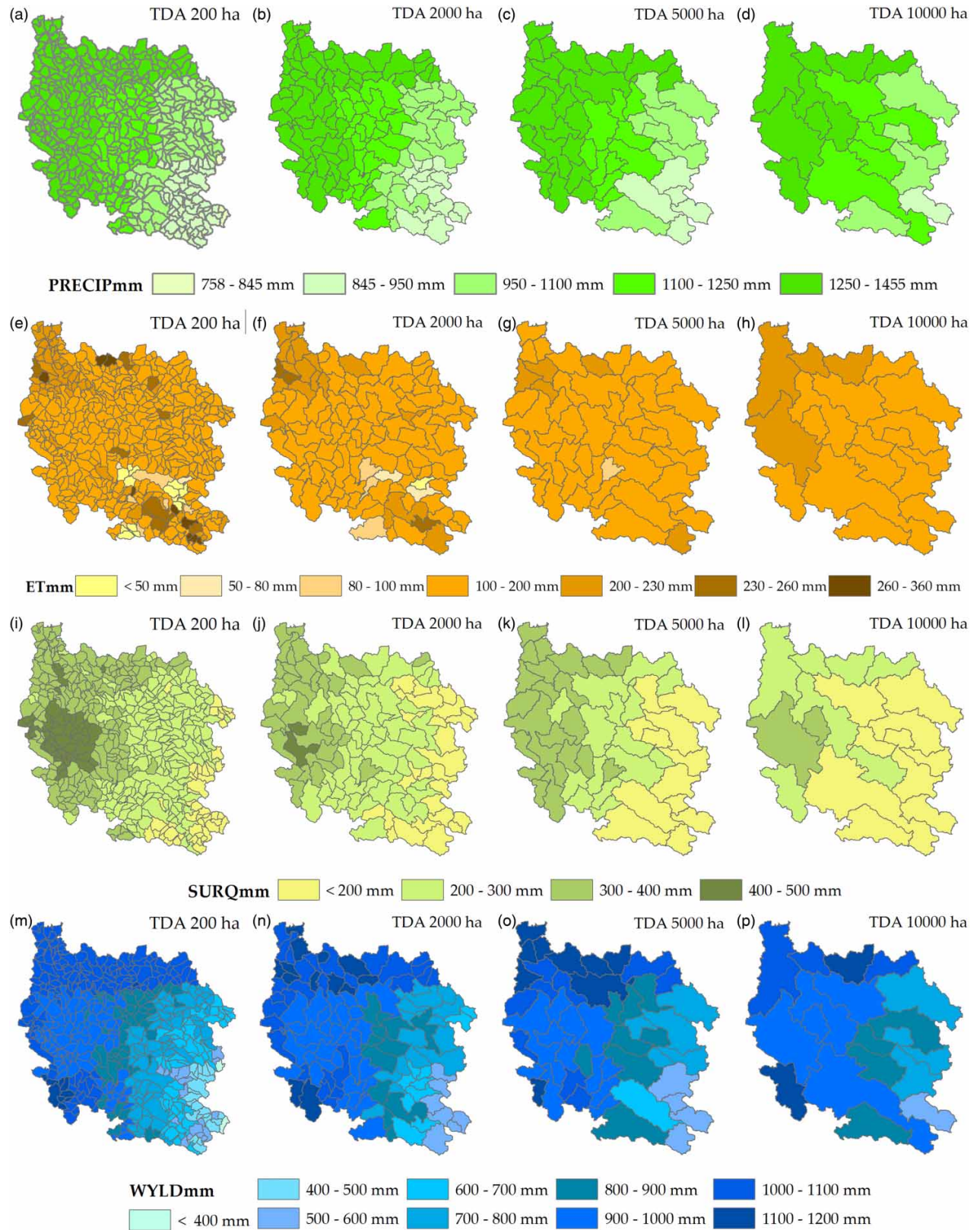
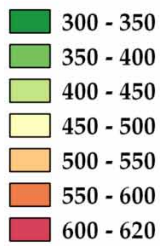


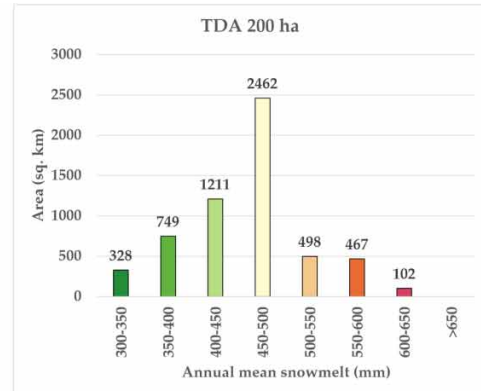
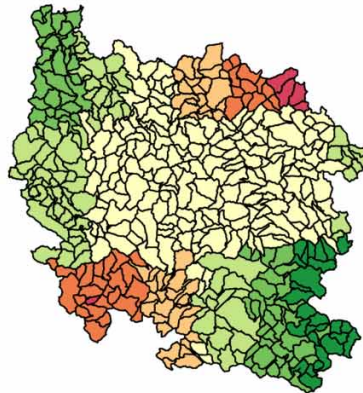
Figure 7 | Spatial variation of annual mean values of some water balance components under four TDA schemes: PRECIP, precipitation (a–d); ET, actual evapotranspiration (e–h); SURQ, surface runoff (i–l); and WYLD, water yield (m–p).

(a) TDA 200 ha

Annual mean snowmelt (mm)

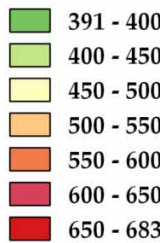


10 0 10 20 30 40 50 km

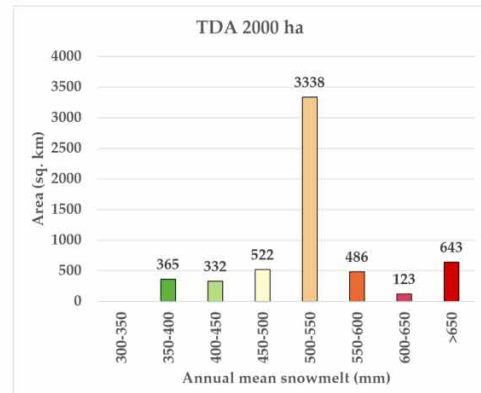
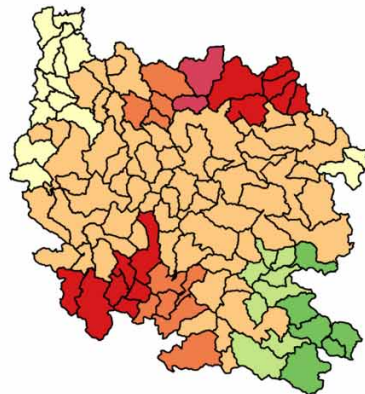


(b) TDA 2000 ha

Annual mean snowmelt (mm)

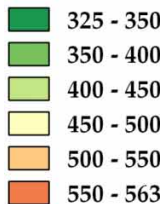


10 0 10 20 30 40 50 km

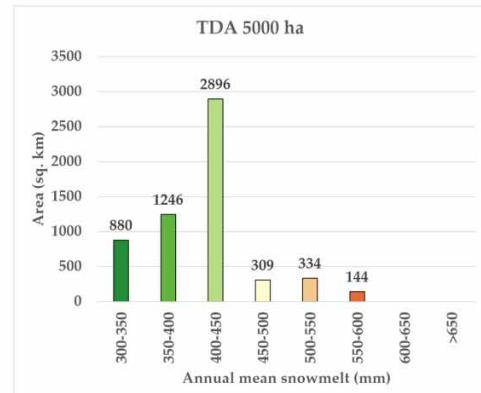
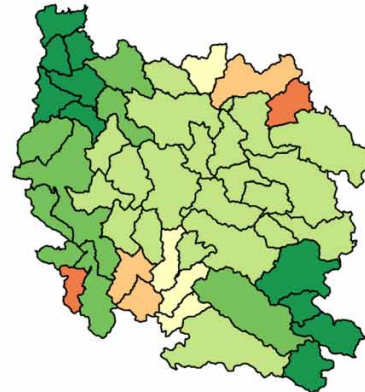


(c) TDA 5000 ha

Annual mean snowmelt (mm)

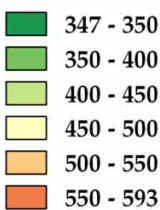


10 0 10 20 30 40 50 km



(d) TDA 10000 ha

Annual mean snowmelt (mm)



10 0 10 20 30 40 50 km

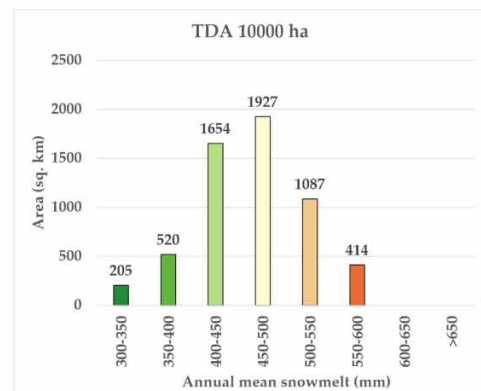
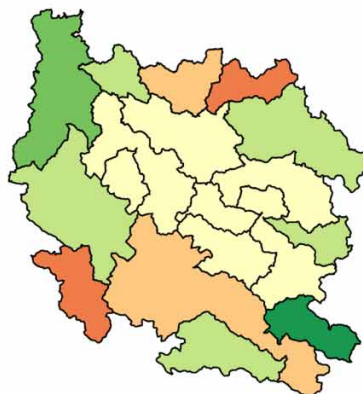


Figure 8 | Spatial variation of annual mean snowmelt runoff volume (1998–2007) under four TDA schemes. Please refer to the online version of this paper to see this figure in colour: <http://dx.doi.org/10.2166/wcc.2021.173>.

However, the maximum and minimum amounts of snowmelt runoff as well as the areas of sub-basins dominating by snowmelt are somewhat different among four TDAs. The reason could be that the fine TDA schemes have higher land-use composition, which could result in decreasing snow albedo and accelerate the snowmelt process (Szczypta *et al.* 2015). Therefore, the higher values of maximum snowmelt volume were found in the fine schemes. Moreover, the fitted model parameters were somewhat different among four TDA schemes during the calibration process (Supplementary Tables S1– S5). This could result in the differences in calculated snowmelt runoff across the watershed.

Furthermore, it is obvious from Figure 8 that the fine TDAs 200 ha (Figure 8(a)) and 2,000 ha (Figure 8(b)) generated finer and higher ranges of annual mean snowmelt volume across the watershed. Also, TDAs 200 and 2,000 ha could point out some hotspot locations of snowmelt volume within the watershed (marked with dark red colors). The relatively high annual mean value of snowmelt runoff volume and its large impacted areas were detected in the central section of the watershed. However, magnitude and impacted areas were inconsistent among four TDAs. For example, the annual mean snowmelt of 450–500 mm accounted for the largest area with 2,462 km², calculated from TDA 200 ha, while the annual mean snowmelt of 500–550 mm accounted for the largest impacted area with 3,338 km², achieved from TDA 2,000 ha. TDA 5,000 ha had the largest impacted area (2,896 km²) regarding the annual mean snowmelt of 400–450 mm. Similar to TDA 200 ha, TDA 10,000 ha detected the largest impacted area (1,927 km²) regarding the annual mean snowmelt of 450–500 mm. Based on the spatial distribution of simulated snowmelt runoff, it is recommended from the present study that more inspection should be focused on the central parts of the watershed as well as the locations of snowmelt hotspots for better risk management due to high snowmelt volume. Additionally, the central sections of the watershed and locations of snowmelt hotspots are the high mountain areas; therefore, the risks for flash flood or landslide could be high.

The influences of watershed subdivisions on streamflow simulation

For each TDA scheme, the simulation result of monthly streamflow during a 10-year period, from 1998 to 2007, was averaged for each hydro-gauging station, and all the results were plotted as shown in Figure 9. According to Figure 9, all TDA schemes

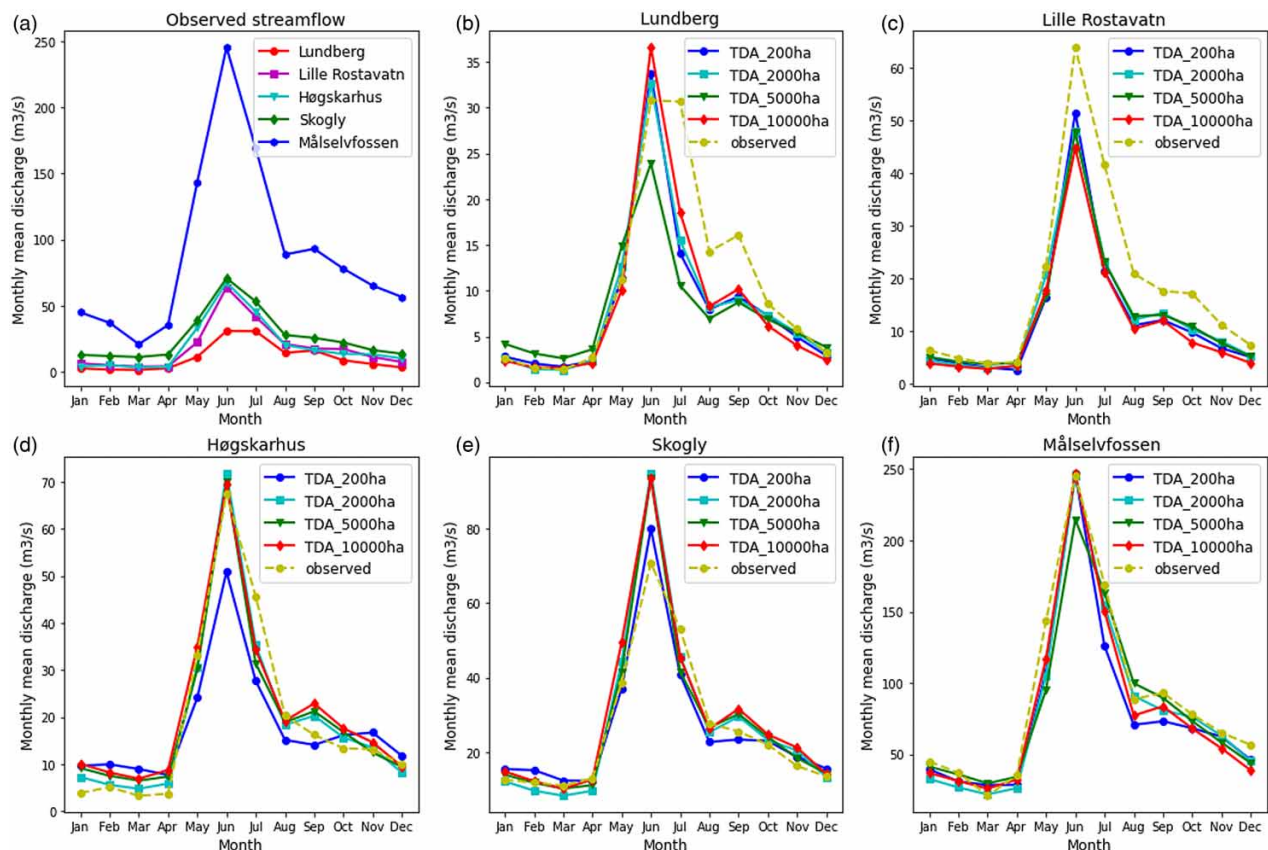


Figure 9 | Monthly mean streamflow (1998–2007) under four TDAs at five hydro-gauging stations.

had capacities to simulate the observed tendency of monthly mean streamflow at all five hydro-gauging stations. However, the accuracy of simulation of monthly mean peak discharge was heterogeneous among TDA schemes as well as among five hydro-gauging stations. For example, the finest scheme TDA 200 ha performed quite well in simulating peak flow at Lundberg and Målselvossen, while the coarsest scheme 10,000 ha was able to capture the peak flow at Høgskarhus and also at Målselvossen. Lille Rostavatn was only the station where all TDA schemes yielded similarly the simulations of peak flows.

Therefore, the present study found that the accuracy of streamflow simulation did not totally depend on the levels of watershed discretization, but may also be controlled by other factors such as the geographic location and/or topographic characteristics of the sub-basins surrounding the investigated hydro-gauging stations. Unlike the homogeneous effects of watershed subdivisions on streamflow simulation in the previous studies, heterogeneous effects were found in the present study. For example, a previous study concluded that the accuracy of streamflow prediction was only increased (Mamillapalli *et al.* 1996) or decreased (Rouhani *et al.* 2009) when the number of sub-watersheds increased. Thus, it could be revealed that because of the complexity of hydrological cycles in the Arctic conditions as well as the topographic characteristics of the watershed, it could result in the heterogeneous effects of watershed subdivisions on streamflow simulations at different locations within the watershed. Furthermore, the heterogeneous effects of watershed subdivisions on the simulation results of streamflow hydrograph from the present study could help to explain the impacts of topographic variation compared to the homogeneous effects of watershed subdivisions in a flat watershed, e.g., the 152.29-km² Little Washita watershed, USA (Norris & Haan 1993). For example, that study found that the simulated peak flow linearly increased with the increase of number of sub-watersheds (Norris & Haan 1993).

Figure 10 illustrates the spatial variation of annual mean streamflows resulting from different TDA schemes. Under the finest TDA 200 ha, five levels of stream order were generated and displayed the high variation of the annual mean streamflow

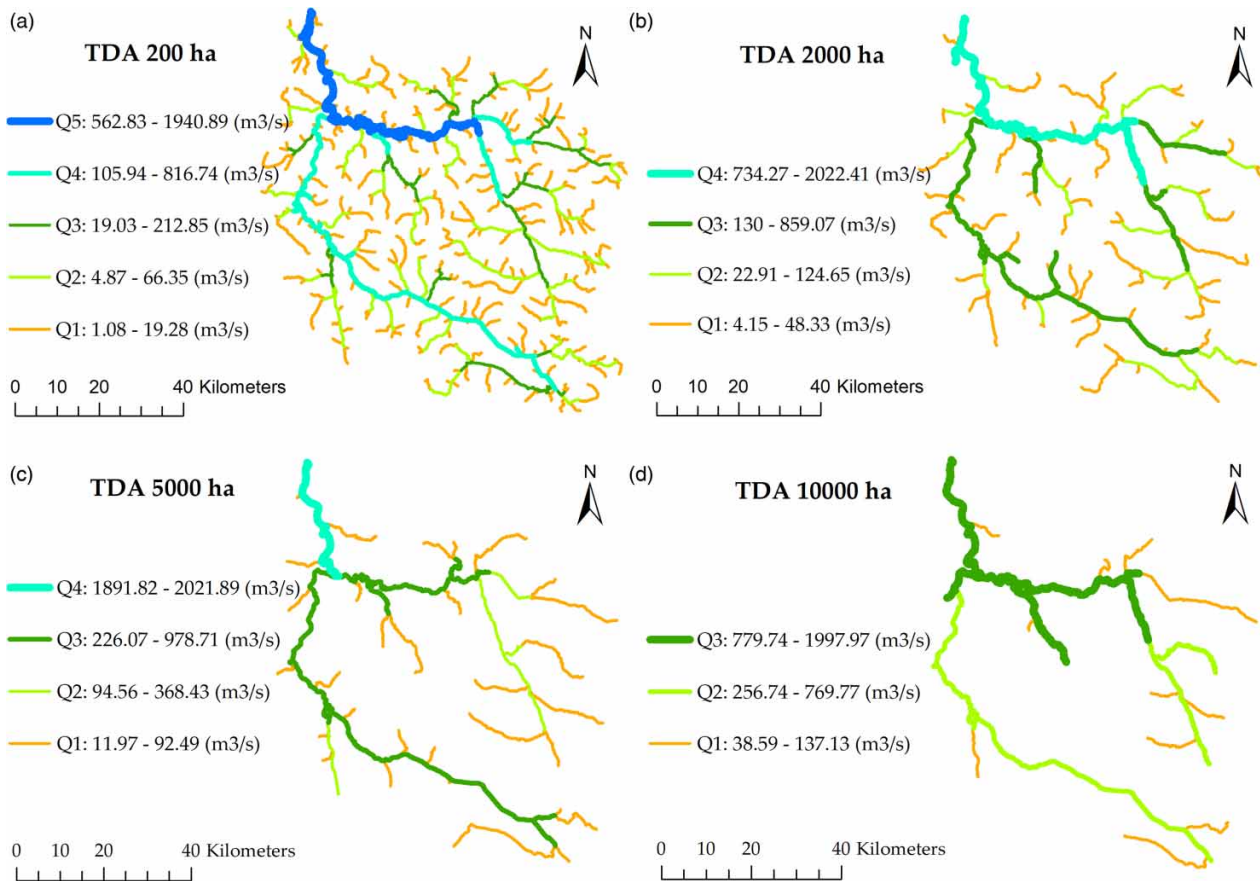


Figure 10 | Spatial variation of annual mean streamflow (1998–2007) in different stream order levels in each TDA scheme. Q1–Q5 denote streamflows in stream order levels 1–5, respectively.

across the entire watershed (Figure 10(a)). Levels of stream order gradually declined in the coarser schemes TDA 2,000 ha (Figure 10(b)), TDA 5,000 ha (Figure 10(c)), and TDA 10,000 ha (Figure 10(d)) because of the decrease in number of sub-basins and the increase in sub-basins' sizes. As a consequence, flow data in the coarser schemes were only detected in the major streams. In contrast, the finest TDA scheme was able to detect some minor streams and their flow values within the watershed; however, such minor streams may not be realistic and may not exist on ground.

Additionally, discrepancies in stream order levels from the fine schemes to the coarse schemes resulted in differences in the spatial distribution of streamflow values. For example, range of values and spatial distribution of streamflow data Q1 (for stream order level 1), Q2 (for stream order level 2), Q3 (for stream order level 3), Q4 (for stream order level 4, except TDA 10,000 ha), and Q5 (for stream order level 5, and only defining in TDA 200 ha) were inconsistent from the finest scheme to the coarsest scheme. This might affect the management of water resources by zones subdivisions. The coarser schemes simplified the stream networks and may lose some important in-stream processes. Loss of minor streams and their flow data may also affect local flood risk analysis (if this task would be planned to carry out in the future studies). For example, total stream length (e.g., minor streams) and drainage density generated from the coarsest TDA 10,000 ha reduced approximately 75% compared to those from the finest TDA 200 ha.

The influences of spatial density of the integrated weather grids on hydrological simulations

In the SWAT model, the nearest neighbor search (NNS) method is used to pick up the weather grid point representative for each sub-basin. According to this technique, one weather grid point closest to the centroid of a sub-basin is selected. The areal rainfall was then calculated for each sub-basin based on the rainfall data from the selected weather grid point. It was observed in this study that the number of weather grid points dropped from 21 grids in TDA 200 ha to 20 grids (−5%), 18 grids (−14.3%), and 14 grids (−33.33%) in TDAs 2,000, 5,000, and 10,000 ha, respectively (Figure 4). Fewer weather grid points produced more uniform distribution of areal rainfall across the watershed (Figure 7(b)–7(d)). As a result, the spatial variation of other water balance components was also influenced (Figure 7(e)–7(p)), since rainfall is the main input to generate water resources in the watershed.

The influences of watershed subdivisions on the sensitivity of model parameters

Global sensitivity analysis in the SUFI-2 algorithm in the SWAT-CUP program detected the most sensitive model parameters among 18 model parameters used for calibration. It was found in the present study that the number of sensitive model parameters and their ranks changed significantly under different TDA schemes. Figure 11 provides the sensitivity changes of each calibrated parameter, which is classified into four different hydrological subgroup processes, while Figure 12 provides the sensitivity rank for all 18 calibrated parameters, based on the values of *t*-stat (magnitude of sensitivity) and *p*-value (significance of sensitivity), under each TDA scheme. Herein, the sensitivity rank, from highest to lowest, is the bottom-up order.

Regarding the surface runoff subgroup process (Figure 11(b)), runoff curve number CN2 showed its higher impacts (e.g., higher sensitivity rank) on the formation of runoff than the remaining parameter when the number of sub-watersheds changed (decreased). This is because CN2 depends strongly on land-use and soil characteristics of the watershed (Tegegne *et al.* 2019). Therefore, the discrepancies in land-use/soil composition by changing TDAs (e.g., the coarsest TDA 10,000 ha lost 4 land-use groups (−36.36%) compared to the finest TDA 200 ha) resulted in high fluctuation of CN2 values. The findings from the present study contradicted findings from the previous study in the Yongdam watershed in South Korea and in the Gilgelabay watershed in Ethiopia, since the sensitivity of CN2 in those studies increased when the number of sub-watersheds increased (Tegegne *et al.* 2019).

Parameters of soil properties, which governed the lateral flow process, fluctuated under changes of TDAs (Figure 11(c)). However, these soil parameters were not ranked in high sensitivity levels. Based on soil map, there are not many soil types in the Målselv watershed, and sandy loam dominates the major area. Therefore, the fluctuation of soil parameters resulted from changes in land-use composition rather than from changes in soil textures/types. The consequences of land-use change on soil properties such as soil moisture, infiltration capacity, and water storage were well validated in previous studies (Moges *et al.* 2013).

Several parameters in the snowmelt subgroup process had higher sensitivity rank orders compared to parameters of other subgroup processes (Figure 11(d)). The changes in watershed subdivision scales also resulted in the fluctuation of these parameters. The reason could be the changes in land-use structure in the watershed. For example, high/low density of land cover significantly affects the amount of snowfall accumulated on the ground, snow interception, sublimation process of snow, snow surface radiation balance (by the shading of trees), and snow albedo (Szczypta *et al.* 2015).

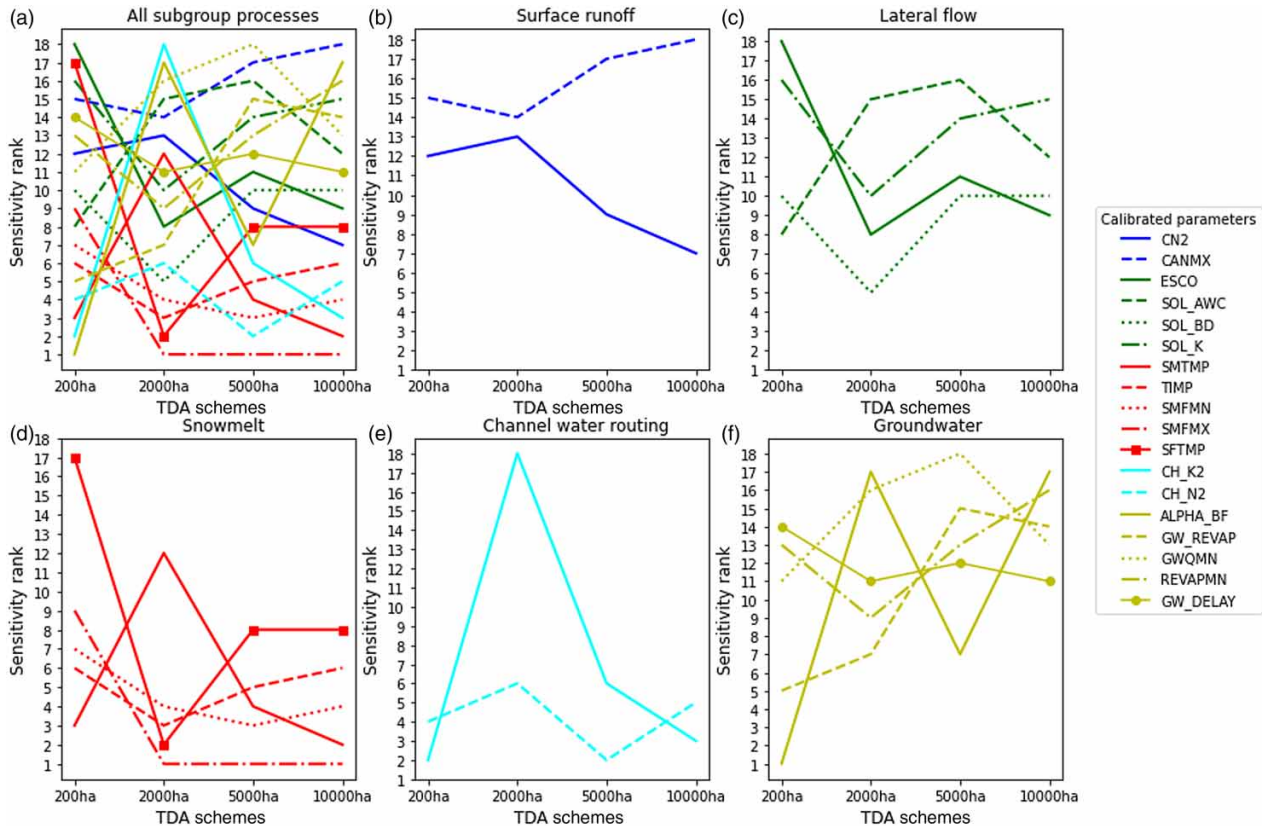


Figure 11 | Changes in sensitivity ranks of all 18 calibrated parameters, under five hydrological subgroup processes, by changes in TDAs.

Changes in TDAs also resulted in the fluctuation of the sensitivity ranks of parameters in channel water routing (Figure 11(e)). However, the sensitivity ranks of the Manning's value (n) for the main channel (CH_N2) were more stable than those of the effective hydraulic conductivity in the main channel (CH_K2) in the channel subgroup process. The variation of parameters in the channel water routing process could result from the discrepancies in terrain complexity and the topographic attributes such as average overland sub-basins slope, streams length, average streams slope, and streams width (Table 3).

Most of the parameters in the groundwater subgroup process had low sensitivity rank and highly fluctuated (except GW_DELAY) when the number of sub-watersheds decreased (Figure 11(f)). The reasons for the fluctuation of parameters in the groundwater subgroup process could be the consequences of the changes in land-use structures and the associated soil properties, which affected the processes of infiltration, groundwater recharge, water transmission in soil, as well as evaporation from soil layers.

CONCLUSIONS

Watershed delineation is an important preliminary step for setting up the hydrological models. The application of the TDA technique for watershed subdivisions has a significant impact on hydrological simulation results. This study used the TDA technique to discretize the Målselv watershed, an Arctic watershed in the North of Norway. Four different TDA schemes, from the finest to the coarsest one, including 200, 2,000, 5,000, and 10,000 ha, were designed. The aim was to evaluate the impacts of different TDA schemes and spatial density of weather grid integration on hydrological simulations. The simulation results of water balance components, snowmelt runoff volume, and streamflow were evaluated. The main conclusions were drawn from the present study as follows:

1. The complexity of terrain and topographic attributes changed significantly with increasing TDA values such as decreasing total stream length, average stream slope, and drainage density. Stream order levels also declined as TDA increased.

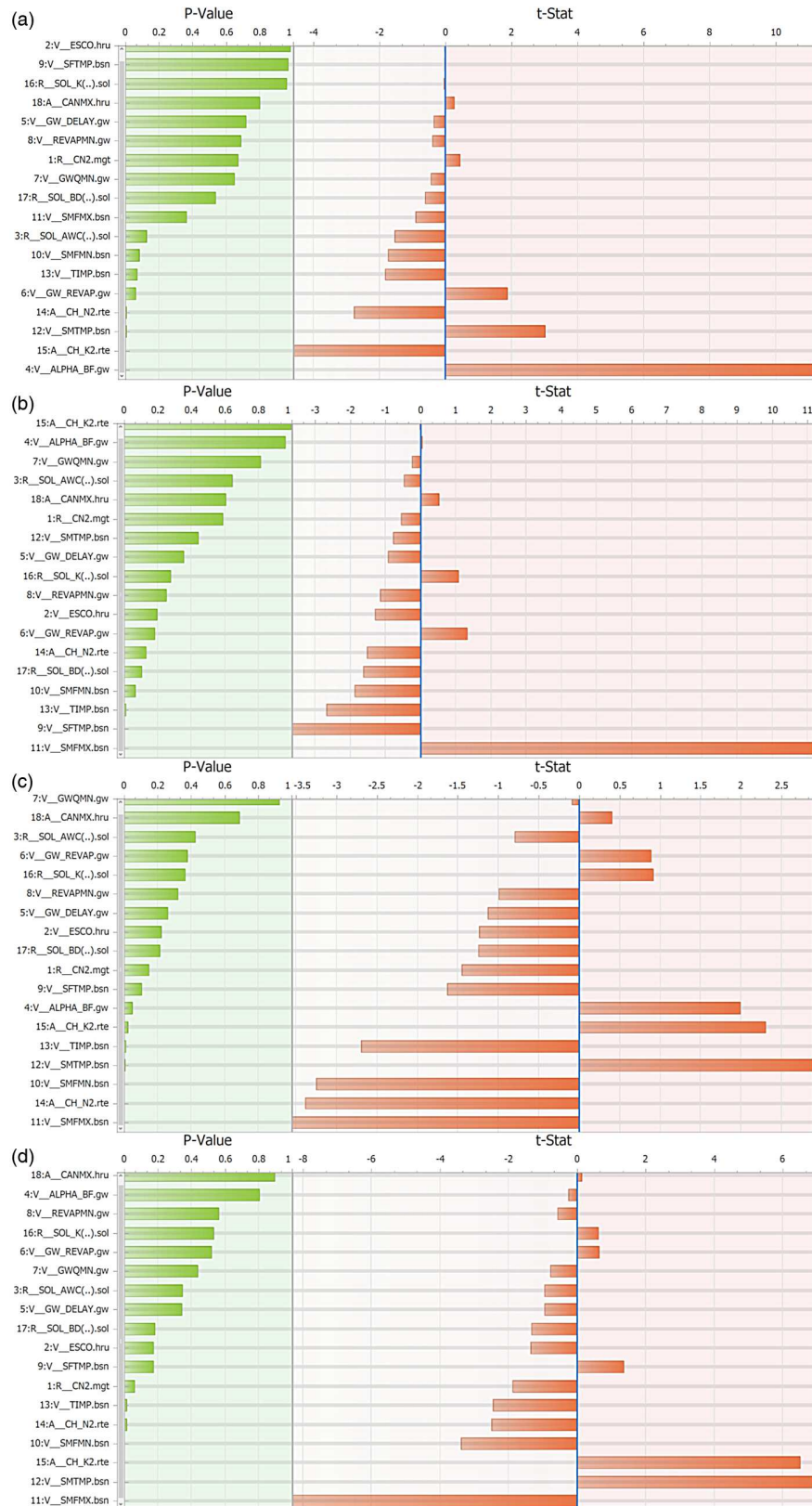


Figure 12 | Sensitivity ranks (in bottom-up orders) of 18 calibrated parameters by global sensitivity analysis in SWAT-CUP: (a) TDA 200; (b) TDA 2,000; (c) TDA 5,000; and (d) TDA 10,000 ha.

2. The spatial density of weather grid point integration decreased from -5 to -33.33% in the coarse schemes 2,000, 5,000, and 10,000 ha compared to the finest scheme 200 ha. Fewer numbers of weather grid points produced more uniform distribution of areal rainfall across the watershed, particularly TDA 10,000 ha.
3. Watershed subdivision did not strongly affect the model performances during the calibration period at Lille Rostavatn and Målselvfossen hydro-gauging stations compared to the remaining stations in upstream.
4. Watershed subdivisions affected the spatial variation of areal rainfall across the watershed, but the total rainfall amount for the whole watershed was only slightly changed.
5. The changes in annual mean values of water balance components from the finest TDA 200 ha to the coarsest TDA 10,000 ha: rainfall (increased), PET and ET (decreased), surface runoff (increased), lateral flow (decreased), and WYLD (increased). However, the magnitudes of changes were not significant. The coarsest TDA 10,000 ha simplified land-use composition (e.g., loss of 4 land-use groups compared to TDA 200 ha with 11 groups) resulted in decreasing PET and ET.
6. The fine TDAs produced finer variation of snowmelt runoff volume and higher values of maximum snowmelt runoff volume across the watershed. Most TDAs detected similarly the most vulnerable areas by high snowmelt runoff volume, which are located in the central sections of the watershed and dominated by highly mountainous terrain. Therefore, high inspection should be focused on the central parts for better risk management, especially the risks of flash flood, erosion, and landslide.
7. All four TDA schemes had similar capacities to replicate the observed tendency of monthly mean streamflow hydrograph at all five hydro-gauging stations within the watershed. However, monthly mean peak flow had slight discrepancies among TDA schemes and among five hydro-gauging stations. Lille Rostavatn station was the only one where all four TDA schemes produced similar simulations of monthly mean peak flows.
8. The finest TDA scheme 200 ha could generate a high spatial variation of streamflow and could reveal the flow values of the minor streams, while other coarser schemes only showed streamflow in the major streams. Therefore, using the coarse schemes could influence the accuracy/detail of local flood risk analysis or finding flood hotspots in case such studies would be planned in future.
9. Watershed subdivisions strongly affected the calibration process regarding the changes in numbers and disordering the sensitivity ranks among the 18 calibrated model parameters.
10. One of the advantages of using the coarse TDA schemes was highlighted in the calibration process since the calibration time for approximately 5,913 km² watershed, and for simulation with monthly time step, decreased (approximately 5.7–34%) when the number of sub-watersheds decreased (from 459 to 18). This would benefit the users who have limitations in time and the available resources for running the model.

In brief, according to findings from the present study, it would be recommended that choosing the suitable threshold of TDA for watershed subdivision could depend on several factors including the purposes of studies, the expected level of accuracy in the output variables, the limited/allowed time, or the available resources that using the fine schemes or the coarse schemes would be an appropriate choice. Moreover, findings from the present study could help to enrich knowledge in designing the TDA for watershed delineation in hydrological models, particularly in the Arctic environment.

ACKNOWLEDGEMENTS

The authors acknowledge the Department of Technology and Safety, University of Tromsø – The Arctic University of Norway – for their financial support in this study. We recognize the in-kind contribution from Foundation CSDI WaterTech.

DATA AVAILABILITY STATEMENT

All relevant data are included in the paper or its Supplementary Information.

REFERENCES

- Abbaspour, K. C., Yang, J., Maximov, I., Siber, R., Bogner, K., Mieleitner, J., Zobrist, J. & Srinivasan, R. 2007 *Modelling hydrology and water quality in the pre-alpine/alpine Thur watershed using SWAT*. *Journal of Hydrology* **333** (2–4), 413–430.
- Abbaspour, K. C. 2015 *SWAT-CUP: Swat Calibration and Uncertainty Program – A User Manual, Eawag*. Swiss Federal Institute of Aquatic Science and Technology, Dübendorf, Switzerland.

- Abbaspour, K. C., Rouholahnejad, E., Vaghefi, S., Srinivasan, R., Yang, H. & Klove, B. 2015 A continental-scale hydrology and water quality model for Europe: calibration and uncertainty of a high-resolution large-scale SWAT model. *Journal of Hydrology* **524**, 733–752.
- Aouissi, J., Benabdallah, S., Chabaane, Z. L. & Cudennec, C. 2013 Sensitivity analysis of SWAT model to the spatial rainfall distribution and watershed subdivision in streamflow simulations in the Mediterranean context: a case study in the Joumine watershed, Tunisia. In: *2013 5th International Conference on Modeling, Simulation and Applied Optimization (Icmsao)*.
- Aouissi, J., Benabdallah, S., Chabaane, Z. L. & Cudennec, C. 2018 Valuing scarce observation of rainfall variability with flexible semi-distributed hydrological modelling – Mountainous Mediterranean context. *Science of the Total Environment* **643**, 346–356.
- Arabi, M., Govindaraju, R. S., Hantush, M. M. & Engel, B. A. 2006 Role of watershed subdivision on modeling the effectiveness of best management practices with SWAT. *Journal of the American Water Resources Association* **42** (2), 513–528.
- Argent, R. M., Podger, G. M., Grayson, R. B., Fowler, K. & Murray, N. 2006 *E2 Catchment Modelling Software, User Guide*.
- Bardossy, A. & Das, T. 2008 Influence of rainfall observation network on model calibration and application. *Hydrology and Earth System Sciences* **12** (1), 77–89.
- Bingner, R. L., Garbrecht, J., Arnold, J. G. & Srinivasan, R. 1997 Effect of watershed subdivision on simulation runoff and fine sediment yield. *Transactions of the ASAE* **40** (5), 1329–1335.
- Boyle, D. P., Gupta, H. V., Sorooshian, S., Koren, V., Zhang, Z. Y. & Smith, M. 2001 Toward improved streamflow forecasts: value of semidistributed modeling. *Water Resources Research* **37** (11), 2749–2759.
- Chaplot, V., Saleh, A. & Jaynes, D. B. 2005 Effect of the accuracy of spatial rainfall information on the modeling of water, sediment, and NO₃-N loads at the watershed level. *Journal of Hydrology* **312** (1–4), 223–234.
- Chaplot, V. 2014 Impact of spatial input data resolution on hydrological and erosion modeling: recommendations from a global assessment. *Physics and Chemistry of the Earth* **67–69**, 23–35.
- Chaubey, I., Haan, C. T., Grunwald, S. & Salisbury, J. M. 1999 Uncertainty in the model parameters due to spatial variability of rainfall. *Journal of Hydrology* **220** (1–2), 48–61.
- Chen, M., Cui, Y., Gassman, P. W. & Srinivasan, R. 2021 Effect of watershed delineation and climate datasets density on runoff predictions for the Upper Mississippi River Basin using SWAT within HAWQS. *Water* **13** (4), 422.
- Chiang, L. C. & Yuan, Y. P. 2015 The NHDPlus dataset, watershed subdivision and SWAT model performance. *Hydrological Sciences Journal* **60** (10), 1690–1708.
- Daofeng, L., Ying, T., Changming, L. & Fanghua, H. 2004 Impact of land-cover and climate changes on runoff of the source regions of the Yellow River. *Journal of Geographical Sciences* **14** (3), 330–338.
- Das, T., Bardossy, A., Zehe, E. & He, Y. 2008 Comparison of conceptual model performance using different representations of spatial variability. *Journal of Hydrology* **356** (1–2), 106–118.
- Devi, G. K., Ganasri, B. P. & Dwarakish, G. S. 2015 A review on hydrological models. *Aquatic Procedia* **4**, 1001–1007.
- Dile, Y. T., Berndtsson, R. & Setegn, S. G. 2013 Hydrological response to climate change for Gilgel Abay River, in the Lake Tana Basin – Upper Blue Nile Basin of Ethiopia. *Plos One* **8** (10), 1–13.
- Di Luzio, M. & Arnold, J. G. 2004 Formulation of a hybrid calibration approach for a physically based distributed model with NEXRAD data input. *Journal of Hydrology* **298** (1–4), 136–154.
- Du, J. K., Rui, H. Y., Zuo, T. H., Li, Q., Zheng, D. P., Chen, A. L., Xu, Y. P. & Xu, C. Y. 2013 Hydrological simulation by SWAT model with fixed and varied parameterization approaches under land use change. *Water Resources Management* **27** (8), 2823–2838.
- Dwarakish, G. S. & Ganasri, B. P. 2015 Impact of land use change on hydrological systems: a review of current modeling approaches. *Cogent Geoscience* **1** (1), 1–18.
- EPA 2013 *Watershed Modeling to Assess the Sensitivity of Streamflow, Nutrient, and Sediment Loads to Potential Climate Change and Urban Development in 20 U.S. Watersheds (Final Report)*. U.S. Environment Protection Agency, Washington, DC.
- FitzHugh, T. W. & Mackay, D. S. 2000 Impacts of input parameter spatial aggregation on an agricultural nonpoint source pollution model. *Journal of Hydrology* **236** (1–2), 35–53.
- Flugel, W. A. 1995 Delineating hydrological response units by geographical information-system analyses for regional hydrological modeling using PRMS/MMS in the drainage-basin of the River Brol, Germany. *Hydrological Processes* **9** (3–4), 423–436.
- Flugel, W. A. 1997 Combining GIS with regional hydrological modelling using hydrological response units (HRUs): an application from Germany. *Mathematics and Computers in Simulation* **43** (3–6), 297–304.
- Gassman, P. W., Reyes, M. R., Green, C. H. & Arnold, J. G. 2007 The soil and water assessment tool: historical development, applications, and future research directions. *Transactions of the ASABE* **50** (4), 1211–1250.
- Geonorge 2013 *Height DTM 10*. Available from: <https://kartkatalog.geonorge.no/metadata/kartverket/dtm-10-terrengmodell-utm33/>.
- Gong, Y. W., Shen, Z. Y., Liu, R. M., Wang, X. J. & Chen, T. 2010 Effect of watershed subdivision on SWAT modeling with consideration of parameter uncertainty. *Journal of Hydrologic Engineering* **15** (12), 1070–1074.
- Goodrich, D. C. 1992 An overview of the USDA-ARS climate change and hydrology program and analysis of model complexity as a function of basin scale. In: *Proceedings of a Workshop: Effects of Global Climate Change on Hydrology and Water Resources at Catchment Scale*, Tsukuba, Japan, pp. 233–242.
- Han, E. J., Merwade, V. & Heathman, G. C. 2012 Implementation of surface soil moisture data assimilation with watershed scale distributed hydrological model. *Journal of Hydrology* **416**, 98–117.

- Haverkamp, S., Srinivasan, R., Frede, H. G. & Santhi, C. 2002 Subwatershed spatial analysis tool: discretization of a distributed hydrologic model by statistical criteria. *Journal of the American Water Resources Association* **38** (6), 1723–1733.
- Her, Y., Frankenberger, J., Chaubey, I. & Srinivasan, R. 2015 Threshold effects in HRU definition of the Soil and Water Assessment Tool. *Transactions of the ASABE* **58** (2), 367–378.
- Jha, M., Gassman, P. W., Secchi, S., Gu, R. & Arnold, J. 2004 Effect of watershed subdivision on swat flow, sediment, and nutrient predictions. *Journal of the American Water Resources Association* **40** (3), 811–825.
- Kalin, L., Govindaraju, R. S. & Hantush, M. M. 2003 Effect of geomorphologic resolution on modeling of runoff hydrograph and sedimentograph over small watersheds. *Journal of Hydrology* **276** (1–4), 89–111.
- Karvonen, T., Koivusalo, H., Jauhainen, M., Palko, J. & Weppling, K. 1999 A hydrological model for predicting runoff from different land use areas. *Journal of Hydrology* **217** (3–4), 253–265.
- Kumar, S. & Merwade, V. 2009 Impact of watershed subdivision and soil data resolution on SWAT model calibration and parameter uncertainty. *Journal of the American Water Resources Association* **45** (5), 1179–1196.
- Lacroix, M. P. 1999 *Spatial Scale and Hydrological Model Response*. PhD Thesis, University of Saskatchewan.
- Mamillapalli, S., Srinivasan, R., Arnold, J. & Engel, B. A. 1996 Effect of spatial variability on basin scale modeling. In: *Proceedings of the Third International Conference/Workshop on Integrating GIS and Environmental Modeling*, Santa Fe, New Mexico.
- Moges, A., Dagnachew, M. & Yimer, F. 2013 Land use effects on soil quality indicators: a case study of Abo-Wonsho Southern Ethiopia. *Applied and Environmental Soil Science* **2013**, 1–9.
- Moriasi, D. N., Arnold, J. G., Van Liew, M. W., Bingner, R. L., Harmel, R. D. & Veith, T. L. 2007 Model evaluation guidelines for systematic quantification of accuracy in watershed simulations. *Transactions of the ASABE* **50** (3), 885–900.
- Muleta, M. K., Nicklow, J. W. & Bekele, E. G. 2007 Sensitivity of a distributed watershed simulation model to spatial scale. *Journal of Hydrologic Engineering* **12** (2), 163–172.
- Mulungu, D. M. M. & Munishi, S. E. 2007 Simiyu River catchment parameterization using SWAT model. *Physics and Chemistry of the Earth* **32** (15–18), 1032–1039.
- Munoth, P. & Goyal, R. 2019a Effects of area threshold values and stream burn-in process on runoff and sediment yield using QSWAT model. *ISH Journal of Hydraulic Engineering*, 1–9.
- Munoth, P. & Goyal, R. 2019b Effects of DEM source, spatial resolution and drainage area threshold values on hydrological modeling. *Water Resources Management* **33** (9), 3303–3319.
- Nazari-Sharabian, M., Taheriyoun, M. & Karakouzian, M. 2020 Sensitivity analysis of the DEM resolution and effective parameters of runoff yield in the SWAT model: a case study. *Journal of Water Supply Research and Technology – AQUA* **69** (1), 39–54.
- Neitsch, S. L., Arnold, J. G., Kiniry, J. R. & Williams, J. R. 2009 Overview of soil and water assessment tool (SWAT) model. In: *Soil and Water Assessment Tool (SWAT): Global Application* (Arnold, J., Srinivasan, R., Neitsch, S., George, C., Abbaspour, K., Gassman, P., Fang, H. H., Av, G., Gosain, A., Debels, P., Kim, N. W., Somura, H., Ella, V., Leon, L., Jintrawet, A., Reyes, M. & Sombatpanit, S., eds). The World Association of Soil and Water Conservation (WASWC), Bangkok, pp. 3–23.
- Ning, J. C., Gao, Z. Q. & Lu, Q. S. 2015 Runoff simulation using a modified SWAT model with spatially continuous HRUs. *Environmental Earth Sciences* **74** (7), 5895–5905.
- Norris, G. & Haan, C. T. 1993 Impact of subdividing watersheds on estimated hydrographs. *Applied Engineering in Agriculture* **9** (5), 443–445.
- Nour, M. H., Smith, D. W., El-Din, M. G. & Prepas, E. E. 2008 Effect of watershed subdivision on water-phase phosphorus modelling: an artificial neural network modelling application. *Journal of Environmental Engineering and Science* **7**, S95–S108.
- Ogden, F. L. & Julien, P. Y. 1994 Runoff model sensitivity to radar rainfall resolution. *Journal of Hydrology* **158** (1–2), 1–18.
- Ozdemir, A., Leloglu, U. M. & Abbaspour, K. C. 2017 Hierarchical approach to hydrological model calibration. *Environmental Earth Sciences* **76** (8), 1–10.
- Pignotti, G., Rathjens, H., Cibin, R., Chaubey, I. & Crawford, M. 2017 Comparative analysis of HRU and grid-based SWAT models. *Water* **9** (4), 1–20.
- Premanand, B. D., Satishkumar, U., Maheshwara Babu, B., Parasappa, S. K., Dandu M, M., Kaleel, I., Rajesh, N. L. & Biradar, S. A. 2018 QSWAT model calibration and uncertainty analysis for stream flow simulation in the Patapur micro-watershed using Sequential Uncertainty Fitting Method (SUFI-2). *International Journal of Current Microbiology and Applied Sciences* **7** (4), 831–852.
- Reed, S., Koren, V., Smith, M., Zhang, Z., Moreda, F., Seo, D. J. & Participants, D. 2004 Overall distributed model intercomparison project results. *Journal of Hydrology* **298** (1–4), 27–60.
- Reggiani, P. & Rientjes, T. H. M. 2005 Flux parameterization in the representative elementary watershed approach: application to a natural basin. *Water Resources Research* **41** (4), 1–18.
- Rouhani, H., Willems, P. & Feyen, J. 2009 Effect of watershed delineation and areal rainfall distribution on runoff prediction using the SWAT model. *Hydrology Research* **40** (6), 505–519.
- Santhi, C., Arnold, J. G., Williams, J. R., Dugas, W. A., Srinivasan, R. & Hauck, L. M. 2001 Validation of the SWAT model on a large river basin with point and nonpoint sources. *Journal of the American Water Resources Association* **37** (5), 1169–1188.
- Savvidou, E., Tzoraki, O. & Skarlatos, D. 2014 Delineating hydrological response units in a mountainous catchment and its evaluation on water mass balance and model performance. In: *Second International Conference on Remote Sensing and Geoinformation of the Environment (Rscy2014)*, p. 9229.

- Sexton, A. M., Sadeghi, A. M., Zhang, X., Srinivasan, R. & Shirmohammadi, A. 2010 Using nexrad and rain gauge precipitation data for hydrologic calibration of swat in a northeastern watershed. *Transactions of the ASABE* **53** (5), 1501–1510.
- Sildre 2020 *Real-Time Hydrological Data*. The Norwegian Water Resources and Energy Directorate (NVE). Available from: <http://sildre.nve.no/> (accessed 18 November 2019).
- Smith, M. B., Koren, V. I., Zhang, Z., Reed, S. M., Pan, J. J. & Moreda, F. 2004 Runoff response to spatial variability in precipitation: an analysis of observed data. *Journal of Hydrology* **298** (1–4), 267–286.
- Srinivasan, R., Zhang, X. & Arnold, J. 2010 Swat ungauged: hydrological budget and crop yield predictions in the Upper Mississippi River Basin. *Transactions of the ASABE* **53** (5), 1533–1546.
- Szczypta, C., Gascoin, S., Houet, T., Hagolle, O., Dejoux, J. F., Vigneau, C. & Fanise, P. 2015 Impact of climate and land cover changes on snow cover in a small Pyrenean catchment. *Journal of Hydrology* **521**, 84–99.
- TAMU 2012 *CFSR: Global Weather Data for SWAT*. Available from: <https://globalweather.tamu.edu/> (accessed 5 July 2020).
- Tegegne, G., Kim, Y. O., Seo, S. B. & Kim, Y. 2019 Hydrological modelling uncertainty analysis for different flow quantiles: a case study in two hydro-geographically different watersheds. *Hydrological Sciences Journal* **64** (4), 473–489.
- Thielen, A. H., Lucke, A., Diekkruger, B. & Richter, O. 1999 Scaling input data by GIS for hydrological modelling. *Hydrological Processes* **13** (4), 611–630.
- Tripathi, M. P., Raghuvanshi, N. S. & Rao, G. P. 2006 Effect of watershed subdivision on simulation of water balance components. *Hydrological Processes* **20** (5), 1137–1156.
- Van Liew, M. W., Arnold, J. G. & Garbrecht, J. D. 2003 Hydrologic simulation on agricultural watersheds: choosing between two models. *Transactions of the ASAE* **46** (6), 1539–1551.
- Waterbase 2007a *Land Use*. Available from: http://www.waterbase.org/download_data.html (accessed 14 February 2021).
- Waterbase 2007b *Soil*. Available from: http://www.waterbase.org/download_data.html (accessed 14 February 2021).
- Woo, M. K. 1980 Hydrology of a small lake in the Canadian high Arctic. *Arctic and Alpine Research* **12** (2), 227–235.
- Wood, E. F., Sivapalan, M., Beven, K. & Band, L. 1988 Effects of spatial variability and scale with implications to hydrologic modeling. *Journal of Hydrology* **102** (1–4), 29–47.
- Zhang, Z. Y., Koren, V., Smith, M., Reed, S. & Wang, D. 2004 Use of next generation weather radar data and basin disaggregation to improve continuous hydrograph simulations. *Journal of Hydrologic Engineering* **9** (2), 103–115.

First received 30 April 2021; accepted in revised form 8 July 2021. Available online 28 July 2021

Supplementary material

Table S1. Model parameters and their ranges for calibration of TDA 200 ha scheme.

Parameter_Name	Fitted_Value	Min_value	Max_value
1:R_CN2.mgt	-0.140419	-0.225354	0.051306
2:V_ESCO.hru	0.137255	0.067328	0.202062
3:R_SOL_AWC(..).sol	-0.719963	-1	-0.58141
4:V_ALPHA_BF.gw	0.092278	0	0.120625
5:V_GW_DELAY.gw	313.35376	260.054504	321.814941
6:V_GW_REVAP.gw	0.185378	0.11655	0.185724
7:V_GWQMN.gw	3,284.766357	2,215.622559	3,318.970215
8:V_REVAPMN.gw	353.454437	252.175049	382.858124
9:V_SFTMP.bsn	-1.478742	-2.722426	0.990062
10:V_SMFMN.bsn	5.327663	1.767545	6.470475
11:V_SMFMX.bsn	2.905475	1.9135	5.743518
12:V_SMTMP.bsn	-0.563781	-3.189911	2.556543
13:V_TIMP.bsn	0.153424	0.145087	0.308557
14:A_CH_N2.rte	0.210441	0.144594	0.227212
15:A_CH_K2.rte	22.005863	-0.01	70.780556
16:R_SOL_K(..).sol	7.302452	4.482007	7.976982
17:R_SOL_BD(..).sol	0.527241	0.402725	0.635465
18:A_CANMX.hru	4.49081	4.016488	12.05584

Table S2. Model parameters and their ranges for calibration of TDA 2,000 ha scheme.

Parameter_Name	Fitted_Value	Min_value	Max_value
1:R_CN2.mgt	-0.202589	-0.244324	-0.109258
2:V_ESCO.hru	0.141132	0.126909	0.217501
3:R_SOL_AWC(..).sol	-0.770458	-0.898907	-0.696625
4:V_ALPHA_BF.gw	0.080682	0.060437	0.125955
5:V_GW_DELAY.gw	280.552307	260.572845	299.825226
6:V_GW_REVAP.gw	0.128529	0.128006	0.152908
7:V_GWQMN.gw	2,933.4104	2,632.426514	3,242.94165
8:V_REVAPMN.gw	353.934723	319.5625	386.827148
9:V_SFTMP.bsn	-0.776701	-2.957009	-0.235027
10:V_SMFMN.bsn	6.132335	4.344446	6.532805
11:V_SMFMX.bsn	2.101861	0.052462	2.643358
12:V_SMTMP.bsn	-1.44298	-2.561037	-0.226889
13:V_TIMP.bsn	0.162583	0.087159	0.195061
14:A_CH_N2.rte	0.216995	0.148336	0.2189
15:A_CH_K2.rte	20.01582	-0.01	28.804127
16:R_SOL_K(..).sol	7.47199	6.671738	8.134722
17:R_SOL_BD(..).sol	0.465665	0.408225	0.553643
18:A_CANMX.hru	7.735365	5.416529	8.378006

Table S3. Model parameters and their ranges for calibration of TDA 5,000 ha scheme.

Parameter_Name	Fitted_Value	Min_value	Max_value
1:R_CN2.mgt	-0.218662	-0.2305	-0.042592
2:V_ESCO.hru	0.038918	0.027637	0.143937
3:R_SOL_AWC(..).sol	-0.831782	-0.981414	-0.71469
4:V_ALPHA_BF.gw	0.054165	0.036839	0.110565
5:V_GW_DELAY.gw	293.679962	262.611511	302.088562
6:V_GW_REVAP.gw	0.147794	0.147637	0.2
7:V_GWQMN.gw	2,724.644775	1,953.468628	2,863.948242
8:V_REVAPMN.gw	313.664642	297.182465	387.248932
9:V_SFTMP.bsn	-1.872779	-3.593377	-0.537253
10:V_SMFMN.bsn	3.98527	3.232036	6.162907
11:V_SMFMX.bsn	2.285399	0.750716	4.079747
12:V_SMTMP.bsn	0.010809	-1.848708	1.088918
13:V_TIMP.bsn	0.357964	0.216262	0.358676
14:A_CH_N2.rte	0.16136	0.134631	0.196361
15:A_CH_K2.rte	17.719742	-0.01	42.507366
16:R_SOL_K(..).sol	7.125256	5.856942	8.608164
17:R_SOL_BD(..).sol	0.523839	0.481252	0.638398
18:A_CANMX.hru	9.633927	7.147029	13.411258

Table S4. Model parameters and their ranges for calibration of TDA 10,000 ha scheme.

Parameter_Name	Fitted_Value	Min_value	Max_value
1:R_CN2.mgt	-0.26423	-0.335077	-0.077451
2:V_ESCO.hru	0.041533	0.000554	0.13491
3:R_SOL_AWC(..).sol	-0.541184	-0.82821	-0.484466
4:V_ALPHA_BF.gw	0.076619	0.043474	0.130468
5:V_GW_DELAY.gw	255.968231	255.570694	299.74176
6:V_GW_REVAP.gw	0.12278	0.100737	0.157403
7:V_GWQMN.gw	2,586.822021	2,393.70459	3,010.693359
8:V_REVAPMN.gw	360.228058	288.296051	360.589508
9:V_SFTMP.bsn	-1.541736	-4.205944	-0.741434
10:V_SMFMN.bsn	3.64668	0.918192	4.620346
11:V_SMFMX.bsn	1.543673	0.566868	4.018476
12:V_SMTMP.bsn	-1.379928	-2.279684	0.945248
13:V_TIMP.bsn	0.193803	0.18602	0.26795
14:A_CH_N2.rte	0.188068	0.124717	0.193057
15:A_CH_K2.rte	10.059103	-0.01	45.551552
16:R_SOL_K(..).sol	6.843474	5.661222	8.021008
17:R_SOL_BD(..).sol	0.465102	0.304835	0.525285
18:A_CANMX.hru	3.596716	1.23811	8.450973

Note:

- The term "A_" explains that a given value is added to the existing parameter value.
- The term "R_" explains that an existing parameter value is multiplied by (1 + a given value).
- The term "V_" explains that the existing parameter value is replaced by a given value.

Table S5. Description of calibrated model parameters.

Parameter Name	Description	Subgroup process
CN2.mgt	SCS runoff curve number f	surface runoff
CANMX.hru	Maximum canopy storage	surface runoff
ESCO.hru	Soil evaporation compensation factor	lateral flow
SOL_AWC(..).sol	Available water capacity of the soil layer	lateral flow
SOL_BD(..).sol	Moist bulk density	lateral flow
SOL_K(..).sol	Saturated hydraulic conductivity	lateral flow
SMTMP.bsn	Snow melt base temperature	snowmelt
TIMP.bsn	Snow pack temperature lag factor	snowmelt
SMFMN.bsn	Minimum melt rate for snow during the year (occurs on winter solstice)	snowmelt
SMFMX.bsn	Maximum melt rate for snow during year (occurs on summer solstice)	snowmelt
SFTMP.bsn	Snowfall temperature	snowmelt
CH_K2.rte	Effective hydraulic conductivity in main channel alluvium	Channel water routing
CH_N2.rte	Manning's "n" value for the main channel	Channel water routing
ALPHA_BF.gw	Baseflow alpha factor (days)	ground water
GW_REVAP.gw	Groundwater "revap" coefficient	ground water
GWQMN.gw	Threshold depth of water in the shallow aquifer required for return flow to occur (mm)	ground water
REVAPMN.gw	Threshold depth of water in the shallow aquifer for "revap" to occur (mm)	ground water
GW_DELAY.gw	Groundwater delay (days)	ground water

Paper IV

Bui, Minh Tuan; Lu, Jinmei; Nie, Linmei. Projections of future floods in Norwegian Arctic catchments under climate change context (manuscript).

1 **Projections of future floods in Norwegian Arctic**
2 **catchments under climate change context**

3
4
5
6

7 **Minh Tuan Bui** ^{1,*}, **Jinmei Lu** ¹, **Linmei Nie** ²

8 ¹ Department of Technology and Safety, Faculty of Science and Technology, UiT The Arctic University of Norway,
9 9037 Tromsø, Norway; jinmei.lu@uit.no

10 ² Centre for Sustainable Development and Innovation of Water Technology, Foundation CSDI WaterTech, 0373 Oslo,
11 Norway; linmei.nie@csdi.no

12
13
14
15
16
17

* Corresponding author at: Department of Technology and Safety, Faculty of Science and Technology, UiT The Arctic
University of Norway, 9037 Tromsø, Norway
E-mail address: minh.t.bui@uit.no (Minh Tuan Bui)

18 **Abstract**

19 Climate change (CC) is expected to alter hydrological cycle in the Arctic, which may lead to increase intensity
20 and frequency of hydrological extremes, including floods. The changes in flooding due to CC are expected to
21 significantly impact on human life, infrastructures, the environment, ecosystem, and socio-economic
22 development of the affected areas. However, projections of flood changes may be more complicated in the
23 region with highly heterogeneous hydrological regimes like Norway. Thus, this study conducted an
24 investigation of CC impacts on future changes in magnitude and frequency of floods. Six Norwegian Arctic
25 catchments, which were further categorised into two rainfall-dominated, three snowmelt-dominated, and one
26 mixed rainfall/snowmelt catchments, were investigated. The state-of-the-art Soil and Water Assessment Tool
27 (SWAT) was coupled to five ensemble Global and Regional Climate Models, developed by EURO-CORDEX
28 initiative project, to perform flood projections. Nine flood quantiles, i.e., 2-,5-,10-,20-,50-,100-,200-,500-, and
29 1000-year floods were estimated, of which the 200-,500-, and 1000-year floods were defined extreme floods,
30 while the 2-, and 5-year floods were small floods. High emission scenario (RCP8.5) was applied to examine
31 flood changes from the reference period (1976-2005) to the near future (2041-2070). This study found that
32 upward trend of annual air temperature was projected (+1.2 to +5.0°C), while annual rainfall would be high
33 fluctuation (-46.0 to +36%). Noticeably, the reduction of rainfall would be higher for rainfall-dominated
34 catchments than that for snowmelt-dominated catchments. This would result in decreases (-25 to <-5%) but
35 increases (>1 to <22%) of the (median) future flood magnitudes for rainfall-dominated catchments and
36 snowmelt-dominated catchments, respectively. The mixed catchment is expected to experience both decrease
37 (small flood, >-2%) and increase (<4 to <14%) patterns. Compared to the reference period, extreme flood
38 events in the near future period are projected to occur more frequent, but with lower magnitudes, in northern
39 (snowmelt-dominated) and southern (rainfall-dominated) catchments. Such behaviors would oppose to inland
40 catchments in the centre of the Norwegian Arctic with snowmelt regimes. The changes in future small flood
41 events would be in the opposite behaviors to those of the extreme floods. Furthermore, the changes in future
42 extreme flood events are expected to be complicated in the rainfall-dominated catchment and near the coast
43 due to high variation of future rainfall in this region. Finally, uncertainties in floods projection were detected
44 in the climate-hydrology modelling chain, and level of uncertainty was dissimilar regarding catchments'
45 scales, and the dominant flood regimes.

46 **Keywords:** Norwegian Arctic, climate change, global and regional climate models, SWAT, future floods,
47 rainfall/snowmelt regime.
48

49 **Funding source:**

50

51 This work was supported by Department of Technology and Safety, Faculty of Science and Technology, UiT

52 The Arctic University of Norway.

53

54 Introduction

55 Flooding is one of the most destructive natural hazards (Xu *et al.* 2019; Engeland *et al.* 2020), which has a
56 significantly impact on human life, infrastructures, the environment, ecosystem, and the socio-economic
57 development of the affected areas (McGrath *et al.* 2015; Vinet 2017; Quintero *et al.* 2018; Talbot *et al.* 2018).
58 It has been stated in various studies that the economic damages and other consequences caused by flooding are
59 increasing together because of climate change (Field *et al.* 2012; Murray & Ebi 2012; Hirabayashi *et al.* 2013;
60 Alfieri *et al.* 2017; Engeland *et al.* 2020). Noticeably, climate change have increased the magnitude and
61 frequency of floods (IPCC 2013; Quintero *et al.* 2018), which result in severely impacts on the society (Nemry
62 & Demirel 2012; Doocy *et al.* 2013). Magnitude and frequency of floods are defined as important indicators of
63 flood hazard indexes for flood risk assessment and mitigation (Richter *et al.* 1996; Logsdon & Chaubey 2013;
64 Xu *et al.* 2019). Recently, several international studies concluded that the magnitude and frequency of design
65 floods, particularly the extremely high floods, are influenced by climate change and landuse change, among
66 other impact factors (Rojas *et al.* 2013; Madsen *et al.* 2014; Alfieri *et al.* 2015; Mallakpour & Villarini 2015).
67 According to that, it is necessary to estimate the changes in the future magnitude and frequency of floods
68 compared to the historical scenarios under climate change. It aims to support for flood mitigation measures to
69 resist the future climate changes.

70 However, projections of floods exists numerous challenges regarding to the reliability of future climate change
71 data (e.g., the selections of climate change scenarios, climate models, and the ways to transfer climate change
72 information from global scale to catchment scale) as well as uncertainties (e.g., in the climate-hydrology
73 modelling chain) of the projections. Normally, flood frequency is estimated based on time series data of river
74 discharge at an interested hydro-gauging station. However, future streamflows are not available and normally
75 estimated based on modelling. Recently, coupling climate models and hydrological models is preferred by the
76 scientists to estimate future streamflows under the climate change impacts (Lawrence & Hisdal 2011; Meresa
77 *et al.* 2016). The methodology of such coupling models is running the hydrological models using climate data
78 inputs which are projected by the General Circulation Models (GCMs). The GCMs are the great and common
79 tools to produce the projected climate data for the future climate conditions (Chen *et al.* 2021). However, their
80 spatial resolutions are usually coarse (approx. 111-222 km grid (Flato *et al.* 2013)) and they do not have
81 capacities to simulate accurately the physical and dynamical processes of the climate system at the watershed
82 scales or local scales (Chen *et al.* 2021). Although the GCMs are physically based, there still exist numerous
83 empirically numerical approximations of the sub-grid processes (IPCC 2015). Such simplifications may cause
84 significant mistakes when directly transferring the climate model outputs into the impacts models (IPCC 2015).
85 Thus, outputs from the GCMs are seldom directly used as inputs for the hydrological models for impacts
86 assessment because of the biases. Instead, downscaling and/or bias-correction of climate data outputs from the
87 GCMs, e.g. using the Regional Climate Models (RCMs), are normally performed prior to drive the hydrological
88 models (Wilby *et al.* 2002; Zhang 2005; Schmidli *et al.* 2006; Chen *et al.* 2011a). Various bias correction
89 methods, such as the simple-skill mean-based linear scaling (correcting the mean values between climate model
90 simulations and observation data), or the higher-skill distribution-based quantile mapping (taking into account
91 the higher moments of a distribution), have been applied to significantly reduce biases of the climate models
92 outputs (Piani *et al.* 2010; Teutschbein & Seibert 2013; Chen *et al.* 2018; Chen *et al.* 2019; Gutierrez *et al.*
93 2019; Chen *et al.* 2021). However, most of bias correction methods work based on the hypothesis of stationary
94 bias, but ignore the nonstationary of the future climate conditions. It means that the magnitude of bias/error is
95 assumed to be constant over the time, from historical to future period (Chen *et al.* 2021). In addition, bias
96 correction methods normally adjust the climate variables independently and disregard the inter-variable
97 dependence, which is very important to correct evaluation of climate change impacts. Because of the limitations
98 of bias correction methods for the climate model simulations, the reliability of bias correction is questioned
99 among scientific community (Maraun 2012; Chen *et al.* 2015; Hui *et al.* 2019; Chen *et al.* 2020). Therefore, the
100 parallel use of raw and bias-corrected climate model outputs in hydrological modelling has been investigated.
101 Some previous studies found that using raw climate model outputs to drive the hydrological model yielded
102 reliable projections of future flood risk (Meresa & Romanowicz 2017; Xu *et al.* 2019).

103 Moreover, there are always high uncertainties in the assessment of climate change impacts on hydrology and
104 water resources (Jones 2000; Heal & Kristrom 2002; Collins *et al.* 2006; Ghosh & Mujumdar 2007; Dunn *et al.*
105 2012; Jung *et al.* 2012). The uncertainties come from (1) future emission scenarios, (2) General Circulation

106 Models-GCMs (e.g., initial conditions of the GCMs), (3) techniques for downscaling the GCMs or bias
 107 correction of the raw GCMs' outputs, and (4) hydrological models (e.g., structures and parameterization of the
 108 hydrological models) etc. (Kay *et al.* 2009; Zhang *et al.* 2014; Meresa & Romanowicz 2017). Of the uncertainty
 109 sources, the structures of the GCMs are the most uncertain sources (Kay *et al.* 2009; Chen *et al.* 2011b;
 110 Woldemeskel *et al.* 2012). However, other studies argued that the significant sources of uncertainties could be
 111 from (a) future emission scenarios (Maurer 2007), (b) downscaling techniques (Khan *et al.* 2006), or (c)
 112 hydrological models (Najafi *et al.* 2011). Thus, there has not been a scientific consensus on the sources of
 113 uncertainties in climate change impacts assessment on water resources systems yet. In addition, the uncertainties
 114 sources could be highly variant among the studied catchments around the world with different characteristics
 115 and climate conditions (Chen *et al.* 2017; Chen *et al.* 2021). Therefore, investigation of the uncertainties of
 116 future projections in climate change impacts has been highly recommended by the scientific communities for
 117 adaption strategies (Katz *et al.* 2013). Taking into that concern, the uncertainties of the projections of future
 118 flood frequency, and subsequent flood risk assessment in the extreme climate like the Arctic should be included
 119 together with the projection analysis.

120 Consideration of the above issues, projections of changes in future floods may be more complicated in the
 121 region with highly heterogeneous hydrological regimes like Norway. Thus, this study contributed to shed more
 122 light on how future climate change could alter flooding in the region having complex hydrological processes,
 123 and highly sensitive to climate change compared to rest of the world. In particular, this study coupled state-of-
 124 the-art Soil and Water Assessment Tool (SWAT) (Jayakrishnan *et al.* 2005; Setegn *et al.* 2011; Ficklin *et al.*
 125 2012; Zhang *et al.* 2013; Xu *et al.* 2019) with multiple ensemble GCM_RCM simulations (both raw and bias
 126 correction) to project the changes in magnitude and frequency of floods, from the reference period (1976-2005)
 127 to the near future (2041-2070) of the 21st century, in six Norwegian Arctic catchments. Those catchments were
 128 classified into three different flood regimes, i.e., rainfall-dominated, snowmelt-dominated, and mixed
 129 rainfall/snowmelt regimes. Uncertainties of the projections were also investigated. Findings from this study
 130 aimed to answer the following research questions:

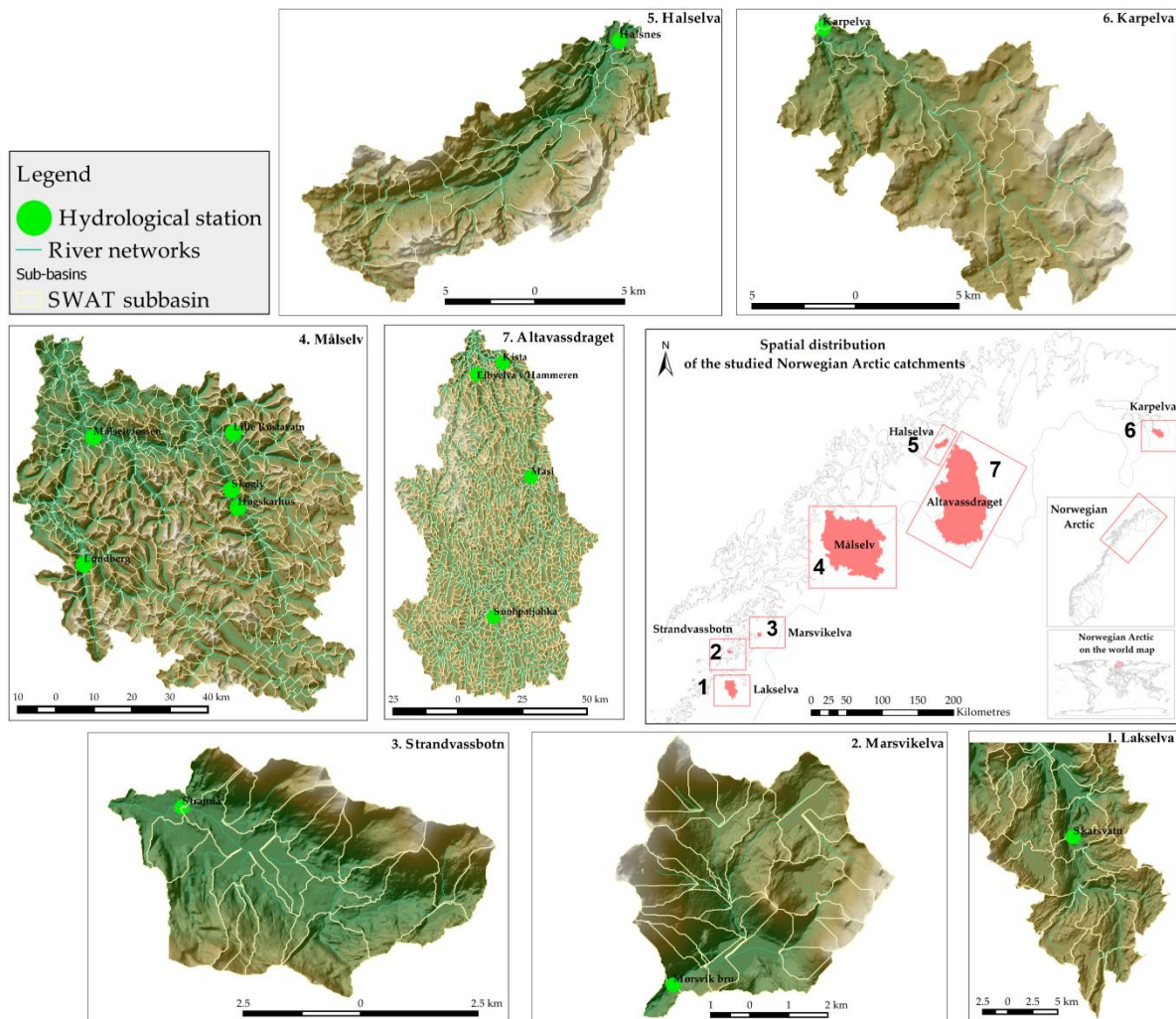
131 When investigating the impacts of climate change on future floods (in 2041-2070 period) in different
 132 Norwegian Arctic catchments with variation in geographical distribution, latitudes, characteristics,
 133 scales/sizes, and the dominant hydrological regimes:

- 134 1. How are the performances of the hydrological SWAT model to reconstruct/estimate the daily
 135 streamflows in different Norwegian Arctic catchments quantified?
- 136 2. Do bias-corrected and raw climate models' simulations have similar/different performances to project
 137 future climate change as well as to drive the hydrological model SWAT in the Arctic environment?
- 138 3. How are the changes in magnitudes and frequencies of floods under future climate conditions in
 139 different Norwegian Arctic catchments estimated?
- 140 4. How are the future changes in small-size floods and large-size/extreme floods in different Norwegian
 141 Arctic catchments projected?
- 142 5. To what extent are the uncertainties of the projected floods in the Arctic environment measured?

143 **Study area**

144 The selection of studied catchments in this study was based on several criteria: (1) geographical distribution i.e.
 145 from coastal zones to inland areas, and latitude distribution, i.e. from southern region to northern region, and
 146 above the Arctic circle, (2) catchments' scales (i.e. small-scale and large-scale), and (3) flood regimes. The
 147 flood regimes in Norway were classified into three types: (1) rainfall-dominated, (2) snowmelt-dominated, and
 148 (3) mixed rainfall/snowmelt-dominated, according to the Norwegian Water Resources and Energy Directorate
 149 (NVE) (Lawrence & Hisdal 2011). A catchment is identified as rainfall-dominated flood regime if at least two-
 150 thirds percentage (approx. 67%) of annual peak flows occurs inside the period of August-February, when most
 151 of rainfall contributes to peak flows. In contrast, a snowmelt-dominated flood regime is defined if at least two-
 152 thirds percentage of annual peak flows occur inside the snowmelt season from March-July. When a catchment
 153 has glacier cover > 25% of the total catchment area, the snowmelt season could expand to August. In case a
 154 catchment with the percentage of annual peak flow occurring during August-February (rainfall-dominated) and
 155 March-July (snowmelt-dominated) is smaller than 67%, they are recognized as mixed rainfall/snowmelt-
 156 dominated flood regime. This study used 30-year daily observed discharges (1976-2005) for flood regime

157 classification. Totally, six catchments locating above the Arctic circle were selected as study catchments, which
 158 are categorized into two rainfall-dominated, three snowmelt-dominated, and one mixed rainfall/snowmelt
 159 catchments (Fig. 1 and Table 1). In addition, one more large-scale catchment Altavassdraget (Fig. 1, numbered
 160 7) is used for verification of the transferability of the calibrated model parameters from one catchment to
 161 another, according to their geographical proximity and hydrological similarity.
 162



163

164

Fig. 1. Map of study areas and the Norwegian Arctic subcatchments.

166

167

168

169

Table 1. General characteristics of the studied Norwegian Arctic catchments.

Region	Catchment	Area (km ²)	No. of sub-basins	No. of HRUs	Glacial cover (%)	Drainage density (km km ⁻²)	Elevation distribution (m)	Average overland sub-basin slope (%)	Average annual precipitation ^a (mm)	Average annual air temperature ^b (°C)	Gauging stations	Annual peak flow in March-July (%)	Annual peak flow in August-February (%)	Flood regimes classification
Nordland	Lakselva	297	24	220	0	0.33	0-1112	20.09	750-1500	+2 to +8	Skarsvatn	57	43	Mixed
	Strandvassbotn	26	22	146	0	0.93	0-944	36.72	1000-1500	+2 to +10	Strandå	27	73	Rainfall
	Marsvikelva	32	27	168	0	0.85	0-1098	37.14	1000-1500	+2 to +8	Mørsvik bru	20	80	Rainfall
Troms	Målselv	5815	459	5601	~ 5	0.33	0-1718	25.95	<500-1500	-5 to +6	Lundberg	93	7	Snowmelt
											Lille Rostavatn	100	0	Snowmelt
											Høgestadhus	100	0	Snowmelt
											Skogly	100	0	Snowmelt
											Målselvfossen	100	0	Snowmelt
Finnmark	Alavassdraget	6902	1376	8320	0	0.55	2-973	6-54	<500-750	-3 to +6	Masi	100	0	Snowmelt
											Kista	100	0	Snowmelt
											Halsnes	100	0	Snowmelt
	Karpelva	129	27	169	0	0.57	3-404	7.80	500-750	-1 to +4	Karpelva	100	0	Snowmelt

^{a,b} averaged values based on 30-year observed data (1991-2020) (source: The Norwegian Water Resources and Energy Directorate - NVE).

170

170 Materials and methods

171 1.1. QSWAT model

172 The QSWAT model was used in this research (version 1.9), which is a coupling of physically-based, semi-
 173 distributed SWAT model (version 2012) (Neitsch *et al.* 2009) and the open source QGIS (version 2.6.1). The
 174 SWAT model includes two important phases to describe the hydrological cycle in a catchment, including land
 175 phase and routing phase (Du *et al.* 2013). The land phase works according to the following water balance
 176 equation (Eq. (1)):
 177

$$SW_t = SW_0 + \sum_{i=1}^t (R_i - Q_i - E_i - P_i - QR_i), \quad (1)$$

178 Where

- 179 • SW_t : soil water content at time t (mm),
- 180 • SW_0 : the initial soil water content (mm),
- 181 • R_i : amount of precipitation on day i (mm),
- 182 • Q_i : amount of surface runoff on day i (mm),
- 183 • E_i : amount of evapotranspiration on day i (mm),
- 184 • P_i : amount of percolation on day i (mm), and
- 185 • QR_i : amount of return flow on day i (mm).

186 While, the routing phase simulates various in-stream processes i.e. water movement, sediments, flow mass,
 187 transformation of chemicals in the stream and streambed.

188 1.2. Data acquisition

189 To run SWAT model, intensive spatial-temporal data were gathered (Table 2), including climate data (e.g.,
 190 precipitation, maximum and minimum air temperature, wind speed, relative humidity, solar radiation), and
 191 spatial data i.e. land use (Waterbase 2007a), soil (Waterbase 2007b) and topography (typically digital elevation
 192 model (DEM), (Geonorge 2013)). This study used climate data from climate forecast system reanalysis (CFSR)
 193 (Saha *et al.* 2010) because of its high-spatial resolution and continuous time series data (Table 2 and Figure 2,
 194 (TAMU 2012)). The high reliability for using CFSR in the Norwegian Arctic has been demonstrated and
 195 validated in a previous study (Bui *et al.* 2021). Moreover, daily time series of river discharge were also collected
 196 from the Norwegian Water Resources and Energy Directorate (Sildre 2020) for calibration and validation of the
 197 SWAT.

198 **Table 2.** Summary of data inputs and their sources for using in the SWAT model.

Data type		Spatial resolution	Temporal resolution	Sources
Spatial data (grid)	DEM	10 x 10 m		(Geonorge 2013)
	Land use	~600 m		(Waterbase 2007a)
	Soil	~5000 m		(Waterbase 2007b)
Temporal data (time series)	Climate data: CFSR	~38 km grid	Daily	(TAMU 2012)
	EURO-CORDEX RCMs	~12.5 km grid	Daily	(Jacob <i>et al.</i> 2014)
	River discharge		Daily	(Sildre 2020)

199
 200
 201
 202
 203
 204

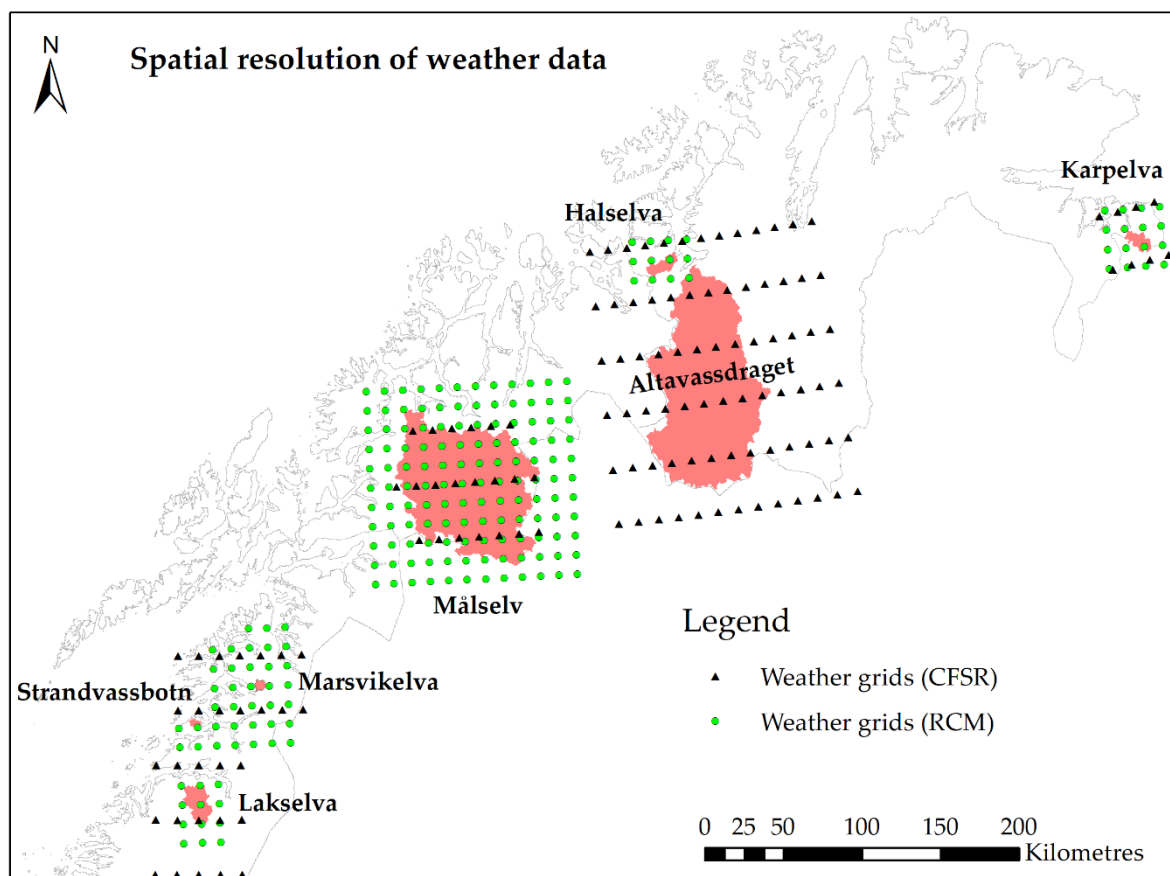


Fig. 2. Spatial resolution of weather inputs from CFSR and GCM_RCMs.

1.3. Climate models data

To conduct climate change impacts assessment, the projected climate change data (e.g., precipitation, max and min air temperature) were collected from five RCMs driven by four GCMs, which were generated by the EURO-CORDEX (Coordinated Downscaling Experiment for Europe) initiative project (Jacob *et al.* 2014). This study used data from the EUR-11 grid with spatial resolution of approx. 12.5 km (Table 3 and Fig. 2).

Table 3. Summary of the climate models data.

GCMs	RCMs	Denote of ensemble models	Institutes	Spatial resolution	RCP	Ensemble	Reference period	Future period	Bias correction method
ICHEC-EC-EARTH	RCA4_v1	GCM_RCM1	SMHI						Not applicable
ICHEC-EC-EARTH	RACMO22E_v1	GCM_RCM2	KNMI						CDFt
MPI-M-MPI-ESM-LR	REMO2009_v1	GCM_RCM3	MPI-CSC	-12.5 km	8.5	r1i1p1	1976-2005	2041-2070	CDFt
CNRM-CERFACS-CNRM-CM5	CCLM4-8-17_v1	GCM_RCM4	CLMcom						CDFt
IPSL-IPSL-CM5A-MR	WRF331F_v1	GCM_RCM5	IPSL-INERIS						CDFt

205
206

207

208

209

210

211

212

213

214 Moreover, the high-emission scenario of the Representative Concentration Pathway (RCP) 8.5 was applied
 215 according to the national guidance for climate change adaption in Norway (Miljøverndepartement 2012). The
 216 30-years time slice of the near future (2041-2070) was used compared to the 30-years time slice of the reference
 217 (1976-2005). Of the five RCMs (Table 3), the outputs of the four RCMs (e.g., precipitation and air temperature)
 218 were bias corrected within the framework of the EURO-CORDEX project using the general Cumulative
 219 Distribution Function transformation method (CDFt) (Vrac *et al.* 2012), and one remaining RCM output was
 220 raw or unbiased-corrected. The purpose of integrating the raw climate model simulation in this study was to
 221 compare performance of the raw and bias-corrected climate data in the projections of future flood changes.

222 1.4. Model running, calibration, and validation

223 Based on input of the CFSR data, the SWAT model picks up the representative weather grid for each sub-basin
 224 based on the method of the nearest neighbor search. The SWAT model run on daily time step from 1995-2007
 225 based on the relatively latest of the available CFSR input. The first three years (1995-1997) was for warming
 226 up, and the remaining ten years (1998-2007) was for model calibration. According to the available climate
 227 inputs of the CFSR dataset, the model was validated from 1981-2005 to verify that the calibrated model
 228 parameters could work well for a long-term period. However, the time length for validation are not the same
 229 among hydro-gauging stations (i.e. variation from 20 to 25 years) and depended on the available measured river
 230 discharges from each of the catchments. In addition, the study employed the Sequential Uncertainty Fitting
 231 Version 2 (SUFI-2) algorithm in the SWAT Calibration Uncertainties Program (SWAT_CUP) for model
 232 calibration, model validation, parameters sensitivity and uncertainty analyses (Abbaspour *et al.* 2007). Total 21
 233 model parameters, which were categorised into five different hydrological subgroup processes i.e. snowmelt,
 234 surface runoff, lateral runoff, channel water routing and ground water, were calibrated and validated
 235 (supplementary Table S1 to Table S7). These parameters were the most sensitivity parameters for streamflow
 236 calibration (Abbaspour *et al.* 2007; Abbaspour *et al.* 2015). 2,000-2,500 simulations were performed for each
 237 catchment to achieve the optimal model parameters. In addition, cross-validation was conducted to verify if the
 238 calibrated model parameters from one catchment could also perform well in another catchment, or the
 239 transferability of the calibrated model parameters. The SUFI-2 algorithm produces all stochastic results
 240 confined in a so-called 95PPU (95 Percent Prediction Uncertainty) band. Such values are calculated at the 2.5%
 241 (lower) and 97.5% (upper) levels of an output hydrological variable, and do not allow 5% of the very bad
 242 simulations.

243 1.5. Evaluation of model performance

244 In this study, three statistical coefficients were employed to quantify the goodness of fit between simulated and
 245 measured data including: (1) the coefficient of determination R^2 (Eq. (2)), measuring the fitness of the linear
 246 relationship between the simulated and observed values; (2) the Nash-Sutcliffe coefficient of efficiency NSE
 247 (Eq. (3)); and (3) root mean square error, divided by the standard deviation-RSR (Eq. (4)).

$$R^2 = 1 - \frac{\sum_{i=1}^n (Y_i^{obs} - Y_{mean}^{obs})(Y_i^{sim} - Y_{mean}^{sim})}{\left[\sum_{i=1}^n (Y_i^{obs} - Y_{mean}^{obs})^2 \right]^{1/2} \left[\sum_{i=1}^n (Y_i^{sim} - Y_{mean}^{sim})^2 \right]^{1/2}} \quad (2)$$

$$NSE = 1 - \frac{\sum_{i=1}^n (Y_i^{obs} - Y_i^{sim})^2}{\sum_{i=1}^n (Y_i^{obs} - Y_{mean}^{obs})^2} \quad (3)$$

$$RSR = \frac{\left[\sum_{i=1}^n (Y_i^{obs} - Y_i^{sim})^2 \right]^{1/2}}{\left[\sum_{i=1}^n (Y_i^{obs} - Y_{mean}^{obs})^2 \right]^{1/2}} \quad (4)$$

248 Where

249 Y_i^{obs} and Y_i^{sim} describe the observed and simulated values at time i ,

250 Y_{mean}^{obs} and Y_{mean}^{sim} describe mean observed and simulated data for the entire evaluation period, and

251 n describes total number of observations/simulations.

252 The thresholds of three statistical coefficient R^2 , NSE and RSR for daily simulation are summarised in Table 4
 253 (Santhi *et al.* 2001; Van Liew *et al.* 2003; Fernandez *et al.* 2005; Moriasi *et al.* 2007; Premanand *et al.* 2018;
 254 Koycegiz & Buyukyildiz 2019).

255 **Table 4.** Thresholds of R^2 , NSE and RSR for evaluation of the hydrological model's performance.

Model performance	R^2	NSE	RSR
Very good	$0.75 < R^2 \leq 1.00$	$0.75 < NSE \leq 1.00$	$0.00 \leq RSR \leq 0.50$
Good	$0.60 < R^2 \leq 0.75$	$0.60 < NSE \leq 0.75$	$0.50 < RSR \leq 0.60$
Satisfactory	$0.50 < R^2 \leq 0.60$	$0.36 < NSE \leq 0.60$	$0.60 < RSR \leq 0.70$
Unsatisfactory	$0.25 < R^2 \leq 0.50$	$0.00 < NSE \leq 0.36$	$RSR > 0.70$

256 1.6. Establishing the ensemble of the hydrological projections

257 In the studies of climate change impacts, because of the uncertainties associated with climate change scenarios,
 258 the ensemble approaches i.e. using multiple models and/or multiple scenarios are normally recommended to
 259 achieve a wide spectrum of the possible outcomes. To achieve that, this study forced the SWAT model with
 260 inputs from five different RCMs driven by four different GCMs to gain the historical and future daily
 261 streamflows. Such simulated and projected streamflows were used in the later stage for estimating the changes
 262 in magnitudes and frequencies of the future floods.

263 1.7. Flood frequency analysis

264 The target of flood frequency analysis is to estimate a flood magnitude with a certain occurrence probability or
 265 return period (Cunnane 1989; Wilson *et al.* 2011). Various statistical distributions models have been developed
 266 for estimation of flood frequency at the specific sites such as Log-normal, Gumbel (Generalized Extreme Value
 267 Type I-EV1), Generalized Extreme Value (GEV), Gamma, Log-Pearson, Gaussian Normal, Pareto, Weibull,
 268 etc. (Cunnane 1989; Wilson *et al.* 2011). Of them, the distribution models producing the best fit to Norwegian
 269 catchments are normally either the Gumbel distribution (with two model parameters i.e. location parameter and
 270 scale parameter) or the GEV (with three model parameters i.e. location parameter, scale parameter, and shape
 271 parameter) (Midttømme *et al.* 2011; Wilson *et al.* 2011). However, for the length of river discharge time series
 272 data from 30-50 years, the Gumbel distribution is more recommended than the GEV distribution (Wilson *et al.*
 273 2011). In addition, the previous practical applications found that the GEV distribution model was highly
 274 sensitive to the outlying events, and the frequency curve could follow the specific peculiarities of the dataset
 275 distribution because of the high flexibility of the model with high number of parameters (Cunnane 1985;
 276 Saelthun & Andersen 1986; Wilson *et al.* 2011). Moreover, the shape parameter of the GEV distribution model
 277 is hard to estimate with short time series data and could yield high uncertainty of estimated extreme flood events
 278 with large return period quantiles (Odry & Arnaud 2017). According to the previous references, this study
 279 selected the Gumbel distribution for estimation of flood frequency based on each 30-year time series of the
 280 streamflow in the reference period (1976-2005) and the near future period (2041-2070). The Gumbel
 281 distribution has its cumulative distribution function (cdf) as follows (Singh 1998):

$$F(x) = \exp[-\exp^{-y}] \quad (5)$$

Where

$y = a(x - b)$: reduced variate

x : peak flow data

$a > 0$: a concentration parameter

$-\infty < b < x$: a parameter for measure of central tendency

Parameter a and b were estimated by the most popular method of moments (MOM) (Lowery & Nash 1970; Landwehr *et al.* 1979; Singh 1998)

Estimate the reduced variate y_t for a given return period T :

$$y_t = -\ln \left\{ \ln \left(\frac{T}{T-1} \right) \right\} \quad (6)$$

Where

$$T = \frac{1}{1-F}$$

282

283 This study examined the estimated peak flows for 2, 5, 10, 20, 50, 100, 200, 500,1000-years return periods
284 based on each daily flow dataset for the reference period (1976-2005) and the near future period (2041-2070),
285 and for every six investigated catchments.

286 **1.8. Uncertainties analysis**

287 Quantifying uncertainties in the estimation of floods is an indispensable procedure to minimize the over/under-
288 estimation of the flood scenarios, so does the planning of the flood mitigation measures (Wiltshire 1987; Wilson
289 *et al.* 2011). This study addressed the multiple uncertainty sources coming from the hydrological model SWAT
290 and the weather inputs from GCM_RCMs. Thus, the estimated flood frequencies were provided in tandem with
291 their uncertainties bands/envelopes. Herein, the 95PPU (95 Percent Prediction Uncertainty) band were applied,
292 where the optimal/expected results were present at the mean/median curve together with the upper limited curve
293 (at 97.5%) and lower limited curve (at 2.5%) of the uncertainty band. By doing this way, it is possible to produce
294 a wide spectrum of the projected results. The SWAT-CUP program generated the stochastic results of daily
295 simulated streamflow distributed within the 95PPU band. Such daily streamflows were generated from each
296 input of five GCM_RCMs for both reference period (1976—2005) and near future period (2041-2070). The
297 flood frequencies were, therefore, estimated for each option of GCM_RCMs input with their uncertainty
298 envelopes. According to the distribution of such uncertainty envelopes driven by each GCM_RCM input, the
299 uncertainty of the projected flood changes could be quantified. Moreover, the uncertainties were also identified
300 and compared among six catchments with three different flood regimes.

301 **Results and discussion**

302 **1.9. Evaluation of model performance**

303 Table 5 revealed that model performances were somewhat different among six catchments. Particularly, 60%
304 of the investigated gauging sites had good performances, while the remaining 40% of gauging sites had
305 satisfactory performances. The general trend could be observed that the simulation of daily streamflow by
306 SWAT model was better for the snowmelt-dominated catchments than that for the rainfall-dominated and mixed
307 catchments. The rainfall-dominated catchment locating nearby the coastal zone had lower performance than the
308 inland catchment. This could be because highly variant and the domination of precipitation in the coastal area
309 compared to the farther inland area. Moreover, the SWAT performed better for the large-scale catchments than
310 the smaller ones (supplementary Fig. S1- Fig. S4). Furthermore, model performances were different among
311 gauging stations at the large-scale and snowmelt-dominated catchment, e.g. the Målselv (Table 5,
312 supplementary Fig. S2 and Fig. S4). This explained high variation of local climate condition and catchments'
313 characteristics of the Norwegian Arctic catchments. Regarding model validation, this study verified that the
314 model could work well with the calibrated parameters for the long-term period (20-25 years). Thus, this study
315 concluded that the calibrated SWAT models were highly reliable for investigating the impacts of future climate
316 on floods.

317 **1.10. Transferability of the calibrated model parameters**

318 Table 6 demonstrated the relatively high transferability of the calibrated model parameters between the donors
319 and the recipients catchments, which have similar flood regimes, and geographical proximity. This finding could
320 open the doors for applying the method of transferring the models parameters between gauged and ungauged
321 catchments in the data-sparse environment. Also, finding from this study could satisfy the expectation of the
322 geographical transferability of the hydrological model's parameters from one to other locations, and that the
323 model parameters have physical relationship (Vörösmarty *et al.* 1989; Xu 1999). However, at the rainfall-
324 dominated catchment Strandvassbotn nearby the coastal, model performance was slightly lower than the
325 satisfactory threshold. This indicated that transferability of the model parameters was harder to perform in the
326 catchment where flow regime is high fluctuation because of high rainfall variation.

Table 5. Model performance in calibration (1998-2007) and validation period (1980s-2005).

Catchments	Total sub-basins	Gauging stations	Calibration (1998-2007)					Validation (1980s-2005)					Performance rating	
			Name	Sub-basin	No. of simulation	R ²	NSE	RSR	Performance rating	No. of simulation	R ²	NSE		RSR
Lakselva	24	Skarsvann	21	2,500	0.65	0.57	0.66	Satisfactory	500	0.67	0.60	0.63	1984-2005	Good
Målselv	459	Lundberg	381	2,000	0.58	0.55	0.67	Satisfactory	250	0.58	0.54	0.68	1981-2005	Satisfactory
		Lille Rostavann	402	2,000	0.76	0.64	0.60	Good	250	0.82	0.74	0.51	1981-2005	Good
		Høgskarhus	408	2,000	0.64	0.62	0.62	Good	250	0.64	0.57	0.66	1981-2005	Satisfactory
		Skogly	412	2,000	0.65	0.50	0.71	Satisfactory	250	0.66	0.37	0.79	1981-2005	Satisfactory
		Målselvfossen	444	2,000	0.61	0.60	0.63	Good	250	0.69	0.64	0.60	1981-2005	Good
Strandvassbom	22	Strandå	21	2,000	0.60	0.51	0.70	Satisfactory	500	0.54	0.42	0.76	1981-2005	Satisfactory
Marsvikelva	27	Mørsvik bru	26	2,000	0.69	0.65	0.59	Good	500	0.71	0.66	0.58	1986-2005	Good
Halselva	35	Halsnes	34	2,500	0.63	0.62	0.61	Good	500	0.65	0.63	0.61	1981-2005	Good
Karpelva	27	Karpelva	26	2,000	0.72	0.71	0.54	Good	500	0.73	0.71	0.53	1985-2005	Good

332

333

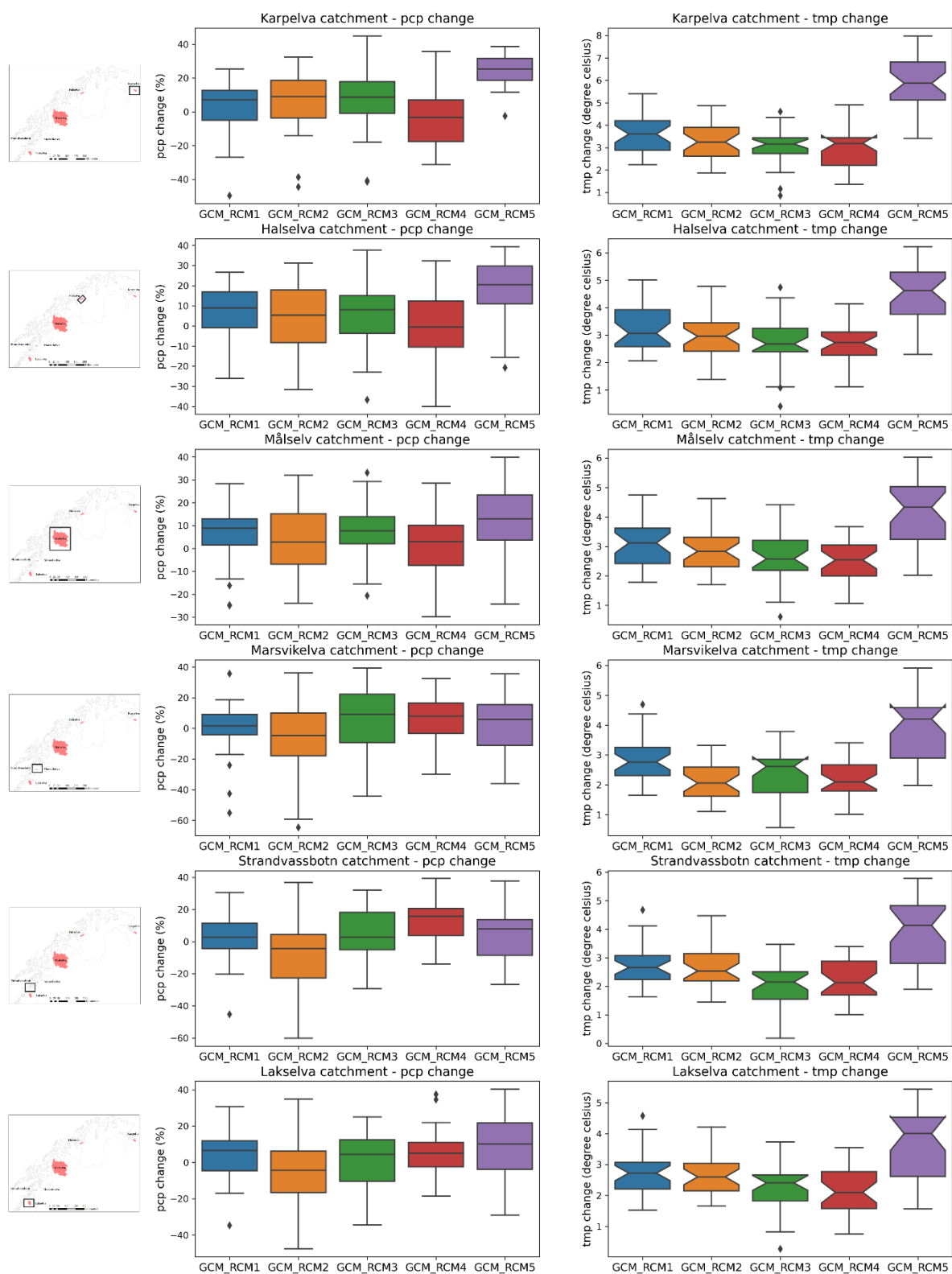
Table 6. Cross-validation of model performances (in 2008-2012 period).

Recipient catchments	Gauging stations	Donor catchments	Sub-basin	R ²	NSE	RSR	p-factor	r-factor	Performance rating
Altavassdraget		Målselv							
	Hammeren		1308	0.71	0.69	0.56	0.58	0.72	Good
	Suohpajohka		1318	0.67	0.65	0.59	0.75	1.05	Good
	Masi		1350	0.69	0.66	0.58	0.77	0.78	Good
	Kista		1370	0.68	0.67	0.58	0.70	0.85	Good
Karpelva	Karpelva	Halselva	26	0.48	0.46	0.73	0.91	0.86	Satisfactory
Halselva	Halsnes	Karpelva	34	0.71	0.69	0.56	0.97	1.45	Good
Marsvikelva	Mørsvik bru	Strandvassbom	26	0.68	0.65	0.59	0.63	1.22	Good
Strandvassbom	Strandå	Marsvikelva	21	0.45	0.35	0.81	0.56	0.37	Unsatisfactory

334

334 1.11. Projected changes in future climate

335 Fig. 3 presented the projected changes in future climate in six Norwegian Arctic catchments.



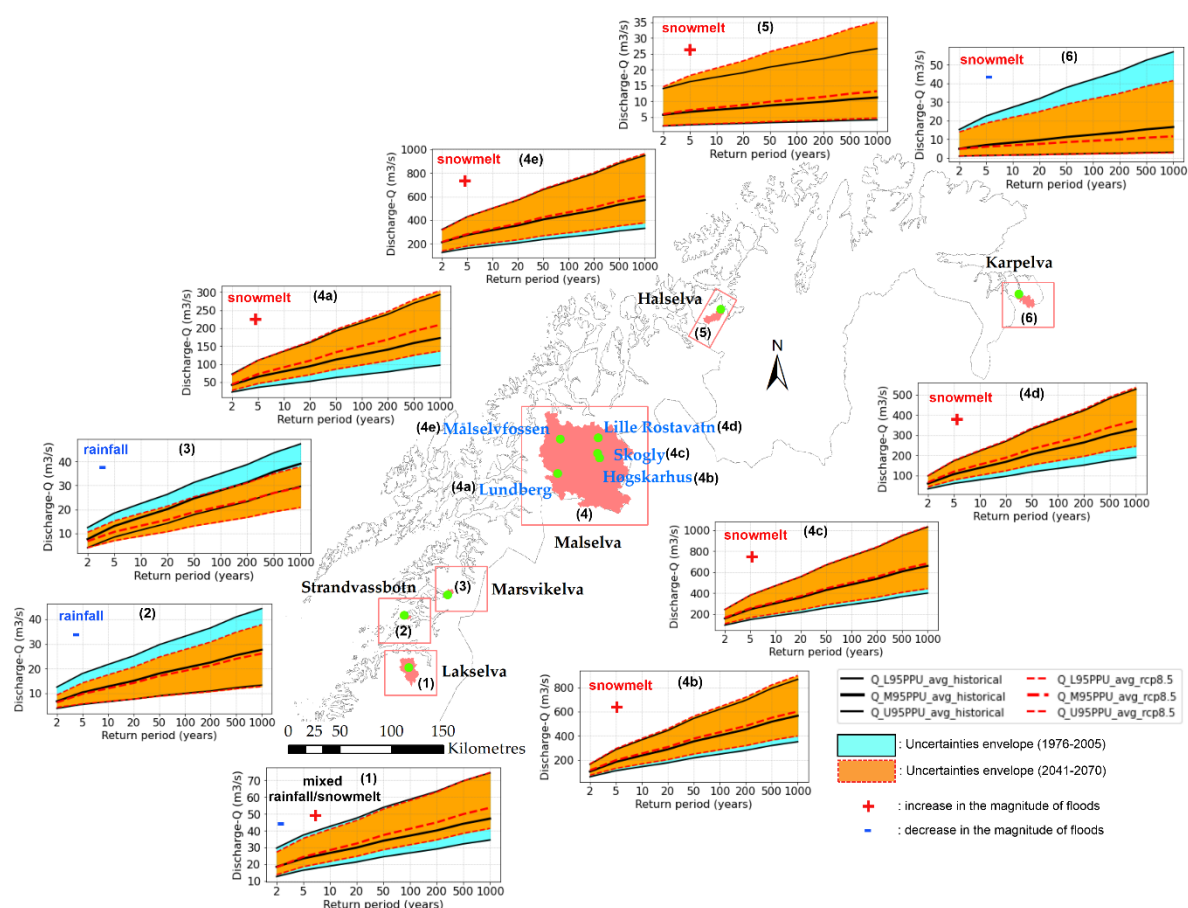
336
337
338

Fig. 3. Deviations in the near future (2041-2070) of annual precipitation-pcp (in %), and annual average air temperature-tmp (in °C) from the reference period (1976-2005), projected from five ensemble GCM_RCMs.

339 In general, annual rainfall in the future period (2041-2070) is expected both increase and decrease trends
 340 compared to that in the reference period (1976-2005). For example, the deviation of annual precipitation,
 341 averaged from five GCM_RCMs, from the 2041-2070 period to the 1976-2005 period is expected to fall in the
 342 range of -32.9 to +33.7%, -35.1 to +35.3%, -46.0 to +35.9%, -24.7 to +32.4%, -31.0 to +33.5%, and -33.8 to
 343 +35.4% for Lakselva, Strandvassbotn, Marsvikelva, Målselv, Halselva, Karpelva catchments, respectively. In
 344 contrast to high fluctuation in the projected rainfall, the average annual air temperature only presented the
 345 upward trend in the near future period. For instance, the average annual air temperature would increase 1.2-
 346 4.3°C, 1.2-4.4°C, 1.3-4.2°C, 1.4-4.7°C, 1.5-5.0°C, and 1.9-5.0°C, at Lakselva, Strandvassbotn, Marsvikelva,
 347 Målselv, Halselva, Karpelva catchments, respectively. Also, magnitudes of the increases in air temperature were
 348 linear to the latitudes of the investigated catchments. This corresponds to the prospect that climate change is
 349 more intensified toward to the north (AMAP 2011; Vormoor *et al.* 2016; AMAP 2017). Noticeably, the
 350 projections from the GCM_RCM5 were much higher than the remaining models (approx. 1.2-2.7 °C and
 351 catchments dependent) and such gaps were linear to the increase in the latitudes. The findings in this study
 352 added further confirmation regarding the catchment dependent of the climate models' performances (Chen *et al.*
 353 2017; Chen *et al.* 2021). The differences in the projections of climate change among five ensemble
 354 GCM_RCMs inputs were expected to result in uncertainties in the estimated flood frequencies and flood
 355 magnitudes.

356 1.12. Projected changes in flood magnitudes

357 Fig. 4 explained the trend and spatial variation of the changes in future flood magnitudes (2041-2070), averaged
 358 from five ensemble GCM_RCMs, compared to those of the reference period (1976-2005).



359

360

361

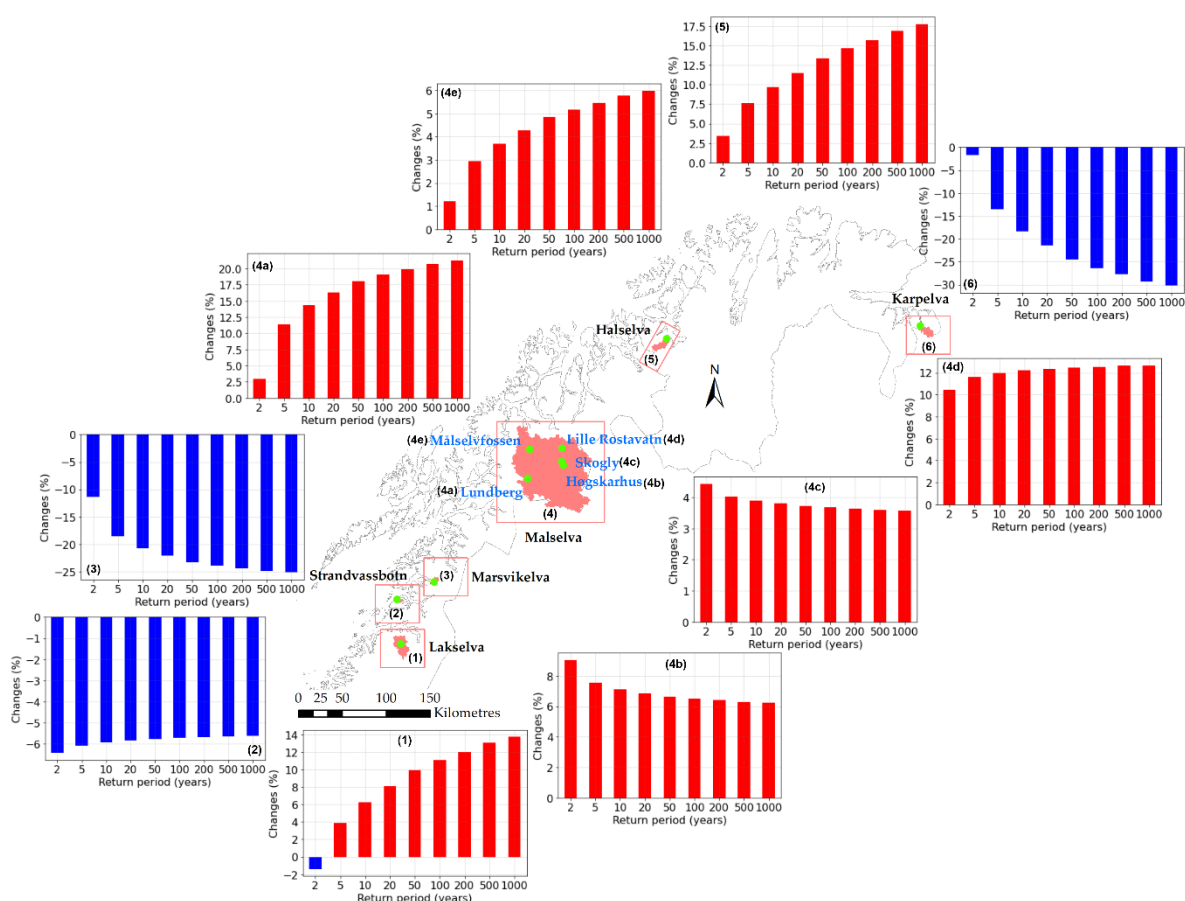
362

363

364

Fig. 4. The average (avg) changes in nine flood quantiles from the historical (1976-2005) to the future (2041-2070) in six Norwegian Arctic catchments (numbered 1-6) under high emission scenario (RCP8.5) of climate change. Q_{U95PPU} , Q_{M95PPU} , and Q_{L95PPU} denote the upper limited (at 97.5%), median and lower limited (at 2.5%) curves of the estimated discharges.

365 Magnitudes of nine flood quantiles were estimated corresponding to nine different flood return periods, in six
 366 Norwegian Arctic catchments. This study found that magnitudes of the future floods were expected to increase
 367 in most of the snowmelt-dominated catchments, excluding the Karpelva. This could explain the strong effects
 368 of the changes in air temperature and precipitation on snow regimes (Vormoor *et al.* 2016). The rising air
 369 temperature plus the occurrence of rain-on-snow events (AMAP 2011, 2017) cause higher snowmelt which
 370 contribute to higher peak flows. In contrast, in the two rainfall-dominated catchments Strandvassbotn and
 371 Marsvikelva, the futures flood magnitudes presented the decreased patterns. The reason was because rainfall
 372 (the main source for generating runoff) in these two catchments were expected to have larger drop (>21%) than
 373 that in the snowmelt-dominated and mixed catchments (Fig. 3). Also, the high increases in air temperature (Fig.
 374 3) would enhance evaporation and may result in reduction of runoff. Further reasons could originate from the
 375 projected results of the selected GCM_RCMs. For example, the projection from the GCM_RCM2 presented
 376 larger decrease (e.g., 15-46% at Strandvassbotn, and 9.5-35% at Marsvikelva) in future rainfall than that from
 377 the remaining GCM_RCMs (Fig. 3). Therefore, the selection of the driven climate models is very important and
 378 high impacts on the projected flood. In the mixed rainfall/snowmelt-dominated catchment Lakselva, future flood
 379 quantiles were projected both decrease (applicable for small flood i.e. the 2-year flood) and increase in the
 380 magnitudes.



381
 382 **Fig. 5.** Median changes (in %) in floods magnitudes from the reference period (1976-2005) to the future (2041-2070) in
 383 six Norwegian Arctic catchments (numbered 1-6) under high emission scenario (RCP8.5) of climate change.

384 Fig. 5 presented the absolute percentage of changes in the median magnitudes of future floods. For example, in
 385 the snowmelt-dominated catchments (excluding the Karpelva), median magnitudes of future floods would have
 386 a slight increase (from >1 to < 22%) and increase linearly with the increase of flood quantiles. Exceptionally,
 387 at Høgskarhus and Skogly gauging stations of Målselv catchment, the percentage increase of floods declined
 388 with the increase of flood quantiles. Regarding to the two rainfall-dominated catchments, the percentages of
 389 decrease in estimated flood magnitudes in the Strandvassbotn catchment, nearby the coastal, were quite low (<
 390 7%) and the reductions were unlinearly with the increase of flood quantiles. In contrast, the ratios of decrease
 391 in future floods magnitudes in the Marsvikelva, somewhat far the coastal, were higher (>10 to < 25%), and the
 392 declines were linearly with the increase of flood quantiles. Furthermore, in the large-scale and snowmelt-

393 dominated catchment Målselv, the predicted rising in flood magnitudes were significantly variant among hydro-
 394 gauging stations. Particularly, the increased flood magnitudes at the upstream stations, i.e. Lundberg, were in
 395 higher range compared to those at the remaining stations. For example, the increased flood magnitudes at
 396 Lundberg station was expected from > 2.5 to < 22%, while it was in the range of >6 to <10%, <3.5 to < 5%,
 397 >10 to <13%, >1 to <6% for Høgskarhus, Skogly, Lille Rostavatn, and Målselvossen stations, respectively.
 398 The snowmelt-dominated catchment Karpelva in the uppermost area was predicted to experience a decrease
 399 pattern of future flood magnitudes, i.e. from <2 up to <31% corresponding to 2-year flood to 1000-year flood.
 400 In short, the (maximum) decreases (in %) in future flood magnitudes were expected to higher (approx. 1.4 times)
 401 than the increases pattern, and spatial variation of the changes in flood magnitudes were also highlighted in the
 402 near future (2041-2070) for Norwegian Arctic catchments.

403 1.12.1. Projected changes in magnitudes of small floods

404 In this study, the small floods i.e. 2-year and 5-year floods were considered. It was found that the median
 405 magnitudes, between the future (2041-2070) and the reference (1976-2005) period, of the small floods were
 406 expected to decrease in the northern catchment (i.e. Karpelva, snowmelt-dominated) and the southern
 407 catchments (i.e. Marsvikelva, and Strandvassbotn (rainfall-dominated), and the mixed catchment Lakselva (only
 408 2-year flood)), whereas they were projected to increase in the remaining catchments (Table 7).

409 **Table 7.** Median changes in future magnitudes of small and extreme floods.

Catchments	Area (km ²)	Flood regimes	Small floods		Extreme floods		
			2-year flood	5-year flood	200-year flood	500-year flood	1000-year flood
Karpelva	129	Snowmelt	-1.7	-8.8	-27.8	-29.3	-30.3
Halselva	143	Snowmelt	+3.4	+7.6	+15.7	+16.9	+17.8
Målselv	5815	Snowmelt					
at Lundberg		Snowmelt	+3	+11.4	+19.9	+20.7	+21.3
at Lille Rostavatn		Snowmelt	+10.5	+11.6	+12.5	+12.6	+12.7
at Høgskarhus		Snowmelt	+9.1	+7.6	+6.4	+6.3	+6.2
at Skogly		Snowmelt	+4.4	+4.0	+3.6	+3.6	+3.6
at Målselvossen		Snowmelt	+1.2	+2.9	+5.5	+5.8	+6.0
Marsvikelva	32	Rainfall	-11.4	-18.6	-24.3	-24.8	-25.2
Strandvassbotn	26	Rainfall	-6.4	-6.1	-5.7	-5.7	-5.6
Lakselva	297	Mixed	-1.4	+3.9	+12.0	+13.1	+13.7

410

411 1.12.2. Projected changes in magnitudes of extreme floods

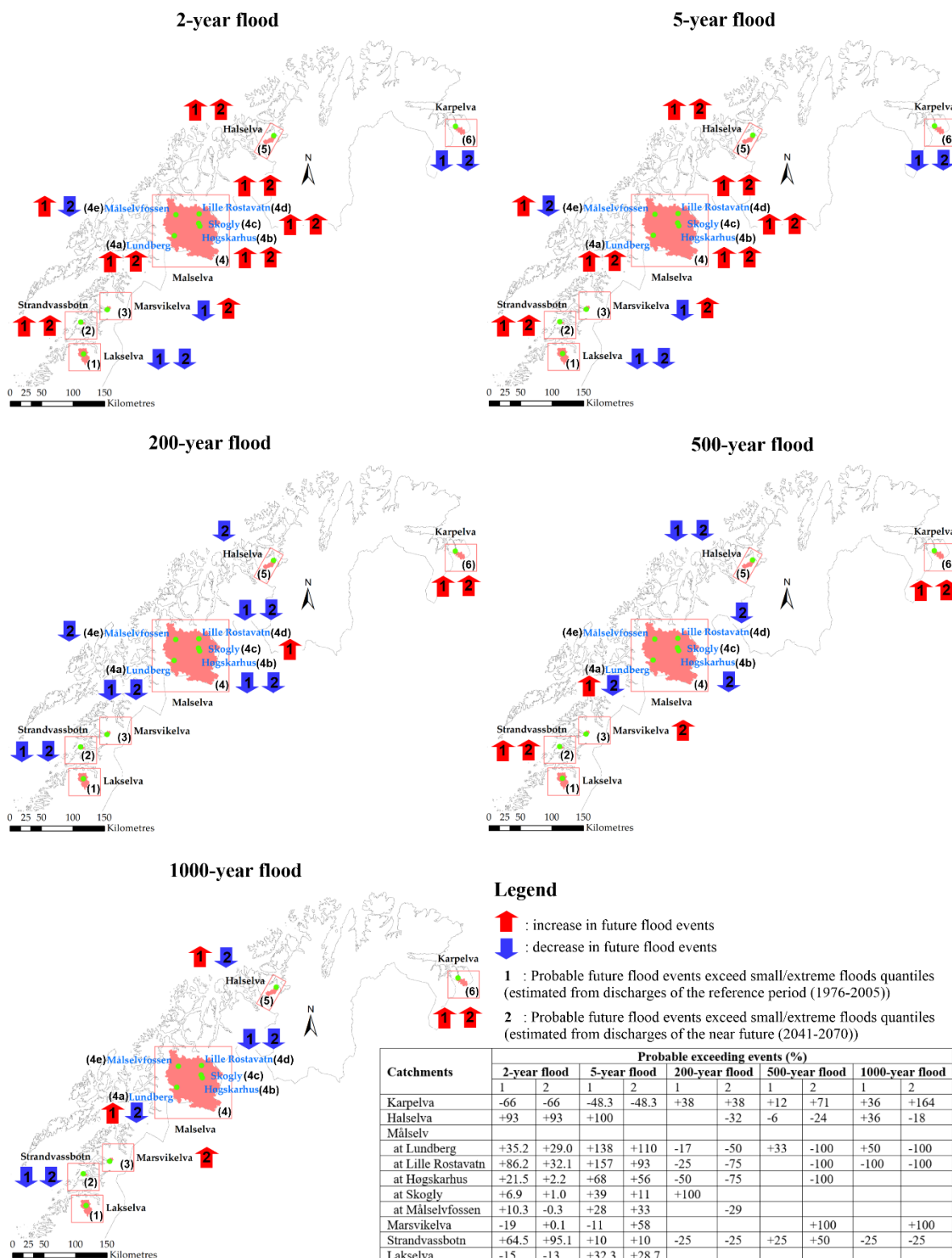
412 The trends of median changes in magnitudes of the extreme floods i.e. 200-year, 500-year and 1000-year floods
 413 in six Norwegian Arctic catchments was found to be similar to those of the small floods. However, the absolute
 414 values of the changes in the extreme floods would be more significant than those of the small floods, excluding
 415 at Høgskarhus and Skogly hydro-gauging stations of the Målselv catchment and Strandvassbotn catchment
 416 (Table 7).

417 1.13. Projected changes in likelihood exceedance

418 1.13.1. Projected changes in likelihood exceedance of small floods

419 Table S8, Table S9 (in supplementary material), and Fig. 6 provided the probable median changes in future
 420 flood events (in %) exceeding the 2-year, and 5-year floods. In general, the projections of the likelihood
 421 exceedance of small floods in the future were highly variation among ensemble GCM_RCM inputs. However,
 422 the average results revealed that small flood events would reduce in the northern catchment (Karpelva,
 423 snowmelt-dominant) and southern catchments (Marsvikelva, rainfall-dominated). In the rainfall-dominated
 424 catchment nearby the coastal, small floods would occur more frequent in the future although their magnitudes
 425 would slightly decrease (Table 7). Regarding the mixed catchment Lakselva, both decrease (for 2-year flood)
 426 and increase (for 5-year flood) of exceeding events were projected. In the central regions of the Norwegian
 427 Arctic with snowmelt-dominated regimes (e.g., Målselv and Halselva), small flood events in the future would
 428 occur more frequent compared to those in the reference period.

429



430
431
432

Fig. 6. Projected changes in likelihood exceedance of small and extreme floods, averaged from five ensemble GCM_RCMs inputs.

433 *1.13.2. Projected changes in likelihood exceedance of extreme floods*

434 The probable median changes in future flood events (in %) exceeding the 200, 500 and 1000-year floods were
435 presented from Table S10 to Table S12 (in supplementary material), and Fig. 6. Additionally, Fig. S5 and Fig.
436 S7 (in supplementary) presented hydrographs of future annual peak flood events (or maximum annual peak
437 flows) which could exceed extreme floods (estimated by discharge data of the reference period (1976-2005)).
438 Also, Fig. S6 and Fig. S8 (in supplementary) were the same but using both estimated flood quantiles by
439 discharge data of the reference period (1976-2005) and the future (2041-2070).

440 The projection of future changes in likelihood exceedance of extreme floods were found to totally oppose to
 441 those of the small floods. For example, in the southernmost and nearby the coastal (rainfall-dominated), and in
 442 the northernmost areas (snowmelt-dominated) of the Norwegian Arctic, extreme flood events could occur more
 443 frequent but with lower magnitudes compared to the historical conditions (Table 7). In contrast, extreme flood
 444 events would reduce, but with increased floods magnitudes (Table 7), in the central regions of the Norwegian
 445 Arctic, where snowmelt is governing the hydrological regime. Noticeably, in the rainfall-dominated catchment
 446 nearby the coastal (i.e. Strandvassbotn), the changes in future extreme flood events would be more complicated
 447 since it would increase (for 500-year flood) or decrease (for 200-year and 1000-year floods). The reason could
 448 be high fluctuation of future rainfall, which is dominating the hydrological regime in such catchment. The
 449 changes in frequency and intensity of extreme floods under climate change, found in this study, were the
 450 verification for previous studies (IPCC 2013; Rojas *et al.* 2013; Madsen *et al.* 2014; Alfieri *et al.* 2015;
 451 Mallakpour & Villarini 2015; Quintero *et al.* 2018), and the cases in Norway (Vormoor *et al.* 2016). Also, the
 452 results from this study could contribute to additional knowledge in case the measures for flood management
 453 and mitigation, e.g. flood hazard mapping (with 200-year flood) or dam safety management (with 500 and 1000-
 454 year floods) (Wilson *et al.* 2011), would be planned in the same study areas or any other regions with similar
 455 climate and hydrological characteristics.

456 Furthermore, performance of the ensemble GCM_RCM simulations were distinguished in the projections
 457 between small floods and extreme floods. This was because most of the ensemble GCM_RCM inputs could
 458 produce the projection of future changes in the likelihood exceedance of small floods. However, it would be
 459 harder for the projections of extreme floods. For example, only the ensemble GCM_RCM1 could produce the
 460 projected changes in future flood events exceeding the extreme flood quantiles in most of catchments. While,
 461 other ensemble models could only provide the projections in Marsvikelva catchment (by GCM_RCM2 and
 462 GCM_RCM3) and Strandvassbotn (by GCM_RCM3).

463 1.14. Uncertainties analysis in the projection of future floods

464 1.14.1. Uncertainties from the hydrological model SWAT

465 Table 13 provided two statistical measures, i.e. p-factor and r-factor, to quantify uncertainties from the
 466 hydrological model SWAT (Abbaspour *et al.* 2004; Abbaspour *et al.* 2015). The results in Table 13 explained
 467 that the daily observed streamflow could be satisfactorily bracketed by the 95PPU band of the stochastic
 468 simulations, and the uncertain envelopes were quite narrow, or the simulated results were highly reliable.

469 **Table 8.** Quantification of uncertainties from the hydrological model SWAT.

Catchments	p-factor		r-factor			
	Calibration	Optimal	Validation	Calibration	Optimal	Validation
Karpelva	0.94		0.92	1.08		1.08
Halselva	0.82		0.89	1.26		1.21
Målselv at Lunderg	0.56		0.52	0.70		0.72
Målselv at Lille Rostavatn	0.69		0.74	0.60		0.60
Målselv at Høgskarhus	0.56		0.43	0.82		0.86
Målselv at Skogly	0.73	> 0.70	0.67	1.15	< 1.5	1.15
Målselv at Målselvfossen	0.69		0.66	0.95		0.96
Marsvikelva	0.79		0.83	1.12		1.22
Strandvassotn	0.55		0.48	0.45		0.43
Lakselva	0.77		0.77	1.71		1.64

470

471 1.14.2. Uncertainties from the ensemble GCM_RCMs simulations

472 It was stated that inputs from climate models added further sources to uncertainties of the projected hydrology
 473 (Kay *et al.* 2009; Chen *et al.* 2011b; Woldemeskel *et al.* 2012). The results from this study agreed with such
 474 statements. Fig. 7 and Fig. 8 provided in detail uncertainties of the estimated flood frequencies and flood
 475 magnitudes, yielded from different ensemble GCM_RCMs inputs.

476 In general, the widths of uncertain envelopes increased linearly with the increase of flood quantiles. This
 477 explained larger uncertain for the estimation of higher flood quantiles. Most of GCM_RCMs inputs yielded
 478 similar thickness of uncertainties envelopes of estimated flood frequency in snowmelt-dominated catchments
 479 (i.e. Karpelva, Halselva and Målselv) but they produced high variation for the results in rainfall-dominated
 480 catchments (i.e. Marsvikvelva and Strandvassbotn). The high variation of the uncertainties envelopes in the two
 481 rainfall-dominated catchments clarified higher sensitive to climate change in rainfall-dominated catchments.
 482 Other reasons could be from the bias correction methods to adjust the GCM_RCMs simulations. The bias
 483 correction methods could fail to capture the temporal structure of daily rainfall which is critical for hydrological
 484 simulations in the rainfall-dominated catchments (Chen *et al.* 2017). In the mixed catchment (i.e. Lakselva),
 485 only the raw GCM_RCM1 inputs produced dissimilar uncertainties envelopes compared to remaining models.

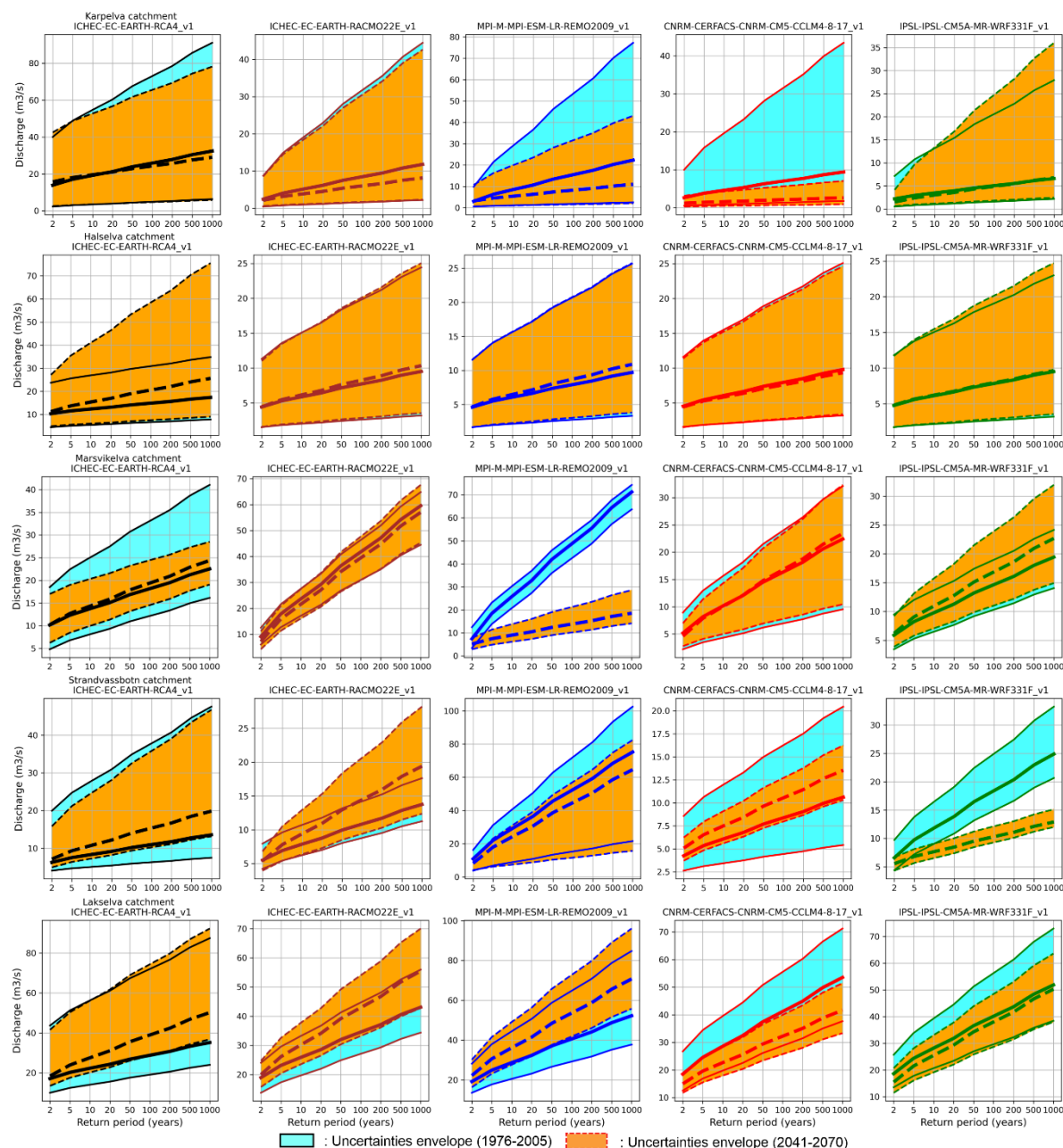
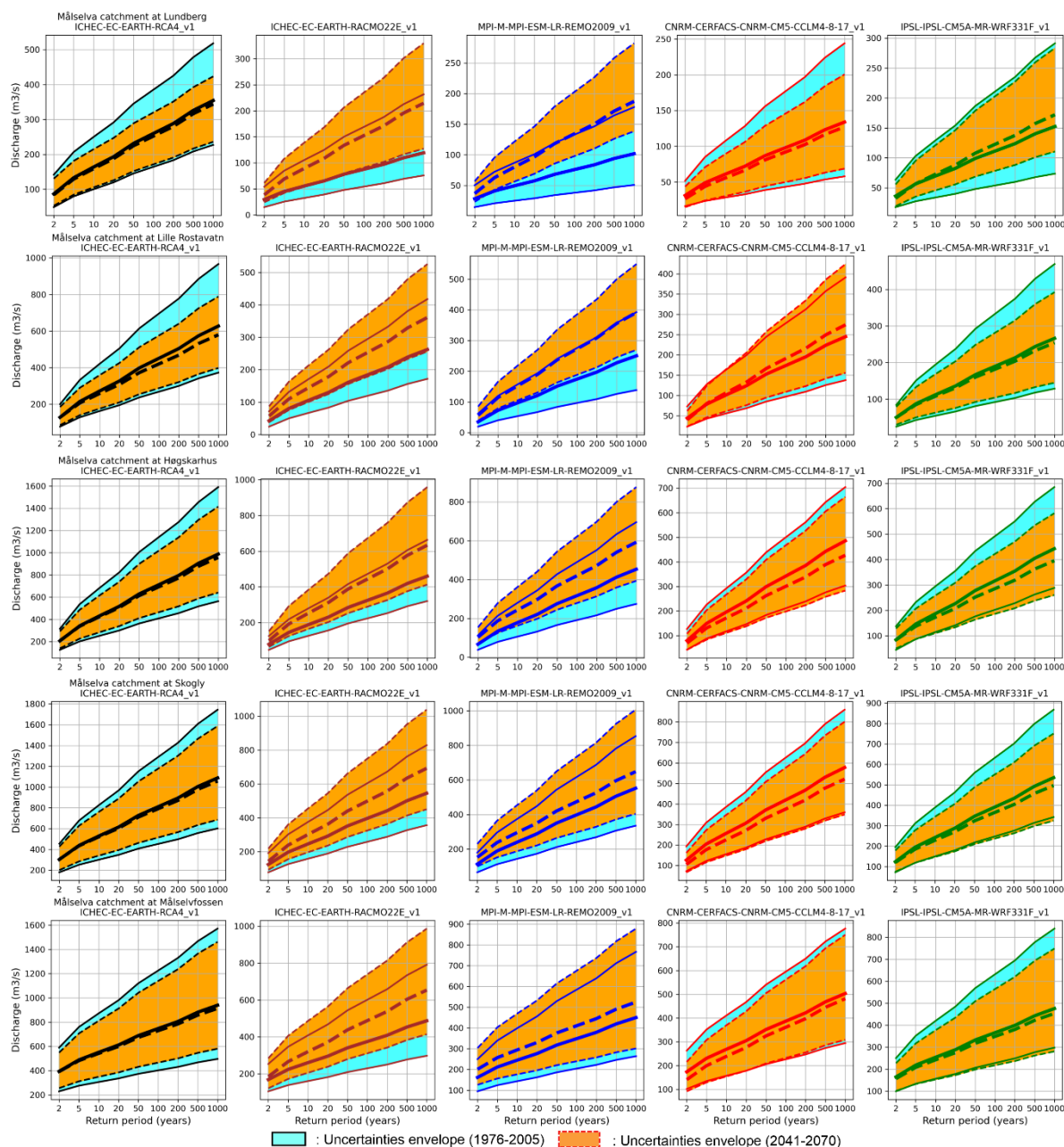


Fig. 7. Uncertainties in the estimation of the probable peak discharges corresponding to different return periods, in the reference period (1971-2005) and the future period (2041-2070), in the small-scale Norwegian Arctic catchments.



489

490

491

Fig. 8. Uncertainties in the estimation of the probable peak discharges corresponding to different return periods, in the reference period (1971-2005) and the future period (2041-2070), in the large-scale Norwegian Arctic catchment Målselv.

492

493

494

495

496

497

498

499

500

Among six investigated catchments, uncertainties envelopes of projected floods in the Karpelva, Halselva were quite broader than those in the remaining catchments. However, the results of calibration and validation of the hydrological models in the Karpelva, Halselva were better than those in the remaining catchments (Table 13). This revealed that uncertainties from the climate models were larger than those from the hydrological models. Findings from this study were agreed with findings from the previous studies (Wilby & Harris 2006; Chen *et al.* 2011a). However, this also agansted to another study, since they concluded that uncertainties from the hydrological model were larger than those from the GCMs (Najafi *et al.* 2011). Nevertheless, this could be because performances of both hydrological models and climate models vary from catchments to catchments (Chen *et al.* 2017; Chen *et al.* 2021).

501

502

503

504

505

Beside the uncertainties envelopes, using different ensemble GCM_RCM inputs resulted in dissimilar absolute values of estimated flood quantiles. This influenced the mean/median values of the projected floods. Also, using different time frame of the ensemble GCM_RCM simulation could yield different results of estimated floods. Thus, it is suggested that using the results of floods projections in this study only applied for the selected ensemble GCM_RCM simulations and within the investigated time frame.

506 Furthermore, it was claimed that using directly raw GCM_RCM to drive impacts models could yield unreliable
 507 projections (IPCC 2015). However, this study found that applications of raw model simulations were still
 508 reliable in some certain cases. For example, magnitudes of the estimated floods by using the raw model
 509 (GCM_RCM1) were similar to those by using the bias-corrected models (e.g., GCM_RCM3 in Karpelva
 510 catchment, or all bias-corrected GCM_RCMs in Lakselva catchment). The possibility of using the raw
 511 GCM_RCM in this study was in the consensus with findings from the previous studies outside the Norwegian
 512 Arctic (Chen *et al.* 2017; Meresa & Romanowicz 2017; Xu *et al.* 2019).

513 **Concluding remarks**

514 Consideration of the severe impacts of flooding on human life, the environment, ecosystem, and socio-economic
 515 development, especially under the context of global climate change, the projections of flood changes in the
 516 future is of great significance for better management and mitigation of the flooding. This study coupled multiple
 517 climate models simulations and hydrological model SWAT to project future floods (in 2041-2070) in six
 518 Norwegian Arctic catchments, which have variation in geographical distribution, scales, and dominant flood
 519 regimes. The key findings from this study were summarised as follows:

- 520 i. The SWAT model demonstrated its high reliability to simulate daily streamflow in the Arctic environment,
- 521 ii. Annual precipitation were expected to experience both increase and decrease patterns, while annual air
 522 temperature were only in the upward trend and more intensified towards the north,
- 523 iii. The median magnitudes of floods were projected to increase in most of snowmelt-dominated catchments,
 524 but decrease in the rainfall-dominated catchments. While the mixed catchment would experience both
 525 decrease (applicable for the small flood) and increase patterns,
- 526 iv. Extreme flood events were expected to occur more frequent, but with lower magnitudes in southern
 527 catchments (rainfall-dominated), and in northern catchment (snowmelt-dominated). This opposed to the
 528 central catchments (snowmelt-dominated),
- 529 v. Changes in extreme flood events in the rainfall-dominated catchment and near the coast were more complex
 530 to project due to high variation of future rainfall regime in this region,
- 531 vi. Future changes in likelihood exceedance of small flood events were projected in the opposite behaviors to
 532 those of extreme floods,
- 533 vii. Five ensemble GCM_RCMs inputs yielded higher variation of the projected floods in the rainfall-dominated
 534 catchments than those in the snowmelt-dominated catchments,
- 535 viii. In the modelling chain for floods projections in the Norwegian Arctic environment, uncertainties from the
 536 ensemble GCM_RCMs were found to be larger than those from the hydrological model SWAT,
- 537 ix. Using the raw climate model simulations to drive the impact models was found to be reliable in some certain
 538 cases. It is, therefore, recommend to consider both raw and bias-corrected climate models in climate change
 539 impacts assessment.

540 Outcomes from this study would support the scientists, decision makers and planners to propose suitable
 541 strategies for flood mitigation and management. Also, this would contribute to sustainable environment and
 542 ecosystem conservation in the Arctic.

543

544 **Acknowledgments**

545

546 The authors would like to acknowledge the Department of Technology and Safety, Faculty of Science and
 547 Technology, UiT The Arctic University of Norway for their financial and administrative supports for this study.
 548 We would like to recognize the in-kind contribution from Foundation CSDI WaterTech, Oslo, Norway.

549

550

551

552 **REFERENCES**

- 553 Abbaspour K. C., Johnson C. A. & van Genuchten M. T. 2004 Estimating uncertain flow and transport parameters
554 using a sequential uncertainty fitting procedure. *Vadose Zone Journal*, **3**(4), 1340-52.
- 555 Abbaspour K. C., Rouholahnejad E., Vaghefi S., Srinivasan R., Yang H. & Klove B. 2015 A continental-scale
556 hydrology and water quality model for Europe: Calibration and uncertainty of a high-resolution large-
557 scale SWAT model. *Journal of Hydrology*, **524**, 733-52.
- 558 Abbaspour K. C., Yang J., Maximov I., Siber R., Bogner K., Mieleitner J., Zobrist J. & Srinivasan R. 2007 Modelling
559 hydrology and water quality in the pre-alpine/alpine Thur watershed using SWAT. *Journal of Hydrology*,
560 **333**(2-4), 413-30.
- 561 Alfieri L., Bisselink B., Dottori F., Naumann G., de Roo A., Salamon P., Wyser K. & Feyen L. 2017 Global
562 projections of river flood risk in a warmer world. *Earths Future*, **5**(2), 171-82.
- 563 Alfieri L., Burek P., Feyen L. & Forzieri G. 2015 Global warming increases the frequency of river floods in Europe.
564 *Hydrology and Earth System Sciences*, **19**(5), 2247-60.
- 565 AMAP 2011 *Snow, water, ice and permafrost in the Arctic (SWIPA) : climate change and the cryosphere*. AMAP, Oslo.
- 566 AMAP 2017 *Snow, Water, Ice and Permafrost in the Arctic (SWIPA) 2017*. Arctic Monitoring and Assessment
567 Programme.
- 568 Bui M. T., Lu J. M. & Nie L. M. 2021 Evaluation of the Climate Forecast System Reanalysis weather data for the
569 hydrological model in the Arctic watershed Malselv. *Journal of Water and Climate Change*, **12**(8), 3481-
570 504.
- 571 Chen J., Arsenault R., Brissette F. P. & Zhang S. B. 2021 Climate Change Impact Studies: Should We Bias Correct
572 Climate Model Outputs or Post-Process Impact Model Outputs? *Water Resources Research*, **57**(5).
- 573 Chen J., Brissette F. P. & Caya D. 2020 Remaining error sources in bias-corrected climate model outputs. *Climatic
574 Change*, **162**(2), 563-82.
- 575 Chen J., Brissette F. P. & Leconte R. 2011a Uncertainty of downscaling method in quantifying the impact of
576 climate change on hydrology. *Journal of Hydrology*, **401**(3-4), 190-202.
- 577 Chen J., Brissette F. P., Liu P. & Xia J. 2017 Using raw regional climate model outputs for quantifying climate
578 change impacts on hydrology. *Hydrological Processes*, **31**(24), 4398-413.
- 579 Chen J., Brissette F. P. & Lucas-Picher P. 2015 Assessing the limits of bias-correcting climate model outputs for
580 climate change impact studies. *Journal of Geophysical Research-Atmospheres*, **120**(3), 1123-36.
- 581 Chen J., Brissette F. P., Poulin A. & Leconte R. 2011b Overall uncertainty study of the hydrological impacts of
582 climate change for a Canadian watershed. *Water Resources Research*, **47**.
- 583 Chen J., Brissette F. P., Zhang X. C. J., Chen H., Guo S. L. & Zhao Y. 2019 Bias correcting climate model multi-
584 member ensembles to assess climate change impacts on hydrology. *Climatic Change*, **153**(3), 361-77.
- 585 Chen J., Li C., Brissette F. P., Chen H., Wang M. N. & Essou G. R. C. 2018 Impacts of correcting the inter-variable
586 correlation of climate model outputs on hydrological modeling. *Journal of Hydrology*, **560**, 326-41.
- 587 Collins M., Booth B. B. B., Harris G. R., Murphy J. M., Sexton D. M. H. & Webb M. J. 2006 Towards quantifying
588 uncertainty in transient climate change. *Climate Dynamics*, **27**(2-3), 127-47.
- 589 Cunnane C. 1985 Factors affecting choice of distribution for flood series. *Hydrological sciences journal*, **30**(1), 25-
590 36.
- 591 Cunnane C. 1989 *Statistical distributions for flood frequency analysis*, WMO Operational hydrology, Geneva,
592 Switzerland.
- 593 Doocy S., Daniels A., Murray S. & Kirsch T. D. 2013 The human impact of floods: a historical review of events
594 1980-2009 and systematic literature review. *PLoS Curr*, **5**.
- 595 Du J. K., Rui H. Y., Zuo T. H., Li Q., Zheng D. P., Chen A. L., Xu Y. P. & Xu C. Y. 2013 Hydrological Simulation
596 by SWAT Model with Fixed and Varied Parameterization Approaches Under Land Use Change. *Water
597 Resources Management*, **27**(8), 2823-38.
- 598 Dunn S. M., Brown I., Sample J. & Post H. 2012 Relationships between climate, water resources, land use and
599 diffuse pollution and the significance of uncertainty in climate change. *Journal of Hydrology*, **434**, 19-35.
- 600 Engeland K., Aano A., Steffensen I., Storen E. & Paasche O. 2020 New flood frequency estimates for the largest
601 river in Norway based on the combination of short and long time series. *Hydrology and Earth System
602 Sciences*, **24**(11), 5595-619.
- 603 Fernandez G. P., Chescheir G. M., Skaggs R. W. & Amatya D. M. 2005 Development and testing of watershed-
604 scale models for poorly drained soils. *Transactions of the Asae*, **48**(2), 639-52.
- 605 Ficklin D. L., Luo Y. Z., Stewart I. T. & Maurer E. P. 2012 Development and application of a hydroclimatological
606 stream temperature model within the Soil and Water Assessment Tool. *Water Resources Research*, **48**.
- 607 Field C. B., Barros V., Stocker T. F. & Dahe Q. 2012 *Managing the Risks of Extreme Events and Disasters to Advance
608 Climate Change Adaptation: Special Report of the Intergovernmental Panel on Climate Change*. New York:
609 Cambridge University Press, New York.

- 610 Flato G., Marotzke J., Abiodun B., Braconnot P., Chou S. C., Collins W., Cox P., Driouech F., Emori S., Eyring V.,
611 Forest C., Gleckler P., Guilyardi E., Jakob C., Kattsov V., Reason C. & Rummukainen M. 2013 Evaluation
612 of Climate Models. In: *Climate Change 2013: The Physical Science Basis. Contribution of Working Group I to*
613 *the Fifth Assessment Report of the Intergovernmental Panel on Climate Change* Stocker TF, Qin D, Plattner G-
614 K, Tignor M, Allen SK, Boschung J, Nauels A, Xia Y, Bex V and Midgley PM (eds), Cambridge
615 University Press, Cambridge, United Kingdom and New York, NY, USA.
- 616 Geonorge 2013 Height DTM 10. [https://kartkatalog.geonorge.no/metadatas/kartverket/dtm-10-terrengmodell-
617 utm33/](https://kartkatalog.geonorge.no/metadatas/kartverket/dtm-10-terrengmodell-utm33/) (accessed 14 February 2021).
- 618 Ghosh S. & Mujumdar P. P. 2007 Nonparametric methods for modeling GCM and scenario uncertainty in
619 drought assessment. *Water Resources Research*, **43**(7).
- 620 Gutierrez J. M., Maraun D., Widmann M., Huth R., Hertig E., Benestad R., Roessler O., Wibig J., Wilcke R.,
621 Kotlarski S., San Martin D., Herrera S., Bedia J., Casanueva A., Manzanos R., Iturbide M., Vrac M.,
622 Dubrovsky M., Ribalaygua J., Portoles J., Raty O., Raisanen J., Hingray B., Raynaud D., Casado M. J.,
623 Ramos P., Zerenner T., Turco M., Bosshard T., Stepanek P., Bartholy J., Pongracz R., Keller D. E., Fischer
624 A. M., Cardoso R. M., Soares P. M. M., Czernecki B. & Page C. 2019 An intercomparison of a large
625 ensemble of statistical downscaling methods over Europe: Results from the VALUE perfect predictor
626 cross-validation experiment. *International Journal of Climatology*, **39**(9), 3750-85.
- 627 Heal G. & Kristrom B. 2002 Uncertainty and climate change. *Environmental & Resource Economics*, **22**(1-2), 3-39.
- 628 Hirabayashi Y., Mahendran R., Koirala S., Konoshima L., Yamazaki D., Watanabe S., Kim H. & Kanae S. 2013
629 Global flood risk under climate change. *Nature Climate Change*, **3**(9), 816-21.
- 630 Hui Y., Chen J., Xu C. Y., Xiong L. H. & Chen H. 2019 Bias nonstationarity of global climate model outputs: The
631 role of internal climate variability and climate model sensitivity. *International Journal of Climatology*,
632 **39**(4), 2278-94.
- 633 IPCC 2013 *Climate Change 2013: The Physical Science Basis. Working Group I Contribution to the Fifth*
634 *Assessment Report of the Intergovernmental Panel on Climate Change*. In, Cambridge University Press,
635 Cambridge, United Kingdom and New York, NY, USA, p. 1535.
- 636 IPCC 2015 *Workshop Report of the Intergovernmental Panel on Climate Change Workshop on Regional Climate*
637 *Projections and their Use in Impacts and Risk Analysis Studies*, IPCC Working Group I, Technical Support
638 Unit, University of Bern, Bern, Switzerland.
- 639 Jacob D., Petersen J., Eggert B., Alias A., Christensen O. B., Bouwer L. M., Braun A., Colette A., Deque M.,
640 Georgievski G., Georgopoulou E., Gobiet A., Menut L., Nikulin G., Haensler A., Hempelmann N., Jones
641 C., Keuler K., Kovats S., Kroner N., Kotlarski S., Kriegsmann A., Martin E., van Meijgaard E., Moseley
642 C., Pfeifer S., Preuschmann S., Radermacher C., Radtke K., Rechid D., Rounsevell M., Samuelsson P.,
643 Somot S., Soussana J. F., Teichmann C., Valentini R., Vautard R., Weber B. & Yiou P. 2014 EURO-
644 CORDEX: new high-resolution climate change projections for European impact research. *Regional*
645 *Environmental Change*, **14**(2), 563-78.
- 646 Jayakrishnan R., Srinivasan R., Santhi C. & Arnold J. G. 2005 Advances in the application of the SWAT model
647 for water resources management. *Hydrological Processes*, **19**(3), 749-62.
- 648 Jones R. N. 2000 Managing uncertainty in climate change projections - Issues for impact assessment - An editorial
649 comment. *Climatic Change*, **45**(3-4), 403-19.
- 650 Jung I. W., Moradkhani H. & Chang H. 2012 Uncertainty assessment of climate change impacts for hydrologically
651 distinct river basins. *Journal of Hydrology*, **466**, 73-87.
- 652 Katz R. W., Craigmile P. F., Guttorp P., Haran M., Sanso B. & Stein M. L. 2013 Uncertainty analysis in climate
653 change assessments. *Nature Climate Change*, **3**(9), 769-71.
- 654 Kay A. L., Davies H. N., Bell V. A. & Jones R. G. 2009 Comparison of uncertainty sources for climate change
655 impacts: flood frequency in England. *Climatic Change*, **92**(1-2), 41-63.
- 656 Khan M. S., Coulibaly P. & Dibike Y. 2006 Uncertainty analysis of statistical downscaling methods using
657 Canadian Global Climate Model predictors. *Hydrological Processes*, **20**(14), 3085-104.
- 658 Koycegiz C. & Buyukyildiz M. 2019 Calibration of SWAT and Two Data-Driven Models for a Data-Scarce
659 Mountainous Headwater in Semi-Arid Konya Closed Basin. *Water*, **11**(1).
- 660 Landwehr J. M., Matalas N. C. & Wallis J. R. 1979 Probability Weighted Moments Compared with Some
661 Traditional Techniques in Estimating Gumbel Parameters and Quantiles. *Water Resources Research*,
662 **15**(5), 1055-64.
- 663 Lawrence D. & Hisdal H. 2011 *Hydrological projections for floods in Norway under a future climate*, The Norwegian
664 Water Resources and Energy Directorate-NVE, Oslo, Norway.
- 665 Logsdon R. A. & Chaubey I. 2013 A quantitative approach to evaluating ecosystem services. *Ecological Modelling*,
666 **257**, 57-65.

- 667 Lowery M. D. & Nash J. E. 1970 A comparison of methods of fitting the double exponential distribution. *Journal*
668 *of hydrology (Amsterdam)*, **10**(3), 259-75.
- 669 Madsen H., Lawrence D., Lang M., Martinkova M. & Kjeldsen T. R. 2014 Review of trend analysis and climate
670 change projections of extreme precipitation and floods in Europe. *Journal of Hydrology*, **519**, 3634-50.
- 671 Mallakpour I. & Villarini G. 2015 The changing nature of flooding across the central United States. *Nature Climate*
672 *Change*, **5**(3), 250-4.
- 673 Maraun D. 2012 Nonstationarities of regional climate model biases in European seasonal mean temperature and
674 precipitation sums. *Geophysical Research Letters*, **39**.
- 675 Maurer E. P. 2007 Uncertainty in hydrologic impacts of climate change in the Sierra Nevada, California, under
676 two emissions scenarios. *Climatic Change*, **82**(3-4), 309-25.
- 677 McGrath H., Stefanakis E. & Nastev M. 2015 Sensitivity analysis of flood damage estimates: A case study in
678 Fredericton, New Brunswick. *International Journal of Disaster Risk Reduction*, **14**, 379-87.
- 679 Meresa H. K., Osuch M. & Romanowicz R. 2016 Hydro-Meteorological Drought Projections into the 21-st
680 Century for Selected Polish Catchments. *Water*, **8**(5).
- 681 Meresa H. K. & Romanowicz R. J. 2017 The critical role of uncertainty in projections of hydrological extremes.
682 *Hydrology and Earth System Sciences*, **21**(8), 4245-58.
- 683 Midttømme G. H., Pettersson L. E., Holmqvist E., Nøtsund Ø., Hisdal H. & Sivertsgård R. 2011 *Retningslinjer for*
684 *flomberegninger (Guidelines for flood calculations)*, The Norwegian Water Resources and Energy
685 Directorate (NVE), Oslo, Norway.
- 686 Miljøverndepartement 2012 *Klimatilpasning i Norge (Climate change adaptation in Norway) Meld. St. nr. 33 (2012–*
687 *2013)*, Miljøvern departement, Oslo, Norway.
- 688 Moriasi D. N., Arnold J. G., Van Liew M. W., Bingner R. L., Harmel R. D. & Veith T. L. 2007 Model evaluation
689 guidelines for systematic quantification of accuracy in watershed simulations. *Transactions of the Asabe*,
690 **50**(3), 885-900.
- 691 Murray V. & Ebi K. L. 2012 IPCC Special Report on Managing the Risks of Extreme Events and Disasters to
692 Advance Climate Change Adaptation (SREX). *J Epidemiol Community Health*, **66**(9), 759-60.
- 693 Najafi M. R., Moradkhani H. & Jung I. W. 2011 Assessing the uncertainties of hydrologic model selection in
694 climate change impact studies. *Hydrological Processes*, **25**(18), 2814-26.
- 695 Neitsch S. L., Arnold J. G., Kiniry J. R. & Williams J. R. 2009 Overview of Soil and Water Assessment Tool (SWAT)
696 Model. In: *Soil and Water Assessment Tool (SWAT): Gobar Application* Arnold J, Srinivasan R, Neitsch S,
697 George C, Abbaspour K, Gassman P, Fang HH, Griensven Av, Gosain A, Debels P, Kim NW, Somura
698 H, Ella V, Leon L, Jintrawet A, Reyes M and Sombatpanit S (eds), The World Association of Soil and
699 Water Conservation (WASWC), Bangkok, pp. 3-23.
- 700 Nemry F. & Demirel H. 2012 *Impacts of Climate Change on transport: a focus on road and rail transport infrastructures.*
701 *JRC72217*, Publications Office of the European Union, Luxembourg (Luxembourg).
- 702 Odry J. & Arnaud P. 2017 Comparison of Flood Frequency Analysis Methods for Ungauged Catchments in
703 France. *Geosciences*, **7**(3).
- 704 Piani C., Haerter J. O. & Coppola E. 2010 Statistical bias correction for daily precipitation in regional climate
705 models over Europe. *Theoretical and Applied Climatology*, **99**(1-2), 187-92.
- 706 Premanand B. D., Satishkumar U., Maheshwara Babu B., Parasappa S. K., M. Dandu M., Kaleel I., Rajesh N. L. &
707 Biradar S. A. 2018 QSWAT Model Calibration and Uncertainty Analysis for Stream Flow Simulation in
708 the Patapur Micro-Watershed Using Sequential Uncertainty Fitting Method (SUFI-2). *International*
709 *journal of current microbiology and applied sciences*, **7**(4), 831-52.
- 710 Quintero F., Mantilla R., Anderson C., Claman D. & Krajewski W. 2018 Assessment of Changes in Flood
711 Frequency Due to the Effects of Climate Change: Implications for Engineering Design. *Hydrology*, **5**(1).
- 712 Richter B. D., Baumgartner J. V., Powell J. & Braun D. P. 1996 A method for assessing hydrologic alteration within
713 ecosystems. *Conservation Biology*, **10**(4), 1163-74.
- 714 Rojas R., Feyen L. & Watkiss P. 2013 Climate change and river floods in the European Union: Socio-economic
715 consequences and the costs and benefits of adaptation. *Global Environmental Change-Human and Policy*
716 *Dimensions*, **23**(6), 1737-51.
- 717 Saelthun N. R. & Andersen J. H. 1986 New Procedures for Flood Estimation in Norway. *Nordic Hydrology*, **17**(4-
718 5), 217-28.
- 719 Saha S., Moorthi S., Pan H. L., Wu X. R., Wang J. D., Nadiga S., Tripp P., Kistler R., Woollen J., Behringer D., Liu
720 H. X., Stokes D., Grumbine R., Gayno G., Wang J., Hou Y. T., Chuang H. Y., Juang H. M. H., Sela J.,
721 Iredell M., Treadon R., Kleist D., Van Delst P., Keyser D., Derber J., Ek M., Meng J., Wei H. L., Yang R.
722 Q., Lord S., Van den Dool H., Kumar A., Wang W. Q., Long C., Chelliah M., Xue Y., Huang B. Y.,
723 Schemm J. K., Ebisuzaki W., Lin R., Xie P. P., Chen M. Y., Zhou S. T., Higgins W., Zou C. Z., Liu Q. H.,

- 724 Chen Y., Han Y., Cucurull L., Reynolds R. W., Rutledge G. & Goldberg M. 2010 The Ncep Climate
725 Forecast System Reanalysis. *Bulletin of the American Meteorological Society*, **91**(8), 1015-57.
- 726 Santhi C., Arnold J. G., Williams J. R., Dugas W. A., Srinivasan R. & Hauck L. M. 2001 Validation of the swat
727 model on a large river basin with point and nonpoint sources. *Journal of the American Water Resources
728 Association*, **37**(5), 1169-88.
- 729 Schmidli J., Frei C. & Vidale P. L. 2006 Downscaling from GCM precipitation: a benchmark for dynamical and
730 statistical downscaling methods. *International Journal of Climatology*, **26**(5), 679-89.
- 731 Setegn S. G., Rayner D., Melesse A. M., Dargahi B. & Srinivasan R. 2011 Impact of climate change on the
732 hydroclimatology of Lake Tana Basin, Ethiopia. *Water Resources Research*, **47**.
- 733 Sildre 2020 Real-time hydrological data. The Norwegian Water Resources and Energy Directorate (NVE).
734 <http://sildre.nve.no/> (accessed 18 November 2019).
- 735 Singh V. P. 1998 Extreme Value Type 1 Distrffiuion. In: *Entropy-Based Parameter Estimation in Hydrology*, Springer
736 Science+Business Media Dordrecht, pp. 108-36.
- 737 Talbot C. J., Bennett E. M., Cassell K., Hanes D. M., Minor E. C., Paerl H., Raymond P. A., Vargas R., Vidon P.
738 G., Wollheim W. & Xenopoulos M. A. 2018 The impact of flooding on aquatic ecosystem services.
739 *Biogeochemistry*, **141**(3), 439-61.
- 740 TAMU 2012 CFSR: Global Weather Data for SWAT. <https://globalweather.tamu.edu/> (accessed 05 July 2020).
- 741 Teutschbein C. & Seibert J. 2013 Is bias correction of regional climate model (RCM) simulations possible for non-
742 stationary conditions? *Hydrology and Earth System Sciences*, **17**(12), 5061-77.
- 743 Van Liew M. W., Arnold J. G. & Garbrecht J. D. 2003 Hydrologic simulation on agricultural watersheds: Choosing
744 between two models. *Transactions of the Asae*, **46**(6), 1539-51.
- 745 Vinet F. 2017 Flood Impacts on Loss of Life and Human Health. In: *Floods*, pp. 33-51.
- 746 Vormoor K., Lawrence D., Bronstert A., Heistermann M., Schlichting L., Wilson D. & Kwok Wong W. 2016 The
747 changing role of snowmelt- and rainfall dominated floods in Norway under climate change -
748 observations, projections, and uncertainties. In: *EGU General Assembly 2016*, Geophysical Research
749 Abstracts, Vienna, Austria, pp. EPSC2016-12812.
- 750 Vörösmarty C. J., Moore B., Grace A. L., Gildea M. P., Melillo J. M., Peterson B. J., Rastetter E. B. & Steudler P. A.
751 1989 Continental scale models of water balance and fluvial transport: An application to South America.
752 *Global Biogeochem. Cycles*, **3**(3), 241-65.
- 753 Vrac M., Drobinski P., Merlo A., Herrmann M., Lavaysse C., Li L. & Somot S. 2012 Dynamical and statistical
754 downscaling of the French Mediterranean climate: uncertainty assessment. *Natural Hazards and Earth
755 System Sciences*, **12**(9), 2769-84.
- 756 Waterbase 2007a Land use. http://www.waterbase.org/download_data.html (accessed 14 February 2021).
- 757 Waterbase 2007b Soil. http://www.waterbase.org/download_data.html (accessed 14 February 2021).
- 758 Wilby R. L., Dawson C. W. & Barrow E. M. 2002 SDSM - a decision support tool for the assessment of regional
759 climate change impacts. *Environmental Modelling & Software*, **17**(2), 147-59.
- 760 Wilby R. L. & Harris I. 2006 A framework for assessing uncertainties in climate change impacts: Low-flow
761 scenarios for the River Thames, UK. *Water Resources Research*, **42**(2).
- 762 Wilson D., Fleig A. K., Lawrence D., Hisdal H., Pettersson L.-E. & Holmqvist E. 2011 *A review of NVE's flood
763 frequency estimation procedures*, Norwegian Water Resources and Energy Directorate, Oslo, Norway.
- 764 Wiltshire S. E. 1987 *Statistical techniques for regional flood frequency analysis*. Unpublished PhD thesis, Newcastle
765 University.
- 766 Woldemeskel F. M., Sharma A., Sivakumar B. & Mehrotra R. 2012 An error estimation method for precipitation
767 and temperature projections for future climates. *Journal of Geophysical Research-Atmospheres*, **117**.
- 768 Xu C. Y. 1999 Climate change and hydrologic models: A review of existing gaps and recent research
769 developments. *Water Resources Management*, **13**(5), 369-82.
- 770 Xu X., Wang Y. C., Kalcic M., Muenich R. L., Yang Y. C. E. & Scavia D. 2019 Evaluating the impact of climate
771 change on fluvial flood risk in a mixed-use watershed. *Environmental Modelling & Software*, **122**.
- 772 Zhang C., Chu J. G. & Fu G. T. 2013 Sobol's sensitivity analysis for a distributed hydrological model of Yichun
773 River Basin, China. *Journal of Hydrology*, **480**, 58-68.
- 774 Zhang X. C. 2005 Spatial downscaling of global climate model output for site-specific assessment of crop
775 production and soil erosion. *Agricultural and forest meteorology*, **135**(1), 215-29.
- 776 Zhang X. J., Xu Y. P. & Fu G. T. 2014 Uncertainties in SWAT extreme flow simulation under climate change.
777 *Journal of Hydrology*, **515**, 205-22.

778

779

Supplementary material

1 Supplementary Table for

2

3

4 **Projections of future floods in Norwegian Arctic**
5 **catchments under climate change context**

6

7 **Minh Tuan Bui ^{1,*}, Jinmei Lu ¹, Linmei Nie ²**

8

9

10 ¹ Department of Technology and Safety, Faculty of Science and Technology, UiT The Arctic University of Norway, 9037
11 Tromsø, Norway; jinmei.lu@uit.no

12 ² Centre for Sustainable Development and Innovation of Water Technology, Foundation CSDI WaterTech, 0373 Oslo,
13 Norway; linmei.nie@csti.no

14

15 * Corresponding author: Minh Tuan Bui

16 E-mail address: minh.t.bui@uit.no

17

18 **Table S1**

19 Description of the calibrated model parameters.

Parameter Name	Description	Subgroup process
SMTMP.bsn	Snow melt base temperature	
TIMP.bsn	Snow pack temperature lag factor	
SMFMN.bsn	Minimum melt rate for snow during the year (occurs on winter solstice)	
SMFMX.bsn	Maximum melt rate for snow during year (occurs on summer solstice)	Snowmelt
SFTMP.bsn	Snowfall temperature	
SNO50COV	Snow water equivalent that corresponds to 50% snow cover	
SNOCOVMX	Minimum snow water content that corresponds to 100% snow cover	
TLAPS	Temperature lapse rate	
CN2.mgt	SCS runoff curve number f	Surface runoff
CANMX.hru	Maximum canopy storage	
ESCO.hru	Soil evaporation compensation factor	
SOL_AWC(..).sol	Available water capacity of the soil layer	Lateral flow
SOL_BD(..).sol	Moist bulk density	
SOL_K(..).sol	Saturated hydraulic conductivity	
CH_K2.rte	Effective hydraulic conductivity in main channel alluvium	Channel water routing
CH_N2.rte	Manning's "n" value for the main channel	
ALPHA_BF.gw	Baseflow alpha factor (days)	
GW_REVAP.gw	Groundwater "revap" coefficient	
GWQMN.gw	Threshold depth of water in the shallow aquifer required for return flow to occur (mm)	Ground water
REVAPMN.gw	Threshold depth of water in the shallow aquifer for "revap" to occur (mm)	
GW_DELAY.gw	Groundwater delay (days)	

20
21

22 **Table S2**

23 Model parameters and their ranges for calibration at Lakselva catchment.

Parameter_Name	Fitted_Value	Min_value	Max_value
1:V__SNO50COV.bsn	0.372068	0.194828	0.373678
2:V__TLAPS.sub	4.783616	3.632595	8.009101
3:V__SNOCOVMX.bsn	148.8052	73.77092	189.386124
4:R__CN2.mgt	-0.19771	-0.36305	-0.168306
5:V__ESCO.hru	0.172988	0.094391	0.219745
6:R__SOL_AWC(..).sol	8.232051	6.303628	8.613116
7:V__ALPHA_BF.gw	0.656814	0.440427	0.668443
8:V__GW_DELAY.gw	59.9978	15.00158	190.084167
9:V__GW_REVAP.gw	0.123949	0.113642	0.171224
10:V__GWQMN.gw	1629.057	1621.968	2266.496338
11:V__REVAPMN.gw	291.2728	232.0549	349.784393
12:V__SFTMP.bsn	-2.59797	-4.54422	0.969232
13:V__SMFMN.bsn	7.109924	3.697446	9.054555
14:V__SMFMX.bsn	2.679136	0	6.075138
15:V__SMTMP.bsn	-0.04044	-4.61297	2.346734
16:V__TIMP.bsn	0.613599	0.359165	0.627839
17:A__CH_N2.rte	0.179857	0.139561	0.202035
18:A__CH_K2.rte	393.1027	313.3356	454.516235
19:R__SOL_K(..).sol	59.72704	35.81412	69.35257
20:R__SOL_BD(..).sol	1.601312	1.336435	1.875899
21:A__CANMX.hru	61.31247	51.09523	77.226265

24 *Note:*

- 25 • The term "A_" explains that a given value is added to the existing parameter value.
- 26 • The term "R_" explains that an existing parameter value is multiplied by (1 + a given value).
- 27 • The term "V_" explains that the existing parameter value is replaced by a given value.

28
29

30 **Table S3**

31 Model parameters and their ranges for calibration at Strandvassbotn catchment.

Parameter_Name	Fitted_Value	Min_value	Max_value
1:V__SNO50COV.bsn	0.771824	0.548834	0.9
2:V__TLAPS.sub	-1.24694	-2.86481	2.337343
3:V__SNOCOVMX.bsn	244.4058	183.3297	361.394226
4:R__CN2.mgt	0.574274	0.455392	0.697514
5:V__ESCO.hru	0.631558	0.382975	0.761335
6:R__SOL_AWC(..).sol	3.472722	1.975952	5.401056
7:V__ALPHA_BF.gw	0.913628	0.821175	1
8:V__GW_DELAY.gw	219.9303	128.291	292.225311
9:V__GW_REVAP.gw	0.131683	0.091036	0.15628
10:V__GWQMN.gw	212.0551	0	2058.787354
11:V__REVAPMN.gw	134.0218	106.6393	194.685883
12:V__SFTMP.bsn	0.501128	-3.33046	6.519385
13:V__SMFMN.bsn	9.598757	5.922366	9.993673
14:V__SMFMX.bsn	8.117971	6.764509	12.2001
15:V__SMTMP.bsn	0.002693	-6.95033	2.613663
16:V__TIMP.bsn	0.434026	0.428843	0.774345
17:A__CH_N2.rte	0.269336	0.205497	0.286
18:A__CH_K2.rte	249.631	239.995	315.868683
19:R__SOL_K(..).sol	45.61824	43.86684	65.488998
20:R__SOL_BD(..).sol	1.647193	1.297402	1.78662
21:A__CANMX.hru	26.76851	15.48557	36.496628

32 **Table S4**

33 Model parameters and their ranges for calibration at Marsvikelva catchment.

Parameter_Name	Fitted_Value	Min_value	Max_value
1:V__SNO50COV.bsn	0.469691	0.007047	0.473893
2:V__TLAPS.sub	-2.51483	-3.22829	-0.515536
3:V__SNOCOVMX.bsn	463.3235	395.5084	500
4:R__CN2.mgt	0.355821	0.156518	0.391268
5:V__ESCO.hru	0.667015	0.460346	0.789962
6:R__SOL_AWC(..).sol	10.79056	6.38537	11.661043
7:V__ALPHA_BF.gw	0.933666	0.744764	0.943818
8:V__GW_DELAY.gw	346.9136	310.885	451.073975
9:V__GW_REVAP.gw	0.047743	0.035708	0.10294
10:V__GWQMN.gw	7.997381	0	727.034607
11:V__REVAPMN.gw	201.9666	129.1458	273.918671
12:V__SFTMP.bsn	-1.02481	-4.14995	4.70313
13:V__SMFMN.bsn	9.95223	6.091054	12.152555
14:V__SMFMX.bsn	2.007376	0	4.551873
15:V__SMTMP.bsn	-0.70504	-6.57072	2.35726
16:V__TIMP.bsn	0.279031	0.13264	0.287224
17:A__CH_N2.rte	0.24621	0.207118	0.267726
18:A__CH_K2.rte	241.0897	193.0853	278.048767
19:R__SOL_K(..).sol	59.75678	45.51609	65.488998
20:R__SOL_BD(..).sol	0.987031	0.755555	1.226993
21:A__CANMX.hru	16.23683	6.319052	31.684206

34 **Table S5**

35 Model parameters and their ranges for calibration at Målselva catchment.

Parameter_Name	Fitted_Value	Min_value	Max_value
1:V__SNO50COV.bsn	0.446531	0.33627	0.586296
2:V__TLAPS.sub	4.28545	0.04978	7.627006
3:V__SNOCOVMX.bsn	305.6337	236.138	412.0764
4:R__CN2.mgt	-0.2507	-0.26087	-0.16924
5:V__ESCO.hru	0.075634	0.063548	0.238712
6:R__SOL_AWC(..).sol	0.841821	-0.19871	1.404575
7:V__ALPHA_BF.gw	0.571225	0.45284	0.603266
8:V__GW_DELAY.gw	138.7014	49.41261	148.2928
9:V__GW_REVAP.gw	0.106467	0.104251	0.143121
10:V__GWQMN.gw	1679.324	1143.926	2152.208
11:V__REVAPMN.gw	401.8657	321.9861	440.6779
12:V__SFTMP.bsn	-4.02599	-8.37578	-2.97231
13:V__SMFMN.bsn	6.398767	5.234928	8.45886
14:V__SMFMX.bsn	7.01304	6.44629	11.13017
15:V__SMTMP.bsn	0.647612	-1.76791	4.347335
16:V__TIMP.bsn	0.013455	0	0.101167
17:A__CH_N2.rte	0.083273	0.017849	0.110649
18:A__CH_K2.rte	274.74	190.8205	332.8163
19:R__SOL_K(..).sol	11.74589	11.73347	14.21723
20:R__SOL_BD(..).sol	-0.10295	-0.11483	0.01862
21:A__CANMX.hru	74.25598	68.92331	82.7744

36 **Table S6**

37 Model parameters and their ranges for calibration at Halselva catchment.

Parameter_Name	Fitted_Value	Min_value	Max_value
1:V__SNO50COV.bsn	0.077217	0	0.136668
2:V__TLAPS.sub	-3.17052	-4.67426	-2.459617
3:V__SNOCOVMX.bsn	321.6501	223.5091	463.462769
4:R__CN2.mgt	0.168899	0.166434	0.283828
5:V__ESCO.hru	0.824999	0.725746	0.830776
6:R__SOL_AWC(..).sol	3.519947	2.683237	4.879325
7:V__ALPHA_BF.gw	0.09354	0.022898	0.168552
8:V__GW_DELAY.gw	113.7252	0	134.905304
9:V__GW_REVAP.gw	0.026366	0.02	0.041579
10:V__GWQMN.gw	2415.427	2140.499	3455.947021
11:V__REVAPMN.gw	136.1137	87.5749	262.805389
12:V__SFTMP.bsn	4.056153	-2.07028	4.440275
13:V__SMFMN.bsn	2.097047	1.286147	3.860434
14:V__SMFMX.bsn	15.73803	15.27752	19.66333
15:V__SMTMP.bsn	-0.57026	-4.65451	2.375171
16:V__TIMP.bsn	0.712901	0.614402	0.734376
17:A__CH_N2.rte	0.281275	0.244184	0.286
18:A__CH_K2.rte	206.3314	197.3828	302.660187
19:R__SOL_K(..).sol	30.00618	29.11426	30.423979
20:R__SOL_BD(..).sol	0.415157	0.192496	0.512872
21:A__CANMX.hru	87.53735	79.26406	95.91053

38 **Table S7**

39 Model parameters and their ranges for calibration at Karpelva catchment.

Parameter_Name	Fitted_Value	Min_value	Max_value
1:V__SNO50COV.bsn	0.121458	0	0.223679
2:V__TLAPS.sub	-1.62143	-5.96032	-1.228701
3:V__SNOCOVMX.bsn	320.3033	283.6223	415.095337
4:R__CN2.mgt	0.286459	0.027319	0.435413
5:V__ESCO.hru	0.786523	0.523386	0.806634
6:R__SOL_AWC(..).sol	6.72311	5.63689	7.532562
7:V__ALPHA_BF.gw	0.140534	0.068671	0.335821
8:V__GW_DELAY.gw	391.9123	356.6408	452.227478
9:V__GW_REVAP.gw	0.116913	0.08721	0.136964
10:V__GWQMN.gw	1652.137	0	1657.108398
11:V__REVAPMN.gw	282.6724	201.7739	296.836761
12:V__SFTMP.bsn	13.17356	7.336163	14.986744
13:V__SMFMN.bsn	7.710621	6.51554	15.238759
14:V__SMFMX.bsn	5.631604	1.943751	6.582559
15:V__SMTMP.bsn	0.04126	-3.33755	2.931115
16:V__TIMP.bsn	0.56778	0.377529	0.677137
17:A__CH_N2.rte	0.011258	-0.01961	0.048228
18:A__CH_K2.rte	213.2674	211.6405	336.788971
19:R__SOL_K(..).sol	10.9921	6.980662	14.739726
20:R__SOL_BD(..).sol	1.190092	0.501049	1.438523
21:A__CANMX.hru	83.83518	65.53342	100

40

41

42 **Table S8**

43 Median changes in the probable future flood events exceeding the 2-year flood.

Catchments	Area (km ²)	Flood regimes	Probable exceeding events (%)													
			GCM_RCM1		GCM_RCM2		GCM_RCM3		GCM_RCM4		GCM_RCM5		Average			
			1 ^c	2 ^d	1	2	1	2	1	2	1	2	1	2		
Karpelva	129	Snowmelt	+3.4	+3.4	-100	-100					-100	-100			-66	-66
Halselva	143	Snowmelt			+300	+300	+167	+167	-75	-75	-20	-20			93	93
Målselva	5815	Snowmelt														
at Lundberg		Snowmelt	-3.3	-3.3	+83.3	+83.3	+160	+140	-22.2	-33.3	-41.7	-41.7			35.2	29.0
at Lille Rostavatn		Snowmelt		-7.7	+55.6	+44.4	+116.7	+100					-8.3		86.2	32.1
at Høgskarhus		Snowmelt		-7.7	+20		+66.7	+55.6	-10	-30	+9.1	-9.1			21.5	2.2
at Skogly		Snowmelt			-7.1	-7.1	+50	+41.7	-7.7	-7.7	-7.7	-7.7			6.9	1.0
at Målselvfossen		Snowmelt			+42.9	+12.9	+77.8	+77.8	-54.5	-54.5	-25	-37.5			10.3	-0.3
Marsvikelva	32	Rainfall	-6.7			+7.1	-36.4	-36.4	-45.5	-45.5	+12.5	+7.5			-19	0.1
Strandvassbotn	26	Rainfall	+45.5	+54.5	+62.5	+75	-26.7	-6.7	+300	+400	-58.8	-47.1			64.5	95.1
Lakselva	297	Mixed	+8.3	+8.3	+5.6	+5.6	+5.3	+5.3	-47.1	-47.1	-44.4	-38.9			-15	-13

^c Probable future flood events exceed the extreme floods quantiles (estimated from discharges of the reference period (1976-2005))

^d Probable future flood events exceed the extreme floods quantiles (estimated from discharges of the future period (2041-2070))

“+”: increase of exceeding events

“-”: decrease of exceeding events

49 **Table S9**

50 Median changes in the probable future flood events exceeding the 5-year flood.

Catchments	Area (km ²)	Flood regimes	Probable exceeding events (%)													
			GCM_RCM1		GCM_RCM2		GCM_RCM3		GCM_RCM4		GCM_RCM5		Average			
			1 ^e	2 ^f	1	2	1	2	1	2	1	2	1	2		
Karpelva	129	Snowmelt	+3.4	+3.4			-100	-100							-48.3	-48.3
Halselva	143	Snowmelt			+100		+100				+100				100	
Målselva	5815	Snowmelt														
at Lundberg		Snowmelt	+5.6	-11.1	+600	+400	+100	+100	-50	-50	+33				138	110
at Lille Rostavatn		Snowmelt	+18.8	-12.5	+100		+600	+500	-33	-67	+100	-50			157	93
at Høgskarhus		Snowmelt	+12.5	-18.8	+100	+100	+300	+300	-50	-50	-25	-50			68	56
at Skogly		Snowmelt	+5	+5	+150	+150	+100	+100	-100	-100					39	11
at Målselvfossen		Snowmelt	+12		+100	+100	+100	+100			-100	-100			28	33
Marsvikelva	32	Rainfall	+133	+233	-66.7	-66.7	-100	-75		+100		+100			-11	58
Strandvassbotn	26	Rainfall	+100	+100	+100	+100	-60	-60			-100	-100			10	10
Lakselva	297	Mixed	+100	+100	+42.9	+28.6	+75	+75	-89	-89					32.3	28.7

^e Probable future flood events exceed the extreme floods quantiles (estimated from discharges of the reference period (1976-2005))

^f Probable future flood events exceed the extreme floods quantiles (estimated from discharges of the future period (2041-2070))

“+”: increase of exceeding events

“-”: decrease of exceeding events

56 **Table S10**

57 Median changes in the probable future flood events exceeding the 200-year flood.

Catchments	Area (km ²)	Flood regimes	Probable exceeding events (%)													
			GCM_RCM1		GCM_RCM2		GCM_RCM3		GCM_RCM4		GCM_RCM5		Average			
			1 ^g	2 ^h	1	2	1	2	1	2	1	2	1	2		
Karpelva	129	Snowmelt	+38	+38											38	38
Halselva	143	Snowmelt														-32
Målselva	5815	Snowmelt														
at Lundberg		Snowmelt	-17	-50											-17	-50
at Lille Rostavatn		Snowmelt	-25	-75											-25	-75
at Høgskarhus		Snowmelt	-50	-75											-50	-75
at Skogly		Snowmelt	+100												100	
at Målselvfossen		Snowmelt		-29												-29
Marsvikelva	32	Rainfall			+100	+100	-100	-100							0	0
Strandvassbotn	26	Rainfall					-25	-25							-25	-25
Lakselva	297	Mixed														

^g Probable future flood events exceed the extreme floods quantiles (estimated from discharges of the reference period (1976-2005))

^h Probable future flood events exceed the extreme floods quantiles (estimated from discharges of the future period (2041-2070))

“+”: increase of exceeding events

“-”: decrease of exceeding events

66 **Table S11**

67 Median changes in the probable future flood events exceeding the 500-year flood.

Catchments	Area (km ²)	Flood regimes	Probable exceeding events (%)											
			GCM_RCM1		GCM_RCM2		GCM_RCM3		GCM_RCM4		GCM_RCM5		Average	
			1 ⁱ	2 ^j	1	2	1	2	1	2	1	2	1	2
Karpelva	129	Snowmelt	+12	+71									12	71
Halselva	143	Snowmelt	-6	-24									-6	-24
Målselva	5815	Snowmelt												
at Lunderg		Snowmelt	+33	-100									33	-100
at Lille Rostavatn		Snowmelt		-100										-100
at Høgskarhus		Snowmelt		-100										-100
at Skogly		Snowmelt												
at Målselvfossen		Snowmelt												
Marsvikelva	32	Rainfall			+100									100
Strandvassotn	26	Rainfall					+25	+50					25	50
Lakselva	297	Mixed												

68 ⁱ Probable future flood events exceed the extreme floods quantiles (estimated from discharges of the reference period (1976-2005))69 ^j Probable future flood events exceed the extreme floods quantiles (estimated from discharges of the future period (2041-2070))

70 “+”: increase of exceeding events

71 “-”: decrease of exceeding events

72

73 **Table S12**

74 Median changes in the probable future flood events exceeding the 1000-year flood.

Catchments	Area (km ²)	Flood regimes	Probable exceeding events (%)											
			GCM_RCM1		GCM_RCM2		GCM_RCM3		GCM_RCM4		GCM_RCM5		Average	
			1 ^k	2 ^j	1	2	1	2	1	2	1	2	1	2
Karpelva	129	Snowmelt	+36	+164									36	164
Halselva	143	Snowmelt	+36	-18									36	-18
Målselva	5815	Snowmelt												
at Lunderg		Snowmelt	+50	-100									50	-100
at Lille Rostavatn		Snowmelt	-100	-100									-100	-100
at Høgskarhus		Snowmelt												
at Skogly		Snowmelt												
at Målselvfossen		Snowmelt												
Marsvikelva	32	Rainfall			+100									100
Strandvassotn	26	Rainfall					-25	-25					-25	-25
Lakselva	297	Mixed												

76 ^k Probable future flood events exceed the extreme floods quantiles (estimated from discharges of the reference period (1976-2005))77 ^j Probable future flood events exceed the extreme floods quantiles (estimated from discharges of the future period (2041-2070))

78 “+”: increase of exceeding events

79 “-”: decrease of exceeding events

80

1 Supplementary Figure for

2
3

4 **Projections of future floods in Norwegian Arctic** 5 **catchments under climate change context**

6

7 **Minh Tuan Bui** ^{1,*}, **Jinmei Lu** ¹, **Linmei Nie** ²

8

9

10 ¹ Department of Technology and Safety, Faculty of Science and Technology, UiT The Arctic University of Norway, 9037
11 Tromsø, Norway; jinmei.lu@uit.no

12 ² Centre for Sustainable Development and Innovation of Water Technology, Foundation CSDI WaterTech, 0373 Oslo,
13 Norway; linmei.nie@csti.no

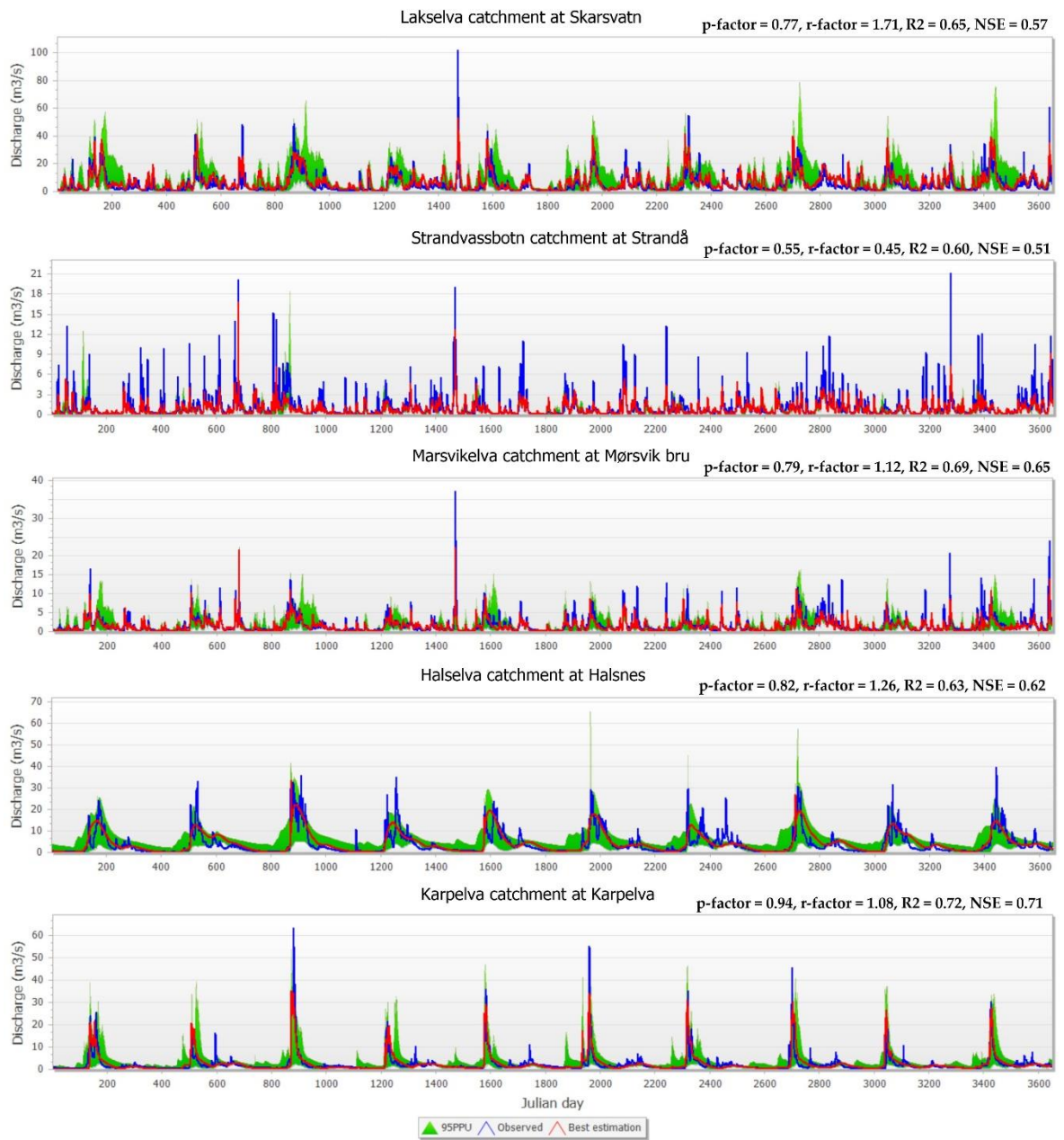
14

15

16 * Corresponding author: Minh Tuan Bui

17 E-mail address: minh.t.bui@uit.no

18



19

20

21

Fig. S1. Model performance during the calibration period (1998-2007) in the small-scale Norwegian Arctic catchments: Lakselva, Strandvassbotn, Marsvikelva, Halselva and Karpelva.

22

23

24

25

26

27

28

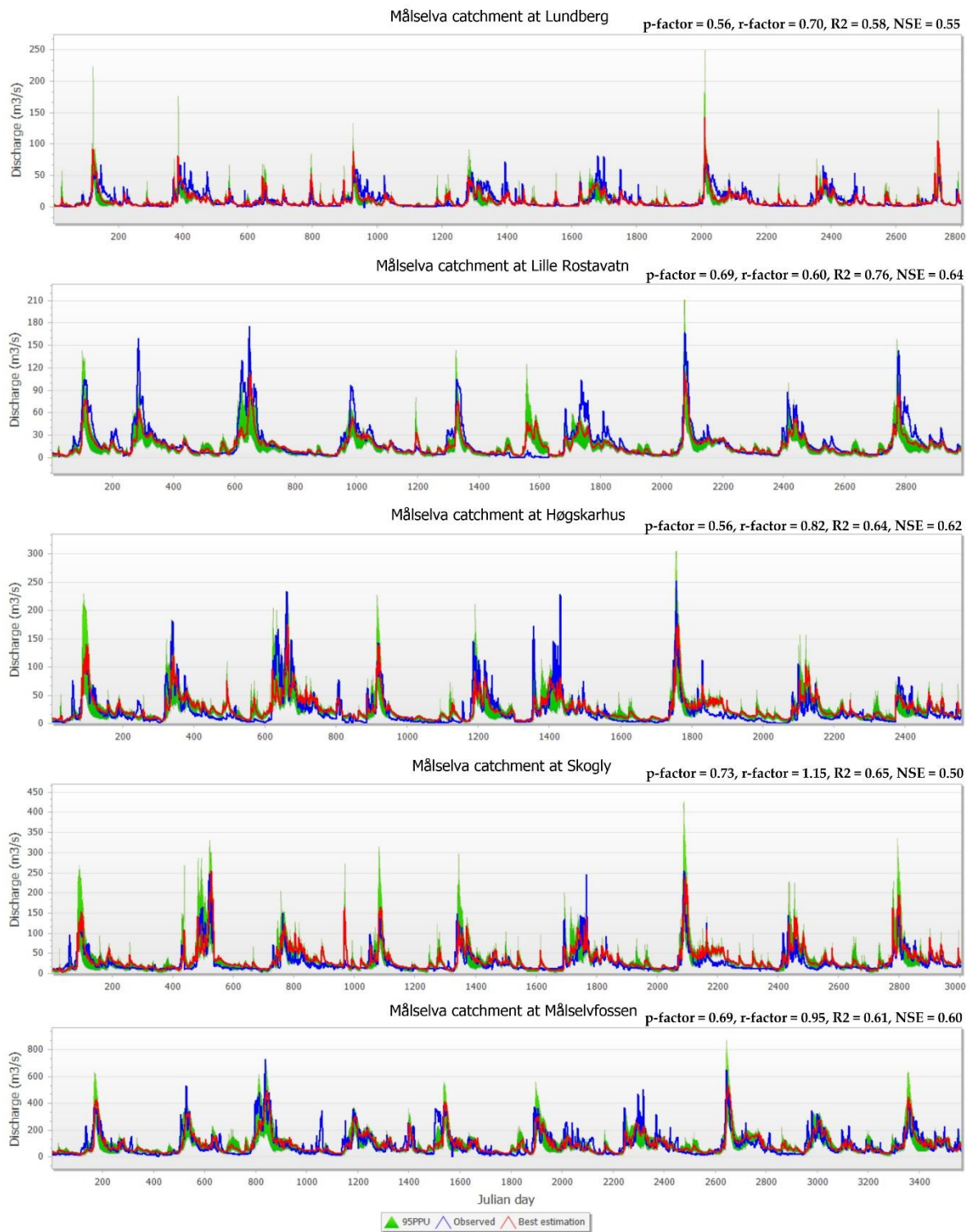
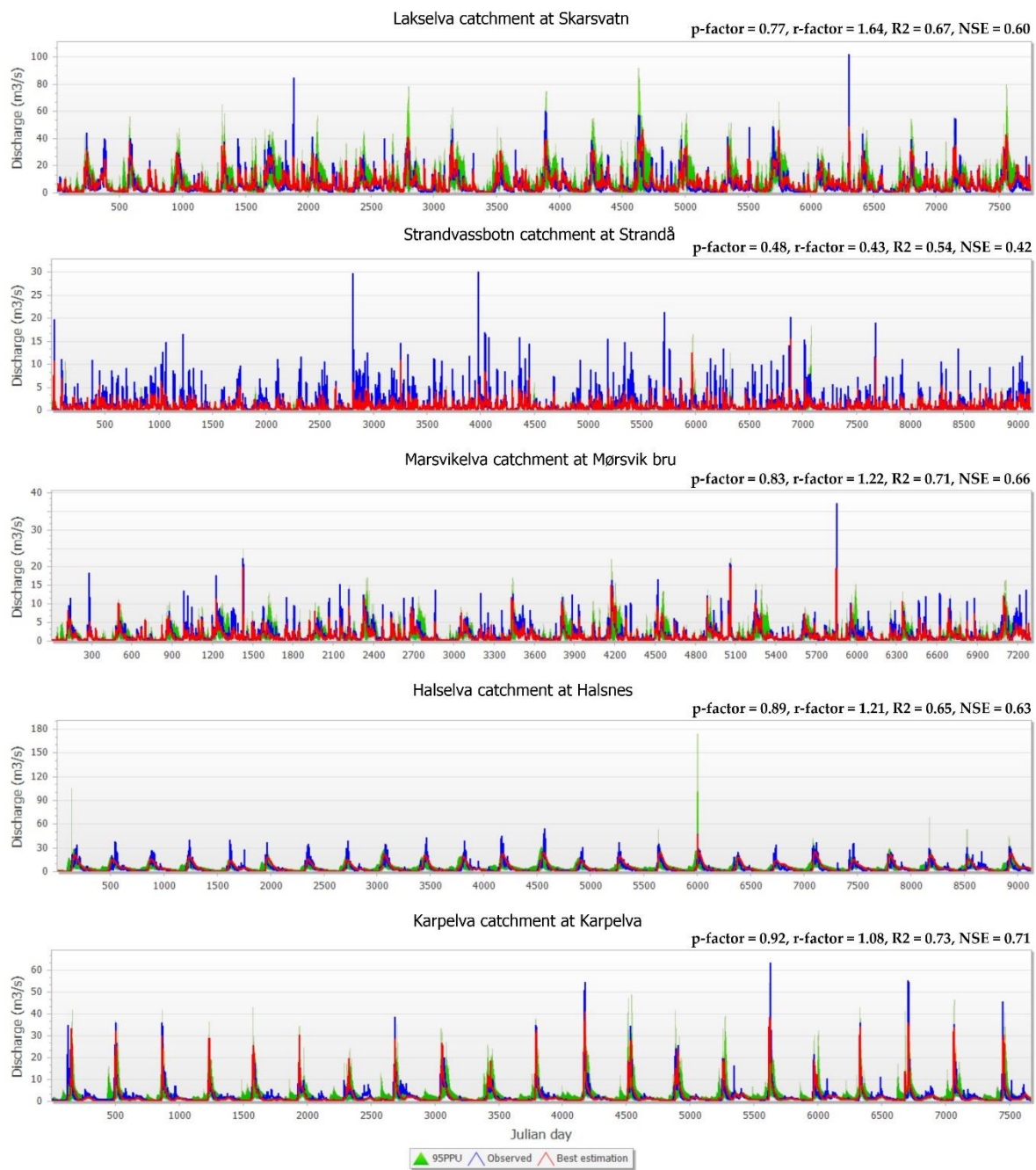


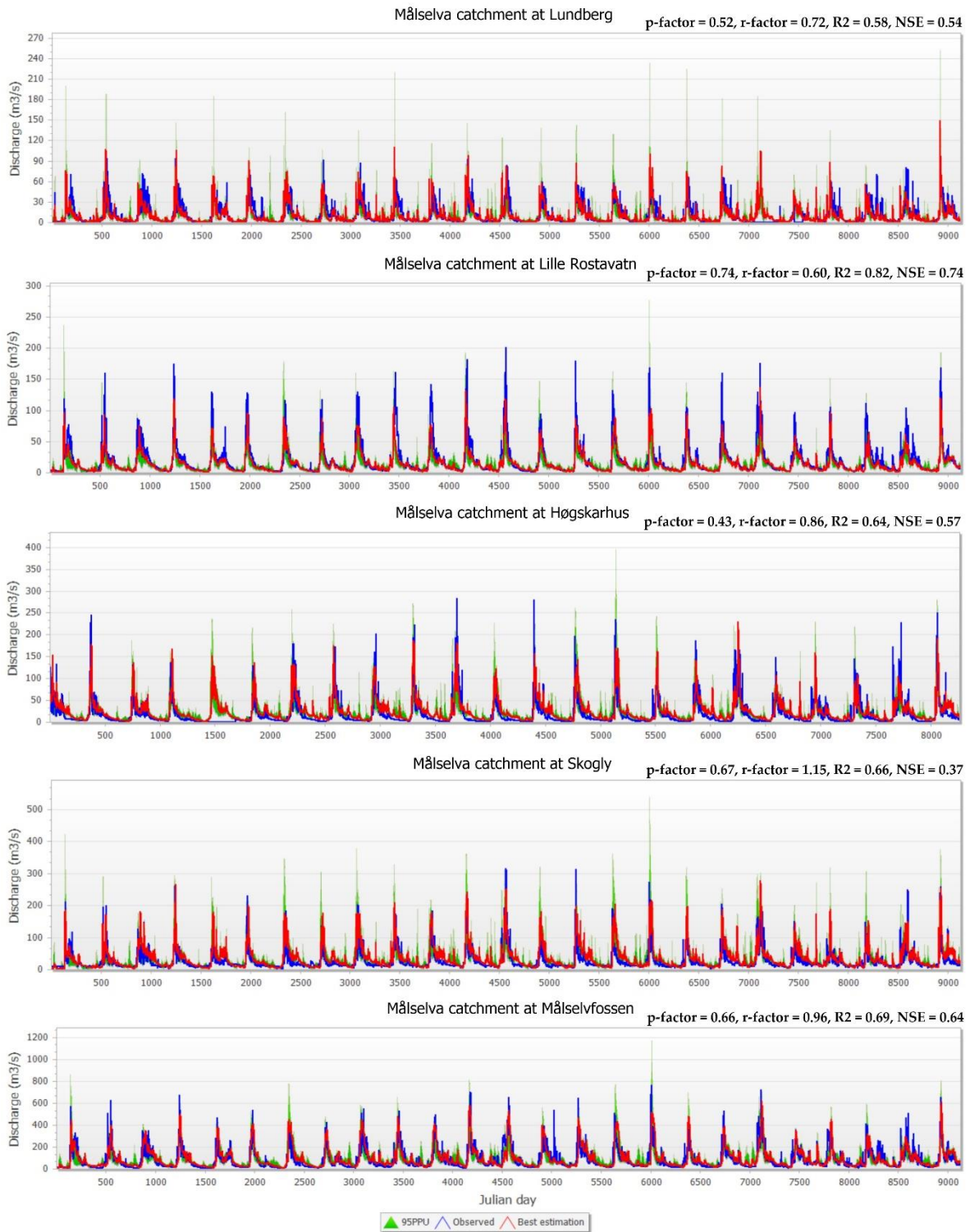
Fig. S2. Model performance during the calibration period (1998-2007) in the large-scale Norwegian Arctic catchment Målselva (Målselv).

29
30
31
32



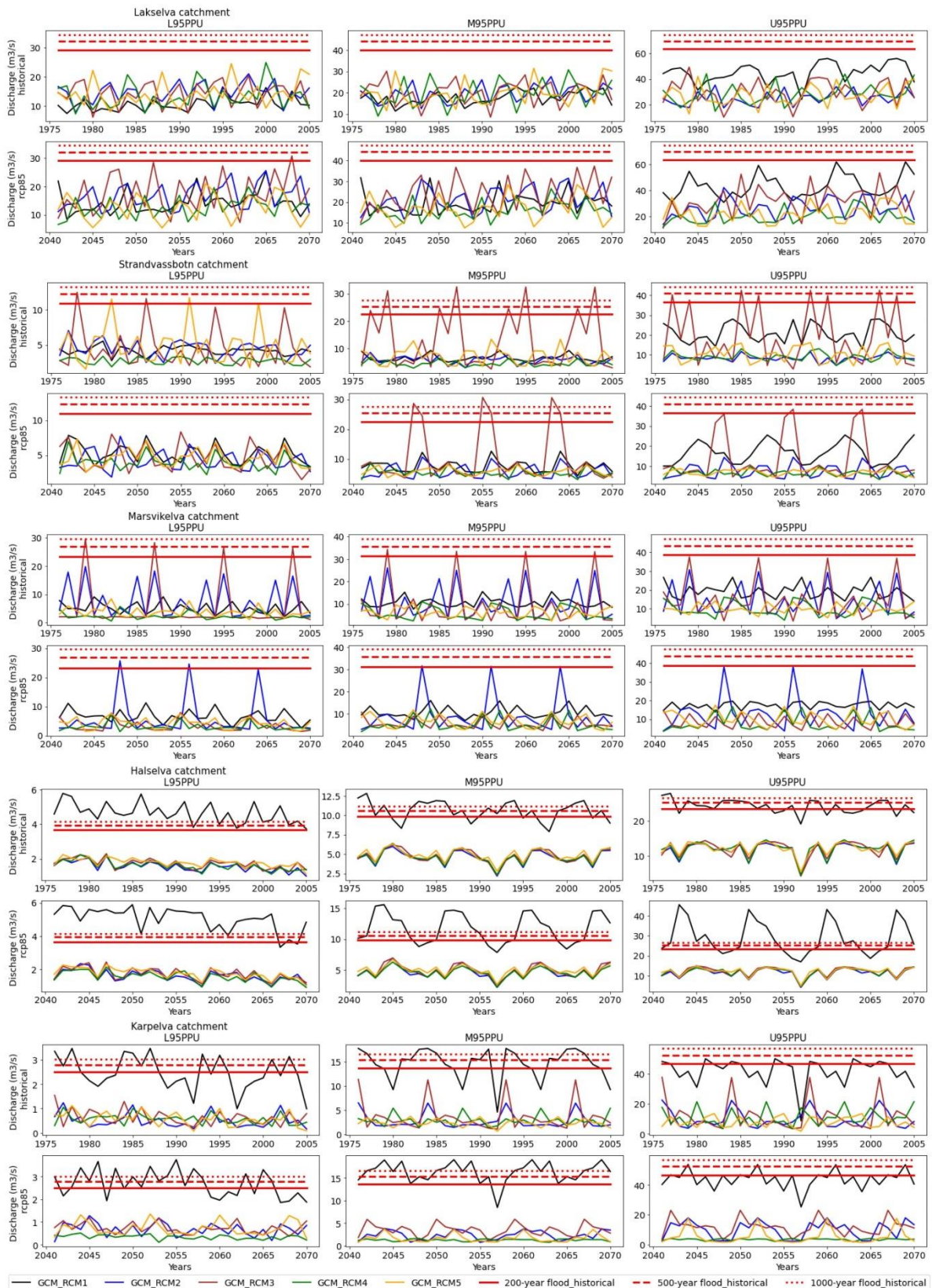
33
 34
 35
 36
 37
 38
 39
 40
 41
 42

Fig. S3. Model performance during the validation period (1980s-2005) in the small-scale Norwegian Arctic catchments: Lakselva, Strandvassbotn, Marsvikelva, Halselva and Karpelva.



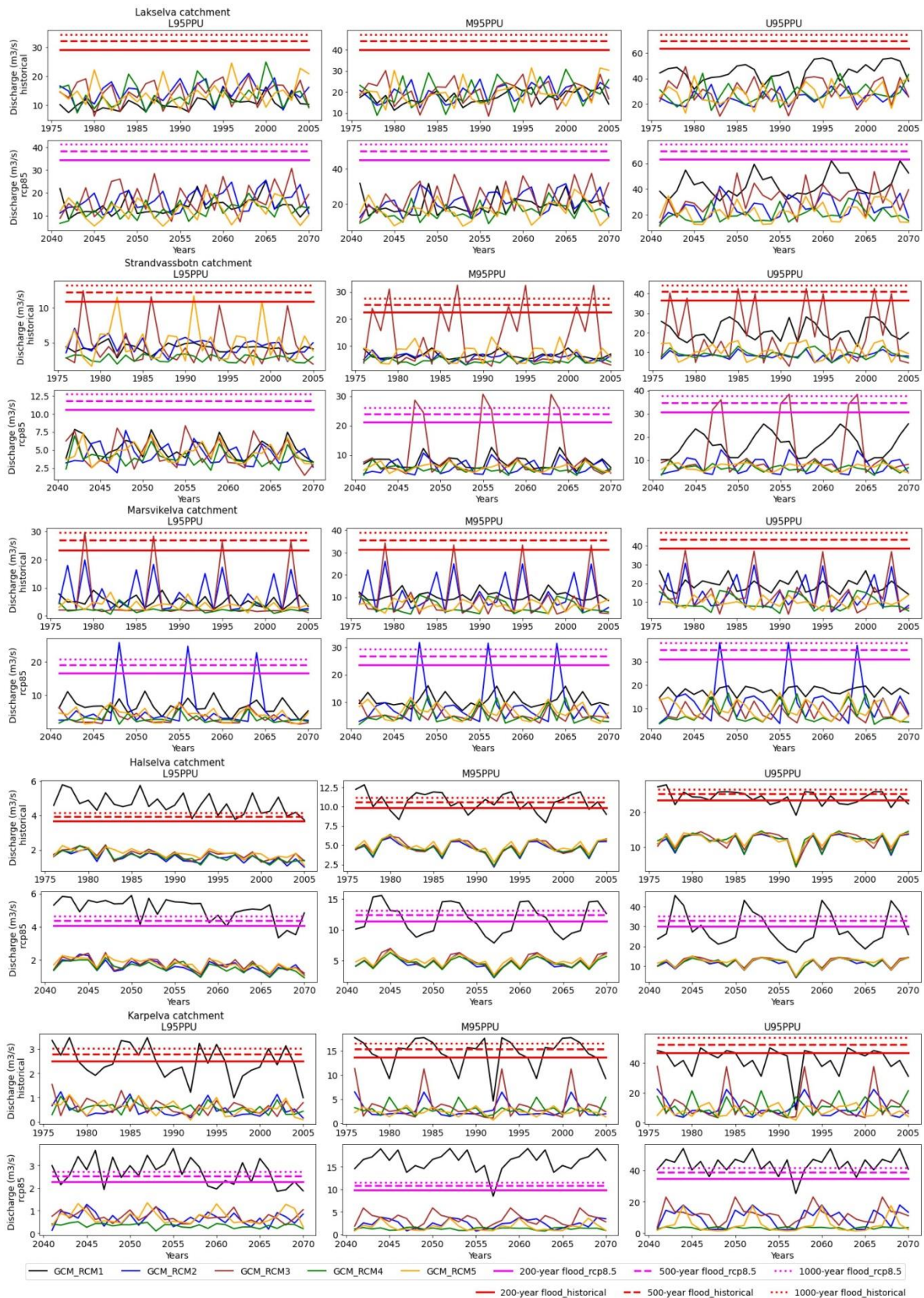
43
 44
 45
 46

Fig. S4. Model performance during the validation period (1980s-2005) in the large-scale Norwegian Arctic catchment Målselva (Målselv).



47
48
49
50
51
52
53

Fig. S5. The estimated number of future maximum annual peak flows (at three levels, i.e., upper limited-U95PPU (at 97.5%), median-M95PPU, and lower limited-L95PPU (at 2.5%) of the discharge data) exceeding the extreme flood quantiles (estimated by discharge of the reference period (1976-2005)), by using five different ensemble Global and Regional Climate Models inputs (GCM_RCM1-5), in the small-scale Norwegian Arctic catchments: Lakselva, Strandvassbotn, Marsvikelva, Halselva, and Karpelva.



54
55
56
57
58
59
60

Fig. S6. The changes in estimated magnitudes of extreme flood quantiles, and number of maximum annual peak flows (at three levels i.e. upper limited-U95PPU (at 97.5%), median-M95PPU, and lower limited-L95PPU (at 2.5%) of the discharge data) exceeding those floods, from the reference period (1976-2005) to the near future (2041-2070), by using five different ensemble Global and Regional Climate Models inputs (GCM_RCM1-5), under high emission scenario (RCP8.5), in the small-scale Norwegian Arctic catchments: Lakselva, Strandvassbotn, Marsvikelva, Halselva and Karpelva.

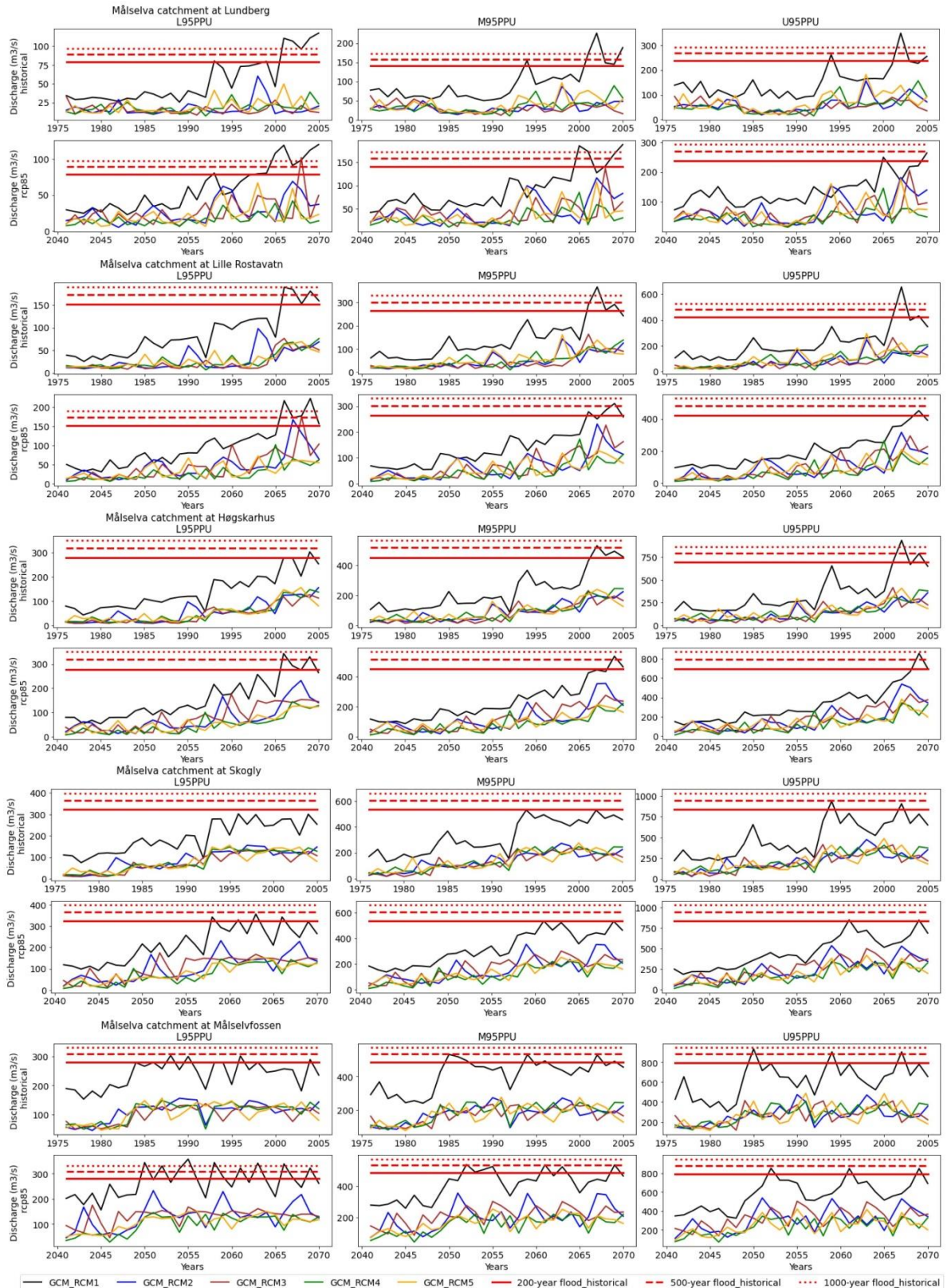


Fig. S7. The estimated number of future maximum annual peak flows (at three levels i.e. upper limited-U95PPU (at 97.5%), median-M95PPU, and lower limited-L95PPU (at 2.5%) of the discharge data) exceeding the extreme flood quantiles (estimated by discharge of the reference period (1976-2005)), by using five different ensemble Global and Regional Climate Models inputs (GCM_RCM1-5), in the large-scale Norwegian Arctic catchment Måselva (Måselv).

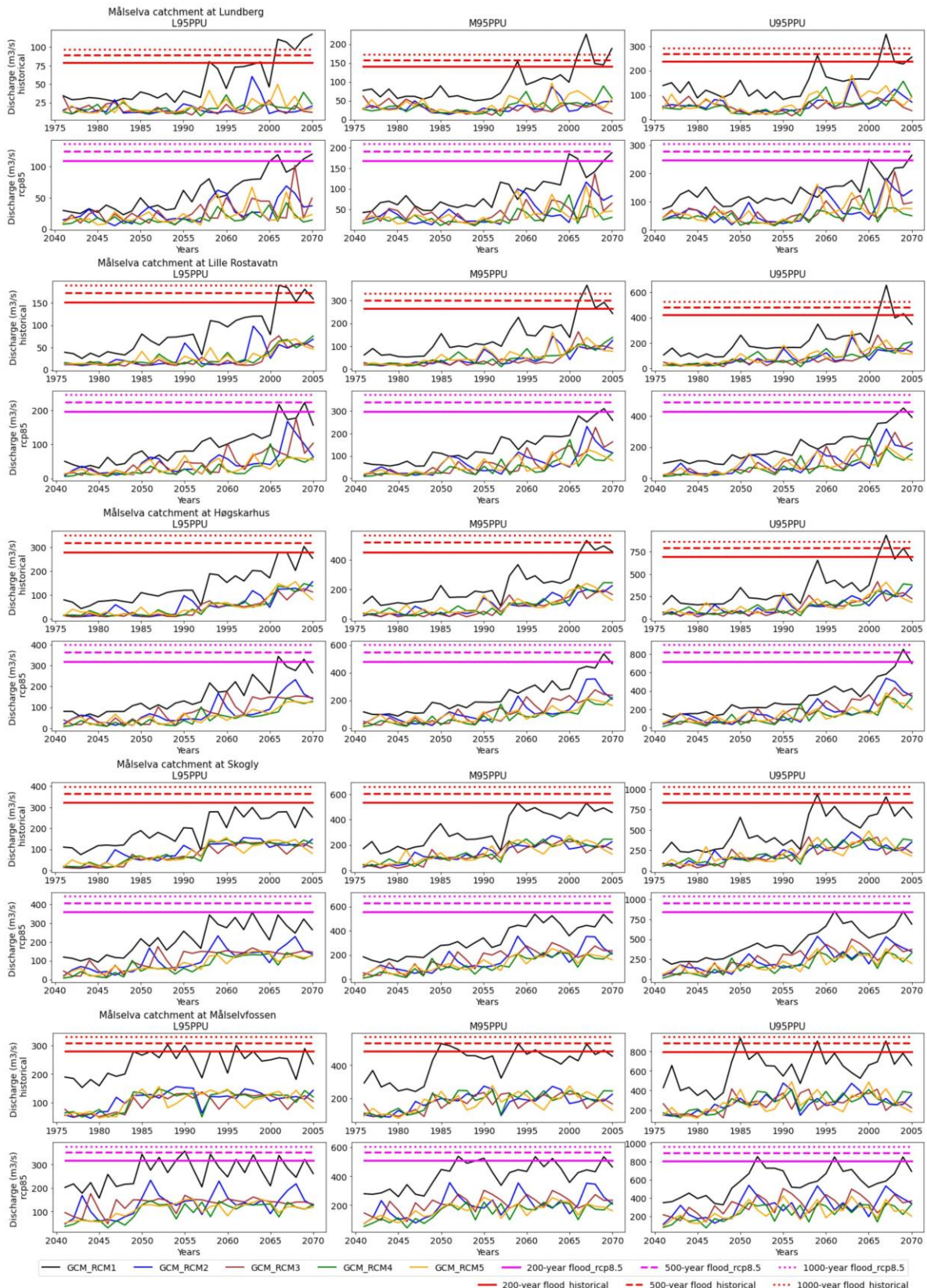


Fig. S8. The changes in estimated magnitudes of extreme flood quantiles, and number of maximum annual peak flows (at three levels i.e. upper limited-U95PPU (at 97.5%), median-M95PPU, and lower limited-L95PPU (at 2.5%) of the discharge data) exceeding those floods, from the reference period (1976-2005) to the near future (2041-2070), by using five different ensemble Global and Regional Climate Models inputs (GCM_RCM1-5), under high emission scenario (RCP8.5), in the large-scale Norwegian Arctic catchment Målselva (Målselv).

68
 69
 70
 71
 72
 73
 74

